An L(2)representationofthecontinuuminheavyparticlecollisio

Robin Nicholas Hewitt

AN L^2 REPRESENTATION OF THE CONTINUUM IN HEAVY PARTICLE COLLISIONS

by

Robin Nicholas Hewitt, B.Sc. (York)

A thesis submitted to the University of Durham
in candidature for the degree of
Doctor of Philosophy

Department of Physics,
University of Durham,
England.

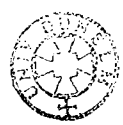

September, 1987.

ABSTRACT

This thesis is concerned with the use of L^2 or square integrable functions as a representation of the electronic continua in ion-atom collisions. An exact representation of the continuum states is considered for comparison. The L^2 functions are optimised in an attempt to remove some of the arbitrary features present in such calculations.

The original work of this thesis is mainly concerned with the calculation of single electron processes in collisions between He^{2+} ions and neutral lithium atoms. The cross sections for single electron capture were calculated in a close-coupled approximation, using the semi-classical impact parameter method. A maximum of thirty-two atomic orbitals with plane-wave translational factors attached were centred upon the target and projectile. Satisfactory agreement with experimental data is obtained over the He^{2+} laboratory energy range from 8 to 2000 keV. The results show the importance of the continuum over a restricted range of impact energies.

The rest of the research is concerned with direct excitation and ionisation in the same collision system and results are given for He^{2+} laboratory energies between 20 and 6000 keV. The calculations used a similar close-coupled approximation with up to sixty-five basis states. The best ionisation cross sections reproduce the experimental data apart from a normalization factor. The excitation results were more sensitive to basis set choice.

The ionisation cross sections were also investigated using an exact representation of the continuum states, using the First Born Approximation and a t-matrix approximation in an attempt to improve upon the L^2 results.

The relationship between the present calculations and some previous methods are discussed and suggestions for future work are made. These are the first close-coupled estimates of ionisation for this sytem and show that contributions from target d- and f- states dominate the ionisation cross section around its maximum.

ACKNOWLEDGEMENTS

I would like to express my gratitude to my joint supervisors, Professor B.H. Bransden and Dr. D.R. Flower, for their patient supervision of this research.

I wish to thank Dr. A.M. Ermolaev for introducing me to the methods used in Chapter four and for his collaboration during part of the present research. I also wish to thank Dr. R. Shingal who was always willing to help and for the use of his program during some of the calculations. I also thank Dr. C.W. Newby for useful discussions.

I am grateful for the facilities provided by the Physics Department at the University of Durham and especially to the University Computing Centres at Newcastle upon Tyne and Durham for the excellent services they provided. The calculations were made using the IBM 4341 and Amdahl 470/V8 at Durham, and the IBM 370/168 and Amdahl 5860 at Newcastle.

I was financed by an SERC quota award. Finally I am indebted to Ms. M. Chipchase for her organisation and typing of this thesis.

CONTENTS

		Page
ABSTRACT		i
ACKNOWLEDGEMENTS		ii
CHAPTER ONE - INTRODUCTION		
1.1	Single electron processes in ion-atom collisions	1
1.2	Applications of heavy particle collisions	3
1.3	Cross sections and frames of reference	13
1.4	Units for cross sections and other variables	19
CHAPTER TWO - EXISTING THEORY AND APPLICATIONS		22
2.1	Introduction	22
2.2	Quantum mechanical formulation	23
2.3	The impact parameter approximation	34
2.3.1	The impact parameter Schrodinger equation	34
2.3.2	Choosing the expansion functions	42
2.3.3	Solving the impact parameter Schrodinger equation	48
2.4	Atomic and related L^2 expansion methods	66
2.4.1	Basic atomic expansion methods	66
2.4.2	The L^2 approach to representing continuum states	67
2.4.3	L^2 expansions in electron-atom scattering	69
2.4.4	Introduction to L^2 methods in heavy particle collisions	77
2.4.5	Sturmian functions	78
2.4.6	Determination of ionisation cross sections from an L^2 expansion	90
2.4.7	The united atom pseudostate method	100
2.4.8	The three centre expansion method	109
2.4.9	Oscillator strengths and the dipole approximation close coupling method	116

2.4.10 The single centre expansion and related approaches to the calculation of ionisation 130

2.4.11 The classical method 142

CHAPTER THREE - THE TWO-CENTRE PSUEDOSTATE EXPANSION METHOD USING THE IMPACT PARAMETER FORMULATION 144

3.1 Introduction 144

3.2 The impact parameter equations 144

3.3 The single electron effective potential model 155

3.4 The evaluation of the direct and exchange matrix elements 159

3.5 The solution of the close-coupled differential equations 174

3.5.1 Introduction 174

3.5.2 The calculation of the cross sections and numerical methods 175

3.5.3 The computer programs for calculating exchange matrix elements 182

3.5.4 The computer programs for calculating cross sections 185

CHAPTER FOUR - THE FIRST BORN APPROXIMATION AND THE T-MATRIX METHOD FOR CALCULATING IONISATION 190

4.1 Introduction 190

4.1.1 The t-matrix for ionisation 191

4.2 The calculation of the t-matrix elements in prolate spheroidal co-ordinates 204

4.3 The evaluation of the ionisation cross sections 216

CHAPTER FIVE - THE PRESENT CALCULATIONS AND RESULTS 223

5.1 Introduction 223

5.2 A description of the charge transfer models 224

5.2.1 The basis sets and pseudo models for capture from the L-shell 224

5.2.2 K-shell capture from Li and the Independent Electron Model 230

5.2.3 Numerical methods used in the capture calculations 235

5.3 Present results for L-shell capture 238

5.4 Present results for K-shell capture 260

5.5 The calculations of the ionisation of Li by He^{2+} 267

5.5.1 The ionisation basis sets 267

5.5.2 Calculation of the 54 state basis set 269

5.6 Ionisation and excitation results 277

5.7 The t-matrix calculations and results for ionisation 297

5.7.1 Numerical methods 297

5.7.2 The t-matrix ionisation results 300

5.8 Remarks on the present methods 304

CHAPTER SIX - CONCLUSIONS 308

6.1 Discussion of results 308

APPENDIX 1 - Evaluation of the direct primitive matrix elements in the space fixed frame. 312

APPENDIX 2 - The Chebychev interpolation method. 317

APPENDIX 3 - The numerical solution of the Schrodinger equation for the case of the continuum states. 318

APPENDIX 4 - Expressions used in the numerical integration of the body-fixed integrals in terms of the prolate spheroidal coordinates (ξ,η,ϕ). 320

REFERENCES 322

CHAPTER ONE

Introduction

1.1 Single electron processes in ion-atom collisions.

The work presented in this thesis is concerned with the calculation of different electronic processes that an electron can undergo in a collision of a multiply charged bare ion with an atom. The atom will always be treated as an effective one electron system even in the many electron case. The active electron which we consider can undergo a variety of possible transitions. To illustrate these possibilities, let us denote the incident projectile ion by A and the target ion or atom by $(B + e^-)$, so that A and B represent a bare nucleus and possibly multiply charged ionic core respectively. In the collision between A and $(B + e^-)$, we can list the following possibilities:

$$A + (B + e^-) \longrightarrow A + (B + e^-), \text{ elastic;} \qquad (1.1.1a)$$

$$\longrightarrow A + (B + e^-)^*, \text{ excitation} \qquad (1.1.1b)$$

$$\longrightarrow (A + e^-) + B \text{ capture into the ground state} \qquad (1.1.1c)$$

$\longrightarrow$ $(A + e^-)^* + B$, capture to an excited state (1.1.1d)

$\longrightarrow$ $A + B + e^-$, ionisation (1.1.1e)

In (1.1.1a) there is no conversion of kinetic energy into internal energy and this represents elastic scattering. However, in (1.1.1b) the target is excited (an excited system will be hereafter denoted by a *) and this is known as direct excitation because there is no rearrangement of the particles during the collision. Processes (1.1.1c) and (1.1.1d) are electron capture processes, and are in the class of collisions called rearrangement processes. They are also known as charge transfer or charge exchange processes. In the last process (1.1.1e), the final state of the active electron is a continuum state and not a discrete bound state on A or B and this is the ionisation channel.

If A and B are the same, the electron capture process is known as "symmetric", otherwise it is called "asymmetric". Also if there is a zero (or nearly zero) energy defect between the initial and final systems the process is called "resonant". If the energy defect is not zero the term "non-resonant" is used. For example the process

$$H^+ + H(1s) \longrightarrow H(1s) + H^+ \qquad (1.1.2)$$

illustrates symmetrical resonance electron capture. However, the process

$$He^{2+} + H(1s) \rightarrow He^{+}(2s) + H^{+} \qquad (1.1.3)$$

is an example of asymmetrical (or accidental) resonance electron capture.

1.2 Applications of heavy particle collisions

The processes of charge exchange and ionisation have been the subject of much attention in recent years for several reasons. We shall now briefly discuss why this is so with particular reference to the system He^{2+} + Li, which is the focus of the present results in this thesis.

There has been considerable interest over the last decade or more in obtaining laser action in the X-ray frequency region. Several schemes have been proposed. For example, McCorkle (1972) proposed to pass an ion beam through a thin target to produce the reaction

$$A^{+} + C \rightarrow A^{+} + C^{*} \qquad (1.2.1)$$

Because of the large cross sections (which will be defined in the next section) for the selective production of inner-shell vacancies in the ions (or atoms), A^{+}, a population inversion could be achieved. However, a major difficulty of this scheme may be the extremely short

lifetimes of the inverted population due to Auger processes. A different method was proposed by Vinogradov and Sobelman (1973) who considered using an electron capture reaction of the type

$$A^{+q} + B \rightarrow A^{+q-1} + B^{+} \qquad (1.2.2)$$

which preferentially leaves the A^{+q-1} product ion in a highly excited state. This subsequently decays to the ground state with the emission of vacuum ultraviolet (VUV) or an X-ray photon. Indeed two astrophysicists, Silk and Steigman (1969) have shown that the reaction (1.1.2) with B = H and A^{+q} a stripped metal ion, is a probable source for soft X-rays in the interstellar medium.

The fundamental issue in the use of (1.2.2) to produce an X-ray laser is the specific choice of reactants. Other important considerations are the optimum collision velocity for producing a specific electronic level, the possible contamination of lower lying electronic levels that may preclude a population inversion, and whether or not the reaction can be realized experimentally. One of the first restraints to consider is the collision velocity. In general for high-velocity collsions, (V > 2 x 10 cm/sec) the excitation of the A^{+q-1} ion after electron capture tends to be spread over many electron levels (Guffey, Ellsworth and MacDonald, 1977). Thus the cross section for producing a specific electronic state is small, reducing the possibility of generating a population inversion. Also the charge

transfer cross sections decrease rapidly with increasing collision velocity, even when the charge state of A^{+q} is large.

However even in the case of low velocity collisions there is another restraint upon the choice of collision partners. For the more highly charged ions and many electron atomic targets, the reactant state lies in the continuum of the ionization and electron capture process

$$A^{+q} + B \rightarrow A^{+q-1} + B^{2+} + e^{-} \qquad (1.2.3)$$

Hence there may not only be electron capture to high lying states of A^{+q-1} via (1.2.2) but also population of low-lying states of the A^{+q-1} ion via (1.2.2), thus removing the possibility of a population inversion. Winter et al. (1977) have shown the importance of (1.2.3) for collisions of multiply charged ions with many electron targets such as Ne and Ar. Shipsey et al. (1978) after considering several systems using semi-empirical theoretical methods (Olson and Salop (1976)) were led to consider a serious calculation on the He^{2+} + Li system, using a molecular orbital approach at low velocities ($V < 7 \times 10$ cm/sec) and a classical method (Section 2.4.1) for $V > 1 \times 10$ cm/sec. Their calculations indicated that for $V < 6 \times 10$ cm/sec the reaction

$$He^{2+} + Li \rightarrow He^{+*} + Li^{+} \qquad (1.2.4)$$

preferentially produces excited He^+ n=3 states. This prediction was confirmed experimentally by Barrett and Leventhal (1981).

Subsequent to the process (1.2.4), the He^{+*}(31) state will decay directly into its ground state either with the emission of a 256A^o (48.4 ev) photon or by cascading via the He^{+*} (21) level with the emission of 1640A^o (7.6eV) and 304 A (40.8eV) photons. Further experimental and theoretical results concerning this feature will be presented in Chapter 5. Details of some schemes for producing a soft X-ray laser can be found in Louisell, Scully and McKnight (1975) and references therein.

Another very important use of the reaction (1.2.4) is in plasma diagnostics in controlled thermonuclear fusion (Guffey et al. 1977). We will now briefly discuss some aspects of the fusion process and then mention the role of cross section calculations as a tool for unfolding the detailed confinement properties of fusion experiments.

Most effort has been directed towards operating a fusion reactor in which a magnetically confined plasma is heated to a temperature at which fusion occurs, the subsequent energy being used to produce steam to generate electricity in steam turbo-generators. To bring this about requires very high temperatures, in order to overcome the Coulomb repulsion of the nuclei which are to be fused. This means nuclei with small charges must be used and the best isotopes for this purpose are those of hydrogen (deuterium,

D and tritium, T). Deuterium occurs naturally in "heavy water", (D_2O) and is obtained relatively cheaply from natural water sources. One of the major tasks has been concerned with confining the plasma, and one method is to use a combination of magnetic fields to confine the plasma in a torus.

One attractive candidate for the fusion reaction is the so-called D-T reaction.

$$D + T \rightarrow ({}^{4}He^{2+} + 3.52 \text{ Mev}) + (n + 14.05 \text{ Mev}) \qquad (1.2.5)$$

The 3.52 Mev alpha particles remain in the fully ionised plasma where they lose their energy through collisions with other constituents. The neutron energy must be converted into heat by some process. One possible solution is to surround the reactor with a lithium blanket to trap the neutrons inside, and use heat exchangers to enable their kinetic energy to be used to heat steam. The advantage of this idea is that more tritium could be produced by the reaction

$$^{6}Li + n \rightarrow {}^{4}He + T + 4.80 \text{ Mev} \qquad (1.2.6)$$

The ^{6}Li isotope occurs in natural lithium (7.5%) and can be obtained fairly easily. As an idea of the temperatures required, 100 MW power station would need of the order of 10

D T reactions per second, and this corresponds to a temperature of the order 10^8 K.

For a magnetically confined plasma, the energy supplied to heat it is through a process called "ohmic heating", which comes from the toroidal current induced by the magnetic field. However above 2-3 Kev this method is ineffective and at higher energies the alpha particles from the D-T fusion reaction (1.2.5) cannot produce further heating. The most promising approach appears to be heating by neutral beam injection. This is a process whereby an intense beam of neutral D atoms (formed by a charge exchange reaction) is injected into the plasma (which it will not contaminate), through the confining magnetic field.

The D atoms become ionised once inside the plasma, and thus become confined by the magnetic field, losing energy by collisions with the plasma constituents. The actual processes whereby the D atoms are ionised in the plasma are given below

$$D + D^+ \rightarrow D^+ + D \qquad (1.2.7a)$$

$$D + T^+ \rightarrow D^+ + T \qquad (1.2.7b)$$

$$D + D^+ \rightarrow D^+ + D^+ + e^- \qquad (1.2.7c)$$

$$D + T^+ \rightarrow D^+ + T^+ + e^- \qquad (1.2.7d)$$

$$e^- + D \rightarrow D^+ + 2e^- \qquad (1.2.7e)$$

The cross sections for the reactions (1.2.7a) to (1.2.7e) can be found from the measured cross sections for the same

reaction in the $H + H^+$ system, as they are the same at the same relative velocity. The most important of these ionisation reactions above are (1.2.7a) and (1.2.7b) which have cross sections of the order of 10^{-15} cm^2 at beam energies of about 10 Kev. However at an average of 100 kev these same two processes have cross sections of the order of 10^{-17} cm^2 and it is the ionisation reactions (1.2.7c) and (1.2.7d) which are more important with cross sections of the order of 10^{-16} cm^2. The electron ionisation process (1.2.7e) is of little importance at the energies being considered. The production of the initial neutral D beam is done by accelerating a pulsed beam of D ions from an ion source, to about 100 kev. This is passed through a molecular deuterium ga5 (D_2) or a metallic vapour target, where partial conversion to fast neutral atoms or molecules occurs by electron capture, for example

$$D^+ + D_2 \rightarrow D + D_2^+ \qquad (1.2.8)$$

However, the cross section for this process at 100 kev is small and so neutralisation is not very efficient. An alternative is to use the "detachment" reaction

$$D^- + D_2 \rightarrow D + e^- + D_2 \qquad (1.2.9)$$

This has a larger cross section but the formation of the negative D beam is difficult.

The efficiency of such neutral beam heating is lowered by the presence of fully ionised impurity ions such as C^{6+} and O^{8+}, in the plasma. Electron capture into highly excited, short-lived states of these impurity ions, such as

$$X^{9+} + H \rightarrow X^{(9-1)+} + H^{+} \qquad (1.2.10)$$

leads to radiative decay and a loss of power.

Also the ionisation process

$$X^{9+} + H \rightarrow X^{9+} + H^{+} + e^{-} \qquad (1.2.11)$$

produces cold electrons which degrade the density and temperature distribution of the plasma.

Another possible source of energy loss within the plasma is the process

$$H^{+} + X^{9+} \rightarrow H + X^{(9+1)+} \qquad (1.2.12)$$

where X may be He^{2+} or an impurity. The neutral H atoms escape the magnetic confinement and the increase of charge of X leads to further radiation power losses. It is clear that data for many atomic processes is required to improve the performance of a magnetically confined fusion system. For instance data is needed for the electron capture processes

$$He^{2+} + H \rightarrow He^{+} + H^{+} \qquad (1.2.13)$$

$$He^{+} + H \rightarrow He + H^{+} \qquad (1.2.14)$$

This is needed to gain a better understanding of the energy and particle loss mechanisms which are associated with alpha particle heating. This is expected to be the dominant heating mechanism on all reactor-sized fusion experiments. Therefore there is interest in diagnostic techniques that could provide quantitative information about alpha particle physics in the first generation of fusion experiments, such as JET and TFTR. One such proposed diagnostic is the use of a high energy (6 Mev) neutral lithium beam injected into the plasma (Post et al. 1981). The fast alpha particles could be neutralized and escape the plasma by double charge exchange with the neutral lithium in the beams,

$$Li + He^{2+} \rightarrow Li^{2+} + He \qquad (1.2.15)$$

The fast neutral helium atoms would be ionized in the detector and analyzed with energy sensitive detectors.

However the expense and complications of the high energy lithium beam make other simpler techniques desirable.

Plasma diagnostic techniques such as this are a vital area of magnetic fusion research. In fact it has been stated that the most impressive progress in the past twenty years in research in magnetic fusion has been in the area of diagnostics.

In general it is important to be able to measure the parameters of a plasma such as its density and temperature, the concentration of impurity ions, and the depth of penetration of the neutral beam used to heat the plasma, along with many other quantities.

An example of electron capture and ionisation processes being used in plasma diagnostics is provided by Kislyakov and Petrov (1971) who have used 4 to 14 kev beams of hydrogen atoms as probes to investigate a plasma. From the attenuation of the beam and a knowledge of the cross sections for electron capture and ionisation for protons colliding with hydrogen, and for ionisation of hydrogen by plasma electrons, the path-averaged proton density in the plasma can be measured. It is also possible to study the Doppler-shifted radiation emitted by decaying hydrogen atoms, formed by electron capture from the hydrogen atom injected beam by plasma protons, in order to study the temperature of the plasma. This method can also be used for investigating impurities present in the plasma, and to exploit the full potential of this aproach, accurate cross sections for the (n,l) distribution will be essential. More comprehensive discussions of many points which have been mentioned concerning controlled nuclear fusion will be found in McDowell and Ferendici (eds.) (1980).In conclusion we can say that a knowledge of the methods and cross sections that are to be presented in this

thesis have important practical and, hopefully, peaceful applications.

1.3 Cross Sections and frames of reference

In this section we shall discuss the quantities which are calculated in the present work and the units of these quantities. In a collision between two "particles" (such as atoms or molecules etc.) the fundamental or characteristic quantity which is measured is called a cross sections, which is defined as follows: the cross section of a certain type of event in a given collision is the ratio of the number of events of this type per unit time and per unit scatterer, to the relative flux of the incident particles with respect to the target. The cross section as defined must be measured experimentally and we will now indicate how this is done.

In Figure 1.1, we illustrate a simple experiment where an incident beam of particles, A, falls upon a target B after being collimated so that it is very nearly a parallel beam. Further we assume that the beam, A, is very closely monoenergetic. We now suppose that N_A particles A reach the target per unit time. We denote by n_A the average density of particles A in incident beam and by U_L their average velocity with respect to the target B. Then the flux of incident particles relative to the target (that is the number of particles A crossing per unit time a unit area perpendicular to the beam direction and stationary with

Figure 1.1

Schematic diagram of a simple collision experiment.

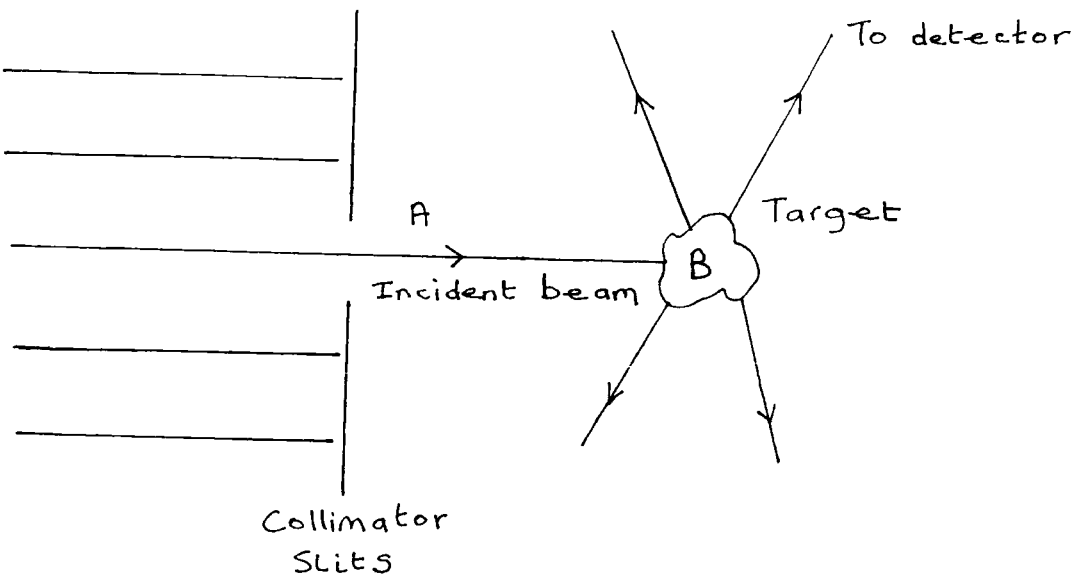

respect to the target) is given by

$$\mathcal{I}_A = n_A u_i = N_A / S \qquad (1.3.1)$$

where S is the cross-sectional area of the beam. We further assume that the target is thin to avoid multiple collision effects. Let n_B be the number of particles B within the "effective" target volume interacting with the incident beam. If the target is a thin layer of thickness l then

$$n_B = S l n_B = S \hat{n}_B \qquad (1.3.2)$$

where n_B is the number of particles B per unit volume of the target and $\hat{n}_B$ is the average surface density of the target particles.

If N_{tot} is the total number of particles A which have interacted per unit time with the scatterers, then under these assumed experimental conditions, N_{tot} is directly proportional to the relative incident flux $\mathcal{I}_A$ and the number n_B of target scatterers. Therefore we have

$$N_{tot} = \sigma_{tot} \mathcal{I}_A n_B \qquad (1.3.3)$$

where the proportionality constant (for a given collision energy) is called the <u>total cross section</u> for the scattering of particle A by particle B. The quantity σ_{tot} has units of area and can be thought of as an effective area which picks

up the incident beam, and is a measure of the strength of the interaction between the particles A and B, at the particular collision energy being considered. It is an intrinsic property of the quantum mechanical system (A + B). The quantity σ_{tot} is the total cross section for all possible collision processes which occur when particles A and B collide. That is to say, it includes elastic scattering

$$A + B \rightarrow A + B, \tag{1.3.4}$$

inelastic scattering

$$A + B \rightarrow A^* + B^* \tag{1.3.5}$$

where, as usual, a * denotes a possible change in the internal quantum state has occurred, and finally reactive scattering

$$A + B \rightarrow C + D \tag{1.3.6}$$

$$A + B \rightarrow C_1 + C_2 + \ldots + C_n \tag{1.3.7}$$

where in the final state two or more particles are produced which are different from A and B.

The reactive processes (1.3.6) and (1.3.7) are called rearrangement collisions if they occur via the exchange of one or more elementary constituent particles. In the case

(1.3.6) where only two particles appear in the final state, it is termed a binary rearrangement collision. For example, a charge exchange process which involves the transfer of one or more electrons between two atomic cores is a binary rearrangement collision. Similarly the process of ionisation which occurs when an electron is ejected from a particle in the collision is a reaction collision. It is possible to introduce total cross sections for particular processes which we shall now proceed to do.

In the case of elastic scattering we can define a <u>total elastic cross section</u> σ_{tot}^{el} in an analagous manner to σ_{tot} in (1.3.3)

$$N_{tot}^{el} = \sigma_{tot}^{el} \Phi_A n_B \qquad (1.3.8)$$

where N_{tot}^{el} is the total number of particles A scattered elastically per unit time. If the collison energy is such that only elastic scattering can occur then clearly $\sigma_{tot} = \sigma_{tot}^{el}$

However, in the general case when inelastic processes occur, we can define the <u>total reaction cross section</u> to include all such processes

$$\sigma_{tot}^{r} = \sigma_{tot} - \sigma_{tot}^{el} \qquad (1.3.9)$$

We note at this point that the term "total" when applied to cross sections can have two different meanings. The

formally correct use is to distinguish between total cross sections and differential cross sections which will be discussed shortly. In the previous discussion we have used the term "total" in its correct sense. However, it is common to find the phrase "total cross section" applied to mean the total cross section for scattering into all possible states being considered, whilst "cross section" means the total cross section for scattering with one or some small number of states.

So far the discussion has not included cross sections which give any information about the angular distribution of the scattered particles. These usually give a more detailed insight into the interaction between the two colliding particles. In order to analyze angular distributions, it is necessary to choose a coordinate reference system. The two most common frames used are the laboratory (Lab.) and centre of mass (CM) frame, often called barycentric system. The laboratory frame is such that the target B is at rest, whereas the centre of mass frame is that where the centre of mass of (A + B) is at rest.

Let us work in the laboratory frame and considering elastic collisions, we denote by dN_{el} the number of particles A scattered per unit time into solid angle $d\Omega_L$ which is centred about the direction (θ_L, ϕ_L) as shown in Figure 1.2. Provided we have a thin target

$$dN_{el} = \sigma_{el}(\theta_L, \phi_L) \oint_A n_B \, d\Omega_L \qquad (1.3.10)$$

The quantity $\sigma_{el}(\theta_L, \phi_L)$ is the <u>laboratory differential cross section</u> for elastic scattering. It is also written as

$$\sigma_{el}(\theta_L, \phi_L) = \frac{d\sigma_{el}(\theta_L, \phi_L)}{d\Omega_L} \qquad (1.3.11)$$

Since Φ_A represents the relative flux of the projectile with respect to the target, we can rewrite the definition (1.3.100 in the centre of mass frame as

$$dN_{el} = \sigma_{el}(\theta_{cm}, \phi_{cm})\, \Phi_A\, n_B\, d\Omega_{cm} \qquad (1.3.12)$$

where

$$\sigma_{el}(\theta_{cm}, \phi_{cm}) = \frac{d\sigma_{el}(\theta_{cm}, \phi_{cm})}{d\Omega_{cm}} \qquad (1.3.13)$$

From equations (1.3.10) asnd (1.3.12) we see that

$$\frac{d\sigma_{el}(\theta_L, \phi_L)}{d\Omega_L}\, d\Omega_L = \frac{d\sigma_{el}(\theta_{cm}, \phi_{cm})}{d\Omega_{cm}}\, d\Omega_{cm} \qquad (1.3.14)$$

and that the total elastic cross section is

$$\sigma_{el} = \int_{\Omega} \frac{d\sigma_{el}}{d\Omega_L}(\theta_L, \phi_L)\, d\Omega_L = \int_{\Omega} \frac{d\sigma_{el}}{d\Omega_{cm}}(\theta_{cm}, \phi_{cm})\, d\Omega_{cm} \qquad (1.3.15)$$

which is independent of the reference frame as any total cross section should be. In a similar manner, we can define differential cross sections for non-elastic scattering.

1.4 Units for cross sections and other variables

Throughout this thesis, unless otherwise stated, we shall use the atomic system of units. This is the system obtained by setting $e = m_e = \hbar = 1$, where e and m_e are the charge and rest mass of the electron respectively. Then in this system the unit of length is the Bohr radius, a_o ($= 0.529 \times 10^{-8}$ cm) which is the radius of the first Bohr orbit of the hydrogen atom. The Bohr radius is given by $a_o = \frac{\hbar^2}{m_e e^2}$. Similarly the units of velocity is the velocity of the electron in the first Bohr orbit of hydrogen, $V_o = \frac{e^2}{\hbar}$. Setting e, m_e and $\hbar$ to one in the expression for the ground state energy of the hydrogen atom, which is $-\frac{m_e e^4}{2\hbar^2}$, gives $-\frac{1}{2}$ in atomic units (a.u.). Therefore the atomic unit of energy is twice the ionisation energy of the hydrogen atom, which is 2*13.6 eV = 27.2eV.

In atomic physics cross sections are often expressed in terms of a_o^2 ($= 2.8 \times 10^{-17}$ cm^2) or in terms of πa_o^2 ($= 8.8 \times 10^{-17}$ cm^2). The units which will be used throughout this thesis for cross sections, unless otherwise stated, will be

10^{-16} cm^2.

It is convenient to measure collision energies in terms of kev, and to refer this to either the laboratory or centre of mass frame. The collision velocity will usually be in terms of atomic units though. If we denote the centre of mass energy by E_{CM}, and the laboratory energy of A by E_L^A (that is E_L^A is the kinetic energy of A in the laboratory frame) and similarly the laboratory energy of B by E, then it is straightforward to show that

$$E_{CM} = \frac{M_B}{M_A + M_B} E_L^A = \frac{M_A}{M_A + M_B} E_L^B \qquad (1.4.1)$$

where M_A and M_B are the masses of A and B respectively. Equation (1.4.1) applies to ion-atom collisions if the electron mass is ignored. It is important to note that the laboratory energy depends upon whether A or B is at rest.

Throughout this work we have used the convention that B is at rest, whilst A is moving. However, unless the meaning is clear, it is necessary to specify which of the colliding entities is the projectile and which is the target when considering laboratory energies. For example we shall use the phrase "the $^4He^{2+}$ laboratory energy" or "the $^4He^{2+}$ projectile energy" to indicate the same fact, that the $^4He^{2+}$ is the projectile. Both these phrases are equivalent. We shall also use the unit of energy obtained by dividing the laboratory energy by the mass of the projectile. For

example taking the $^4He^{2+}$ mass in atomic mass units, (amu) as 4, we can divide the $^4He^{2+}$ laboratory energy by 4 to obtain units of kev amu^{-1}. We note that from (1.4.1) $\frac{E_L^A}{M_A} = \frac{E_L^B}{M_B}$ which is proportional to the square of the relative velocity of A and B, and hence there is no need to specify that A is the projectile. For example, if the laboratory energy is 150 kev amu^{-1} for A incident upon B, it is the same for B incident upon A. We also will make use of the fact that one atomic unit of velocity corresponds to a laboratory energy of 24.97 kev amu^{-1}.

CHAPTER TWO

Existing theory and applications

2.1 Introduction

Processes which involve electron capture or ionisation in ion-atom collisions has generated a vast literature in both review articles and text books, for example, McDowell and Coleman (1970), Bransden (1983), Greenland (1982), Janev, Presnyakov and Shevelko (1985), Basu et al. (1978), Mapleton (1972). The present chapter is not intended to extensively review the subject or to mention every different approach to the problem of calculating charge transfer or ionisation cross sections. It is intended to mention some of the main aspects of the theory of electron capture and ionisation, which are relevant to the work in this thesis, and also illustrate briefly the history of the subject through attempts to improve upon previous calculations.

We shall begin by briefly discussing the full quantum mechanical treatment of the electron capture problem and then discuss the semi-classical impact parameter approximation which is used extensively in theoretical work on ion-atom collisions, and which forms the basis for the results in this thesis. We shall then consider the use of the atomic orbital expansion method, and attempts to improve

upon this, by using various pseudostate expansions. Finally, we shall discuss the use of a completely classical model for calculating ionisation and charge transfer which has recently been applied to calculate cross sections for the same collision system that forms the basis for the present results in this thesis, namely the He + Li system.

2.2 Quantum mechanical Formulation

We shall begin by considering the single electron capture process

$$A + (B + e^-) \rightarrow (A + e^-) + B \qquad (2.2.1)$$

where A and B may represent singly charged ionic cores. As was stated before we shall suppose that A is the projectile ion and B is the target ion. The coordinate system which is to be used to describe the system is shown in Figure 2.1. In Figure 2.1, R denotes the position vector of A with respect to B, $\vec{R}_A$ is the position vector of B with respect to the centre of mass of $(A + e^-)$, $\vec{R}_B$ is the position vector of A with respect to the centre of mass of $(B + e^-)$. The vectors $\vec{r}_A$ and $\vec{r}_B$ are the position vectors of the electron with respect to A and B respectively, and $\vec{r}$ is the position vector of the electron with respect to the centre of mass of A and B. Finally, we let G be the centre

Figure 2.1

Electron capture centre of mass coordinates.

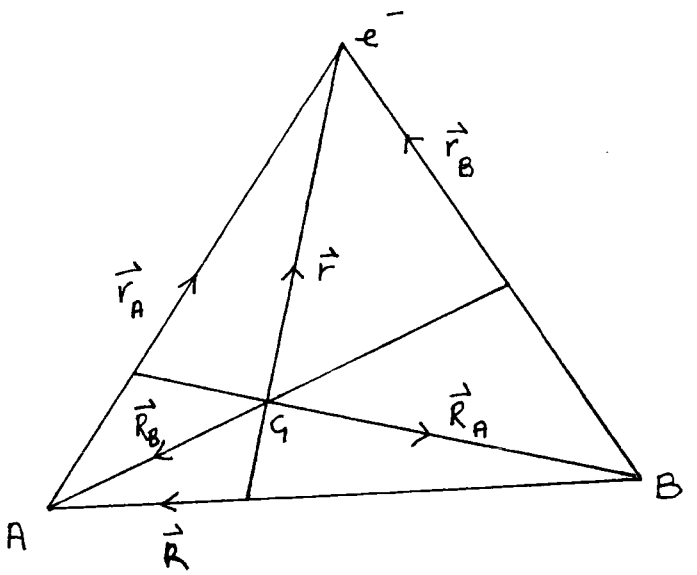

of mass of the whole system ($A + B + e^-$). We shall use M_A and M_B for the masses of A and B respectively, and let M_e be the mass of the electron (we shall use M_e here for the electron mass although it is equal to one in atomic units). Then the total mass of the system is

$$M = M_A + M_B + M_e \qquad (2.2.2)$$

The kinetic energy, T_{CM} of the centre of mass of the system is given by

$$T_{CM} = P_{CM}^2 / 2M \qquad (2.2.3)$$

where P_{CM} is the magnitude of the linear momentum of the centre of mass in the reference frame. It is useful to separate out the centre of mass motion from the scattering problem and work in the frame where the centre of mass is at rest. Hence P_{CM} and T_{CM} (from 2.2.3) will be zero. Then in the system described above, the point G in figure 2.1 is chosen to be at rest. It is usual, in order to describe the dynamics of the system in the centre of mass frame, to choose one of three sets of coordinates, namely $(\vec{r},\vec{R})$, $(\vec{r}_A, \vec{R}_A,)$ or $(\vec{r}_B, \vec{R}_B)$. The centre of mass kinetic energy operator T is now given by

$$T = \frac{P^2}{2\mu} + \frac{P^2}{2m} = \frac{P_A^2}{2\mu_A} + \frac{P_A^2}{2m_A} = \frac{P_B^2}{2\mu_B} + \frac{P_B^2}{2m_B} \qquad (2.2.4)$$

$\vec{P}$, $\vec{P}_A$ and $\vec{P}_B$ are momentum operators conjugate to $\vec{R}$, $\vec{R}_A$ and $\vec{R}_B$ respectively, and similarly $\vec{p}$, $\vec{p}_A$ and $\vec{p}_B$ are momentum operators conjugate to $\vec{r}$, $\vec{r}_A$ and $\vec{r}_B$ respectively. In equation (2.2.4), the various reduced masses are given by

$$\mu = \frac{M_A M_B}{M_A + M_B}, \quad \mu_A = \frac{M_B (M_A + m_e)}{M_A + M_B + m_e}, \quad \mu_B = \frac{M_A (M_B + m_e)}{M_A + M_B + m_e}. \tag{2.2.5}$$

$$m = \frac{m_e (M_A + M_B)}{M_A + M_B + m_e}, \quad m_A = \frac{m_e M_A}{m_e + M_A}, \quad m_B = \frac{m_e M_B}{m_e + M_B}. \tag{2.2.6}$$

In the general theory of collisions it is convenient to introduce the concept of arrangement channels (Bransden (1983), Chapter 4). In the centre of mass frame, the total Hamiltonian of the system, is written as

$$H = H_\alpha + V_\alpha \tag{2.2.7}$$

where the subscript α is variable and denotes a particular grouping of the particles into single particles and aggregates, i.e. different arrangements. We use H_α to denote the Hamiltonian of the system when the separate

particles and aggregates are far apart and then V_α represents the interaction potential. Corresponding to each arrangement channel of H, denoted by α, there are associated a set of channels. Each channel corresponds to a particular state of the system within each arrangement channel.

In the case of the $(A + B + e^-)$ system, the arrangement channels to be considered are the direct arrangement channel, when centre A interacts with the $(B + e^-)$ system, and the rearrangement arrangement channel which corresponds to centre B interacting with the $(A + e^-)$ system. Henceforth we shall omit the word "arrangement" and refer to the direct and rearrangement channels. Ionisation will not be considered here as it is a three body arrangement channel and only two body arrangement channels are being discussed. Hence excitation occurs in the direct channel and charge transfer occurs in the rearrangement channel. In these two channels we shall use the coordinates, $(\vec{r}_B, \vec{R}_B)$ and $(\vec{r}_A, \vec{R}_A)$ respectively to describe the scattering process. In the $(A + B + e^-)$ system the total Hamiltonian is denoted by H. It is given by

$$H = T + V \tag{2.2.8}$$

where T (the kinetic energy operator) was defined in (2.2.4). The potential energy operator V was given by

$$V = V_{eA} + V_{eB} + V_{AB} \tag{2.2.9}$$

V_{eA} and V_{eB} are the potentials between the electron and A and B respectively and V_{AB} is the potential between A and B. If A and B represent bare nuclei, then these three potentials are simply Coulombic in character. We can now decompose the total Hamiltonian into direct and rearrangement channels and write

$$H = H_d + V_d \tag{2.2.10a}$$

or $$H = H_r + V_r \tag{2.2.10b}$$

where d and r refer to the direct and rearrangement channels respectively. Then we have that

$$H_d = T + V_{eB} \tag{2.2.11a}$$

and $$V_d = V_{eA} + V_{AB} \tag{2.2.11b}$$

Similarly

$$H_r = T + V_{eA} \tag{2.2.12a}$$

and $$V_r = V_{eB} + V_{AB} \tag{2.2.12b}$$

We denote by $\Phi_m^B(\vec{r}_B, \vec{R}_B)$ the asymptotic free state for the system being in the mth state in the direct channel. Thus

$$H_d \Phi_m^B = E_m \Phi_m^B \tag{2.2.13}$$

where E_n are energy eigenvalues. In the same way we denote by $\chi_n^A(\vec{r}_A, \vec{R}_A)$ the asymptotic free state for the system being in the nth state in the rearrangement channel. Then

$$H_r \chi_n^A = E_n \chi_n^A \qquad (2.2.14)$$

The asymptotic state for the system being in the initial state i in the direct channel is $\Phi_i^B(\vec{r}_B, \vec{R}_B)$ and this is given by

$$\Phi_i^B(\vec{r}_B, \vec{R}_B) = \exp(i\vec{K}_i \cdot \vec{R}_B)\, \phi_i^B(\vec{r}_B) \qquad (2.2.15)$$

$\vec{k}_i$ is the initial wave vector of A relative to the centre of mass of $(B + e^-)$. The $\phi_i^B(\vec{r}_B)$ is the initial state eigenfunction of the $(B + e^-)$ system with eigenvalue ε_i so we have

$$\left(-\frac{1}{2m_B}\nabla^2_{\vec{r}_B} + V_{eB}\right)\phi_i^B(\vec{r}_B) = \varepsilon_i\, \phi_i^B(\vec{r}_B) \qquad (2.2.16)$$

The total energy E_i and ε_i are related by

$$E_i = \frac{K_i^2}{2\mu_B} + \varepsilon_i \qquad (2.2.17)$$

The m_B and μ_B in (2.2.16) and (2.2.17) have been defined in (2.2.6) and (2.2.5). We shall now consider direct channel

scattering, that is excitation processes. We denote the final asymptotic "free" state in the direct channel by $\Phi_f^B(\vec{r}_B, \vec{R}_B)$. This is given by

$$\Phi_f^B(\vec{r}_B, \vec{R}_B) = \exp(i \vec{K}_f \cdot \vec{R}_B) \phi_f^B(\vec{r}_B) \qquad (2.2.18)$$

where $\vec{k}_i$ is the final wave vector of A relative to the centre of mass of (B + e$^-$). The function of $\phi_f^B(\vec{r}_B)$ satisfies the equation

$$\left(-\frac{1}{2m_B} \nabla^2_{\vec{r}_B} + V_{eB}\right) \phi_f^B(\vec{r}_B) = \varepsilon_f \phi_f^B(\vec{r}_B) \qquad (2.2.19)$$

Then

$$E_f = \frac{K_f^2}{2\mu_B} + \varepsilon_f \qquad (2.2.20)$$

For direct scattering the probability of scattering from an initial state Φ_i^B to a final state Φ_f^B is zero unless we are "on the energy shell", that is to say

$$E_i = E_f = E \qquad (2.2.21)$$

For the direct process i $\rightarrow$ f the scattering amplitude is given by (McDowell and Coleman 1970)

$$f^{d}_{fi}(\hat{K}_i, \hat{K}_f) = -\frac{\mathcal{M}_B}{2\pi} T^{d}_{fi} \qquad (2.2.22)$$

where T^{d}_{fi} is the transition (T) matrix element for direct channel scattering between states denoted by i and f. The T-matrix element T^{d}_{fi} is given by

$$T^{d}_{fi} = \langle \Phi^{B}_{f} | V_d | \Psi^{(+)}_{i} \rangle \qquad (2.2.23)$$

$\Psi^{(+)}_{i}$ is the complete scattering solution corresponding to initial state i, and satisfies the Schrodinger equation

$$H \Psi^{(+)}_{i} = E \Psi^{(+)}_{i} \qquad (2.2.24)$$

The (+) denotes that outgoing boundary conditions are to be imposed. The differential scattering cross section in the direct channel is given by

$$\frac{d\sigma^{d}_{fi}}{d\Omega} = \frac{K_f}{K_i} | f^{d}_{fi}(\hat{K}_i, \hat{K}_f) |^2 \qquad (2.2.25)$$

$$= \frac{\mathcal{M}_B}{4\pi^2} \frac{K_f}{K_i} | T^{d}_{fi} |^2 \qquad (2.2.26)$$

For the case of rearrangement scattering, corresponding to electron capture, we write the final asymptotic state as $\chi^{A}_{f}(\vec{r}_A, \vec{R}_A)$. This is given by

$$\chi^{A}_{f}(\vec{r}_A, \vec{R}_A) = \exp(-i\vec{k}_f \cdot \vec{R}_A)\, \chi^{A}_{f}(\vec{r}_A) \qquad (2.2.27)$$

where $\vec{k}_f$ is now the final wave vector of the centre of mass of $(A + e^-)$ relative to B. $\chi^{A}_{f}(\vec{r}_A)$ is the final state eigenfunction of the $(A + e^-)$ system and satisfies

$$\left(-\frac{1}{2m_A}\nabla^2_{\vec{r}_A} + V_{eA}\right)\chi^{A}_{f}(\vec{r}_A) = \eta_f\, \chi^{A}_{f}(\vec{r}_A) \qquad (2.2.28)$$

where η_f is the final state energy eigenvalue of the (A + e) system. The total energy corresponding to the final state f is E_f and we have

$$E_f = \frac{k_f^2}{2\mu_A} + \eta_f \qquad (2.2.29)$$

The m_A and μ_A in (2.2.28) and (2.2.29) have been given in (2.2.6) and (2.2.5) and are the reduced masses of A and e^-, and B and $(A + e^-)$ respectively. Again it is necessary to

be on the energy shell and so

$$E_i = E_f = E \tag{2.2.30}$$

Then the scattering amplitude for the rearrangement process $i \rightarrow f$ is given by (McDowell and Coleman, 1970)

$$f^r_{fi}(\hat{K}_i, \hat{K}_f) = -\frac{\mu_A}{2\pi} T^r_{fi} \tag{2.2.31}$$

where T^r_{fi} is the T-matrix element for the rearrangement process $i \rightarrow f$ and is given by

$$T^r_{fi} = \langle \chi^A_f \mid V_r \mid \Psi^{(+)}_i \rangle \tag{2.2.32}$$

The corresponding differential scattering cross section is given by

$$\frac{d\sigma^r_{fi}}{d\Omega} = \frac{\mu_B}{\mu_A}\frac{K_f}{K_i} \mid f^r_{fi}(\hat{K}_i, \hat{K}_f) \mid^2 \tag{2.2.33}$$

$$= \frac{\mu_A \mu_B}{4\pi^2}\frac{K_f}{K_i} \mid T^r_{fi} \mid^2 \tag{2.2.34}$$

The total scattering cross sections for direct and rearrangement scattering are given respectively by

$$\sigma_{fi}^{d} = \int_{\Omega} \frac{d\sigma_{fi}^{d}}{d\Omega} \, d\Omega \tag{2.2.35}$$

$$\sigma_{fi}^{r} = \int_{\Omega} \frac{d\sigma_{fi}^{r}}{d\Omega} \, d\Omega \tag{2.2.36}$$

The asymptotic boundary conditions imposed upon the scattering wave function $\Psi_i^{(+)}$ corresponding to outgoing spherically scattered waves are given by

$$\Psi_i^{(+)} \underset{R_B \to \infty}{\sim} \sum_m \phi_m^B(\vec{r}_B) \left[\delta_{mi} \exp(i\vec{K}_i \cdot \vec{R}_B) + f_{mi}^{d} \frac{\exp iK_m R_B}{R_B} \right] \tag{2.2.37}$$

$$\underset{R_A \to \infty}{\sim} \sum_n f_{ni}^{r} \frac{\exp iK_n R_A}{R_A} \cdot \chi_n^A(\vec{r}_A) \tag{2.2.38}$$

Equation (2.2.37) corresponds to the direct (excitation) channel, with the first term being an incident plane wave of momentum $\vec{K}_i$ (with $\hbar = 1$). The second term represents outgoing spherical waves describing particle A scattering from the (B + e^-) system which is in the mth level represented by the eigenfunction $\phi_m^B(\vec{r}_B)$.

Expression (2.2.38) corresponds to the rearrangement (electron capture) channel which has no incident plane-wave and this expression represents particle B scattering off the (A + e^-) system which is in the nth level represented by the eigenfunction $\chi_n^A(\vec{r}_A)$.

To solve the scattering problem at low energies, the scattering wavefunction can be expanded using an atomic or

molecular orbital basis of wavefunctions, and after a partial wave decomposition is made, the problem is one of solving a set of coupled second-order differential equations. Alternatively, at high energies when $\Psi_i^{(+)}$ is expected to be only weakly perturbed by the collision, the Born approximation or a distorted wave method can be employed, along with many other variations. However the full quantum mechanical treatment is impractical when the collision energy is in some intermediate region. The large masses of the two centres A and B however as compared to the electronic mass makes it possible to treat the internuclear motion classically due to the associated de Broglie wavelength being very small as compared to the typical atomic dimensions. The result is called the semi-classical impact parameter approximation and will be considered in more detail in the next section.

2.3 The Impact Parameter Approximation

2.3.1 The Impact Parameter Schrodinger equation

In the previous section the quantum mechanical treatment of ion-atom collisions was considered and it was noted that this method was impractical to employ in the intermediate energy region. The use of the word intermediate is of course, arbitrary here but we can introduce the notion of a low and high energy region more

explicitly as follows. The laboratory energy of an ion or atom of mass M (in atomic units) on a stationary target is $E = 25 \times M\ v^2$ keV where v is the laboratory velocity of the ion in atomic units. Then it is reasonable to take the low energy region as $E < 25 \times M\ v_o^2$ keV and the high energy region as $E >> 25 \times M\ v_o^2$ keV where v_o is the Bohr velocity mentioned in (1.4). The intermediate energy region refers to some energy region in which neither a low energy approximation or a high energy approximation is adequate to describe the scattering solution. Generally the de Broglie wavelength for the motion of centres A and B must be very much smaller than some typical atomic dimension of the system in order that the paths of A and B can be considered as classical trajectories. In quantitative terms this means that the collision energy E must be such that

$$E \gtrsim \text{eV amu}^{-1} \qquad (2.3.1)$$

Also if E is much greater than the typical change in electronic energy which occurs during the collision, then the nuclear motion of A and B can be considered as being independent of the electronic motion. This independence of nuclear and electronic motion will generally be in assured if

$$E \gtrsim 100 \text{ eV amu}^{-1} \qquad (2.3.2)$$

For example consider a proton with a laboratory energy of 1 keV. The associated de Broglie wavelength is 0.0027 a.u. which by conventional reasoning is justification for describing its path by a classical trajectory. All laboratory energies considered in the present work will be greater than 1 keV amu^{-1}.

We shall now briefly derive the time dependent impact parameter Schrodinger equation, for the usual system consisting of the two centres A and B and a single active electron. The total Hamiltonian for this three body system is given by

$$H = T + V \tag{2.3.3}$$

$$= -\frac{1}{2\mu}\nabla^2_{\vec{R}} - \frac{1}{2m}\nabla^2_{\vec{r}} + V_{eA} + V_{eB} + V_{AB} \tag{2.3.4}$$

which comes from equations (2.2.4), (2.2.8) and (2.2.9). μ is the reduced mass of A and B, and m is the reduced mass of the electron and the (A + B) system. (Equations (2.2.5) and (2.2.6)). Because the electronic mass is very small compared to the mass of A or B, we can put $m \simeq m_e = 1$ in atomic units. We now rewrite the Schrodinger equation (2.3.4) as follows

$$\left(-\frac{1}{2\mu}\nabla^2_{\vec{R}} + W(R) + H_{el} - E\right)\Phi(\vec{R}, \vec{r}) = 0 \tag{2.3.5}$$

where the electronic Hamiltonian H_{el} is given by

$$H_{el} = -\frac{1}{2}\nabla^2_{\vec{r}} + V_{eA} + V_{eB} + \left(V_{AB} - W(\vec{R})\right) \qquad (2.3.6)$$

and $\Phi(\vec{R},\vec{r})$ is the wavefunction of the system. W(R) is a potential which is a function of R only, which we assume determines the relative motion of the two heavy particles A and B in all channels. For example it could be taken as the average static interaction potential in the incident channel so that

$$W(\vec{R}) = \int |\phi_i(\vec{r}_B)|^2 \left(V_{AB} + V_{eA}\right) d\vec{r}_B \qquad (2.3.7)$$

Unfortunately $W(\vec{R})$ is far from unique in the three body problem. The nuclear motion will then be described by a wavefunction $F(\vec{R})$ which satisfies the potential scattering equation

$$\left(-\frac{1}{2\mu}\nabla^2_{\vec{R}} + W(\vec{R}) - E\right) F(\vec{R}) = 0 \qquad (2.3.8)$$

In most cases of interest we ignore the initial binding energy of the electron in its initial state when calculating E so that

$$E = \frac{K_i^2}{2\mu} + \varepsilon_i \simeq \frac{K_i^2}{2\mu} = \frac{1}{2}\mu v^2 \qquad (2.3.9)$$

where v is the relative velocity of the centres A and B and K_i is the wavenumber associated with the motion of A and B.

We now write the wavefunction of the system $\Phi(\vec{R},\vec{r})$ as the product of the nuclear wavefunction and a wavefunction for the electronic motion $\Psi(\vec{R},\vec{r})$ so that

$$\Phi(\vec{R},\vec{r}) = F(\vec{R})\,\Psi(\vec{R},\vec{r}) \qquad (2.3.10)$$

Substituting for $\Phi(\vec{R},\vec{r})$ into (2.3.5) we find that

$$-\frac{1}{2\mu} F(\vec{R})\,\nabla^2_{\vec{R}}\Psi(\vec{R},\vec{r}) - \frac{1}{\mu}\vec{\nabla}_{\vec{R}}F(\vec{R})\cdot\vec{\nabla}_{\vec{R}}\Psi(\vec{R},\vec{r}) + F(\vec{R})\,H_{el}\Psi(\vec{R},\vec{r}) = 0 \qquad (2.3.11)$$

We approximate the nuclear wavefunction by

$$F(\vec{R}) = \exp(i\,S(\vec{R})) \qquad (2.3.12)$$

where

$$S(\vec{R}) \simeq \int ds\,[2\mu(E-\omega(\vec{R}))]^{1/2} \qquad (2.3.13)$$

which is consistent with the nuclear motion being described by a classical trajectory and the integration in (2.3.13) is

along this trajectory. This trajectory can be written in terms of an impact parameter vector b and a parameter t as

$$\vec{R} = \vec{R}(b,t) \qquad (2.3.14)$$

The approximations defined by (2.3.12) and (2.3.13) are the starting point of the semi-classical eikonal approximation (Bransden, 1983) and $F(\vec{R})$ in (2.3.12) is called the eikonal wavefunction. At sufficiently high energies (in fact as low as a few hundred eV for proton-hydrogen collisions) the heavy particle deflection is mainly into a forward cone of small angular width and the motion of centres A and B can be approximated closely by a straight line trajectory so that

$$\vec{R} = \vec{b} + \vec{v}t \quad , \quad \vec{b} \cdot \vec{v} = 0 \qquad (2.3.15)$$

The constant velocity vector is taken as parallel to the z-axis. This straight line trajectory case is consistent with the effective internuclear potential, $W(\vec{R})$, being ignored, with the result that the wavefunction $F(\vec{R})$ is a plane wave

$$F(\vec{R}) \simeq \exp i K_i Z_R = \exp i \mu v Z_R \qquad (2.3.16)$$

where z_R is the z-component of $\vec{R}$. Using equation (2.3.16)

for $F(\vec{R})$ in equation (2.3.11) and since μ is a large parameter, then the first term in (2.3.11) is found to be much smaller than the second term, and hence is neglected. The result is that (2.3.11) reduces to

$$H_{el}\,\Psi(\vec{R},\vec{r}) = iv\frac{\partial}{\partial Z_R}\Psi(\vec{R},\vec{r}) \qquad (2.3.17)$$

If we use (2.3.15) then we can rewrite (2.3.17) as

$$H_{el}\,\Psi(\vec{R},t) = i\frac{\partial}{\partial t_{\vec{r}}}\Psi(\vec{r},t) \qquad (2.3.18)$$

where $\frac{\partial}{\partial t}_{\vec{r}}$ means differentiate with respect to time keeping $\vec{r}$ constant. We note that we have identified t here as the classical time as if it were a trivial matter. However (Weinberg 1962) has justified this point of view. Equation (2.3.18) is the time dependent Schrodinger equation or impact parameter Schrodinger equation which will form the basis for the calculations presented in this thesis. If we wanted to use non-linear trajectories for A and B then we would again omit the first term in (2.3.11) and obtain (2.3.18) but this time the trajectory is given by equation (2.3.14) as determined by the particular form of $W(\vec{R})$ being used. Since we have defined the paths of the incident particle A relative to B by a classical trajectory there is now no possibility of interference due to exchange effects in the case of identical nuclei. However, Smith (1964) has shown these effects to be negligible for collision energies

above 15eV or so in the case of protons on hydrogen atoms.

The coordinate system that has been defined by the impact parameter approximation is shown in Figure 2.2 for the case when A and B move along straight line trajectories. In Figure 2.2 the parameter p determines the position of the origin O on the internuclear line AB; p is such that

$$0 < p < 1 \tag{2.3.19}$$

Then

$$\vec{BO} = p\vec{R} \tag{2.3.20a}$$

$$\vec{OA} = (1 - p)\vec{R} \tag{2.3.20b}$$

The quantity b is a two-dimensional impact parameter. $\vec{r}$ is used to denote the electronic coordinate, no matter where the origin O is located upon AB. For the eikonal approximation, which has been discussed in this section, to be valid the results should be independent of the choice of O (i.e. the p parameter) provided it is reasonable. We now have a model problem to solve where the classically determined nuclear motion (external motion) is treated as providing a time dependent perturbation of the electronic motion (internal motion) treated quantum mechanically. In the next section of this chapter we shall consider how to solve the impact parameter equation (2.3.18).

Figure 2.2

Impact parameter coordinate system

for straight line trajectories.

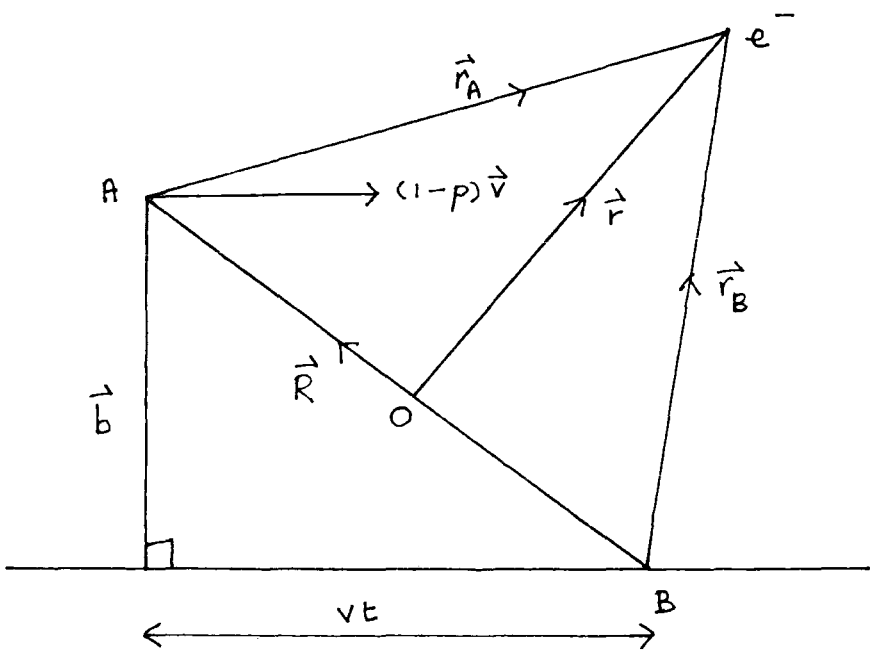

2.3.2 Choosing the expansion functions

In order to obtain an approximate solution of equation (2.3.18) it is usual to make an expansion of the total electronic wavefunction in terms of some finite basis sets about both centres A and B, with time dependent coefficients which are the occupation amplitudes for the states in the basis sets. The parameter which is usually used to decide upon the choice of basis states is

$$\lambda = v / v_e \qquad (2.3.21)$$

where v_e is the characteristic velocity of the electron in the initial target state and v is the incident projectile velocity. When $\lambda << 1$ the electron will end to adjust adiabatically to the internuclear motion and a molecular type of expansion of a few strongly coupled states is appropriate. In this collision energy region both charge exchange and excitation are competing processes whilst ionisation is generally less important. For the case $\lambda >> 1$, charge exchange is not important and only direct excitation and ionisation are the important channels. The appropriate expansion is now in terms of a large number of atomic type orbitals upon the target with only a few atomic orbitals upon the projectile (or even none at all). In the intermediate energy region, however, the most suitable expansion is in terms of several atomic orbitals placed upon

each centre. There are no absolute criteria for the choice of the basis sets used in any expansion basis. However, the need for a basis which is computationally convenient is usually of paramount importance. There are some important restrictions which must be imposed upon any basis set however, if an accurate representation of the physical system is to be obtained.

Firstly the initial channel of the system must be accurately contained in the basis so that the correct asymptotic behaviour for large negative times is guaranteed. Correspondingly the most important final channels must be represented as accurately as possible in the basis so that the asymptotic behaviour at large positive times can closely match the actual physical system. However, it is possible to extract cross sections for states not actually represented explicitly in the basis set and this will be illustrated later in the thesis.

The calculations made using the impact parameter method that will be considered in the present work all have as a starting point the following ansatz;

$$\Psi(\vec{r},t) = \sum_{j=1}^{M} b_j(t)\,\Phi_j^B(\vec{r},t) + \sum_{K=1}^{N} a_K(t)\,\chi_K^A(\vec{r},t) \quad (2.3.22)$$

where the functions $\Phi_j^B(\vec{r},\ t)$ and $\chi_K^A(\vec{r},t)$ are the members of

the basis sets to be employed upon the target and projectile respectively. Since the impact parameter equation (2.3.18) is to be solved for each value of b independently it is possible in principle for a different basis set to be used for different b values within a single calculation but this has not been done in the present work.

For convenience the dependence of $\Phi_j^B(\vec{r}, t)$ and $\chi_K^A(\vec{r}, t)$ upon b has not been shown in (2.3.22) and will only be shown if necessary to avoid confusion. The important question of the Galilean invariance of the impact parameter method will be considered next in this section.

We shall chose an inertial frame with an origin at O, as in Figure 2.2 and consider the asymptotic region as $t \to \infty$ for the case of a target centred expansion function. For the moment we shall ignore the possible effects of the long range Coulomb interaction upon the asymptotic region but shall return to it again in Section (2.3.3). Then for a target centred function the only perturbation in the asymptotic region is from the target centre B and equation (2.3.18) reduces to the following

$$\left(-\frac{1}{2}\nabla_{\vec{r}}^2 + V_{eB} - i\frac{\partial}{\partial t}_{\vec{r}}\right)\Phi_j^B(\vec{r}, t) = 0 \qquad (2.3.23)$$

This is for the case when the expansion function $\Phi_j^B(\vec{r}, t)$ is assumed to be an exact eigenstate of the unperturbed (B +

e^-) system with eigenvalue λ_j. Because the time derivative is taken with $\vec{r}$ fixed and not $\vec{r}_B$ this introduces the so-called plane-wave translational factor (PWTF) into the solution. The correct form of $\Phi_j^B(\vec{r}, t)$ which is a solution of (2.3.23) is then given by

$$\Phi_j^B(\vec{r}, t) = \phi_j^B(\vec{r}_B) \exp -i(\lambda_j t + p\vec{v}.\vec{r} + \tfrac{1}{2} p^2 v^2 t) \quad (2.3.24)$$

This is a solution of (2.3.23) for $t \to \pm\infty$ and $r_B \ll r_A$. Similarly if we consider a solution of the unperturbed (A + e^-) system as $t \to \pm\infty$ and $r_A \ll r_B$ then it is found that

$$(-\tfrac{1}{2}\nabla_{\vec{r}}^2 + V_{eA} - i\frac{\partial}{\partial t}_{\vec{r}})\chi_K^A(\vec{r}, t) = 0 \quad (2.3.25)$$

and the corresponding function $\chi_K^A(\vec{r}, t)$ is given by

$$\chi_K^A(\vec{r}, t) = \chi_K^A(\vec{r}_A) \exp -i(\varepsilon_K t - (1-p)\vec{v}.\vec{r} + \tfrac{1}{2}(1-p)^2 v^2 t) \quad (2.3.26)$$

where ε_K is the energy eigenvalue of the state $\chi_K^A(\vec{r}_A)$.

The results in (2.3.24) and (2.3.26) follow from the fact that the time derivative operator $\frac{\partial}{\partial t}_{\vec{r}}$ can be written as follows

$$\left(\frac{\partial}{\partial t}\right)_{\vec{r}} = \left(\frac{\partial}{\partial t}\right)_{\vec{r}_B} + p\vec{v}\cdot\vec{\nabla}_{\vec{r}} \qquad (2.3.27)$$

$$\left(\frac{\partial}{\partial t}\right)_{\vec{r}} = \left(\frac{\partial}{\partial t}\right)_{\vec{r}_A} - (1-p)\vec{v}\cdot\vec{\nabla}_{\vec{r}} \qquad (2.3.28)$$

The factors $\exp -i(\frac{1}{2}p^2v^2t + p\vec{v}.\vec{r})$ and $\exp -i(\frac{1}{2}(1-p)^2 v^2 t - (1-p)\vec{v}.\vec{r})$ in the expressions (2.3.24) and (2.3.26) are the plane wave translation factors. They are required to account for the fact that an electron is riding along with either centre A and B and if it is transferred from one centre to another it will acquire a momentum v due to the relative motion of A and B. They also ensure that the impact parameter formulation is invariant under a Galilean transformation, so that the probability amplitudes that are determined are independent of the choice of origin of coordinates. They were first recognised as necessary in electron capture theory by Bates and McCarroll (1958) in the formulation using molecular basis functions, and again by Bates (1958) in the case of an atomic basis expansion.

The choice of the translational factors which account for the change of momentum of the electron in the rearrangement channels is not unique, except in the asymptotic region. Translational factors with more general functional forms can be used to try to allow for the fact that at small internuclear distances the electron is not

associated with either centre, as opposed to the case when t $\rightarrow \pm \infty$.

The so-called switching functions are used to modify the usual plane wave translational factors to account for the adiabatic relaxation of the system at small internuclear separations. Newby (1983) investigated the system

$$^4He^{2+} + H(1s) \rightarrow {}^4He^{+} (n = 2) + H(1s)$$

using a two state approximation. The general conclusion was that below impact energies (of the $^4He^{2+}$ ion) of 24 keV, the agreement with a two state calculation using the usual plane wave translational factor was very good.

However, at higher energies the switching function calculations diverged rapidly from experiment and the plane wave results (e.g. by a factor of about 100 at a $^4He^{2+}$ impact energy of 200 keV). All the present calculations in this thesis use the plane wave translational factors as defined by (2.3.24) and (2.3.26).

Finally, concerning the use of plane wave translation factors, we note that Greenland (1982) has shown how they arise naturally by solving the perturbed stationary state equations in the asymptotic region assuming straight line trajectories are used to describe the nuclear motion. He also showed how the factors are modified when a Coulomb trajectory is employed.

At this point we shall briefly review the model that

has been used to represent the collision of two heavy particles in the single active electron approximation. The two nuclei are assumed to follow classically predetermined trajectories, and this produces a time dependent perturbation of the electron which is treated quantum mechanically. The appropriate ansatz is to be based upon (2.3.22) but as yet the expansion functions $\Phi_j^B(\vec{r}, t)$ and $\chi_K^A(\vec{r}, t)$ have not been defined completely. The main problem is to determine the unknown time dependent amplitudes $b_j(t)$ and $a_K(t)$ in (2.3.22) and then to evaluate the cross sections. This will be the subject of the next section.

2.3.3 Solving the impact parameter Schrodinger equation

In this section we shall define the form of the basis functions that are used in the ansatz (2.3.22) in the present work. Then the equations which determine the occupation amplitudes in (2.3.22) (that is the quantities $b_j(t)$ and $a_K(t)$) will be described.

Firstly we shall concentrate upon the form of the expansion functions used in (2.3.22) which are denoted by $\Phi_j^B(\vec{r}, t)$ and $X_K^A(\vec{r}, t)$. It has already been stated that plane wave translational factors have been used throughout the present work (in Section 2.3.2) and hence from equation (2.3.24) and equation (2.3.26) the so far unspecified quantities are the functions given by

$$\phi_j^B(\vec{r}_B)\exp -i\lambda_j t \tag{2.3.29}$$

and

$$\chi_K^A(\vec{r}_A)\exp -i\Sigma_K t \tag{2.3.30}$$

These functions in equations (2.3.29) and (2.3.30) must be combined with corresponding plane wave translation factors to obtain the expansion states used in expression (2.3.22). Throughout the present work all the basis functions $\phi_j^B(\vec{r}_B)$ and $\chi_K^A(\vec{r}_A)$ that have been used in impact parameter calculations have been determined from a diagonalization procedure, which results in some important properties of these functions. At this point we will concentrate on the target basis functions $\phi_j^B(\vec{r}_B)$ for convenience. The target Hamiltonian for the system $(B + e^-)$ is given by

$$H_B = -\frac{1}{2}\nabla^2_{\vec{r}_B} + V_{eB} \tag{2.3.31}$$

Then it is well known that if the states $\phi_j^B(\vec{r}_B)$ (j = 1, ..., M) have been obtained from a diagonalization (variational)

procedure using H as the Hamiltonian, the following results are true (Weissbluth (1978))

$$\langle \bar{\phi}^{B}_{j}(\vec{r}_B) \mid H_B \mid \bar{\phi}^{B}_{j'}(\vec{r}_B) \rangle = \lambda_j \delta_{jj'} \quad (2.3.32)$$

$$\langle \bar{\phi}^{B}_{j}(\vec{r}_B) \mid \bar{\phi}^{B}_{j'}(\vec{r}_B) \rangle = \delta_{jj'} \quad (2.3.33)$$

The results in equations (2.3.32) and (2.3.33) are true for $1 < j < M$ and $1 < j' < M$, and the usual Dirac notation is employed. We note that a bar is placed above any state which has been obtained from a variational procedure as described above. Similar results apply to the projectile basis functions which have been obtained from a diagonalization procedure using the Hamiltonian of the (A + e) system

$$H_A = -\frac{1}{2}\nabla^2_{\vec{r}_A} + V_{eA} \quad (2.3.34)$$

That is to say the following results are true

$$\langle \bar{\chi}^{A}_{K}(\vec{r}_A) \mid H_A \mid \bar{\chi}^{A}_{K'}(\vec{r}_A) \rangle = \Sigma_K \delta_{KK'} \quad (2.3.35)$$

$$\langle \bar{\chi}^{A}_{K}(\vec{r}_A) \mid \bar{\chi}^{A}_{K'}(\vec{r}_A) \rangle = \delta_{KK'} \qquad (2.3.36)$$

In equations (2.3.35) and (2.3.36) we have 1 K < N and 1<K' < N. Some further useful results will now be given as they will be used later on in this section. We shall, at this point, take the origin O in Figure 2.2 to be the midpoint of AB. Then the parameter $p = {}^{1}/_{2}$ in the expressions for the plane wave translational factors. We shall now consider a target expansion state $\bar{\Phi}^{B}_{j}(\vec{r}, t)$ from the ansatz (2.3.22), which is of the form (see Equation (2.3.24))

$$\bar{\Phi}^{B}_{j}(\vec{r}, t) = \bar{\phi}^{B}_{j}(\vec{r}_B) \exp -i(\lambda_j t + \tfrac{1}{2}\vec{v}\cdot\vec{r} + \tfrac{1}{8}v^2 t) \qquad (2.3.37)$$

where the function $\phi^{B}_{j}(\vec{r}_B)$ satisfies equations (2.3.32) and (2.3.33). Then using equations (2.3.27), (2.3.32) and (2.3.33) it is straightforward to show that

$$0 = \langle \bar{\Phi}^{B}_{j}(\vec{r}, t) \mid H_B - i\frac{\partial}{\partial t}_{\vec{r}} \mid \bar{\Phi}^{B}_{j'}(\vec{r}, t) \rangle \qquad (2.3.38)$$

for 1<j < M and 1<j'<M, and H_B is given by equation (2.3.31). In a similar fashion we can consider a projectile state from ansatz (2.3.22), $\bar{\chi}^{A}_{K}(\vec{r}, t)$, which has the form (see equation (2.3.26))

$$\bar{\chi}^{A}_{K}(\vec{r},t) = \bar{\chi}^{A}_{K}(\vec{r}_A)\exp -i(\varepsilon_K t - \tfrac{1}{2}\vec{v}.\vec{r} + \tfrac{1}{8}v^2 t) \quad (2.3.39)$$

and where $\bar{\chi}^{A}_{K}(\vec{r}_A)$ satisfies equations (2.3.35) and (2.3.36). Then using equations (2.3.28), (2.3.35) and (2.3.36) it is straightforward to show that

$$\langle \bar{\chi}^{A}_{K}(\vec{r},t) \mid H_{el} - i\frac{\partial}{\partial t}_{\vec{r}} \mid \bar{\chi}^{A}_{K'}(\vec{r},t)\rangle = 0 \quad (2.3.40)$$

where H_A is given by equation (2.3.34) and we have $1<K<N$ and $1<K'<N$. The results in equations (2.3.38) and (2.3.40) for expansion states which contain variationally determined wavefunctions ($\bar{\phi}^{B}_{J}(\vec{r}_B)$ and $\bar{\chi}^{A}_{K}(\vec{r}_A)$) and the corresponding variational energy values (λ_J and ε_K respectively) are analagous to equations (2.3.23) and (2.3.25) which only hold true for the case when exact eigenfunctions [and corresponding eigenvalues] are employed in the expressions for the expansion states. However (2.3.38) and (2.3.40) will turn out to be sufficiently strong enough conditions for the present discussion.

The next part of this section will be based upon Shakeshaft (1975). Throughout the following discussion we shall use the notation that Shakeshaft used for convenience.

The model Shakeshaft considered was for proton-hydrogen scattering in the linear trajectory classical impact parameter formulation. The full Hamiltonian of the system is denoted by H(t). Then the time-dependent Schrodinger equation is given by

$$H(t)\,|\Psi(t)\rangle = i\frac{\partial}{\partial t}\,|\Psi(t)\rangle \qquad (2.3.41)$$

We remember that $\frac{\partial}{\partial t}$ stands for $\frac{\partial}{\partial t}_{\vec{r}}$ in (2.3.41). $|\Psi(t)\rangle$ is the full electronic state vector for the problem, subject to a suitable boundary condition. We shall use α to denote either the target proton (A) or incident proton (B) Let $|\Phi_{K\alpha}(t)\rangle$, where α denotes A or B, be a normalized state vector of the electron bound to proton in an unperturbed state K of the hydrogen atom. This state will hereafter be denoted by $K\alpha$. Also let $|\Psi^{\beta}_{K\alpha}(t)\rangle$ be the solution of equation (2.3.41) which satisfies the boundary condition

$$|\Psi^{\beta}_{K\alpha}(t)\rangle \rightarrow |\phi_{K\alpha}(t)\rangle \quad , \quad \beta t \rightarrow -\infty \qquad (2.3.42)$$

where β = + or -. The quantity to be determined is the transition amplitude for the electron to be in a final state $f_{\alpha'}$ if initially it was in the state $i\alpha$. This quantity is

defined by

$$A_{i\alpha}^{f\alpha'} = \langle \Psi_{f\alpha'}^{-}(t) \mid \Psi_{i\alpha}^{+}(t) \rangle$$
$$= \lim_{t\to\infty} \langle \phi_{f\alpha'}(t) \mid \Psi_{i\alpha}^{+}(t) \rangle \qquad (2.3.43)$$

We now make an approximation by replacing the exact solution $|\Psi_{K\alpha}^{\beta}(t)\rangle$ by a trial solution $|\hat{\Psi}_{K\alpha}^{\beta}(t)\rangle$. The symbol $\wedge$ denotes the fact that a particular quantity, $\hat{X}$, is the trial approximation to the exact quantity X. $|\hat{\Psi}_{K\alpha}^{\beta}(t)\rangle$ consists of a finite number, J, of normalizable basis vectors $|\psi_j(t)\rangle$, where $1<j<J$, with time dependent coefficients (this is the same approximation as in the expression (2.3.22)). Now we suppose these time dependent coefficients are determined by solving the set of coupled differential equations formed by substituting $|\hat{\Psi}_{K\alpha}^{\beta}(t)\rangle$ into the impact parameter Schrodinger equation (equation (2.3.41)) and then projecting this onto every basis function, that is to say

$$\langle \psi_j(t) \mid H(t) - i\frac{\partial}{\partial t} \mid \hat{\Psi}_{K\alpha}^{\beta}(t) \rangle = 0 \,, \qquad (2.3.44)$$

for all $1 \le j \le J$.

Then if $|\hat{\Psi}_{K\alpha}^{\beta}(t)\rangle$ satisfies the same boundary condition as

$|\Psi^{\beta}_{K\alpha}(t)\rangle$ the approximate transition amplitude is defined, in analogy with (2.3.43) by

$$\hat{A}^{f\alpha'}_{i\alpha} = \langle \hat{\Psi}^{-}_{f\alpha'}(t) | \hat{\Psi}^{+}_{i\alpha}(t) \rangle$$
$$= \lim_{t\to\infty} \langle \Phi_{f\alpha'}(t) | \hat{\Psi}^{+}_{i\alpha}(t) \rangle \qquad (2.3.45)$$

Now ideally one would like to choose an expansion basis for the $|\psi_j(t)\rangle$ functions so that as the basis is enlarged, $\hat{A}^{f\alpha'}_{i\alpha}$ from expression (2.3.45) converges towards $A^{f\alpha'}_{i\alpha}$ from expression (2.3.43). However, if the trial vector $|\hat{\Psi}^{\beta}_{K\alpha}(t)\rangle$ does not satisfy the same boundary conditions as $|\Psi^{\beta}_{K\alpha}(t)\rangle$ then $\hat{A}^{f\alpha'}_{i\alpha}$ as defined by expression (2.3.45) does not exist in general, and therefore neither does the transition probability, $|\hat{A}^{f\alpha'}_{i\alpha}|^2$. For example if the boundary condition associated with the final state $f\alpha'$, is not satisfied, then the quantity $|\langle \Phi_{f\alpha'}(t) | \hat{\Psi}^{+}_{i\alpha}(t)\rangle|$ tends to a constant term plus a term which oscillates without limit as $t \to \infty$ (Gallaher and Wilets (1968)). It is possible however to obtain well-defined variational estimates of $A^{f\alpha'}_{i\alpha}$ for arbitrary initial and final states by modifying the boundary conditions satisfied by the trial state vector $|\hat{\Psi}^{\beta}_{K\alpha}(t)\rangle$. This modification will now be described. Let $H_{\alpha}(t)$ denote the Hamiltonian of the electron in the field of proton

alone, where the time dependence arises because the coordinate system used has its origin at the midpoint of the internuclear distance. We shall now introduce a set of orthonormal functions $|\hat{\Phi}_{K\alpha}(t)\rangle$, $1<k<J$, which are obtained from a diagonalizatin procedure so that the Hylleraas-Undheim theorem (Hylleraas and Undheim (1930)) applies. This means that the expectation value $\langle \hat{\Phi}_{j\alpha}(t)| H_{\alpha}(t)| \hat{\Phi}_{j\alpha}(t)\rangle$ is an upper bound to the jth energy level of the hydrogen atom. That is to say $|\hat{\Phi}_{j\alpha}(t)\rangle$ is a trial approximation to the state vector $|\hat{\Phi}_{j\alpha}(t)\rangle$ which represents the jth state of the hydrogen atom. Then Shakeshaft proves that if the trial state vector satisfies the boundary conditions

$$|\hat{\Psi}^{\beta}_{K\alpha}(t)\rangle \rightarrow |\hat{\Phi}_{K\alpha}(t)\rangle, \quad \beta t \rightarrow -\infty \tag{2.3.46}$$

and the approximate transition amplitude is now defined by

$$\begin{aligned} \hat{A}^{f\alpha'}_{i\alpha} &= \langle \hat{\Psi}^{-}_{f\alpha'}(t) | \hat{\Psi}^{+}_{i\alpha}(t)\rangle \\ &= \lim_{t\rightarrow\infty} \langle \hat{\Phi}_{f\alpha'}(t) | \hat{\Psi}^{+}_{i\alpha}(t)\rangle \end{aligned} \tag{2.3.47}$$

then $\hat{A}^{f\alpha'}_{i\alpha}$ is a variational estimate of $A^{f\alpha'}_{i\alpha}$. The term variational as used here means that the difference between $\hat{A}^{f\alpha'}_{i\alpha}$ and $A^{f\alpha'}_{i\alpha}$ is a second order term in the differences

between the exact and trial wave functions. It is straightfoward to extend the analysis of Shakeshaft to the case where non-Coulombic potentials are involved as is the case in this thesis. We will now apply the results just obtained to derive the equations which must be solved in order to obtain the occupation amplitudes in expression (2.3.22).

Firstly we recall that the equation to be solved is given by (see Equation 2.3.18)

$$H_{el}\,\Psi(\vec{r},t) = i\frac{\partial}{\partial t}_{\vec{r}}\,\Psi(\vec{r},t) \qquad (2.3.48)$$

Then we expand $\Psi(\vec{R},t)$ according to expression (2.3.22) where we now use the symbol $\hat{}$ to denote that a function is obtained from a diagonalization calculation, so that our trial function $\Psi_T(r,t)$ is given by

$$\Psi_T(\vec{r},t) = \sum_{j=1}^{M} b_j(t)\,\hat{\Phi}_j^B(\vec{r},t) + \sum_{K=1}^{N} a_K(t)\,\hat{\chi}_K^A(\vec{r},t) \qquad (2.3.49)$$

We note that for convenience we do not attach a symbol $\hat{}$ to the occupation amplitudes $b_j(t)$ and $a_K(t)$, or express the dependence of the amplitudes and the functions, $\hat{\Phi}_j^B(\vec{r},t)$ and $\hat{\chi}_K^A(\vec{r},t)$ upon the impact parameter, b. Then we insert the

trial function in expression (2.3.49) into the equation (2.3.48) and project this onto each function contained in the trial function. That is we obtain the set of coupled first order differential equations given by

$$\int d\vec{r}\ \hat{\Phi}^{*}_{j}(\vec{r},t)\left(H_{el}-i\frac{\partial}{\partial t}_{\vec{r}}\right)\Psi_{T}(\vec{r},t)=0 \qquad (2.3.50)$$

$$\int d\vec{r}\ \hat{\chi}^{*}_{K}(\vec{r},t)\left(H_{el}-i\frac{\partial}{\partial t}_{\vec{r}}\right)\Psi_{T}(\vec{r},t)=0 \qquad (2.3.51)$$

For convenience to avoid too many labels we have dropped the letters A and B from the functions in the trial function. After some simplification and using some of the previous results given in this section we obtain a set of differential equations which we give in matrix form as follows

$$i\left[\underset{\sim}{b}(t)+\underset{\sim}{N}\,\underset{\sim}{\dot{a}}(t)\right]=\underset{\sim}{H}\,\underset{\sim}{a}(t)+\underset{\sim}{K}\,\underset{\sim}{b}(t) \qquad (2.3.52)$$

$$i\left[\underset{\sim}{N}^{\dagger}\,\underset{\sim}{\dot{b}}(t)+\underset{\sim}{\dot{a}}(t)\right]=\underset{\sim}{\bar{K}}\,\underset{\sim}{a}(t)+\underset{\sim}{\bar{H}}\,\underset{\sim}{b}(t) \qquad (2.3.53)$$

where the symbol $\dagger$ denotes Hermitian adjoint. We can

combine expressions (2.3.52) and (2.3.53) into the compact form

$$i \underset{\sim}{S} \dot{\underset{\sim}{A}}(t) = \underset{\sim}{M} \underset{\sim}{A}(t) \tag{2.3.54}$$

where

$$\underset{\sim}{S} = \begin{pmatrix} \underset{\sim}{I} & \underset{\sim}{N} \\ \underset{\sim}{N}^{+} & \underset{\sim}{I} \end{pmatrix} \tag{2.3.55}$$

$$\underset{\sim}{M} = \begin{pmatrix} \underset{\sim}{H} & \underset{\sim}{K} \\ \underset{\sim}{\bar{K}} & \underset{\sim}{\bar{H}} \end{pmatrix}$$

and $\underset{\sim}{I}$ is the unit matrix. We also have

$$\underset{\sim}{A}(t) = \begin{pmatrix} \underset{\sim}{b}(t) \\ \underset{\sim}{q}(t) \end{pmatrix} \tag{2.3.56}$$

The boundary conditions which must be imposed upon the amplitudes in solving equation (2.2.54) are

$$|b_j(-\infty)| = \delta_{ji} \quad , \quad q_K(-\infty) = 0 \tag{2.3.57}$$

where index i corresponds to the initial state of the

$(B + e^-)$ system. For $t \to \infty$ then the amplitudes become the transition amplitudes as defined by (2.3.47), that is

$$b_{ji}(\vec{b}) = \lim_{t \to \infty} \langle \hat{\Phi}_j(\vec{r}, t) \mid \Psi_T(\vec{r}, t) \rangle \qquad (2.3.58)$$

which is the probability amplitude for finding the electron in state j of the $(B + e^-)$ system and when the initial state of the system was given by (2.3.57) above. Similarly the probability amplitude for finding the electron in the kth state of the $(A + e^-)$ system after the collision is given by

$$a_{Ki}(\vec{b}) = \lim_{t \to \infty} \langle \hat{\chi}_K(\vec{r}, t) \mid \Psi_T(\vec{r}, t) \rangle \qquad (2.3.59)$$

From the results given by Shakeshaft (1975) which have been discussed earlier in this section, the probability amplitudes $b_{ji}(\vec{b})$ and $a_{Ki}(\vec{b})$ in equations (2.3.58) and (2.3.59) are variationally correct amplitudes. We will now consider in more detail the matrices given in equations (2.2.52) and (2.2.53), which contain the matrix elements given below

$$N_{jK}(t) = \int d\vec{r}\, \hat{\Phi}_j^*(\vec{r}, t)\, \hat{\chi}_K(\vec{r}, t) \qquad (2.3.60)$$

$$H_{JK}(t) = \int d\vec{r}\, \hat{\Phi}_j^*(\vec{r},t)\left(H_{el} - i\frac{\partial}{\partial t}\right)\hat{\Phi}_K(\vec{r},t) \qquad (2.3.61)$$

$$\bar{H}_{JK}(t) = \int \hat{\chi}_j^*(\vec{r},t)\left(H_{el} - i\frac{\partial}{\partial t_{\vec{r}}}\right)\hat{\chi}_K(\vec{r},t)\, d\vec{r} \qquad (2.3.62)$$

$$K_{JK}(t) = \int \hat{\Phi}_j^*(\vec{r},t)\left(H_{el} - i\frac{\partial}{\partial t_{\vec{r}}}\right)\hat{\chi}_K(\vec{r},t)\, d\vec{r} \qquad (2.3.63)$$

$$\bar{K}_{JK}(t) = \int \hat{\chi}_j^*(\vec{r},t)\left(H_{el} - i\frac{\partial}{\partial t_{\vec{r}}}\right)\hat{\Phi}_K(\vec{r},t)\, d\vec{r} \qquad (2.3.64)$$

The $\underset{\sim}{N}$ matrix is known as the overlap matrix. The $\underset{\sim}{H}$ and $\underset{\sim}{\bar{H}}$ matrices are known as the direct matrices, since they involve functions attached to only one centre, whereas the $\underset{\sim}{K}$ and $\underset{\sim}{\bar{K}}$ matrices involve two centre integrals and are known as exchange matrices.

Several important results can be derived for the set of equations given in equation (2.3.54). Firstly Green (1965)

has shown that since the Hamiltonian H_{el} is Hermitian this implies that the trial function $\Psi_T(\vec{r},t)$ conserves probability (the unitarity property) that is to say

$$\frac{d}{dt} \langle \Psi_T(\vec{r},t) | \Psi_T(\vec{r},t) \rangle = 0 \qquad (2.3.65)$$

From this it can be shown that

$$i \underset{\sim}{\dot{S}} = \underset{\sim}{M}^{\dagger} - \underset{\sim}{M} \qquad (2.3.66)$$

and from this it can be shown that

$$i \underset{\sim}{\dot{N}} = \underset{\sim}{\bar{K}}^{\dagger} - \underset{\sim}{K} \qquad (2.3.67)$$

A further useful result of probability conservation is Greens unitarity relation (1965).

$$\underset{\sim}{A}^{\dagger} \underset{\sim}{S} \underset{\sim}{A} = 1 \qquad (2.3.68)$$

Probability conservation can also be expressed as the fact that

$$\sum_{j=1}^{M} |b_j(+\infty)|^2 + \sum_{K=1}^{N} |a_K(+\infty)|^2 = 1 \qquad (2.3.69)$$

This means no electron flux is lost during the collision process. The expressions in equations (2.3.66) to (2.3.69) are very useful in actual calculations and provide a check on the accuracy of the numerical procedures being used.

Another very useful relation is due to the time reversal properties of the system. Green (1965) has shown

$$|b_{ji}(+\infty)|^2 = |b_{ij}(+\infty)|^2 \qquad (2.3.70)$$

and

$$|a_{Ki}(+\infty)|^2 = |a_{iK}(+\infty)|^2 \qquad (2.3.71)$$

Tai and Gerjuoy (1973) demonstrate that the use of detailed balance as given in equations (2.3.70) and (2.3.71) is a much more sensitive test of numerical accuracy than the

unitarity test given in equation (2.3.68). Unfortunately it is also more expensive in terms of computational time. Browne (1965) has also considered the question of detailed balance.

We shall now give the expressions for the cross sections that are obtained from the transition amplitudes. The cross section for excitation of the jth state of the target is given by integrating $|b_{ji}(\vec{b})|^2$, from expression (2.3.58), over all two-dimensional impact parameter space, that is

$$\sigma_{ji}^{d} = \int d\vec{b}\, |b_{ji}(\vec{b})|^2 = 2\pi \int_0^\infty db\, b\, |b_{ji}(b)|^2 \qquad (2.3.72)$$

Similarly the cross section for capture into the kth state on the projectile is given by a similar expression (using (2.3.59))

$$\sigma_{ki}^{r} = \int d\vec{b}\, |a_{ki}(\vec{b})|^2 = 2\pi \int_0^\infty db\, b\, |a_{ki}(b)|^2 \qquad (2.3.73)$$

The factors of 2π in expressions (2.3.72) and (2.3.73) are due to the azimuthal symmetry.

Finally in this section we shall mention the role of the internuclear potential in the impact parameter approximation. It can be shown (Fennema, 1968) that the addition of an internuclear potential which is a function of R, the internuclear distance, only affects the phase of the transition amplitudes $b_{ji}(t)$ and $a_{Ki}(t)$. Hence the total cross section for excitation and for capture will not be affected as they are calculated from $|b_{ji}(\infty)|^2$ and $|a_{Ki}(\infty)|^2$, which are independent of the phase. However, it is possible (Bransden 1983) to calculate differential cross sections within the impact parameter aproximation and these will indeed be dependent upon the phase of the transition amplitudes, and hence the form of the internuclear potential that is used. Also the total elastic cross section will depend upon the internuclear potential as it is calculated from $b_{ii}(\infty)-1$ which is phase dependent.

We have described the impact parameter approximation in this section which is the basic method used to obtain the cross sections presented in this thesis. In the next section we shall consider how the particular choice of basis set functions can be optimised to obtain cross sections which are close to the actual experimental cross sections.

2.4 Atomic and related L^2 expansion methods.

2.4.1 Basic atomic expansion methods

We have discussed in section 2.3.3 how the impact parameter approximation is formulated using an atomic basis expansion for the trial function, given by expression (2.3.49). This expansion is appropriate in the intermediate to high energy region where the electron will spend most of its time associated with one of the nuclear centres, A or B. One of the main problems in this formulation is the expensive computing time that is needed to evaluate the matrix elements and to solve the coupled differential equations which have been given in equations (2.3.52), (2.3.53) and (2.3.54). It is therefore, usual to try to select a small set of strongly interacting states, and this is called the close coupling expansion. To estimate how successful this expansion is in representing the wavefunction at a particular energy, it is usual to add or remove a small number of basis states and repeat the calculation to see if the cross sections change greatly. This gives an idea of the convergence properties of the particular basis set used.

Therefore, it is clear that unless the continuum states of either particle A or particle B, or possibly both, are somehow represented in the collision, accurate cross

sections cannot be produced, for certain processes over specific energy regions. In the next section we shall discuss how this problem may be approached in a pragmatic fashion.

However, it is clear that over certain energy regions, an expansion basis for the trial function which only includes atomic states with negative expectation energy values will not be adequate to obtain convergent cross sections if the continuum states of the true scattering wave function plays an important role in the collision process.

2.4.2 The L^2 approach to representing continuum states

The problem of describing the continuum in an atomic collision process is made difficult because of the fact that the eigenfunctions of the Hamiltonian operator which correspond to continuum states obey different boundary conditions to those eigenfunctions which describe the bound atomic states. The specification of these boundary conditions alone is not a trivial matter in the case of ionisation (see for example, Peterkop (1977)).

However, since the physical requirements of the problem determine that the electronic wavefunction is at all times a normalizable quantity, we can suppose that we can describe the time evolution of the electronic wave function without leaving the Hilbert (L^2) space of the problem. The term L^2 in the case refers to functions $\chi(\vec{R})$ such that

$$\int d\vec{R} \; |\chi(\vec{R})|^2 < \infty \qquad (2.4.1)$$

where the integral in expression (2.4.1) is a Lebesque integral. Then the function $\chi(\vec{R})$ is called Lebesque square-integrable (Taylor (1983)). From now on we shall use the phrase "an L^2 function" to indicate that the function concerned satisfies expression (2.4.1).

One should always be able to work totally in the Hilbert space of the problem and obtain physical results, within the restrictions of the model used to represent the physical system. The great advantage of using purely L^2 functions in a collision problem is that it can be attacked using existing computational methods, designed for bound state problems, with relatively minor modifications to computer codes and this reduces the problem to a level where it is much more likely to be solved. Formally, of course, we may use any complete L^2 basis, with which to expand the total wavefunction, but in practice we are restricted for reasons already given (see Section 2.4.1).

The question of how to optimize this choice of truncated basis, and at the same time retain the most important physical properties of the system in order to produce reliable results, is one of the problems to which much of the work to be presented in this thesis has been

directed. If the initial model of the physical system is at all a reasonable one then it should be possible, ideally, to demonstrate how the results converge towards the correct values as the size of this truncated basis is increased, but this is a long and time consuming process. It is more prudent to try to use physical or intuitive approaches to the problem a priori to hopefully take into account the most important processes that occur during the collision event. The aim is to try to select a basis set with the view that it can both describe the corresponding regions of the L^2 space for the wavefunction in the collision and is also of a convenient size for numerical computations to be performed. In the next section we shall consider some attempts that have been made to remove some of the typical ad hoc features of describing the continuum.

2.4.3 L^2 expansions in electron-tom scattering

The use of L^2 states as a means of representing the continuum states of a system has a history extending back to the earliest days of quantum mechanics. One of the earliest calculations to make use of this approach was made by Hasse, 1931. This was an example whereby an L^2 function was used in an attempt to approximate the contribution made by the continuum to the polarizability of neutral helium and of the ion, Li^+. A variational principle was used to suggest the form of the L^2 pseudofunction which represented the

continuum.

In electron atom interactions, in particular, the effect of polarization must be included in the calculation, and is of particular importance at low collision energies. The influence of the long range polarization potential was investigated by Temkin (1957, 1960) in the so called method of polarized orbitals. This attempted to include both the effects of polarization and that of exchange in a relatively simple approximation (applied to e^- + H collisions). The effect of the distortion of the hydrogen in the ground state by the incident electron is accounted for by using perturbation theory to obtain the form of the distorted wavefunction, and then further approximations are made to obtain a tractable equation that can be solved, such as retaining only the dipole contribution to the polarization, and requiring that the polarization function vanishes when the incident electron is closer to the nucleus than the target electron. In effect an effective local potential is explicitly introduced as a model of the true optical potential acting in a single open channel. In the case of electrons incident upon a hydrogen atom, it was shown by Castillejo, Percival and Seaton (1960) that the 2p state accounts for about 66% of the total polarizability, while including all the discrete p states will give 81.4% of the total polarizability and hence the p continuum states are needed to account for the missing 18.6%.

This suggests that in the usual close coupling

approximation for electron-hydrogen scattering (Bransden, 1983) the results may converge rather slowly as the number of discrete states in the expansion basis is increased. One approach to this problem was suggested by Damburg and Karule (1967), in order to represent the long range potential fully. They showed that it was possible to add a single L^2 function (or pseudostate) to the expansion basis so that the full polarizability was obtained. It was possible to obtain this function in closed form. For instance, in the case when only a single p state is retained in the expansion the pseudostate given by

$$R_{21} = (32/129)^{1/2} r\left(1+\frac{r}{2}\right)\exp(-r) \qquad (2.4.2)$$

accounts for the full polarizability, while if the 2p state is included in the basis as the only discrete state, then to obtain the full polarizability it is necessary to include the following pseudostate (which is orthogonal to the 2p state)

$$R_{31} = 0.340\, r \exp(-r/2) - 0.966\, r\left(1+r/2\right)\exp(-r) \qquad (2.4.3)$$

Using a basis consisting of the 1s and 2s hydrogenic

functions and the 2p and R_{31} p type pseudostate in expression (2.4.3), Burke et al. (1969) were able to obtain accurate values for the elastic differential cross section in the forward direction, where the long range polariztion potential is particularly important. Thus the p continuum has in some sense been effectively included in the calculation through the use of an L^2 function. A method for constructing pseudostates which will account for the polarizabilities of many electron atoms has been given by Burke and Mitchell (1974). A similar approach has been previously described by Koker and Michels (1965). These approaches are based upon constructing a suitable variational principle from which the pseudostates are determined. The method starts by defining the dipole poarizability of an atomic system, in atomic units, as

$$\alpha = 2 \sum \int dK \frac{| \langle \phi_0 | M_1^0 | \phi_K \rangle |^2}{E_K - E_0} \qquad (2.4.4)$$

where

$$M_1^0 = \sum_{i=1}^{N} z_i \qquad (2.4.5)$$

where N is the number of electrons in the atom. In equation

(2.4.4) the summation and integration are taken over all states ϕ_k including the continuum, coupled to the ground state ϕ_o by the dipole operator defined by expression (2.4.5). The polarized pseudostate ϕ_p is defined by requiring that we can replace the summation and integration in (2.4.4) by a single term so that

$$\alpha = 2 \frac{| \langle \phi_o | M_1^o | \phi_p \rangle |^2}{E_p - E_o} \qquad (2.4.6)$$

where

$$\langle \phi_p | \phi_p \rangle = 1 \qquad (2.4.7)$$

and

$$\langle \phi_p | H | \phi_p \rangle = E_p \qquad (2.4.8)$$

where H is the atomic Hamiltonian.

It can be shown that ϕ_p is given by

$$\phi_p = N^{-1/2} \tilde{\phi}_p \tag{2.4.9}$$

where $\tilde{\phi}_p$ is a solution

$$(H - E_0)\tilde{\phi}_p = M_1^0 \phi_0 \tag{2.4.10}$$

and the factor $N^{-1/2}$ in equation (2.4.9) ensures that equation (2.4.7) is satisfied. To solve equation (2.4.10) the functional J is constucted where

$$J = \langle \tilde{\phi}_p^t | H - E_0 | \tilde{\phi}_p^t \rangle - 2 \langle \tilde{\phi}_p^t | M_1^0 | \phi_0 \rangle \tag{2.4.11}$$

This is stationary for small variations of the trial function $\tilde{\phi}_p^t$ about the exact solution of equation (2.4.10). The trial function is constructed from an orthonormal basis χ_i so that

$$\tilde{\phi}_p^t = \sum_{i=1}^{N'} a_i \chi_i \tag{2.4.12}$$

Variation of the coefficients a_i leads to the equations

$$\sum_{j=1}^{N'} \left(\langle x_i | H | x_j \rangle - \delta_{ij} E_0 \right) a_j = \langle x_i | M_1^0 | \phi_0 \rangle \qquad (2.4.13)$$

for $1 < i < n$.

Equation (2.4.13) can be solved and the function $\tilde{\phi}_p^t$ normalized correctly to obtain ϕ_p^t, the trial pseudostate function. By varying the parameters in the basis set used in expression (2.4.12), the 'best' polarized pseudostate can be determined. Other calculations based on the approach of optimizing the polarizability contribution of the expansion basis have been made by Geltman and Burke (1970) and Damburg and Geltman (1968).

However desirable the optimization of the polarizability is, it is only one of the desirable features that a pseudostate expansion must have for representing the continuum and does not guarantee that other physical properties have correctly determined values. The optimization of the polarizability which depends upon terms of second order, as in equation (2.4.6), will tend to emphasize coordinte values in configuration space which are far from the nucleus, in contrast to the optimization of the energy of a bound state by the usual diagonalization procedure. This may in general be more sensitive to the regions of space closer to the nucleus. This is to say that the unperturbed atomic Hamiltonian operator, H , and the

radial operator, r, will tend to emphasise different regions of the electronic distribution.

Thus we may not in general expect that pseudostates obtained from optimizing the polarizability to be the most effective in a case when we expect the regions of space near the nucleus to be the most important.

Another distinct possibility as to the choice of pseudostates has been investigated by Callaway and Wooten (1974), in the case of e^- + H scattering, using the algebraic variational method (Nesbet (1969), Harris and Michels (1969)). In particular they considered the 1s - 2s and 1s - 2p transitions between 10 eV and 12 eV and the 1s-1s elastic transition between 10 eV and 30 eV. The basis set included the exact 1s, 2s, 2p and 3d hydrogenic states and seven pseudostates. The pseudostates channels were allowed to be open and the pseudostate parameters were chosen so as to avoid the introduction of unphysical pseudoresonances. These exist near the thresholds of the pseudostates. This is an unfortunate consequence of the fact that the discretization of the continuum leads to the inclusion of arbitrary positive energies in the problem which have no real physical significance. However, Callaway and Wooten employed four criteria in their attempt to optimize the basis set expansion, which will be discussed briefly. Firstly the exact 1s, 2s, 2p and 3d states were present. Secondly the 3s and 3p eigenvalues were closely approximated by two of the pseudostate energies. They also

demanded that the eigenphase sum, for L = O and an impact energy of 0.405 a.u., should equal or exceed the values given by Geltman and Burke (1970), and lastly that the S-wave phase shifts for L = 1 and impact energy of 0.245 a.u. should equal or exceed those reported by Matese and Oberoi (1971). As they remark, a considerable arbitrariness still remained in the choice of pseudostates. The pseudostates included three with negative energies and four with positive energies. Their conclusions were that in general good agreement with other calculations was obtained, and also with experimental results for the 1s - 2s cross section except for an impact energy of 0.39 a.u.

So far we have briefly discussed some choices of pseudostates for electron-hydrogen collisions, based upon optimization of certain parameters. However, other choices are possible and the general conclusion seems to be that at low collision energies the use of a basis consisting of the lowest exact states (.e.g. 1s, 2s, 2p) supplemented by several pseudostates produces results very close to elaborate variational calculations. Further details are given by Callaway (1978). We will now concentrate upon the use of pseudostates in heavy particle collisions.

2.4.4 Introduction to L^2 methods in heavy particle collisions

For almost two decades now calculations involving heavy

particle scattering have used the idea of augmenting a basis set consisting of bound states, representing the physical states of a system, in a trial function expansion similar to (2.3.22), by pseudofunctions intended to represent the continuum. In the following sections we shall briefly outline some of the main attempts to achieve the aims outlined in Section (2.4.1), namely to calculate cross sections close to the actual experimental data, using only a reasonable number of judiciously chosen basis states. The first calculation made in the impact parameter formulation which incorporated pseudostate functions was probably that of Gallaher and Wilets (1968), in an investigation of proton-hydrogen collisions, and so we shall begin by discussing how they attempted to include the hydrogenic continuum in their calculation.

2.4.5 Sturmian functions

Gallaher and Wilets (1968) investigated proton-hydrogen collisions in the two centre expansion impact parameter approximation. The basis functions they choose, $f_{nlm}(r)$, contained Sturmian functions, and had the following form

$$f_{nlm}(r) = \frac{1}{r} S_{nl}(r) Y_{lm}(\theta, \phi) \qquad (2.4.14)$$

where $S_{n\ell}(r)$ is a radial function which satisfies

$$\left(-\frac{1}{2}\frac{d^2}{dr^2} + \frac{\ell(\ell+1)}{2r^2} - \frac{\alpha_{n\ell}}{r}\right) S_{n\ell}(r) = E_\ell S_{n\ell}(r) \quad (2.4.15)$$

and

$$E_\ell = -\frac{1}{2(\ell+1)^2} \quad (2.4.16)$$

The Sturmian functions defined by (2.4.15) form an infinite discrete, complete L^2 basis set. So, unlike the usual hydrogenic case, there is no continuum set of states. Equation (2.4.15) is similar to the usual Schrodinger equation except that the energy E_ℓ is treated as a fixed parameter and it is the effective charge $\alpha_{n\ell}$ which acts as the eigenvalue. The necessary boundary conditions to be imposed upon $S_{n\ell}(r)$ are that it be zero at the origin and decay exponentially at infinity. By choosing E_ℓ as in equation (2.4.16), the Sturmian functions are in fact scaled hydrogenic functions, that is

$$S_{n\ell}(r) = \alpha_{n\ell}^{1/2} R_{n\ell}(\alpha_{n\ell} r) \quad (2.4.17)$$

where $R_{nl}(r)$ is the usual radial hydrogenic function. The normalisation is chosen so that

$$\langle f_{nlm}(\vec{r}) \mid f_{nlm}(\vec{r}) \rangle = 1 \qquad (2.4.18)$$

However the usual orthogonalisation condition has to be modified by the inclusion of the factor $\frac{1}{r}$, that is

$$\langle f_{nlm}(\vec{r}) \mid \frac{1}{r} \mid f_{n'l'm'}(\vec{r}) \rangle = \frac{\alpha_{nl}}{n^2} \delta_{(nlm)(n'l'm')} \qquad (2.4.19)$$

It can also be shown that

$$\alpha_{nl} = \frac{n}{l+1} \qquad (2.4.20)$$

and hence the first Sturmian function for each l value coincides with the corresponding hydrogenic function.

We also note that the mean energy is given by

$$\langle f_{nlm}(\vec{r}) \mid -\frac{1}{2}\nabla^2 - \frac{1}{r} \mid f_{nlm}(\vec{r}) \rangle = \frac{-1}{n(l+1)} + \frac{1}{2(l+1)^2} \qquad (2.4.21)$$

It can also be shown that the Sturmian functions are more compact than hydrogenic states in that

$$\langle f_{n\ell m} \left| \frac{1}{r} \right| f_{n\ell m} \rangle = \frac{1}{n(\ell+1)} \qquad (2.4.22)$$

whereas for hydrogenic functions

$$\langle R_{n\ell} \left| \frac{1}{r} \right| R_{n\ell} \rangle = \frac{1}{n^2} \qquad (2.4.23)$$

Most of their calculations were carried out using the four Sturmian basis functions 1s, 2s and 2p , on both centres. However in order to obtain some idea of the convergence characteristics of this type of basis they carried out selective tests with up to five states, one p state and one d state upon each centre. In order to test the effectiveness of their basis set, Gallaher and Wilets calculated the overlap of their basis set with the united atom $He^+(1s)$ state. This is the ground state of the system formed when the two nuclear centres, A and B, are at zero separation. They found the overlap of $He^+(1s)$ with the first three Sturmian s states was 0.92, which compares with

0.76 for the overlap of He^+ (1s) with all the discrete hydrogenic functions. Since the He^+ (1s) state has zero overlap with the 2s Sturmian state, this demonstrates the ability of the Sturmian basis to include the hydrogenic continuum. However, there is a problem with the Sturmian basis connected with the calculation of the transition amplitudes at large values of t, which arises when projecting the basis functions onto exact hydrogenic functions, in accordance with the formula given in expression (2.3.45). The resulting transition amplitudes have oscillating components which do not vanish as $t \rightarrow \infty$. Gallaher and Wilets succeeded in removing these, however, to produce constant transition amplitudes as $t \rightarrow \infty$, which were variationally correct (Shakeshaft 1976). This will be discussed again in Section (2.4.6). Another problem with the eight state basis of Wilets and Gallaher, consisting of the 1s, 2s and $2p_{0,1}$ Sturmian functions on each centre, is the fact that the strong degeneracy coupling between the true 2s and 2p states is not present because the 2s hydrogenic state is not represented exactly in the basis. This will affect both the 2s and 2p excitation and charge transfer cross sections. A comparison with experiment reveals that in general the eight state Sturmian basis is better than a purely hydrogenic basis of the same size, which consists of 1s, 2s and $2p_{0,1}$ states placed upon each centre, especially for the 2p exchange cross section at incident proton energies between 1keV and 25keV. However a

very dramatic improvement is found for the total exchange probability for 3^{o} scattering, as a function of incident proton energy, which has been measured by Helbig and Everhart (1965). The eight state hydrogenic expansion produces a curve which is out of phase with experiment but the Sturmian basis produces a curve in excellent agreement with experiment at all laboratory energies between 1keV and 100keV. This calculation therefore showed the importance of including the hydrogenic continuum, but larger calculations were needed to establish the convergence properties of the Sturmian basis functions, and we shall now describe some other investigations using these functions.

An advantage of the Sturmian basis set over some other basis sets is that the difficult and time consuming exchange matrix elements, which have been defined by the equations (2.3.63) and (2.3.64), can be evaluated by solving a set of coupled differential equations, which are derived by using certain recurrence relations for the Sturmian functions. This fact has been employed by Shakeshaft (1975), who also investigated the proton-hydrogen collision system. His Sturmian basis was based upon the same choice of parameters as used by Gallaher and Wilets (1968), as given in expressions (2.4.15), (2.4.16) etc. Using a basis of up to ten Sturmian functions of s symmetry only on each centre, Shakeshaft obtained convergent results for the amplitudes for elastic scattering, 2s excitation and capture into 1s and 2s states, at an impact energy of 25keV and an impact

parameter of 1.0 a.u. This convergence includes the effect of the s continuum states on both centres only and the inclusion of higher l states will change the final amplitudes. In further work using a Sturmian basis set, Shakeshaft (1976) used a two centre basis consisting of six s states and six p states centred about each proton. The exact 1s and 2p hydrogenic states were included in the Sturmian basis and the 2s hydrogenic state was closely approximated by an eigenvector of the diagonalized Sturmian s type basis set. However, the degeneracy between the 2s and 2p states was satisfied to within 0.6%. Reasonably good agreement was obtained between the theoretical and experimental cross sections for excitation of the n = 2 level, and also for charge transfer into the 2s state over the impact energy range 15keV to 200keV. There was however a large disagreement of about 45% between the results of Shakeshaft and the results obtained by Cheshire, Gallaher and Taylor (1970), for the peak in the excitation of the n = 2 level. Cheshire et al. used a seven state basis upon each centre consisting of the exact 1s, 2s and 2p , hydrogenic states with the addition of an s and a p type pseudostate. Their results obtained using only the exact 1s, 2s and 2p, states upon each centre were in better agreement with those of Shakeshaft than their pseudostate basis results. Shakeshaft attributed these differences to the fact that near the cross section peak for n = 2 excitation, the ionisation cross section is also large and

the continuum states can be represented more accurately in his basis than in the basis of Cheshire, Gallaher and Taylor. This is because Shakeshaft's basis functions include more extended orbitals than those of Cheshire et al. for representing the continuum, and the electron flux will presumably be less likely to return back into the bound state during the collision from these extended orbitals, than is the case for the pseudostates used by Cheshire et al.

Shakeshaft also considered the charge transfer cross section into the 1s state, which agreed well with the results of Cheshire et al. at low incident energies but worsens slightly for increasing energies. Shakeshaft explained this disagreement by noting that for high energies the second Born term is thought to be the dominant contribution to the cross section for charge transfer in the forward direction (see for example Shakeshaft and Spruch (1973), Dettmann and Leibfried (1969)), and this corresponds to the classical picture of the electron being scattered twice through 60^{o}, firstly towards the target proton and then by the target proton before emerging with the velocity of the incident proton. In this picture the electron is scattered into an intermediate continuum state which is formed from states with a large range of angular momentum values since the electron is scattered through a large angle into a small solid angle. Hence neither Shakeshaft nor Cheshire et al. can account precisely for this effect with

their limited basis sets (with only s and p angular momentum) but presumably Shakeshaft's basis represents the s and p subspace of the continuum states more effectively than does the basis of Cheshire et al. Shakeshaft also estimated the cross section for ionisation using a projection technique which we shall describe in the next section as it will be much used later on in the discussion of the present results obtained for this thesis. The results obtained by Shakeshaft for the probability of ionisation, using a trial wave function containing s states only at a single impact parameter, for a single energy, show that reasonable convergence is obtained when five or six wavefunctions are used on each centre. However, the convergence is not monotonic.

Further calculations using a Sturmian basis have been made by Winter (1982), in a study of charge transfer in the collision systems

$$H^{+} + He^{+} \rightarrow H + He^{2+} \qquad (2.4.24a)$$

$$He^{2+} + H \rightarrow He^{+} + H^{+} \qquad (2.4.24b)$$

The basis sets used consisted of between nineteen and twenty-four basis functions. The same approach was taken as in Shakeshaft (1975). That is to say the basis sets on each centre were diagonalized to produce approximate atomic states corresponding to each centre, and the occupation

amplitudes for these approximate states were used directly to obtain the physical cross sections.

Firstly we consider the process given in expression (2.4.24b). At $^4He^{2+}$ impact energies of 20keV and 70 eV, the Sturmian expansion was used to obtain the total cross section for charge transfer into all states of $^4He^{2+}$ and these were only about 9% lower than the corresponding results obtained using a molecular basis with plane wave translation factors by Hatton, Lane and Winter (1979) and Winter and Hatton (1980). Comparing the Sturmian results and those of Winter and Hatton (1980) the impact parameter dependence for the total electron transfer probability is also in similar agreement, especially near the peaks in the impact parameter dependence. The Sturmian result for the $^4He^{2+}$ energy of 20keV is also within 1% of the calculation of Kimura and Thorson (1981a) who used a ten molecular state basis with optimized translational factors. However, in the second reaction considered, given by (2.4.24a), the agreement is not so good. At a centre-of-mass energy of 4keV the Sturmian basis results for capture into the H(1s) state are 7% below the result of Winter, Hatton and Lane (1980) and 6% above the result of Kimura and Thorson (1981a), for the same transition. However, at a centre-of-mass energy of 14keV, the Sturmian result for 1s capture is 28% above the corresponding result of Winter, Hatton and Lane (1980). This suggests, as noted by Winter, that the molecular state result has not converged, probably due to

the neglect of the continuum, as convergence tests of the Sturmian basis suggested that further additions to it would only slightly raise the capture cross section.

A comparison can be made with an eight state bound atomic expansion used by Bransden and Noble (1981) and Winter (1980). This basis consisted of the exact 1s, 2s and $2p_{0,1}$, atomic states placed on both centres. Both eight state calculations were in excellent agreement with each other for $^4He^{2+}$ impact energies between 20keV and 200keV. Firstly, we compare the capture into all states for reaction (2.4.24b). The eight state results are about 10% below the Sturmian results at $^4He^{2+}$ impact energies between 20keV and 70keV but at 200keV the disagreement is about 41% due to the neglect of charge transfer states with $n > 3$. Bransden, Newby and Noble (1980) have estimated the contribution for $n > 3$ using two-state calculations and their total result at 200keV is within 7% of the Sturmian result.

We now consider the second reaction (2.4.24a). At the lowest centre-of-mass energy of 4keV the eight state result for capture into all states is within 10% of the Sturmian result but at 14keV it is 50% below the Sturmian result and at 120keV it is 20% too low. This suggests that for reaction (2.4.24a) the continuum states have an important role to play. Bransden and Noble (1981) suggest an explanation for this as follows. In reaction (2.4.24b) the initial H(1s) state and the $n = 2$ states of He^+ have the same energy, and are strongly coupled. Therefore the

influence of intermediate states, including continuum intermediate states, is expected to be small for energies near the cross section maximum. In contrast, in reaction (2.4.24a) the energy difference between the initial state He (1s) and the H(1s) state is large and hence the coupling will be weak and hence continuum intermediate states may be important even at low energies. The Sturmian results of Winter can also be compared to experimental results. For reaction (2.4.24a) total electron transfer cross sections have been measured by Peart, Grey and Dolder (1977) and Angel, Dunn, Sewell and Gilbody (1978). At centre-of-mass energies below 25keV the Sturmian basis results lie above the upper error bars of Peart et al. by up to 20%. However, between 40keV and 120keV centre-of-mass energies the Sturmian results are within the error bars of Angel et al. Cross sections for total electron transfer in reaction (2.4.24a) have been measured by Shah and Gilbody (1978) and Olson, Salop, Phaneuf and Meyer (1977) and the Sturmian basis results are in excellent agreement with experiment for $^4He^{2+}$ impact energies between 20keV and 200keV.

In this section we have discussed the attempts to represent the continuum by Sturmian functions and the general conlusion seems to be that possibly five or more Sturmian functions of a given l value are needed to obtain reasonable convergence and also to ensure the exact bound states are adequately represented, but that good agreement with experiment is possible for certain processes where the

continuum plays a role.

However the Sturmian basis approach is best applied to a system with a hydrogenic centre and subsequently we shall discuss various approaches to the more general problem. However, firstly we shall describe in more detail how unambiguous ionisation cross sections may be obtained from an L^2 basis set.

2.4.6 Determination of ionisation cross sections from an L^2 expansion

We start by using the fact that since the Sturmians basis functions overlap the hydrogenic continuum, then the trial function (see expression (2.3.49)), which is found by solving equations similar to equation (2.3.54), must contain some information about the ionised probability of the electron at some large time t. We suppose that the trial function $\Psi_T(\vec{r},t)$ has been expanded in a basis set, which consists of states which have been obtained from a diagonalization procedure using the hydrogen atom Hamiltonian, as described in Section (2.3.3). These variationally determined states will be labelled as $\Phi_{K\alpha,tr}(\vec{r},t)$ and from the Hylleraas-Undheim theorem we have the result that $\Phi_{K\alpha,tr}(\vec{r},t)$ is an approximation to the exact hydrogenic state $\Phi_{K\alpha}(\vec{r},t)$, with its variational energy being an upper bound to the corresponding exact energy of $\Phi_{K\alpha}(\vec{r},t)$. The label K refers to the Kth atomic state of

the hydrogen atom, attached to centre α where α is either A or B. Hence we can write the trial function in the limit as t becomes infinite as

$$\Psi_T(\vec{r},t) = \sum_{j=1}^{M} b_j(t)\,\Phi_{jB,tr}(\vec{r},t) + \sum_{K=1}^{N} a_K(t)\,\Phi_{KA,tr}(\vec{r},t) \qquad (2.4.25)$$

(which is analagous to equation (2.3.49)), and where the labels A and B as usual refer to the projectile and target respectively. The summations in expression (2.4.25) are over all trial states included in the basis. We note that the label i which denotes the initial state of the system before the collision has been dropped for convenience in this discussion, but is contained implicitly in expression (2.4.25). For convenience we will now concentrate on the target centred part of expression (2.4.25) asking what is the probability of a transition into an exact final state $\Phi_{qB}(r,t)$ after the collision?

The probability is given by the following expression

$$P'_{qB,tr} = \lim_{t\to\infty} |\langle \Phi_{qB}(\vec{r},t) | \Psi_T(\vec{r},t)\rangle|^2$$

$$= \lim_{t\to\infty} \frac{1}{t}\int_{t}^{2t} dt' |\langle \Phi_{qB}(\vec{r},t) | \Psi_T(\vec{r},t)\rangle|^2 \qquad (2.4.26a$$

provided the limit in expression (2.4.26a) exists. Shakeshaft (1976) shows that it does exist and that the probability $P'_{qB,tr}$ is given by

$$P'_{qB,tr} = \sum_{j=1}^{M} |b_j(\infty) < \Phi_{qB}(\vec{r}) | \Phi_{jB,tr}(\vec{r}) >|^2 \qquad (2.4.26b)$$

where the time dependence has been removed because of the modulus operation. We note that the probability in expression (2.5.26b) is that calculated by Gallaher and Wilets (1968). This is to be compared with the transition probability that would be obtained by using equation (2.3.58), for the transition into the final trial state $\Psi_T(r,t)$ which is given by

$$P_{qB,tr} = |b_q(\infty)|^2 \qquad (2.4.27)$$

As Shakeshaft remarks, the quantity $< \Phi_{qB}(\vec{r}) / \Phi_{jB,tr}(\vec{r}) >$ is $= \delta_{qj}$ to second order in the error in $\Phi_{jB,tr}(\vec{r},t)$ and it has been stated already in section (2.3.3) that expression (2.4.27) is also a variational probability estimate. Hence it is not obvious which of the expressions (2.4.26b) or (2.4.27) provides the best estimate for the transition probability for a finite basis set. Evidently though both

expressions will give the same value as the size of the basis set is increased. We shall now consider expression (2.4.26b) again, which gives the probability for a transition into the exact final qth bound state on the target.

We now calculate the sum of all such probabilities into all final exact target bound states, $\Phi_{qB}(\vec{r},t)$ which will be given by

$$\sum_{\text{all } q} P'_{qB,tr} = \sum_{\text{all } q} \sum_{j=1}^{M} |b_j(\infty)|^2 \, |\langle \Phi_{qB}(\vec{r}) | \Phi_{jB,tr}(\vec{r}) \rangle|^2 \quad (2.4.28)$$

The summation $\sum_{\text{all } q}$ is over all the exact target bound states.

The total probability for the electron to be attached to the target, no matter what final state it is in, is given by

$$P_B = \sum_{J=1}^{M} |b_j(\infty)|^2 \quad (2.4.29)$$

and hence the probability that the electron is in the continuum states of the target after the collision is given by subtracting expression (2.4.28) from expression (2.4.29) to obtain

$$P_{ion,B} = \sum_{j=1}^{M} |b_j(\infty)|^2 \left(1 - \sum_{\text{all } q} |\langle \Phi_{qB}(\vec{r}) | \Phi_{jB,tr}(\vec{r}) \rangle|^2\right) \quad (2.4.30)$$

where $P_{ion,B}$ is the target ionisation probability. We can rewrite the term in brackets in expression (2.4.30), by using the completeness relation

$$\hat{I} = \sum_{\text{all } q} |\Phi_{qB}(\vec{r})\rangle\langle\Phi_{qB}(\vec{r})| + \int_{\text{all } \vec{k}} d\vec{k}\, |\Phi_{B}(\vec{k},\vec{r})\rangle\langle\Phi_{B}(\vec{k},\vec{r})| \quad (2.4.31)$$

where $|\Phi(\vec{k},\vec{r})\rangle$ is a suitably normalized hydrogenic continuum state of the target centre B, and $\hat{I}$ is the unit operator.

Then

$$\Gamma_{jB} = 1 - \sum_{\text{all } q} |\langle \Phi_{qB}(\vec{r}) | \Phi_{jB,tr}(\vec{r}) \rangle|^2$$

$$= \int_{\text{all } \vec{k}} d\vec{k}\, |\langle \Phi_{B}(\vec{k},\vec{r}) | \Phi_{jB,tr}(\vec{r}) \rangle|^2 \quad (2.4.32)$$

where in the second step we have used the result in (2.3.33) and thus we rewrite expression (2.4.30) as

$$P_{ion,B} = \sum_{j=1}^{M} \Gamma_{jB} \, |b_j(\infty)|^2 \qquad (2.4.33)$$

with Γ_{jB} defined by expression (2.4.32). This is an important result as it relates the probability for ionisation to occur to the probabilities $b_j(\infty)$ which are for transition into discretized pseudostates. $P_{ion,B}$ as defined relates only to the target and is therefore a measure of the direct ionisation probability. However, a similar analysis can be applied to the projectile transition amplitudes and it is straightforward to show that the corresponding probability for a transition into the continuum states centred upon the projectile, which are denoted by $|\Phi_A(\vec{k},\vec{r},\,)>$, and are suitably normalized, will be given by the following expression

$$P_{ion,A} = \sum_{K=1}^{N} \Gamma_{KA} \, |q_K(\infty)|^2 \qquad (2.4.34)$$

where $a_K(\infty)$ is obtained from equation (2.3.59) and Γ_{KA} is defined by

$$\Gamma_{KA} = \int_{\text{all } \vec{k}} d\vec{k} \; |<\Phi_A(\vec{k},\vec{r})|\,\Phi_{KA,tr}(\vec{r})>|^2 \qquad (2.4.35)$$

in analogy to expression (2.4.32).

Therefore the final result is that the total combined probability for a transition into a continuum state centred around either the projectile centre of the target centre is given by the expression

$$P_{ion} = P_{ion,A} + P_{ion,B}$$

$$= \sum_{K=1}^{N} \Gamma_{KA} |a_{Ki}(\infty)|^2 + \sum_{j=1}^{M} \Gamma_{jB} |b_{ji}(\infty)|^2 \quad (2.4.36)$$

We can interpret the expression (2.4.36) for the total probability of ionisation as follows. For a projectile centred state we have that $|a_K(\infty)|^2$ is the probability for a transition into the state denoted by K and must be multiplied by the corresponding probability that this state is in the continuum set of states centred upon the projectile, which is given by Γ_{KA}. Similarly the probability $|b_j(\infty)|^2$ for a transition into a target state, denoted by j, must be multiplied by the corresponding probability that this state is in the continuum set of states centred upon B, which is given by Γ_{jB}. The analysis above has been for the case of proton hydrogen collisions but it can be extended immediately to the cases where one or both centres represent an effective potential in which a single active electron is moving, which will be the basic system to be studied in this thesis.

We note also at this point that we shall call the cross sections obtained through the use of expression (2.4.36) the projected cross section. The projected cross sections will be determined in the same fashion as the usual cross sections, that is through the use of equations analagous to (2.3.72) and (2.3.73). Thus we can write that the total ionisation cross section, obtained from the probabilities in expression (2.4.36), is given by

$$\begin{aligned} \sigma_{im} &= 2\pi \sum_{K=1}^{N} \Gamma_{KA} \int_0^\infty b\, |a_{Ki}(\infty)|^2\, db \\ &\quad + 2\pi \sum_{j=1}^{M} \Gamma_{jB} \int_0^\infty b\, |b_{ji}(\infty)|^2\, db \\ &= \sum_{K=1}^{N} \Gamma_{KA}\, \sigma_{Ki}^{r} + \sum_{j=1}^{M} \Gamma_{jB}\, \sigma_{ji}^{d} \end{aligned} \qquad (2.4.37)$$

In the second line of expression (2.4.37) we use the fact that the quantities and as defined by expressions (2.4.35) and (2.4.32) are independent of the impact parameter, b. Then in the last line of expression (2.4.37) we have obtained the reaction cross section, , and direct cross section, , as defined by expressions (2.3.72) and (2.3.73). Thus it is clear that the total ionisation cross section, as obtained from a two centre expansion, separates naturally into two distinct contributions. The first summation term in expression (2.4.37) is the contribution due to the projectile centred states and is usually called

charge transfer into the continuum (or CTTC) and this abbreviation will be used from this point. The second summation term in expression (2.4.36) is the direct ionisation cross section.

Finally in this section we shall describe how other probabilities can be projected using formula analogous to expression (2.4.36). We return to expression (2.4.26b) which is the variational probability that the exact final bound state, denoted by $\Phi_{q_B}(\vec{r})$ for a target centred state, is occupied and is given by

$$P'_{q_B,tr} = \sum_{j=1}^{M} |b_j(\infty)|^2 |\langle \Phi_{q_B}(\vec{r}) | \Phi_{j_B,tr}(\vec{r}) \rangle|^2$$

$$= \sum_{j=1}^{M} \prod_{q_B,j_B} |b_j(\infty)|^2 \qquad (2.4.38)$$

where we define

$$\prod_{q_B,j_B} = |\langle \Phi_{q_B}(\vec{r}) | \Phi_{j_B,tr}(\vec{r}) \rangle|^2 \qquad (2.4.39)$$

Since Φ_{q_B} represents an exact bound state on the target, then expression (2.4.38) is analogous to the expression (2.4.33) for the direct ionisation probability, and we calculate the cross section for the transition into an exact final bound target state, denoted by $\Phi_{q_B}(r)$, as follows,

$$\sigma'_{qB} = 2\pi \int_0^\infty db\, b \sum_{j=1}^{M} \Pi_{qB,jB} |b_{ji}(\infty)|^2$$

$$= \sum_{j=1}^{M} \Pi_{qB,jB} \sigma_{ji}^{d} \qquad (2.4.40)$$

where we have used expression (2.3.72) in the second line. We shall call the cross section, obtained for an exact final state $\underset{\sim}{\Phi}_{qB}$ as in expression (2.4.40), a projected cross section for the state $\underset{\sim}{\Phi}_{qB}(r)$.

Similarly we can define the projected cross section for charge transfer into the exact state $\underset{\sim}{\Phi}_{SA}(r)$ on the projectile centre as follows

$$\sigma'_{SA} = 2\pi \int_0^\infty db\, b \sum_{K=1}^{N} \Pi_{SA,KA} |a_{Ki}(\infty)|^2$$

$$= \sum_{K=1}^{N} \Pi_{SA,KA} \sigma_{Ki}^{r} \qquad (2.4.41)$$

where we have used expression (2.3.73) in the last line, and where we define $\Pi_{SA,KA}$ as follows

$$\Pi_{SA,KA} = \left| \langle \underset{\sim}{\Phi}_{SA}(\vec{r}) | \underset{\sim}{\Phi}_{KA,tr}(\vec{r}) \rangle \right|^2 \qquad (2.4.42)$$

Thus we have obtained expressions for the cross sections for transitions into exact final states, representing both bound and continuum electrons, on both the target and projectile centres, in formula (2.4.37), (2.4.40) and (2.4.41). These

formula will be used extensively later on and therefore their derivation has been considered in detail.

Now we shall return to the discussion of L^2 basis sets in the impact parameter approximation, which can be applied in more general situations than the purely hydrogenic case.

2.4.7 The united atom pseudostate method.

The calculation of Cheshire, Gallaher and Taylor (1970) for the proton-hydrogen collision system has been mentioned in the previous section and we shall now describe it in more detail. Cheshire et al. based their choice of basis set upon the following considerations. Firstly to avoid the problems associated with the degeneracy of the 2s and 2p states (encountered in the Sturmian basis method by Gallaher and Wilets (1968)), the 1s, 2s and 2p states must be represented exactly to allow completely for the long range coupling.

Secondly they reasoned that at small interproton separations intermediate states of the united atom He^+ are formed and these should be adequately represented in the expansion basis. Finally, they selected the basis so that the time consuming exchange matrix elements (equations (2.3.63) and (2.3.64)) could be evaluated using the fast differential equation method of Cheshire (1967), which restricts the number of exponents which should be included. Due to computational limitations only a single 3s

pseudostate and a single 3p pseudostate could be included in the basis and these have the following radial wavefunctions respectively (using the notation of Cheshire et al.)

$$S_{11}(r) = (600/17)^{1/2} \exp(-r)\left(1 - \frac{16r}{15} + \frac{r^2}{5}\right) \quad (2.4.43)$$

$$S_{21}(r) = \frac{1}{2}(5/6)^{1/2} \exp(-r/2)(1 - r/2) \quad (2.4.43a)$$

The basis set consisting of the 1s, 2s, 3s, $2p_{0,1}$ and $\bar{3}p_{0,1}$ states give the overlap integrals with the three lowest He^+ states shown in table 2.1.

The results in table 2.1 show that the pseudostate basis represents the united atom states rather better than the complete set of hydrogenic states and includes significant contributions from the hydrogenic continuum states. The total charge exchange cross section was computed by projecting the $\bar{3}s$ and $\bar{3}p$ pseudostates onto the exact bound states as described in section (2.4.6), and was in good agreement with the experiment of Bayfield (1969). However, the total charge transfer probability corresponding to a scattering angle of 3^o, although in agreement with the experimental data of Lockwood and Everhart (1962), at high incident proton energies (between 15 keV and 60 keV), was in worse disagreement at lower energies than the eight state

Table 2.1 *)

Overlap intergrals with the first three states of He^+

N	$\sum_{n=1}^{N} \lvert \langle He^+(1s) \mid \phi_{ns} \rangle \rvert^2$	$\sum_{n=1}^{N} \lvert \langle He^+(2s) \mid \phi_{ns} \rangle \rvert^2$	$\sum_{n=1}^{N} \lvert \langle He^+(2p) \mid \phi_{ns} \rangle \rvert^2$
1	0.70233	0.25000	-------
2	0.74227	0.56215	0.55493
3	0.9215	0.91509	0.86322
4	0.99227	0.98203	0.96599
5	0.99699	0.99560	0.96632
H(∞) a)	0.76	0.66	0.70

a) The last row corresponds to the complete set of hydrogenic bound states. N=1,2 corresponds to hydrogenic wavefunctions and higher values of N correspond to pseudostates.

*) This table is reproduced from Table 1. in Cheshire et al. ,1970.

Sturmian results of Gallaher and Wilets (1968) near the cross section minima which is puzzling. The general conclusion was that the inclusion of the $\bar{3}s$ and $\bar{3}p$ pseudostates improved the wavefunction and the cross sections derived from it when compared with available experimental data.

We shall now return to the idea of relating the choice of pseudostates used, which must include the continuum to improve the convergence characteristics of a basis, to the eigenfunctions of the united atom limit of the collision system. Firstly, we consider the low impact velocity region. It is reasonable to expect that for such collisions, where the time for the projectile to cross the target atomic interaction region is large compared with the characteristic orbital period of the active electron in the target, a quasimolecule is almost adiabatically formed about the two centres of charge. Non-adiabatic couplings arising from the relative nuclear motion will cause excitation of the virtual molecule, leading to charge transfer and other excitation processes. In this region it is usual to try to represent the electronic distribution by a small set of strongly coupled molecular orbitals rather than to use atomic orbitals. Asymptotically, as the two collision centres move far apart, the molecular orbital must tend to an atomic orbital on one of the two centres (in the homonuclear case the limit is a linear combination of atomic orbitals on both centres). For vanishingly small

internuclear distances the united atom limit is approached. Usually the internuclear axis is taken as the axis of quantization and the system can be described in the coordinate system shown in figure 2.3, which is for the single electron system consisting of the particles ABe as in section 2.1.

The total Hamiltonian of the system is given by

$$H = T_{nuc} + H_{el} \tag{2.4.44}$$

where T_{nuc} is the kinetic energy operator associated with the nuclear motion, where

$$T_{nuc} = -\frac{1}{2\mu} \nabla^2_{\vec{R}} \tag{2.4.45}$$

where μ is the reduced mass of the nuclei,

$$\mu = \frac{m_A m_B}{m_A + m_B} \tag{2.4.46}$$

and the electronic Hamiltonian H_{el} is given by

$$H_{el} = -\frac{1}{2} \nabla^2_{\vec{r}} + V_{eA} + V_{eB} + V_{AB} \tag{2.4.47}$$

where the electronic mass, m_e, has been ignored compared to the masses of A and B (see equations (2.3.5) and (2.3.6)).

The adiabatic molecular orbitals $\hat{\psi}(\vec{R},\vec{r})$ are defined as the bounded solutions of the eigenvalue problem

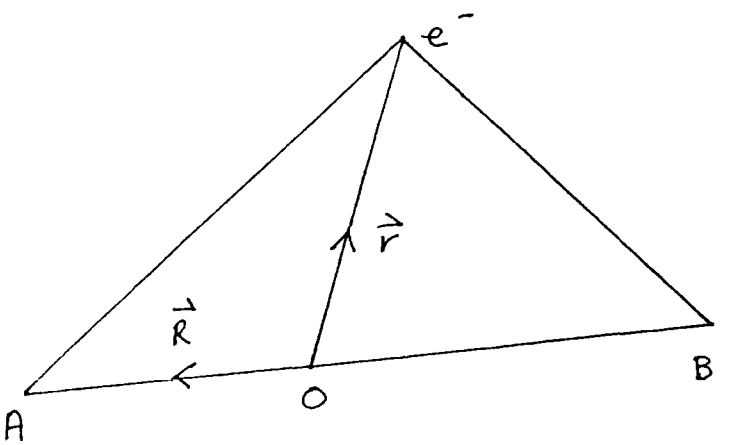

Figure 2.3

Molecular (adiabatic) coordinates for the system ABe^-. O is the centre of mass of AB.

$$H_{el}\,\psi_n(\vec{R},\vec{r}) = E_n(R)\,\psi_n(\vec{R},\vec{r}) \qquad (2.4.48)$$

The internuclear potential is a constant, for fixed R, so that the total energy $E_n(R)$ is the sum of V_{AB} and the electronic energy, that is

$$E_n(R) = V_{AB} + E_n(R) \qquad (2.4.49)$$

The system is symmetrical for rotations about the internuclear axis so that the angular momentum component along this axis, denoted by λ, is a good quantum number. Due to invariance under reflections where $(\vec{r} \to -\vec{r}, \vec{R} \to -\vec{R})$ the eigenvalues $E_n(R)$ depend only upon $|\lambda|$. Two other quantum numbers must be specified to specify the molecular orbital. One way to choose these is to consider the united atom limit, $(R \to 0)$ where the wavefunction becomes an atomic orbital described by three quantum numbers, n, ℓ, m. In this unit λ corresponds to m. Thus the orbitals can be labelled by the united atom quantum numbers, n, ℓ and the symbols, $\sigma, \pi, \delta \ldots$ which denote $|\lambda| = 0,1,2\ldots$. This gives the notation for the orbitals as $1s\sigma$, $2p\sigma$, $2p\pi$, ... etc. For more than one electron the total component of angular momentum along the axis is conserved and is denoted by $\Sigma, \Pi, \Delta, \ldots$ which represents $|\sum_i \lambda_i| = 0,1,2, \ldots$ etc. As the internuclear separation tends to infinity then the molecular orbital tends to an atomic orbital (or a linear combination

of these) with quantum numbers $|\lambda|\, n\ell'$, and therefore a given molecular orbital can be designated either by its united atom limit $n\ell|\lambda|$ or separated atom limit $|\lambda|\, n\ell'$. If the two nuclei are the same then the system is invariant under the transformation $\vec{r} \rightarrow -\vec{r}$ and the molecular states are labelled gerade (g) or ungerade (u) which denote even or odd parity solutions respectively.

Now an important aid used for constructing the united atom basis set is the set of adiabatic potential energy curves which show $E_n(R)$ as a function of R. This is called a potential energy correlation diagram which correlates the united atom limit with the atomic orbitals in the separated atom limit, (see Bransden (1983)). An important theorem (the non-crossing theorem) states that if j and k belong to the same symmetry class, the curves of $E_j(R)$ and $E_k(R)$ cannot cross as R varies between 0 and ∞. For a heteronuclear system this theorem requires two curves with the same $|\lambda|$ may not cross (Von Neumann and Wigner, 1929). In the case of a one electron system, states with the same values of S and $|\lambda|$ cannot cross, where S is a separation constant arising because of the extra symmetry of the problem. The scattering equations in the molecular basis can be set up (Bransden, 1983) and one obtains a set of coupled equations analagous to the atomic orbital coupled equations (Section 2.3.3).

As in the case of the atomic orbital expansion, the matrix elements involving two molecular orbitals, denoted by

j and k, include a phase factor which depends upon the difference between the two adiabatic energy levels of the states in the matrix element. If this energy difference, $E_j - E_k$, is large for all R then the two states will be only weakly coupled. However, if the energy difference, $E_j - E_k$, vanishes for some particular R, they will in general be strongly coupled. For two states which have the same symmetry, and therefore obey the non-crossing rule previously mentioned, the energy curves can sometimes closely approach each other at what is called a pseudo-crossing, and the radial coupling between the states is large resulting in strong coupling between the two states. In selecting a molecular basis the main criteria is to choose a small basis set which consists of the most strongly coupled states as indicated by the appropriate correlation diagram. We shall now consider how an atomic orbital expansion can be selected also by considering the same correlation diagram. Fritsch and Lin (1982) based their so-called modified atomic orbital expansions, which we shall denote by AO+, upon this idea in order to investigate charge transfer in $H^+ + H$ and $He^+ + H^+$ collision system. In the case of $H^+ + H$ the largest basis set typically used consisted of the 1s, 2s and $2p_{o,1}$ states of both the separated atom limit and the united atom limit, which were placed upon both centres giving a total of sixteen states. This choice of basis both ensured that the eight state basis of Bransden and Noble (1982) was contained completely in it,

and also that the united atom orbitals to which the lowest molecular orbitals correlate for the H^+ system were included.

A similar basis chosen in the same fashion was also used for the study of the $He^+ + H$ system, that is it consisted of the separated atom and united atom 1s, 2s and $2p_{o,1}$ states. Diagonalizing the two centre Hamiltonian for the $He^+ + H^+$ system in the space spanned by the sixteen state atomic expansion produced correlation energy curves differing by less than 1% from the exact molecular orbital curves for all internuclear separations. The basis sets on each centre were subsequently diagonalized using the corresponding separated atom Hamiltonian to produce an orthogonalized pseudostate basis which contained both positive and negative expectation energies and thus included a contribution from the continuum states of both separated atoms, He^+ and H . A similar procedure was applied to the basis for $H^+ + H$ collisions, with a subsequent partial representation of the continuum of the H atom on both centres. The 3d united atom orbital was also included on both centres to produce a twenty two state basis for some calculations.

The results for 1s capture in $H^+ + H$ collisions were in agreement with the other pseudostate calculations of Cheshire et al. (1970), described previously in this section, and of Shakeshaft (1978) who used 68 orbitals derived from scaled hydrogenic basis sets, and also with

the experiment of McClure (1966). The sixteen state AO+ results for H(2s) capture oscillated around the ten state molecular orbital results of Kimura and Thorson (1981b) but the twenty-two AO+ results are in excellent agreement with the molecular results up to an impact energy of 50 keV, which indicates the effectiveness of the AO+ expansion because the 2s capture is a small process compared to the 1s and 2p capture at low energy and also because the calculation of Kimura and Thorson used sophisticated molecular translation factors. However, both these calculations overestimate the measured 2s transfer cross section at the highest energies, whereas Shakeshaft (1978), using sixty eight basis states, is in agreement with experiment. This indicates that the AO+ expansion must include a better representation of the n = 3 orbitals and also of the continuum to obtain convergence. For $H^+ + He^+$ collisions the total transfer cross sections obtained from the sixteen state AO+ expansion are again in agreement with the ten molecular orbital calculation of Winter et al. (1980) for H^+ impact energies between 1.5 keV and 8 keV and above this they are within 1% of the Sturmian expansion results of Winter (1981) previously discussed, which indicates that both the Sturmian expansion and the AO+ expansion are effectively accounting for the dominant part of the electronic wave function but by seemingly different means. Fritsch and Lin conclude that above an H^+ impact energy of 25 keV a better representation of the separated atom continuum may be needed to ensure that

convergence of their expansion. This is because the united atom orbitals included in the expansion give rise, after diagonalization of the basis on each centre, to high values for the positive energies in the pseudostate basis and thus the important low positive energy region is not represented, and this will be the important region for collision velocities > 1 a.u.

2.4.8 The three centre expansion method

So far we have only described how the impact parameter approximation has been used with expansion functions placed upon both the heavy particle centres throughout the collision process. However there is no reason in principle why other expansion functions should not be placed upon a third or more centres during the collision. This approach was considered by Anderson, Antal and McElroy (1974) for $H^+ + H$ collisions. Since the results of Gallaher and Wilets (1968) and Cheshire et al. (1970) had already shown the importance of the hydrogenic continuum and the united atom states in the charge exchange process it was decided to explicitly introduce united atom states into the expansion basis with the expansion states to be placed upon three centres. The formulation of the problem proceeds along similar lines to the two centre expansion as described in Section (2.3.3). The exact 1s and 2s hydrogenic states were placed upon each proton centre and the united atom $He^+(1s)$ state was placed upon the midpoint, O, of the internuclear vector, $\vec{AB}$, which is also the centre of charge of the system

as shown in figure 2.3.

If the coordinate origin is taken as being at O then any expansion function placed upon centre O does not need a plane wave translational factor attached to it. In formulating the problem the expectation energy associated with the united atom orbital in the phase (see equations (2.3.37) and (2.3.39) is the usual eigenvalue associated with $He^{+}(1s)$. However, the computational difficulties are greater than for the usual two centre expansion because three centre integrals have to be calculated, instead of only two centre integrals for the exchange matrix elements. For H^{+} impact energies between 2 keV and 20 keV the five state three-centre expansion were almost identical to those from the fourteen pseudostate expansion of Cheshire et al. (1970), for the total charge exchange probability for 3° scattering. The three centre expansion also gave the cross section for charge transfer into the 1s state at 10 keV as $8.6\ \pi a_o^2$ compared to the experimental value of $8.2\ \pi\ a_o^2$ and the value of $3.4\ \pi a_o^2$ which is obtained when the united atom orbital is omitted from the expansion. However, not enough results were obtained to suggest whether the three-centre expansion converges more rapidly than the usual two centre pseudostate expansion. We shall now consider how the continuum is represented in the three centre expansion. It is clear that any orbitals placed upon the internuclear midpont in the three centre expansion cannot contribute to either the direct or exchange bound channels as $t \to \infty$ and

hence all the electronic flux into these orbitals can be considered as representing ionisation. We note, however, that the expectation energy of these orbitals does not have to be positive in order that they represent the continuum. However, if these same orbitals were placed upon either of the centres A or B, then because they would in general overlap with the bound states corresponding to that centre, the flux into these orbitals represents a combination of possible transitions. However the triple centre expansion may be able to represent processes that would otherwise require a much larger two centre expansion to model them. It is clear that in order to represent a single s state placed upon the internuclear midpoint requires many states, including angular momentum greater than zero, to be placed upon either nuclear centre. A similar point was made in Section (2.4.5). Further motivation for using three centre approach to represent the continuum through the use of united atom orbitals on the third centre was given by Antal, McElroy and Anderson (1975). They considered the use of correlation diagrams, as described in Section (2.4.7), and showed that the introduction of a single united atom orbital placed at the internuclear midpoint could dramatically improve the energy obtained (as a function of internuclear distance) for the H_2^+ molecular ion as compared to a simple LCAO approximation which retains only the hydrogenic 1s function on both nuclear centres. They then proposed that the correlation diagrams suggest the major pathways that the

charge exchange reactions

$$H^+ + H(1s) \rightarrow H(2s) + H^+ \qquad (2.4.50)$$

and $$H^+ + H(1s) \rightarrow H(1s) + H^+ \qquad (2.4.51)$$

proceed along, via intermediate united atom and molecular orbitals. Thus the three centre expansion as proposed by Antal et al. is closely related to the united atom approach of Fritsch and Lin which was described in Section (2.4.7). Lin, Winter and Fritsch (1982) investigated the three centre approach for $H^+ + H(1s)$ collisions using only the hydrogenic 1s functions on the nuclear centres and the united atom $He^+(1s)$ state placed upon the internuclear midpoint, in order to assess the improvement this produces over the two-state approximation which neglects the $He^+(1s)$ state. They also used a basis consisting of the hydrogenic 1s state and an orthonormalized $He^+(1s)$ state placed upon each nuclear centre. The impact parameter probability distributions for charge transfer into the H(1s) state for all three basis sets were very similar at an H^+ impact energy of 25 keV but the three centre expansion gave increasingly different results for small impact parameters (less than 1 a.u.) as the energy decreases. Since small impact parameters only contribute a small amount to the total integrated cross section then a more sensitive test is required to

differentiate between different theoretical models, such as the 3^{o} scattering data of Helbig and Everhart (1965) previously referred to. Both expansions which included the united atom orbitals gave very similar results and predicted the maxima and minima in the total charge transfer probability more accurately than the simple two-state approximation. The largest calculations so far attempted in the three centre approximation were made by Winter and Lin (1984) in a treatment of ionisation in low energy $H^{+} + H$ collisions. In particular they attempted to take into account the Wannier mechanism in which the electron will not be removed in a slow collision unless it is asymptotically at the point of unstable equilibrium between the colliding nuclei. That is to say the electron must move along the equipotential point (the internuclear midpoint for $H^{+} + H$ collisions) as the two nuclei slowly separate in order to become free. The first order perturbation calculation, within a molecular basis, of Sethuraman, Thorson and Lebeda (1973) showed that gerade states have contributed less than 0.2% to ionisation for H^{+} impact energies between 0.1 keV and 0.5 keV. Winter and Lin therefore mainly considered an ungerade basis expansion and found that the minimum size basis consisted completely of bound states as follows:
all ungerade combinations of hyrogenic exact states up to n = 3 were used on each proton centre (i.e. a combined total of ten states on both centres) and the united atom He^{+} states with symmetry $2p_{\sigma,1}$, $3p_{\sigma,1}$, $4p_{\sigma,1}$ and $4f_{\sigma,1,2,3}$ on

the third centre at the internuclear midpoint. Therefore only the states upon the third centre could give any continuum contribution in the collision process. Winter and Lin checked the convergence of the expansion by the addition of further ungerade combinations of s and p states on the nuclear centres, A and B, with positive expectation energies such that they represented the low energy region of the continuum. At impact energies between 1.563 keV and 11.11 keV these changed the maximum values of bP(b) (where P(b) is the total ionisation probability at an impact parameter value b) by about 15%. It was also found that a three centre expansion using gerade combinations of states was less reasonably converged with respect to the addition of similar s and p gerade combinations of states upon centres A and B, but the change in the gerade probability was only about 10% of the ungerade total ionisation probability at an energy of 11 keV.

Thus the conclusion was that at these energies the bound united atom orbitals upon the equipotential point are the primary ionisation channels. Further tests, involving the addition of further p and f united atom states to the third centre suggested that the initial basis had converged to within 20% or so, as far as the ionisation probability was concerned. The final ionisation cross sections from the three centre expansion were an improvement over the existing pseudostate calculations of Fritsch and Lin (1983a) at the lowest energies where the experimental data for ionisation

of Fite, Stebbings, Hummer and Blackman (1960) is available. Fritsch and Lin used a two centre pseudostate basis with eight s and six p states upon each proton centre. They underestimate the lower experimental error limit by a factor of four, whereas this limit is "only" 46% above the value from the three centre expansion. At the highest energy considered, which is 15 keV, the three centre expansion is about 50% above the value of the two centre expansion but uncertainty in the normalisation of the experimental data available makes comparison difficult. However, this work shows that up to impact energies of 15 keV the fundamental ionisation mechanism is probably due to continuum states localized near the equipotential point and can be intrinsically represented by the three centre expansion whereas it is difficult to account for this using only a reasonably large two centre expansion.

We have described in this section how the continuum may best be represented in the low energy collision region, through the introduction of a third expansion centre motivated by the Wannier approach to ionisation. In the next section we shall consider another approach motivated by the high energy behaviour of the ionisation and excitation cross sections.

2.4.9 Oscillator strengths and the dipole approximation close coupling method.

In the previous section we have considered how an approach to the representation of the continuum is suggested in the low energy collision region through the use of wavefunctions attached to a third centre. However, for the case of intermediate and high collision energies another approach is more appropriate. In order to investigate this we shall initially consider the case of a bare ion of nuclear charge Z, denoted by A^{Z+}, colliding with a single active electron atom, in a reaction of the type

$$A^{Z+} + B \rightarrow A^{Z+} + B^{*} \qquad (2.4.52)$$

where the target atom, B, is left in an excited state. In the usual impact parameter approximation the corresponding time dependent ion-atom interaction will be of the form

$$V(\vec{r}_B, \vec{R}(t)) = - \frac{Z}{|\vec{R}(t) - \vec{r}_B|} \qquad (2.4.53)$$

where $\vec{r}_B$ and $\vec{R}(t)$ are shown in figure (2.2)

The relative velocity of A and B is V. The time dependent potential given by expression (2.4.53) can be

expanded as follows (Weissbluth 1978)

$$V(\vec{r}_B, \vec{R}(t)) = -Z \sum_{\ell=0}^{\infty} \frac{r_<^{\ell}}{r_>^{\ell+1}} P_{\ell}(\cos\omega) \qquad (2.4.54)$$

where $r_<$ is the smaller of the two quantities $|\vec{R}(t)|$ and $|\vec{r}_B|$, and $r_>$ is the larger of the same two quantities. $P_{\ell}(\cos w)$ is the Legendre polynomial of degree ℓ and argument cos w, where w is the angle between the unit vectors in the directions of $\vec{R}(t)$ and $\vec{r}_B$. Since $P_0(\cos w) = 1$ and $P_1(\cos w) = \cos w$ then we can rewrite expression (2.4.54) as follows

$$V(\vec{r}_B, \vec{R}(t)) = -Z \left(\frac{1}{R(t)} + \frac{r_<}{r_>^2} \cos\omega + \ldots \right) \qquad (2.4.55)$$

In the region of space where $R(t) > r_B$ then the expression (2.4.55) becomes

$$V(\vec{r}_B, R(t)) = -Z \left(\frac{1}{R(t)} + \frac{\vec{r}_B \cdot \vec{R}(t)}{|\vec{R}(t)|^3} + \ldots \right) \qquad (2.4.56)$$

Janev and Presnyakov (1980) have considered a model where only the first two terms in expression (2.4.56) are retained in the impact parameter approximation. The first term in expression (2.4.56) can be neglected as it depends only upon

the internuclear separation, R(t).

For the case of excitation they retained only the initial and final states in the expansion basis. However for the case of ionisation they introduced a third state to account for the effect of transitions into the continuum through intermediate discrete states. The approximation based upon the second term of expression (2.4.56) is known as dipole-approximation close coupling (denoted by the initials DACC) theory.

In the case of excitation from an initial s state, $|ns\rangle$, into a final p_o state, $|n'p_o\rangle$, or p_1 state, $|n\ p_1\rangle$, the following set of coupled equations are obtained for the corresponding occupation amplitudes which we denote by a, b_o and b_1;

$$i\frac{da}{dt} = \frac{Z\lambda}{R^2}\left(b_o\cos\theta + b_1\sin\theta\right)\exp(-i\omega t) \qquad (2.4.57)$$

$$i\frac{db_o}{dt} = \frac{Z\lambda}{R^2}\cos\theta\,\exp(i\omega t)\,a \qquad (2.4.58)$$

$$i\frac{db_1}{dt} = \frac{Z\lambda}{R^2}\sin\theta\,\exp(i\omega t)\,a \qquad (2.4.59)$$

$$\cos\theta = \frac{vt}{R} \qquad (2.4.60)$$

$$\sin\theta = \frac{b}{R} \tag{2.4.61}$$

$$\lambda = (f_{01}/2\omega)^{1/2} \tag{2.4.62}$$

where f_{01} is the oscillator strength for the transition between the s and the p states and ω is the energy difference between the s and p states involved. The quantities vt and b are defined in figure (2.2). The oscillator strength for the transition between an s and a p type state is given by the formula (Bethe and Saltpeter 1977)

$$f_{01} = 2\omega |\langle n'P_0 | r\cos\theta | nS \rangle|^2 \tag{2.4.63}$$

The coupled equations (2.4.57) to (2.4.59) are solved subject to the usual boundary conditions, $a(-\infty) = 1$ and $b_{0,1}(-\infty) = 0$. The solution is found by transforming to the new set of variables $K_i(t) = -ib_i(t)/a(t)$ (Presnyakov 1964) and then solving for the functions $K_i(t)$ by the method of Vainshtein, Presnyakov and Sobel'man (1962). The resulting probability for the $ns \rightarrow n'p$ transition is given by W(b) where

$$W(b) = W_0(b) + W_1(b) \tag{2.4.64}$$

$$W_0(b) = |b_0(+\infty)|^2 = \frac{P_0}{1 + P_0 + P_1} \tag{2.4.65}$$

$$W_1(b) = |b_1(+\infty)|^2 = \frac{P_1}{1 + P_0 + P_1} \tag{2.4.66}$$

$$P_0 = \left(\int_{-\infty}^{\infty} dt \; \frac{z\lambda v t}{R^3} \sin\left\{ \int_0^t \left[w^2 + 4\left(\frac{z\lambda}{R^2(t')}\right)^2 \right]^{1/2} dt' \right\} \right)^2 \tag{2.4.67}$$

$$P_1 = \left(\int_{-\infty}^{\infty} dt \; \frac{z\lambda b}{R^3} \cos\left\{ \int_0^t \left[\left(\frac{w}{2}\right)^2 + \left(\frac{z\lambda}{R^2(t')}\right)^2 \right]^{1/2} dt' + \frac{wt}{2} \right\} \right)^2 \tag{2.4.68}$$

The transition probability given by expression (2.4.64) has the important property that it is properly normalized and has non-singular behaviour as $b \to 0$. Janev and Presnyakov introduced the scaling transformation

$$b = \frac{z\lambda}{v} y \tag{2.4.69}$$

$$vt = \frac{z\lambda}{v} x \tag{2.4.70}$$

and the dimensionless parameter β where

$$\beta = \frac{z\lambda w}{v^2} \tag{2.4.71}$$

Then after integrating W(b) over all impact parameters the

following expression is obtained for the excitation cross section, σ_{exc},

$$\sigma_{exc} = 2\pi \left(\frac{z\lambda}{\omega}\right) D(\beta) \qquad (2.4.72)$$

where

$$D(\beta) = \beta \int_0^\infty y\,dy \, \frac{P_0(y,\beta) + P_1(y,\beta)}{1 + P_0(y,\beta) + P_1(y,\beta)} \qquad (2.4.73)$$

For values of $\beta << 0.01$, which corresponds to the region where the Born approximation is valid, the excitation cross section has the approximate form

$$\sigma_{exc}^{Born} = 8\pi \left(\frac{z\lambda}{v}\right)^2 \ln\left(\frac{1.4\,v^2}{z\lambda\omega}\right) \qquad (2.4.74)$$

This expression for the excitation cross section can also be found from the general Bethe-Born theory (Landau and Lifschitz 1977). From the expression (2.4.77) it is found that the excitation cross section reaches its maximum for $\beta_{max} = 0.28$ which corresponds to a collision velocity given by

$$v_{max} \simeq 1.89\,(z\lambda\omega)^{1/2} \qquad (2.4.75)$$

and the corresponding maximum cross section is given by

$$\sigma_{exc,max} \simeq 0.82 \frac{\pi Z \lambda}{\omega} \qquad (2.4.76)$$

Thus the position of v_{max} scales as $Z^{1/2}$ whereas the cross section maximum depends linearly upon Z. Janev and Presnyakov then proposed to calculate the ionisation cross section in a similar fashion to the excitation cross section. To do this they introduced the idea of a single pseudostate with an energy corresponding to zero, and an oscillator strength, f_{cont}, equal to the total oscillator strength for transitions between the initial state of the system and the complete set of continuum states. Thus f_{cont} is defined as follows

$$f_{cont} = \frac{2}{3}(E_f - E_i)\int_0^\infty |\langle \psi_{Ep}(\vec{r}) | r | \psi_{ns}(\vec{r}) \rangle|^2 \qquad (2.4.77)$$

where $\psi_{Ep}(\vec{r})$ is a suitably normalized continuum state and $\psi_{ns}(\vec{r})$ is the initial state of the system. A further factor, S, is introduced here to allow for the fact that transitions into the continuum occur through higher multipoles than the dipole term in the potential and thus the important quantity is the effective oscillator strength, f_{eff}, defined by

$$f_{eff} = S f_{cont} \qquad (2.4.78)$$

This concept of an effective oscillator strength was first

introduced by van Regemorter (1962) in a perturbational approach to electron-atom collision.

The numerical values of S and f_{cont} have to be found by quantum-mechanical calculations, as shown in Vainshtein, Sobelman and Yakov, 1979. For the case of hydrogen we have $f_{cont} = 0.4350$ and $S = 1.5$. Thus the same equations as were used in the case of discrete excitation can now be used to treat ionisation. The parameter λ given by expression (2.4.62) is now given by

$$\lambda_{eff} = \left(\frac{f_{eff}}{2 w_{ion}} \right)^{1/2} \qquad (2.4.79)$$

where w_{ion} is the ionisation potential of the atom. The ionisation cross section is given by the expression (2.4.72) with the appropriate values of β_{eff} obtained from expression (2.4.71), that is

$$\beta_{eff} = \frac{2 \lambda_{eff} w_{ion}}{v^2} \qquad (2.4.80)$$

Janev and Presnyakov used this method to calculate the ionisation cross section for the reaction

$$H^+ + H(1s) \rightarrow H^+ + H^+ + e \qquad (22.4.81)$$

Their results were in reasonable agreement with experiment for H^+ impact energies between 5 keV and 500 keV except

around the cross section maximum. The theory consistently underestimated experiment because of the neglect of transitions into the continuum through intermediate discrete states. Janev and Presnyakov estimated the contribution of the two step processes represented by transitions from the 1s state into the 2p state (the dominant excitation state) and then into either the s or d continuum states using the same dipole approximation close coupling theory and obtained the following expression for the total ionisation cross section

$$\sigma_{ion} = 2\pi Z \left(\frac{\lambda_{eff}}{\omega_{ion}} D(\beta_{eff}) + \frac{1}{8} \frac{\lambda_{or}}{\omega_{or}} D(\beta_{or}) \right) \quad (2.4.82)$$

where the first term comes from transitions directly into the p pseudostate, and the second term represents the intermediate transitions contribution via the so called intermediate resonant state. The parameters λ_{or}, and β_{or} in expression (2.4.82) are the quantities corresponding to expressions (2.4.62) and (2.4.71) for the ground to intermediate state transition. Similarly w , in expression (2.4.82) is the energy difference between the intermediate and ground states. The function D is defined as before by expression (2.4.73). The second term in expression (2.4.82) due to the intermediate state was found to contribute a maximum of 20% to the total cross section around the maximum. For $v<<1$ or $v>>1$ only direct transitions

represented by the first term are important. It was found that the inclusion of the intermediate state contribution improved the agreement of the theory with experiment for reaction (2.4.81). The inclusion of intermediate states other than the 2p state was estimated to contribute less than 5% to the total ionisation cross section. Encouraged by the initial good agreement of their method with experiment Janev and Presnyakov also used the intermediate state version of the DACC method to calculate the ionisation of helium by bare ions, A^{Z+}, with nuclear charge $2<Z<32$, and their results were again in good agreement with the experimental data of Hvelplund, Haugen and Knudsen (1980) and Haugen et al. (1982). However, similar DACC calculations for the ionisation of hydrogen by bare ions, A^{Z+}, with $2<Z<32$, show significant disagreement by a factor of approximately two at the cross section maximum, when the data is plotted in a reduced representation (Janev and Hvelpund 1981) against the data of Shah and Gilbody (1981a, 1981b, 1982). This disagreement occurs for ion impact energies of less than 200 keV/amu/Z in the reduced representation. However, in this region it is known that the capture into continuum states contributes significantly to the ionisation of hydrogen by protons (Shakeshaft 1978), and this is a process evidently not accounted for by the DACC method, but may be important in other collision systems also. This suggests that the close agreement of experiment with the DACC theory applied to the ionisation of hydrogen

by protons is somewhat fortuitous rather than being the result of any completely correct theory. The basic idea of the DACC method is however a very reasonable one, namely that the oscillator strengths for certain transitions should be used to select the pseudostate basis in order to calculate ionisation. This approach was considered in the work of Bransden, Noble and Chandler (1982) who investigated the collision systems He^{2+} + H(1s) and H^{+} + He^{+}(1s). The pseudostates that were used in these calculations were based upon the pseudostates used by Callaway and Wooten in their investigation of electron-hydrogen scattering. These pseudostates were discussed in Section (2.4.3) and by correctly scaling the basis parameters they can be used on either the H centre or the He^{+} centre. Firstly we shall consider the results for the excitation of H(1s) by He^{+} impact. Bransden et al. used various basis sets on both atomic centres in order to estimate the region of validity of the DACC method. The smallest basis consisted of the hydrogenic 1s and $2p_{0,1}$ states on the hydrogen target with no diagonal interactions, which is the starting point from which Janev and Presnyakov derive their DACC theory. The largest basis consisted of the Callaway and Wooten pseudostates placed upon the hydrogen target with the exact 1s, 2s and 2p states upon the He^{2+} projectile.

The results for excitation of the n = 2 states of hydrogen indicate that an approximation which retains only the 1s and 2p target states is not accurate below He^{2+}

impact energies of 1000 keV or so. This is well above the region where Janev and Presnyakov applied their DACC model for excitation. From an analysis of their own results, Janev and Presnyakov concluded that it was accurate to within a factor of two below the cross section maximum but should improve in the higher energy region. We shall now compare the DACC and close coupled results for excitation. From equation (2 .4.75) the cross section maximum in the DACC model for excitation of H(2p) by He^{2+} occurs at a velocity given by

$$v_m = 1.89 \, (z \lambda_{2p} \omega_{2p})^{1/2} \qquad (2.4.83)$$

where from equation (2.4.57) we find that

$$\lambda_{2p} = 0.745 \qquad (2.4.84)$$

Hence $v_m = 1.89*(2*0.745 \times 0.375)^{1/2} = 1.41$ a.u. which corresponds to an He^{2+} impact energy of 200 keV. Bransden et al. calculated that the H(2p) excitation cross section obtained by using the 1s and $2p_{0,1}$ target basis (with no diagonal interactions) and also using the Callaway-Wooten pseudostates on the target has the respective values of 5.2×10^{-16} cm^2 and 1.67×10^{-16} cm^2 at an He^{2+} impact energy of 100 keV, and the corresponding values of 3.27×10^{-16} cm^2 and 2.15×10^{-16} cm^2 at an impact energy of 500 keV. These results show that the DACC approach for excitation may be

quite unreliable around the cross section maximum. The case of ionisation for the same reaction will now be discussed. The cross sections for the ionisation were obtained, from the basis consisting of the Calloway-Wooten pseudostates upon the target, by simply considering the flux into the positive energy pseudostates as representing ionisation and thus no projection method was used (as was described in Section (2.4.6)). The Callaway-Wooten pseudostate basis has two s states, two p states and a single d state lying in the continuum energy range (that is with positive expectation energies). In the spirit of the DACC approach the oscillator strengths of these states can be computed. The oscillator strength sum for transitions from the H(1s) state into all the p pseudostates is found to be equal to 0.996 as compared to the exact value of 1.000, as given by Cowan 1982. The sum of the oscillator strengths for the p pseudostates lying in the continuum is 0.51 as compared to the exact continuum contribution of 0.44. Since the p pseudostate provides the largest contribution to the ionisation cross section this suggests that simply taking the flux into the positive energy p states as representing ionisation may be an overestimate of the true continuum contribution.

Similarly the positive energy s pseudostates overestimate the exact continuum oscillator strength but this is only a small contribution to the total for all the s states and is probably not very important. However the d

pseudostates significantly overestimate the positive energy contribution although the total d state oscillator sum is equal to the exact value, the calcuated and exact values for transitions from the 2p state into the continuum being 0.41 and 0.18 respectively.

The results obtained by Bransden et al. for ionisation using this basis were in reasonable agreement with the experimental data of Shah and Gilbody (1981a), above He^{2+} impact energies of 400 keV, where they overestimated experiment by about 25%. Below this energy charge exchange channels, which were not included, would reduce the cross section and improve the agreement with experiment. As stated previously in this section, the DACC results underestimate the experiment by about 50% at the maximum and approach the experimental data more slowly than the close coupled results as the collision energy increases.

The general conclusion as far as ionisation is concerned is that the use of a relatively small basis with reasonably accurate oscillator strengths sums for certain transitions can produce ionisation cross sections of the correct order, while the DACC method is rather less successful, probably because of the neglect of transitions between states not included in the theory.

In this section we have discussed how it is possible to base the choice of pseudostates, chosen to represent the continuum, upon the idea of either effective oscillator strengths (as in the DACC method) or by using oscillator

sums for certain explicit transitions to suggest whether the basis is a reasonable choice or not. These ideas will be reconsidered later in this thesis because the choice of pseudostates for the calculations to be presented was based upon a similar line of reasoning, and this section shows that there is some a priori justification for such a choice. In the next section we shall consider how ionisation cross sections have been calculated using a method which will provide further justification for one type of basis set used in the present calculations, separately from the results of this section.

2.4.10 The single centre expansion and related approaches to the calculation of ionisation.

In this section we shall discuss the use of certain basis expansions which have been designed specifically for the efficient numerical computation of ionisation of atoms by fully stripped ions. It is well known that for high collision energies the direct channels dominate the exchange channels and the cross sections for direct excitation and ionisation can be obtained using the Born Series expansion. This is discussed for example in McDowell and Coleman (1970) and by Inokuti (1971). We note that for very highly charged ions relativistic effects become important before the Born approximation is valid, except possibly for the excitation of low lying excited states. The fact that the direct channels only remain important for high collision velocities follows from the observtion that the exchange matrix

elements defined in expressions Section (2.3.3) contain the oscillatory factor exp($\pm$iv.r) which will dramatically reduce their value for high values of v. Therefore it is completely reasonable to make an atomic expansion about the target centre only and to neglect all charge exchange channels in the usual impact parameter approximation. This type of expansion is called a one-centre expansion (which we shall denote by OCE). Fitchard, Ford and Reading (1977) used an expansion of this type consisting of ten s states, eleven p states and seven d states, with expectation energies representing both bound and continuum states, centred upon the target in calculations for protons colliding with hydrogen atoms. When summed over all magnetic quantum numbers their final basis included fifty-three states on the target, which presented a formidable numerical calculation. However because there were no exchange matrix elements to compute they could solve the problem efficiently using their time-development U-matrix method, first used by Zimmerman (1972) and subsequently by Shakeshaft (1976). The ionisation cross sections were obtained by summing over all states except those that represented exact bound states, with the condition that bound states which were not well represented had small excitation cross sections. The fifty three state basis contained a total of twenty-two bound states and thirty-one states representing the continuum with all n = 2 and n = 3 states represented. The ionisation results were

corrected to allow for angular momentum states with $l > 2$ by adding on the full first Born results obtained for all higher partial waves.

The results obtained for n = 2 and n = 3 excitation were in excellent agreement with experiment for impact energies above 50 keV. The same conclusion applied to the ionisation results. It is no surprise that below 50 keV the OCE fails at this energy when we consider the results from the large two centre expansion of Shakeshaft (1978). Shakeshaft calculated that at this energy the total charge exchange cross section is 9.2×10^{-16} cm^2 and the total excitation cross section is 11.0×10^{-16} cm^2. The separate contributions from direct ionisation and from the charge exchange into the continuum process are estimated from figure 5 of Shakeshafts paper to be respectively 8.9×10^{-16} cm^2 and 7.0×10^{-16} cm^2. Thus the exchange channels are effectively as important as the direct channels at this energy thus making the agreement of the OCE with experiment probably fortuitous as was the case with the DACC method described in the first section, for the same collision system, at low collision energies. For the case where the incident projectile has a much smaller charge, Z_A, than the corresponding target nucleus, Z_B, K-shell hole production in the target can be treated by using a large OCE in the projectile energy region $v < 1$, where v is the projectile laboratory velocity, as shown by Ford, Fitchard and Reading (1977). This was an extension of earlier work by Reading,

Ford and Fitchard (1976). Essentially the same approach was taken as in the calculation for proton-hydrogen collisions previously described. The incident projectile was taken as a proton and the target was a neutral atom with nuclear charge Z_B = 13 to 30. The target pseudostates were formed by diagonalization of the target Hamiltonian in a basis set of functions of the type

$$u_j(r) = r^{l} \exp(-c_l r / (a_n (1 - \alpha \exp i\phi_j))) Y_{lm}(\theta, \phi) \quad (2.4.85)$$

where ϕ_j are equally spaced in the interval 0 to 2π and a_n is the Bohr radius of the hydrogenic atom of charge Z_B. These functions can be shown to form a complete set. A large basis containing up to fifty four states with $0 < l < 2$ was used in the same U-matrix approach as in the previously proton-hydrogen calculation. However in this case only the first and second Born amplitudes were calculated and for consistency only terms to order Z_B^3 were retained in the final expressions, as was done by Holt and Moiseiwitch (1968). The results for K-shell hole production in nickel, titanium and aluminium by protons were typically 10% - 20% below experiment which could be due to uncertainty in the experimental normalization or due to the neglect of configuration-interaction wave functions. Ford et al. also concluded that they had calculated the ionisation contributions to an accuracy of 2% within the context of the independent particle model which they were using for the

K-shell. In an extension of the OCE approach, Reading et al. (1979) considered charge transfer by protons colliding with argon and fully stripped He, C and O ions colliding with copper. They demonstrated an important result concerning the continuum representation for the target atom. The charge transfer cross sections were obtained from a t-matrix approach using the solution of the Schrodinger equation from the OCE method, which is denoted by (r, t). Then the Schrodinger equation is of the form

$$i\frac{\partial}{\partial t}\psi^{+} = \left[-\frac{1}{2}\nabla^{2}_{\vec{r}_B} + u(\vec{r}_B) + W(\vec{R}) + V(\vec{r}_B - \vec{R}(t))\right]\psi^{+} \quad (2.4.86)$$

where $u(\vec{r}_B)$ is a single-electron Hartree-Fock potential representing the target atom, $W(\vec{R})$ is some internuclear potential function and $V(\vec{r}_B - \vec{R}(t))$ is the interaction between the projectile and target electron. Equation (2.4.86) is solved up to the terms representing the second Born approximation by a time-development operator approach using only target pseudostates in the expansion for $\psi^{+}(\vec{r}_B, t)$.

The T-matrix for charge transfer into a projectile state ϕ_{CT} is then given by an expression of the form

$$t_{CT} = \int_{-\infty}^{\infty} dt \; \langle \phi_{CT} | u + w | \psi^{+} \rangle \quad (2.4.87)$$

Reading et al. found that the charge transfer mechanism for K and L shell capture from target atoms with high nuclear charge by light ions was by a two stage process.

The target electron was initially excited into a target continuum state with an energy of approximately $\frac{1}{2}v^2$, where v is the projectile velocity relative to the target. Then the electron was captured by the projectile. If the diagonalization of the target basis states did not produce a pseudostate with an energy close to that needed in order to represent this process, then the important part of the continuum would not be well represented by that particular basis. As the size of the basis were increased the important energy region may or may not be well represented and convergence would be difficult to demonstrate. Reading and Ford (1979) however, had shown that it was possible to introduce the idea of energy intervals, Δ_n, to be associated with each positive energy pseudostate. By using this concept in the charge transfer calculations Reading et al. showed that it was possible to obtain converged results, when only s and p states were retained in the basis. We shall return to the idea of finding an energy interval for each pseudostate in Chapter 5 when we discuss the basis states used in the present calculations. We note that in the work of Reading et al., because the important energy in the continuum is dependent upon the projectile velocity, the pseudostates used to represent this must also be recalculated for each projectile energy.

These calculations were extended by Ford et al. (1979a, 1979b) who studied inner-shell charge transfer and ionisation in proton-argon collisions in the impact energy

range 1 MeV to 12 MeV. This work showed that it was necessary to include d states in the target expansion to obtain agreement with experiment for charge transfer while the ionisation results were virtually unchanged. Subsequently Becker et al. (1980) investigated collisions between He^{2+} and C^{6+} incident upon argon in the energy range 1 MeV to 9 MeV and agreement with experiment was obtained for K-shell ionisation and charge transfer by the C^{6+} ions. Other calculations of this type were made by Ford et al. (1981) for H^{+}, He^{2+} and Li^{3+} incident upon neon (0.4 - 4.0 MeV amu^{-1}) and upon carbon (0.2 to 2.0 MeV amu^{-1}).

Reading et al. (1981) made an interesting improvement to their usual one-centre expansion method to allow for the effects of the charge exchange channels, in a method called the one and a half centre expansion (denoted by OHCE), which we shall describe as it is similar to the approach adopted in some of the present calculations to be discussed in this thesis. A trial expansion is made of the following form

$$\psi_{OHCE}(\vec{r},t) = \sum_{j=1}^{J} a_j(t)\,\phi_j(\vec{r},t) + \sum_{K=1}^{K} c_K(t_L)\,f_K(t)\,\chi(\vec{r},t) \qquad (2.4.88)$$

where the first summation is of the usual form and is centred upon the target. The second summation includes pseudostates upon the projectile to represent the important charge exchange channels. The coefficients $C_K(t_L)$ are the unknown asymptotic occupation amplitudes for the charge

exchange channels, where t_L is some suitably large time which determines the end of the collision.

The functions $f_K(t)$ are restrained to satisfy the initial and final conditions.

$$f_K(t_L) \rightarrow 0 \quad , \quad t \rightarrow -\infty \tag{2.4.89}$$

$$f_K(t_L) \rightarrow 1 \quad , \quad t \rightarrow +\infty \tag{2.4.90}$$

Otherwise the form of $f_K(t)$ is arbitrary. The time dependent amplitudes $a_j(t)$ and the coefficients $c_K(t)$ are determined by applying the conditions that

$$\langle \Phi_j(\vec{r},t) \mid H_{el} - i\frac{\partial}{\partial t}_{\vec{r}} \mid \Psi_{OHCE}(\vec{r},t) \rangle = 0, \text{ for all } j. \tag{2.4.91}$$

and one of two possible sets of constraints:

$$\int_{-t_L}^{t_L} dt \; \langle \chi(\vec{r},t) \mid i\frac{\partial}{\partial t}_{\vec{r}} - H_{el} \mid \Psi_{OHCE}(\vec{r},t) \rangle = 0 \tag{2.4.92}$$

or

$$\int_{-t_L}^{t_L} dt \; f_K(t) \langle \chi(\vec{r},t) \mid i\frac{\partial}{\partial t}_{\vec{r}} - H_{el} \mid \Psi_{OHCE}(\vec{r},t) \rangle = 0 \tag{2.4.93}$$

Other constrations, apart from expressions (2.4.92) and (2.4.93) are possible. The use of expression (2.4.93) can be shown to conserve unitarity as in the usual two centre expansion and its use results in the unitary OHCE.

However, the use of expression (2.4.92) will in general result in a violation of unitarity for the final set of amplitudes and it gives rise to the perturbative OHCE. The final set of equations that determine the amplitudes are of the form of the usual first order differential equations that determine $a_j(t)$ coupled with algebraic inhomogenous equations for the $c_K(t_L)$ amplitudes. The advantage of the OHCE method over a similar two centre expansion is that it has a numerical efficiency similar to the single centre expansion but should give improved results, although not as accurately as those obtained from the two centre expansion in general. It should also overcome the formal difficulty of the two centre expansion which occurs as the basis sets on both centres are increased in size. Because they will not be linearly independent for small internuclear separations, the solution for the corresponding occupation amplitudes will become ill-conditioned. To test the OHCE method Reading et al. investigated proton-hydrogen collisions below 50 keV, where Fitchard et al. (1977) have shown a single centre expansion fails as was discussed earlier in this section. A comparison of the OCE, the unitary OHCE and the perturbative OHCE was made using a basis consisting of eight s states, eighteen p states and

twenty seven d states on the target and the H(1s) state on the projectile. Both the unitary OHCE and perturbative OHCE were in reasonable agreement with each other and with experiment for impact energies above 15 keV for n = 2 and n = 3 excitation and also for ionisation except near the cross section maximum. At this energy there is also fair agreement with the large two-centre calculation of Shakeshaft for both excitation and charge transfer into H(1s), although the ionisation cross sections are above Shakeshaft's by a factor of 1.9 from the perturbative OHCE, and by a factor of 3.5 for the unitary OHCE. However for an impact energy of 100 keV the corresponding ratios are both equal to 0.85. The ratio of the OCE ionisation cross section to the result of Shakeshaft is a factor of 10 at 15 keV and 0.92 at 100 keV. By comparison the first Born approximation of Bates and Griffing (1953) agrees with experiment only for impact energies above 60 keV. This is the energy at which Shakeshaft (1978) found the direct ionisation channel becomes more important than charge transfer into the continuum of the projectile. The conclusion is that the results of Reading et al. suggest their OHCE methods can be successfully extended into the low energy region where a priori justification is not evident, in a manner similar to the DACC method described in section (2.49), for the same collision system (H + H(1s)), but the final agreement with experiment is probably fortuitous.

Reading et al. (1981) and Ford et al. (1982) used the

perturbative OHCE to investigate the ionisation due to proton impact upon He^{2+} and $Li^{+,2+}$ respectively. In the case of protons colliding with He a total of fifty-four target states were used with $0 < \ell < 2$ and only the H(1s) state attached to the projectile. The total electron loss cross section, which is the sum of the calculated ionisation and charge transfer cross sections, was in agreement with experiment down to an impact energy of 80 keV. The comparison with the pure ionisation cross section obtained experimentally as the difference between electron loss and total charge transfer is less favourable possibly because the experimental charge transfer total is overestimated. However, the discrepancy could also be because the basis set used in the OHCE calculations was not large enough to ensure convergence, as it did not include states with values of angular momentum $\ell > 2$. To try to understand these results Ford et al. (1982) studied the more asymmetric system $H^{+} + Li^{+,2+}$ using the perturbative OHCE method.

In both calculations a total of fifty four target states with $0 < \ell < 2$ were used although the distribution of states over ℓ was not identical. As in previous calculations only the H(1s) states was retained upon the target. The two electron Li^{+} system was replaced by a localised Hartree-Fock potential of the form

$$U_L = -\frac{2}{r} - \exp(-3.3954r)/r \qquad (2.4.94)$$

This was used to obtain single electron probabilities which were consequently used in an independent electron model. The results for ionisation were in agreement with the experimental data of Sewell et al. (1980) except for the lowest impact energies below 100 keV where there are large experimental uncertainties. At E = 71keV amu the POHCE results were 28% below the Born ionisation results obtained with the same basis, (which included a contribution from f and g states). Again the experimental ionisation data was obtained as the difference between electron loss and electron capture. The agreement between the theoretical total capture cross section and experiment was particularly poor with theory underestimating experiment by almost a factor of two for impact energies between 70 keV and 253 keV, which is qualitatively the same as the case for $p + He^+$ previously mentioned.

However, their results were in agreement with continuum distorted-wave results of Banyard and Shirtcliffe (1979). The important conclusion, as far as the present work is concerned, is that a large basis set centred upon the target is capable of producing ionisation cross sections in harmony with experiment, in the energy range where the Born approximation is not accurate, and where capture is an important process also. However, this type of expansion can fail as the collision energy decreases as in proton-hydrogen collisions, where the basis must be extended to the projectile centre, to obtain accurate ionisation results. We

shall reconsider this method in Chapter 5 where we shall compare it with other methods of calculating ionisation used in the present work.

2.4.11 The classical method

It is possible to consider the collision system as a collection of various particles which obey the classical equations of motion and then to solve these and extract cross sections for the various processes by examining the final state of the system. The initial problem is to construct an adequate classical representation of the initial quantum-mechanical state of the target atom. This can be done, in the case of a multi electron atom, by using an effective potential which reproduces the experimental energy levels for instance in a single electron model. This leads to a microcanonical ensemble of initial orbits from which the initial conditions are selected at random. The effective three particle system is then described using Hamiltons equations for the coordinates and conjugate momenta. These equations are solved and a statistical analysis applied to the state of the system at a large finite time to obtain cross sections for ionisation, charge transfer and excitation. Each collision corresponds to a trajectory and as the number of trajectories increases the accuracy of the cross sections, in the particular model, increases also. This is the basis of the Classical Trajectory Monte Carlo (CTMC) method. In the context of ion-atom collisions it was first considered by Abrines and

Percival (1966) for the proton-hydrogen system. The method has also been applied to fully stripped ions with $1 < z$ 36 colliding with hydrogen. In the case of charge exchange, agreement with experiment was obtained in general when $v_e < v < 2v_e$ where v is the collision velocity and v_e is the target electron velocity. The results for ionisation are also in agrement with experiment over a limited energy range. In order to understand the energy regions in which the CTMC method can provide reasonable results for both total and partial capture cross sections, and for ionisation also, a detailed comparison with the semi-classical impact parameter method has been made, for the particular system He^{2+} + Li. The CTMC method that was used is based upon Peach et al (1985). The results of these comprehensive calculations are given in Ermolaev, Hewitt and McDowell (1987) and Ermolaev, Hewitt, Shingal and McDowell (1987) and will be discussed in Chapter 5. It is possible that such investigations will establish the CTMC method as an alternative to quantal-based methods under certain conditions where accuracy is less important than savings in computer time and memory. This completes the discussion of some of the methods that have been used in describing collision processes and in the next chapter we shall consider the impact parameter method as applied in the present work.

CHAPTER THREE

The two-centre pseudostate expansion method using the impact parameter formulation.

3.1 Introduction

In this chapter we shall discuss how the close-coupled equations given in section (2.3.3) were derived for the particular collision system that was studied in this thesis, that is the He^{2+} + Li system, and also consider the various numerical methods that were used to obtain the solutions. We shall precede this by describing how the lithium atom was represented by a single active electron approximation for both the K-shell and L-shell calculations that have been performed.

Firstly, however, we shall review the basic impact parameter formulation that has been used in the present calculations, and for convenience we shall collect together the important expressions that have been used.

3.2 The impact parameter equations

In the case of the single active electron approximation the impact parameter Schrodinger equation for the system comprising of the two heavy particles A and B and an

electron, e^-, has the form

$$\left(-\frac{1}{2}\nabla^2_{\vec{r}} + V_{eA} + V_{eB} - i\frac{\partial}{\partial t_{\vec{r}}} \right) \psi(\vec{r},t) = 0 \qquad (3.2.1)$$

as described in section (2.3.1). The potential functions between each pair of particles are as yet unspecified. We next make an expansion of $\psi(\vec{r},t)$ in terms of pseudostates, upon both centres A and B, where the pseudostates are obtained by a diagonalisation process using the isolated atom Hamiltonians corresponding to centres A and B which are given by $H_A = -\frac{1}{2}\nabla^2_{\vec{r}} + V_{eA}$ and $H_B = -\frac{1}{2}\nabla^2_{\vec{r}} + V_{eB}$ respectively.

In figure 3.1 since we have taken the origin to be the midpoint of the internuclear distance between A and B, the factor p in figure 2.2 is $\frac{1}{2}$ and the trial wave function $\psi_T(r,t)$ has the following form

$$\psi_T(\vec{r},t) = \sum_{j=1}^{M} b_j(t)\,\bar{\phi}^B_j(\vec{r}_B)\exp -i(\lambda_j t + \tfrac{1}{2}\vec{v}.\vec{r}. + \tfrac{1}{8}v^2 t) \qquad (3.2.2)$$
$$+ \sum_{K=1}^{N} a_K(t)\,\bar{\chi}^A_K(\vec{r}_A)\exp -i(\varepsilon_K t - \tfrac{1}{2}\vec{v}.\vec{r} + \tfrac{1}{8}v^2 t)$$

as described in section (2.3.3.). Because the pseudostates $\bar{\phi}^B_j(\vec{r}_B)$ and $\bar{\chi}_K(\vec{r}_A)$ are determined from a diagonalsation procedure some important results are satisfied which have been given in expressions (2.3.38), and (2.3.40). We now define

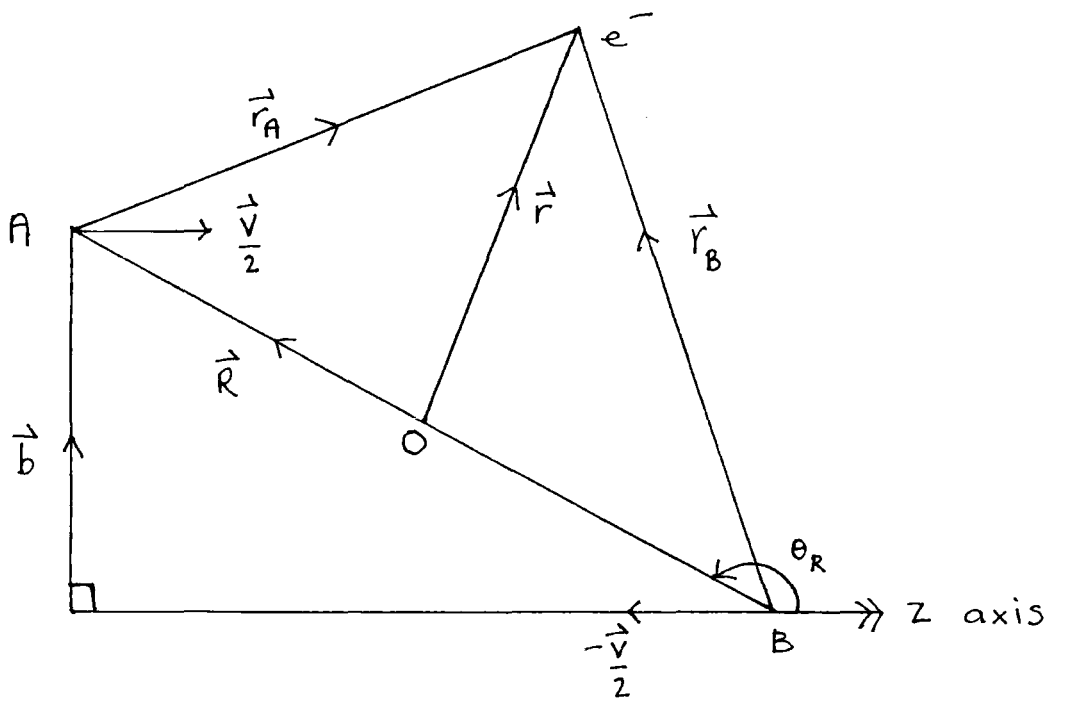

Figure 3.1

The coordinate system for straight line trajectories. O is the midpoint of AB.

$$\chi_K^A(\vec{r},t) = \bar{\chi}_K^A(\vec{r}_A)\exp(-i(\varepsilon_K t - \tfrac{1}{2}\vec{v}.\vec{r} + \tfrac{1}{8}v^2 t)) \qquad (3.2.3)$$

$$\phi_j^B(\vec{r},t) = \bar{\phi}_j^B(\vec{r}_B)\exp(-i(\lambda_j t + \tfrac{1}{2}\vec{v}.\vec{r} + \tfrac{1}{8}v^2 t)) \qquad (3.2.4)$$

Then the form of the close coupled equations obtained by projecting each $\chi_K^A(\vec{r},t)$ and $\phi_j^B(\vec{r},t)$ onto equation (3.2.1) is given by expression (2.3.54) which is equivalent to the equation

$$i\begin{pmatrix} \underset{\sim}{I} & \underset{\sim}{N} \\ \underset{\sim}{N}^{\dagger} & \underset{\sim}{I} \end{pmatrix}\dot{\underset{\sim}{A}}(t) = \begin{pmatrix} \underset{\sim}{H} & \underset{\sim}{K} \\ \bar{\underset{\sim}{K}} & \bar{\underset{\sim}{H}} \end{pmatrix}\underset{\sim}{A}(t) \qquad (3.2.5)$$

where $\underset{\sim}{I}$ is the usual unit matrix. The matrices $\underset{\sim}{N}$, $\underset{\sim}{H}$, $\underset{\sim}{K}$, $\bar{\underset{\sim}{H}}$ and $\bar{\underset{\sim}{K}}$ are defined by expressions (2.3.60) to (2.3.64). The column matrix $\underset{\sim}{A}(t)$ contains the time dependent amplitudes.

That is $\underset{\sim}{A}(t) = \begin{pmatrix} b_1(t) \\ \vdots \\ b_m(t) \\ a_1(t) \\ \vdots \\ a_N(t) \end{pmatrix}$ (3.2.6)

There are two distinct problems therefore which must be solved in order to obtain the final amplitudes, namely the evaluation of the individual matrix elements of the matrices in expression (3.2.5) and then the solution of these

equations to obtain $\underset{\sim}{A}(t)$. We shall now consider further the matrix elements and their evaluation.

Firstly the overlap matrix elements, N_{jK}, can be found using expressions (3.2.3) and (3.2.4) and have the form

$$N_{jK}(t) = \langle \bar{\phi}_j^B(\vec{r}_B) | e^{i\vec{v}.\vec{r}} | \bar{\chi}_K^A(\vec{r}_A) \rangle \exp -i(\varepsilon_K - \lambda_j)t \quad (3.2.7)$$

No further simplification is possible to this form for N_{jK} without making approximations. However, we note that in some calculations at low velocities it is possible to expand the oscillatory exponential term and retain only the first two terms. Next we consider the direct matrix elements, H_{jK} and $\bar{H}_{jK}$. Using expressions (2.3.38) and (2.3.40), (2.3.32) and (2.3.35) it is straightforward to show that the following results are obtained for these matrix elements:

$$H_{jK}(t) = \langle \bar{\phi}_j^B(\vec{r}_B) | V_{eA} | \bar{\phi}_K^B(\vec{r}_B) \rangle \exp i(\lambda_j - \lambda_K)t \quad (3.2.8)$$

$$\bar{H}_{jK}(t) = \langle \bar{\chi}_K^A(\vec{r}_A) | V_{eB} | \bar{\chi}_K^A(\vec{r}_A) \rangle \exp i(\varepsilon_j - \varepsilon_K)t \quad (3.2.9)$$

These matrix elements cannot be reduced any further. We shall now consider the exchange matrix elements defined by

expressions (2.3.63) and (2.3.64). The exact form for K is given by

$$K_{jk}(t) = \langle \bar{\phi}_j^B(\vec{r},t) \mid H_{el} - i\frac{\partial}{\partial t_{\vec{r}}} \mid \chi_K^A(\vec{r},t) \rangle \qquad (3.2.10)$$

Using the expressions in Section (2.3.3), and in particular (2.3.28), it follows that this can be rewritten as

$$K_{jk}(t) = \langle \bar{\phi}_j^B(\vec{r}_B) \mid e^{i\vec{v}.\vec{r}} \left(-\frac{1}{2}\nabla_{\vec{r}}^2 + V_{eA} + V_{eB} - \varepsilon_K\right) \mid \bar{\chi}_K^A(\vec{r}_A) \rangle \qquad (3.2.11)$$
$$\times \exp i(\lambda_j - \varepsilon_K)t$$

Similarly

$$\bar{K}_{jk}(t) = \langle \bar{\chi}_j^A(\vec{r}_A) \mid e^{-i\vec{v}.\vec{r}} \left(-\frac{1}{2}\nabla_{\vec{r}}^2 + V_{eA} + V_{eB} - \lambda_j\right) \mid \bar{\phi}_K^B(\vec{r}_B) \rangle \qquad (3.2.11a)$$
$$\times \exp -i(\lambda_K - \varepsilon_j)t$$

(3.2.11) is the exact form for K_{jk} but unfortunately it contains several terms due to the kinetic energy and potential operators, and these are in general time consuming to evaluate. Also the potential operators are restricted to a certain form if the matrix element is to be evaluated using the fourier transform method of Sin Fai Lam (1967), which

was written as a computer program by Noble (1980). This will be discussed again later on in this chapter.

Furthermore, for certain cases the potentials may not be in a suitable form for using in a calculation even though the wavefunctions are known.

It is desirable therefore, to try to simplify the complicated form for K_{jK} given in expression (3.2.11). Firstly if $\bar{X}_K^A(\vec{r}_A)$ is an eigenfunction of the projectile Hamiltonian then the following relation is true:

$$\left(-\tfrac{1}{2}\nabla_{\vec{r}}^2 + V_{eA} - \mathcal{E}_K\right)\bar{X}_K^A(\vec{r}_A) = 0 \qquad (3.2.12)$$

Similarly if $\bar{\phi}_j^B(\vec{r}_B)$ is an eigenfunction of the target Hamiltonian then it follows that

$$\left(\tfrac{1}{2}\nabla_{\vec{r}}^2 + \lambda_j\right)\bar{\phi}_j^B(\vec{r}_B) = V_{eB}\,\bar{\phi}_j^B(\vec{r}_B) \qquad (3.2.13)$$

Then using expressions (3.2.12) and (3.2.13) the exact form for K_{jK} can be rewritten as follows:

$$\begin{aligned} K_{jK}(t) &= \langle \bar{\phi}_j^B(\vec{r}_B) \,|\, e^{i\vec{v}\cdot\vec{r}} V_{eB} \,|\, \bar{X}_K^A(\vec{r}_A)\rangle \\ &\quad \times \exp i(\lambda_j - \mathcal{E}_K)t \\ &= \langle (\tfrac{1}{2}\nabla_{\vec{r}}^2 + \lambda_j)\bar{\phi}_j^B(\vec{r}_B) \,|\, e^{i\vec{v}\cdot\vec{r}} \,|\, \bar{X}_K^A(\vec{r}_A)\rangle \\ &\quad \times \exp i(\lambda_j - \mathcal{E}_K)t \end{aligned} \qquad (3.2.14)$$

Similarly the exchange matrix element $\bar{K}_{jK}$ defined by

expression (2.3.64) can be rewritten in the following form, by using expressions (3.2.12) and (3.2.13),

$$\bar{K}_{jK}(t) = \langle \left(\tfrac{1}{2}\nabla^2_{\vec{r}} + \varepsilon_j\right)\bar{\chi}^{A}_{j}(\vec{r}_A) \mid e^{-i\vec{v}.\vec{r}} \mid \bar{\phi}^{B}_{K}(\vec{r}_B)\rangle \times \exp i(\varepsilon_j - \lambda_K)t \qquad (3.2.15)$$

The potential operators do not therefore appear explicitly in the exact expressions for K_{jK} and $\bar{K}_{jK}$ given above. This approach was used by Ermolaev, Noble and Bransden (1982) in calculations of charge exchange between Cs^+ and Cs^+ ions, where the wave functions were analytic Hartree-Fock orbitals obtained from Sachdeva and Puri (1976). However, we emphasise that the expressions (3.2.14) and (3.2.15) above are exactly equal to the expressions (2.3.63) and (2.3.64) only for the case where both $\bar{\phi}^{B}_{j}(\vec{r}_B)$ and $\bar{\chi}^{A}_{K}(\vec{r}_A)$ are eigenfunctions of the isolated Hamiltonians as defined by equations (3.2.13) and (3.2.12). It follows that for the case where either $\bar{\phi}^{B}_{j}(r_B)$ or $\bar{\chi}^{A}_{K}(\vec{r}_A)$ is not an eigenfunction, then either equation (3.2.12) or equation (3.2.13) is not satisfied exactly. For example an L^2 pseudostate with a positive expectation energy can never satisfy an eigenvalue equation as it has the incorrect boundary conditions for $r \to \infty$. Subsequently since both (3.2.12) and (3.2.13) have been used in obtaining equations (3.2.14) and (3.2.15), for K_{jK} and $\bar{K}_{jK}$, these matrix elements are approximations to the exact values of K_{jK} and $\bar{K}_{jK}$ obtained from expressions (3.2.11) and (3.2.11a). However, it is clear that the form

of the matrix elements in expressions (3.2.14) and (3.2.15) are considerably simpler than those given in expressions (3.2.11) and (3.2.11a) as the former pair do not involve the potential operators V_{eA} and V_{eB} and hence are both easier to program on the computer and also faster to evaluate. The price to be paid for this advantage is that there will be an uncertainty in the exchange matrix elements involving at least one pseudostate upon either centre, and therefore an associated error in all the amplitudes obtained from such a calculation. In order to test the effect of using the exchange matrix elements evaluated from expressions (3.2.14) and (3.2.15) some initial calculations were made using both of the forms for K_{jK} and $\bar{K}_{jK}$ as given in expressions (3.2.14), (3.2.15), (3.2.11) and (3.2.11a). The results from these calculations will be discussed in the final chapter containing the results of the present calculations.

In this section we have so far considered the form of the close-coupled equations and the matrix elements which are necessary in order to solve them. We shall conclude by describing the basis sets used in obtaining the pseudostates $\bar{\phi}^{B}_{j}(\vec{r}_{B})$ and $\bar{\chi}^{A}_{K}(\vec{r}_{A})$ needed in expression (3.2.2) for the trial function. It is both numerically and physically appropriate to use pseudostates constructed from basis functions which contain Slater-type orbitals (STO's) which have the general form $r^{n} e^{-\alpha r}$. Thus a typical pseudostate, denoted by ψ_{nlm} has the following form

$$\psi_{n\ell m}(\vec{r}) = R_{n\ell}(r)\,\bar{Y}_{\ell m}(\theta,\phi) \tag{3.2.16}$$

The $R_{n\ell}(r)$ functions for given values of n and ℓ are given by

$$R_{n\ell}(r) = \sum_{i=1}^{N} c_i\, r^{n(i)}\, e^{-\alpha_i r} \tag{3.2.17}$$

where C are coefficients. The $\bar{Y}_{\ell m}(\theta,\phi)$ functions are defined by $(m \geq 0)$

$$\bar{Y}_{\ell m}(\theta,\phi) = N_m \left[Y_{\ell m}(\theta,\phi) + Y^{*}_{\ell m}(\theta,\phi) \right] \tag{3.2.18}$$

where

$$N_m = \frac{1}{\sqrt{2}} \quad \text{if} \quad m > 0 \tag{3.2.19}$$

$$N_m = \frac{1}{2} \quad \text{if} \quad m = 0 \tag{3.2.20}$$

The spherical harmonics $Y_{\ell m}(\theta,\phi)$ are given by $(m \geq 0)$

$$Y_{\ell m}(\theta,\phi) = (-1)^m \left[\frac{(2\ell+1)\,(\ell-m)!}{4\pi\,(\ell+m)!} \right]^{1/2} P_\ell^m(\cos\theta)\, e^{im\phi} \tag{3.2.21}$$

where $P_\ell^m(\cos\theta)$ are associated Legendre functions. The $(-1)^m$ phase factor is the same as in the Condon-Shortley phase convention. We note that since the initial state on the target, which is an s state, has a definite symmetry under reflection in the collision plane (the x-z plane in figure

2.2) only states with the same symmetry need to be considered in the calculation (Geltman, 1969). This is why the real spherical harmonics defined in expression (3.2.18) are chosen. For example, in order to represent a d state with $\ell = 2$, we only need to include pseudostates with the angular functions $\bar{Y}_{20}$, $\bar{Y}_{21}$ and $\bar{Y}_{22}$ in the trial function. We note that the normalisation conditions for the pseudostate $\psi_{n\ell m}(\vec{r})$ require that

$$\int_0^\infty R^2_{n\ell}(r)\, r^2\, dr = 1 \qquad (3.2.22)$$

and

$$\int_{\text{all } \Omega} d\Omega\ \bar{Y}^2_{\ell m}(\theta, \phi) = 1 \qquad (3.2.23)$$

We can now write the real spherical harmonics as follows

$$\bar{Y}_{\ell m}(\theta,\phi) = N_m\, C_{\ell m}\, P_\ell^m(\cos\theta)\cos m\phi \qquad (3.2.24)$$

where $C_{\ell m}$ is defined by

$$C_{\ell m} = 2\,(-1)^m \left[\frac{(2\ell+1)\ (\ell-m)!}{4\pi\ (\ell+m)!}\right]^{1/2} \qquad (3.2.25)$$

Thus we can write the trial pseudostates on centres A and B in the following form

$$\bar{\phi}^B_j(\vec{r}_B) = R_{(n_B)_j (\ell_B)_j}(r_B)\ \bar{Y}_{(\ell_B)_j (m_B)_j}(\theta_B, \phi_B) \qquad (3.2.26)$$

$$\bar{X}_{K}(\vec{r}_A) = R_{(n_A)_K (\ell_A)_K}(r_A)\ \bar{Y}_{(\ell_A)_K (m_A)_K}(\theta_A, \phi_A) \qquad (3.2.27)$$

The radial wavefunctions have the form given in (3.2.17) and are expressed as follows

$$R_{(n_B)_j (\ell_B)_j}(r_B) = \sum_{q=1}^{NB(j)} b_{jq}\, r_B^{nb_{jq}}\, e^{-\beta_{jq} r_B} \qquad (3.2.28)$$

$$R_{(n_A)_K (\ell_A)_K}(r_A) = \sum_{p=1}^{NA(K)} a_{Kp}\, r_A^{na_{Kp}}\, e^{-\alpha_{Kp} r_A} \qquad (3.2.29)$$

The angular functions in expressions (3.2.26) and (3.2.27) have the form

$$\bar{Y}_{(\ell_B)_j (m_B)_j}(\theta_B, \phi_B) = N_{(m_B)_j}\, C_{(\ell_B)_j (m_B)_j}\, P^{(m_B)_j}_{(\ell_B)_j}(\cos\theta_B)\, \cos(m_B)_j \phi_B \qquad (3.2.30)$$

$$\bar{Y}_{(\ell_A)_K (m_A)_K}(\theta_A, \phi_A) = N_{(m_A)_K} C_{(\ell_A)_K (m_A)_K} P^{(m_A)_K}_{(\ell_A)_K}(\cos\theta_A) \cos(m_A)_K \phi_A \quad (3.2.31)$$

We have now given the form of the wavefunctions and the matrix elements used in the present calculations. In the next section we shall describe the form of the potential, V_{eB}, used in equation (3.2.1) to describe the lithium target atom in the single active electron approximation.

3.3 The single electron effective potential model

The main calculations of this thesis are concerned with trying to model the collision process between a bare helium nucleus, He^{2+}, and a neutral lithium atom, Li ($1s^2 2s$). This is a three electron problem and consequently very difficult to solve. In order to reduce it to a computationally efficient problem it is necessary to introduce some approximations in order to treat the Li target as a one-electron model problem, which still retains the important physical features of the original system. We shall now describe how this is done for the L shell of

lithium. The neutral lithium atom is represented by the configuration Li($1s^2$ 2s) which represents a single valence electron orbiting two core electrons in the usual central field approximation.

The ionisation energy needed to remove the valence electron is given by

$$-E(1s^2\ {}^1S) + E(1s^2 2s\ {}^2S) = 0.198 \text{ a.u.} \qquad (3.3.1)$$

The ionisation energy needed to remove an inner core electron, weighted to allow for spin, is given by

$$\frac{3}{4}\left(E(1s2s\ {}^3S) - E(1s^2\ {}^1S)\right) \qquad (3.3.2)$$

$$+\frac{1}{4}\left(E(1s2s\ {}^1S) - E(1s^2\ {}^1S)\right) + 0.198 \text{ a.u.}$$

$$= 2.38 \text{ a.u.}$$

The large difference between the first and second ionisation energies suggests that the valence electron interacts rather weakly with the core electrons because it will have a much more diffuse wavefunction than the inner core electrons which are more tightly bound to the nucleus. In particular if the physical features of the atom are mainly determined by the outer valence electron of lithium for a certain range of projectile impact energies then it is well known that some convenient approximations can be made. We assume the Li($1s^2$) core electrons only contribution is to

produce a spherically symmetrical potential in which the outer valence electron moves and that this interaction depends only upon the coordinates of the valence electron and the point where the potential is evaluated, i.e. it is a local potential.

This is in contrast to a non-local potential. The action of a non-local operator upon a wavefunction depends upon the value of the wavefunction at all points in configuration space. Because the inner core is a closed shell $(1s^2)$ configuration this potential is taken to be a spherically symmetrical potential which is a function only of the distance between the valence electron and the nucleus. The idea of using an effective one electron model for lithium was suggested by Seitz (1935) following the work of Prokofjew (1929). Prokofjew showed that this type of model was successful when applied to Na (the next alkali atom above Li). Inside the core region, in general, the wavefunction of a valence electron state will oscillate due to the high kinetic energy and this is partially cancelled by the strong attractive potential due to the nucleus. The oscillations may be viewed as a manifestation of the Pauli principle which requires the valence electron wavefunction to be orthogonal to the core orbitals. The net effect of the effective potential is to replace the oscillations by a smoother wavefunction which keeps the valence electronic charge distribution out of the core region (Abarenkov and Heine, 1965).

If we assume the $(1s^2)$ core electrons have the simple

wavefunction form

$$\phi(r', r'') = N e^{-\alpha(r'+r'')} \qquad (3.3.3)$$

then it is straightforward to show that the potential experienced by another electron at a radial distance r in the field of this charge density, and of a point nucleus with charge z, is given by

$$V(r) = -\frac{z}{r} + \frac{2}{r} - \frac{e^{-2\alpha r}}{r}(2 + 2\alpha r) \qquad (3.3.4)$$

Potentials which are a more generalised version of (3.3.4) have been considered by Danielle (1979) and Klapisch (1967) for various systems. The form of this potential is suitable for use in the present calculations because it can be incorporated into the computer codes used for evaluating matrix elements. However, the addition of terms which correspond to polarization of the core electrons, for example, would be impossibe if it had the mathematical form

$$V_{pol} = -\frac{\alpha_d}{(r^2+r_0^2)^2} \qquad (3.3.5)$$

where α_d and r_o are constants.

The general form of the model potential which we have considered in the present work is given by

$$V = -\frac{Z_1}{r} - \frac{e^{-\gamma r}}{r}(Z_2 + Z_3 r) \qquad (3.3.6)$$

where Z_1, Z_2, Z_3 and γ are constants. This form of model potential can be used also to represent the K-shell electrons as well as the L-shell electron. These constants will be chosen in such a way that the basis sets constructed using V satisfy certain physical criteria appropriate to the physical model which V represents. This will be discussed in chapter 5. Model potentials of the form of (3.3.4) have been used in previous close coupled equations with success (Fritsch and Lin, 1983b). We shall now consider how the matrix elements required in the close-coupled equations are to be evaluated.

3.4 The evaluation of the direct and exchange matrix elements.

In the last section we considered the form of the model potentials that were used in the present work, and in Section (3.2) we considered the form of the wavefunctions that have been used. In this section we shall describe how the form of these potentials and wavefunctions allows the matrix elements defined in equations (3.2.7), (3.2.8),

(3.3.9), (3.3.11), (3.3.11a), (3.3.14) and (3.3.15) to be evaluated in a numerically efficient manner. To begin with we shall consider the direct matrix elements as defined in expressions (3.3.8) and (3.3.9). It will be sufficient to consider the direct matrix element H_{jK} as given in (3.3.8), as this will display all the numerical methods employed for the direct matrix elements. We shall begin by noting that if we included the internuclear potential V_{AB}, then (3.2.8) reduces to a simple form due to the orthonormality of the wavefunctions represented by $\bar{X}^{A}_{j}(\vec{r}_{A})$ and $\bar{X}^{A}_{K}(\vec{r}_{A})$ and the fact that V_{AB} only depends upon the internuclear coordinates.

That is to say we can write expression (3.2.9) as

$$\bar{H}_{jK}(t) = \langle \bar{X}^{A}_{j}(\vec{r}_{A}) \mid V_{eB} \mid \bar{X}^{A}_{K}(\vec{r}_{A}) \rangle \exp i(\varepsilon_{j} - \varepsilon_{K})t + \delta_{jK} V_{AB} \qquad (3.4.1)$$

where δ_{jK} is the usual Kronecker delta function. We shall now concentrate upon the first term in expression (3.4.1) above. Using the form of the model potential for V_{eB}, as given in expression (3.3.6), and the form for the wavefunctions as given in expression (3.1.27) we can write this term as follows (where for convenience we have omitted the exp $i(\varepsilon_{j} - \varepsilon_{K})t$ factor)

$$\bar{P}_{jK} = \langle \bar{X}^A_j(\vec{r}_A) \mid -\frac{Z_1}{r_B} \mid \bar{X}^A_K(\vec{r}_A) \rangle$$
$$+ \langle \bar{X}^A_j(\vec{r}_A) \mid -\frac{Z_2}{r_B} e^{-\gamma r_B} \mid \bar{X}^A_K(\vec{r}_A) \rangle$$
$$+ \langle \bar{X}^A_j(\vec{r}_A) \mid -Z_3 e^{-\gamma r_B} \mid \bar{X}^A_K(\vec{r}_A) \rangle \qquad (3.4.2)$$

The form of the matrix elements defined in (3.4.2) can now be reduced by substituting the expression for the radial wavefunction given in (3.2.29). Thus we finally obtain the following expression for $\bar{D}_{jK}$;

$$\bar{D}_{jK} =$$
$$\sum_{P=1}^{NA(j)} \sum_{q=1}^{NA(K)} a_{jP} a_{Kq} \int d\vec{r}_A \, r_A^{n a_{jP}} e^{-\alpha_{jP} r_A} \bar{y}_{(\iota_A)_j (m_A)_j}(\theta_A, \phi_A) \left[-\frac{Z_1}{r_B} \right]$$
$$\times r_A^{n a_{Kq}} e^{-\alpha_{Kq} r_A} \bar{y}_{(\iota_A)_K (m_A)_K}(\theta_A, \phi_A)$$
$$+ \sum_{P=1}^{NA(j)} \sum_{q=1}^{NA(K)} a_{jP} a_{Kq} \int d\vec{r}_A \, r_A^{n a_{jP}} e^{-\alpha_{jP} r_A} \bar{y}_{(\iota_A)_j (m_A)_j}(\theta_A, \phi_A) \left[-\frac{Z_2}{r_B} e^{-\gamma r_B} \right]$$
$$\times r_A^{n a_{Kq}} e^{-\alpha_{Kq} r_A} \bar{y}_{(\iota_A)_K (m_A)_K}(\theta_A, \phi_A)$$
$$+ \sum_{P=1}^{NA(j)} \sum_{q=1}^{NA(K)} a_{jP} a_{Kq} \int d\vec{r}_A \, r_A^{n a_{jP}} e^{-\alpha_{jP} r_A} \bar{y}_{(\iota_A)_j (m_A)_j}(\theta_A, \phi_A) \left[-Z_3 e^{-\gamma r_B} \right] \qquad (3.4.3)$$
$$\times r_A^{n a_{Kq}} e^{-\alpha_{Kq} r_A} \bar{y}_{(\iota_A)_K (m_A)_K}(\theta_A, \phi_A)$$

It is apparent from expression (3.4.2) that $\bar{D}_{jK} = \bar{D}_{Kj}$ and hence this symmetry can be used to reduce the number of matrix elements that have to be calculated. From the expression (3.4.3) it is clear that there are three basic or primitive types of matrix element which were to be evaluated, which correspond to the three distinct terms in the effective potential. By combining the exponents for the terms involving r in expression (3.4.3) it follows that the three basic types of direct matrix element that have to be evaluated are given by the three following expressions

$$I^{1}_{jK} = \int d\vec{r}_A \, r_A^{n} \, e^{-\alpha r_A} \, \bar{Y}_{(l_A)_j (m_A)_j}(\theta_A, \phi_A) \left(\frac{-z_1}{r_B}\right) \bar{Y}_{(l_A)_K (m_A)_K}(\theta_A, \phi_A) \qquad (3.4.4)$$

$$I^{2}_{jK} = \int d\vec{r}_A \, r_A^{n} \, e^{-\alpha r_A} \, \bar{Y}_{(l_A)_j (m_A)_j}(\theta_A, \phi_A) \left(\frac{-z_2 e^{-\gamma r_B}}{r_B}\right) \bar{Y}_{(l_A)_K (m_A)_K}(\theta_A, \phi_A) \qquad (3.4.5)$$

$$I^{3}_{jK} = \int d\vec{r}_A \, r_A^{n} \, e^{-\alpha r_A} \, \bar{Y}_{(l_A)_j (m_A)_j}(\theta_A, \phi_A) \left(-z_3 e^{-\gamma r_B}\right) \bar{Y}_{(l_A)_K (m_A)_K}(\theta_A, \phi_A) \qquad (3.4.6)$$

The methods used to evaluate these primitive integrals are given in Appendix (A1). From the form of the separate terms in expression (3.4.3) it is clear that for certain values of j and k corresponding to different pairs of wavefunctions,

there will be primitive matrix elements which are duplicated, i.e. the same primitive matrix element will be needed more than once. This is because any two radial wavefunctions for a particular angular momentum are obtained from the same set of basis STO's and only the coefficients which multiply each STO are different.

We shall show this by an example. We define the wavefunctions corresponding to two different sets of quantum numbers as follows

$$\chi_{n\ell m} = \sum_{p=1}^{N_\ell} c_{n\ell p}\, r_A^{n_{\ell p}}\, e^{-\alpha_{\ell p} r_A}\, \bar{Y}_{\ell m}(\theta_A, \phi_A) \qquad (3.4.7)$$

$$\chi_{n'\ell'm'} = \sum_{q=1}^{N_{\ell'}} c_{n'\ell' q}\, r_A^{n_{\ell' q}}\, e^{-\alpha_{\ell' q} r_A}\, \bar{Y}_{\ell' m'}(\theta_A, \phi_A) \qquad (3.4.8)$$

We now consider the first term in the expression (3.4.2) which contains the contribution from the $-z_1$ term in the effective potential. When the expressions (3.4.7) and (3.4.8) are substituted into this term we obtain the following result, which is equivalent to the first term in expression (3.4.3),

$$\bar{D}^{1}_{(n\ell m)(n'\ell'm')} = \sum_{p=1}^{N_\ell} \sum_{q=1}^{N_{\ell'}} c_{n\ell p}\, c_{n'\ell' q} \qquad (3.4.9)$$

$$\times \left[\int d\vec{r}_A\; r_A^{n_{\ell p}} e^{-\alpha_{\ell p} r_A}\, \bar{Y}_{\ell m}(\theta_A, \phi_A) \left[\frac{-z_1}{r_B}\right] r_A^{n_{\ell' q}} e^{-\alpha_{\ell' q}} \bar{Y}_{\ell' m'}(\theta_A, \phi_A) \right].$$

Since the integral in [ ] is independent of the

parameters n and n' which represent the expectation energies of the states, then the same integral will be needed for all the different combinations of n and n' which are possible.

In Appendix A.1 it is shown that the integral in [ ] in expression (3.4.9), which we shall denote by I'_{jK}, can be written as

$$I'_{jK} = I'_{(n\ell m)(n'\ell'm')}$$

$$= \sum_{\ell''} \sum_{m''=-\ell''}^{+\ell''} f'_{\ell''}(\alpha, \bar{n}, |\vec{R}|)\, Y^{*}_{\ell''m''}(\theta_R, \phi_R) \times g(\ell, m, \ell', m', \ell'', m'') \quad (3.4.10)$$

where $\vec{R}$ is the internuclear separation vector with polar angles (θ_R, ϕ_R) and we define

$$\alpha = \alpha_{\ell p} + \alpha_{\ell' q} \quad (3.4.11)$$

$$\bar{n} = n_{\ell p} + n_{\ell' q} \quad (3.4.12)$$

Therefore by substituting expression (3.4.10), for the integral [ ] in the expression (3.4.9), we obtain

$$\bar{D}'_{(n\ell m)(n'\ell'm')}$$

$$= \sum_{\ell''} \sum_{m''=-\ell''}^{\ell''} \left[\sum_{p=1}^{N_\ell} \sum_{q=1}^{N_{\ell'}} c_{n\ell p}\, c_{n'\ell' q}\, f'_{\ell''}(\alpha, \bar{n}, |\vec{R}|) \right] Y^{*}_{\ell'' m''}(\theta_R, \phi_R) \times g(\ell, m, \ell', m', \ell'', m'') \quad (3.4.13)$$

Now since the integral in expression (3.4.9) is independent of n and n', then the value of $f'_{\ell''}(\alpha, \bar{n}, |\vec{R}|)$ as defined by expression (3.4.10) is also independent of n and n'. Therefore we only need to evaluate the function $f'_{\ell''}(\alpha, \bar{n}, |\vec{R}|)$ for all the distinct combinations of the parameters ℓ'', α and $\bar{n}$ which are allowed. The values of α and $\bar{n}$ are determined from equations (3.4.11) and (3.4.12) while the values of ℓ'' are limited as shown in Appendix (A1).

Once these different function values have been evaluated it is then possible to perform the summation over p and q denoted by [ ] in expression (3.4.13), which combines the different function values with the correct coefficients corresponding to the different values of n and n'. Therefore in this manner we need to evaluate each unique integral defined by $f'_{\ell''}(\alpha, \bar{n}, |\vec{R}|)$ only once because, for given values of ℓ and m, each pseudostate denoted by $\psi_{n\ell m}$ comprises the same set of STO's and only the coefficients are different. If, however, each pseudostate had been constructed from a different set of STO's the number of integrals to be evaluated corresponding to the functions $f'_{\ell''}(\alpha, \bar{n}, |\vec{R}|)$ would have been much greater than in the present method. So far we have only considered the first term in expression (3.4.2) due to the Coulomb term in the effective potential but the remarks made following expression (3.4.8) apply equally to each term in expression

(3.4.2) in general, provided the function $f^{l'}_{l''}(\alpha, \bar{n}, |\vec{R}|)$ is replaced by the corresponding function for that particular potential term. We also note that the same method is applied to evaluate the direct matrix elements H_{jk} as defined by (3.2.8), which contain the projectile-electron potential.

We shall now describe how the exchange matrix elements were evaluated. We begin by considering the exchange matrix elements K_{jk} as defined in expression (3.2.11). This is the exact form of the exchange matrix elements, without approximation, in the case of a general pseudostate expansion. To be specific we consider

$$K_{jk}(t) = \langle \bar{\phi}^{B}_{j}(\vec{r}_B) | e^{i\vec{v}.\vec{r}} (-\tfrac{1}{2}\nabla^2_{\vec{r}} + V_{eA} + V_{eB} - \varepsilon_k) | \bar{\chi}^{A}_{k}(\vec{r}_A) \rangle \times \exp i(\lambda_j - \varepsilon_k) t \qquad (3.4.14)$$

In the general case we shall let j and k represent the quantum numbers (nlm) and (n'l'm') respectively, and the potentials V_{eA} and V_{eB} have been defined in Section (3.3). We shall write the wavefunctions represented by $\bar{\phi}^{B}_{j}(\vec{r}_B)$ and $\bar{\chi}^{A}_{k}(\vec{r}_A)$ as follows

$$\bar{\phi}^{B}_{j}(\vec{r}_B) = \bar{\phi}^{B}_{nlm}(\vec{r}_B) = \sum_{p=1}^{N^{B}_{l}} b_{nlp}\, r^{nb_{lp}} e^{-\beta_{lp} r_B} \bar{Y}_{lm}(\theta_B, \phi_B) \qquad (3.4.15)$$

$$\bar{\chi}^{A}_{n'\ell'm'}(\vec{r}_A) = \bar{\chi}^{A}_{K}(\vec{r}_A) = \sum_{q=1}^{N^A_{\ell'}} a_{n'\ell'q}\, r^{n a_{\ell'q}}\, e^{-\alpha_{\ell'q} r_A}\, \bar{Y}_{\ell'm'}(\theta_A, \phi_A) \quad (3.4.15a)$$

For convenience we shall write (3.4.15) and (3.4.16) as follows

$$R^{B}_{\ell p}(r_B) = r_{\ell p}^{n b_{\ell p}}\, e^{-\beta_{\ell p} r_B} \quad (3.4.16)$$

$$R^{A}_{\ell' q}(r_A) = r_A^{n a_{\ell' q}}\, e^{-\alpha_{\ell' q} r_A} \quad (3.4.16a)$$

Upon substituting the expressions (3.4.15) and (3.4.16) into (3.4.14) and operating upon $\bar{X}^{A}_{K}(\vec{r}_A)$ with the operator $-\frac{1}{2}\nabla^2_{\vec{r}}$ produces the following exact form for K_{jK}

$$K_{jK}(t) = \left[A^{BA}_{jK} + B^{BA}_{jK} + C^{BA}_{jK} + D^{BA}_{jK} + E^{BA}_{jK} + F^{BA}_{jK} + G^{BA}_{jK} + H^{BA}_{jK} \right] \times \exp i(\lambda_j - \Sigma_K)t \quad (3.4.17)$$

In expression (3.4.17) the individual terms are as follows

$$A^{BA}_{jK} = \sum_{p=1}^{N^B_\ell} \sum_{q=1}^{N^A_{\ell'}} b_{n\ell p}\, a_{n'\ell' q} \left\{ \tfrac{1}{2}\left(\ell'(\ell'+1) - n a_{\ell' q}(n a_{\ell' q}+1)\right)\right\} \times \langle R^{B}_{\ell p}(r_B)\, \bar{Y}_{\ell m}(\theta_B, \phi_B) \,|\, e^{i\vec{v}\cdot\vec{r}}/r_A^2 \,|\, R^{A}_{\ell' q}(r_A)\, \bar{Y}_{\ell' m'}(\theta_A, \phi_A)\rangle \quad (3.4.18)$$

$$B^{BA}_{jK} = \sum_{p=1}^{N^B_\ell} \sum_{q=1}^{N^A_\ell} b_{n\ell p}\, \alpha_{n'\ell' q} \left\{ \alpha_{\ell' q}(n a_{\ell' q}+1)\right\} \times \langle R^{B}_{\ell p}(r_B)\, \bar{Y}_{\ell m}(\theta_B, \phi_B) \,|\, e^{i\vec{v}\cdot\vec{r}}/r_A \,|\, R^{A}_{\ell' q}(r_A)\, \bar{Y}_{\ell' m'}(\theta_A, \phi_A)\rangle \quad (3.4.19)$$

$$C_{jK}^{BA} = \sum_{p=1}^{N_l^B} \sum_{q=1}^{N_{l'}^A} b_{nlp}\, a_{n'l'q} \left\{ -\tfrac{1}{2} \alpha_{l'q}^2 \right\} \tag{3.4.20}$$
$$\times \left\langle R_{lp}^B(r_B)\, \bar{Y}_{lm}(\theta_B, \phi_B) \left| e^{i\vec{v}\cdot\vec{r}} \right| R_{l'q}^A(r_A)\, \bar{Y}_{l'm'}(\theta_A, \phi_A) \right\rangle$$

$$D_{jK}^{BA} = \sum_{p=1}^{N_l^B} \sum_{q=1}^{N_{l'}^A} b_{nlp}\, a_{n'l'q} \left\{ Z_1^A \right\} \tag{3.4.21}$$
$$\times \left\langle R_{lp}^B(r_B)\, \bar{Y}_{lm}(\theta_B, \phi_B) \left| \frac{e^{i\vec{v}\cdot\vec{r}}}{r_A} \right| R_{l'q}^A(r_A)\, \bar{Y}_{l'm'}(\theta_A, \phi_A) \right\rangle$$

$$E_{jK}^{BA} = \sum_{p=1}^{N_l^B} \sum_{q=1}^{N_{l'}^A} b_{nlp}\, a_{n'l'q} \left\{ Z_1^B \right\} \tag{3.4.22}$$
$$\times \left\langle R_{lp}^B(r_B)\, \bar{Y}_{lm}(\theta_B, \phi_B) \left| \frac{e^{i\vec{v}\cdot\vec{r}}}{r_B} \right| R_{l'q}^A(r_A)\, \bar{Y}_{l'm'}(\theta_A, \phi_A) \right\rangle$$

$$F_{jK}^{BA} = \sum_{p=1}^{N_l^B} \sum_{q=1}^{N_{l'}^A} b_{nlp}\, a_{n'l'q} \left\{ Z_2^B \right\} \tag{3.4.23}$$
$$\times \left\langle R_{lp}^B(r_B)\, \bar{Y}_{lm}(\theta_B, \phi_B) \left| \frac{e^{-\gamma r_B} e^{i\vec{v}\cdot\vec{r}}}{r_B} \right| R_{l'q}^A(r_A)\, \bar{Y}_{l'm'}(\theta_A, \phi_A) \right\rangle$$

$$G_{jK}^{BA} = \sum_{p=1}^{N_l^B} \sum_{q=1}^{N_{l'}^A} b_{nlp}\, a_{n'l'q} \left\{ Z_3^B \right\} \tag{3.4.24}$$
$$\times \left\langle R_{lp}^B(r_B)\, \bar{Y}_{lm}(\theta_B, \phi_B) \left| e^{-\gamma r_B} e^{i\vec{v}\cdot\vec{r}} \right| R_{l'q}^A(r_A)\, \bar{Y}_{l'm'}(\theta_A, \phi_A) \right\rangle$$

$$H_{jK}^{BA} = \sum_{p=1}^{N_l^B} \sum_{q=1}^{N_{l'}^A} b_{nlp}\, a_{n'l'q} \left\{ -\varepsilon_K \right\} \tag{3.4.25}$$
$$\times \left\langle R_{lp}^B(r_B)\, \bar{Y}_{lm}(\theta_B, \phi_B) \left| e^{i\vec{v}\cdot\vec{r}} \right| R_{l'q}^A(r_A)\, \bar{Y}_{l'm'}(\theta_A, \phi_A) \right\rangle$$

In the expression for K given in (3.4.17) the terms A^{BA}_{jK}, B^{BA}_{jK} and C^{BA}_{jK} are produced by the $-\frac{1}{2}\nabla^2_{\vec{r}}$ operator in expression (3.4.14). The term D^{BA}_{jK} is produced by the potential $V_{\in A}$ and the terms E^{BA}_{jK}, F^{BA}_{jK} and G^{BA}_{jK} are produced by the effective potential $V_{\in B}$. The final term H^{BA}_{jK} is derived from the expectation energy $\mathcal{E}_K$ term in expression (3.4.14). It is clear that all of the expressions (3.4.18) to (3.4.25) are of the following general form

$$X^{BA}_{jK} = \sum_{p=1}^{N^B_\ell} \sum_{q=1}^{N^A_{\ell'}} b_{n\ell p}\, a_{n'\ell' q} \{\ldots\} < > . \qquad (3.4.26)$$

where X^{BA}_{jK} represents any of these expressions. The quantities represented by $\{\ldots\}$ in (3.4.26) are all simple coefficients. The matrix elements represented by the quantities < > are all independent of the parameters n and n', which represent the expectation energies of the wavefunctions denoted by j and k. This is an important fact which allows the calculation of the exchange matrix elements to be performed efficiently. This follows because of the expression (3.4.26) which we rewrite as follows

$$X^{BA}_{(n\ell m)(n'\ell'm')} = \sum_{p=1}^{N^B_\ell} \sum_{q=1}^{N^A_{\ell'}} b_{n\ell p}\, a_{n'\ell' q}\, C^{M(\ell,m,p:\ell',m',q)}_{(n\ell)(n'\ell')} \qquad (3.4.27)$$

where $C_{(n\ell)(n'\ell')}$ represents the coefficients $\{\ldots\}$ in expression (3.4.26) and $M(\ell,m,p:\ell',m',q)$ represent the matrix elements in the same expression. The quantities $M(\ell;m,p:\ell',m',q)$ can be evaluated for all unique combinations of the parameters denoted by $(\ell,m,p:\ell',m',g)$. The final matrix elements denoted by $X^{BA}_{(n\ell m)(n'\ell'm')}$ can be formed by combining the quantities $M(\ell,m,p;\ell',m',q)$ with the correct coefficients as in expression (3.4.27). In effect, for given values of the parameters (ℓ,m) and $(\ell'm')$ which are the angular quantum numbers of the two pseudostates, all the required matrix elements $X^{BA}_{(n\ell m)(n'\ell'm')}$ for all the combinations of the parameters n and n' can be constructed from the same set of basic quantities denoted by $M(\ell,m,p;\ell',m',q)$ in expression (3.4.27). This is analogous to the method employed in calculating the direct matrix elements discussed previously in this chapter. It also follows that if the pseudostates, which had the angular quantum number ℓ, were composed of different sets of STO's rather than different combinations of the same set then many more basic matrix elements would have to be calcuated in the evaluation of the final exchange matrix elements (3.4.18) to (3.4.25). Therefore as in the case of the direct matrix elements it is a great advantage, in terms of computer time, to construct all pseudostates for a given value of the angular quantum number ℓ, from the same set of STO's. It is clear that the exchange matrix elements $\bar{K}_{jk}$ defined in

expression (3.2.11a) can be formed in precisely the same manner as the exchange matrix elements K_{jK} in expression (3.4.17). For convenience we shall consider the exchange matrix element $\bar{K}_{Kj}$ which is defined, following expression (3.3.11a), as follows

$$\bar{K}_{K_j}(t) = \langle \bar{\chi}^{A}_{K}(\vec{r}_A) | e^{-i\vec{v}.\vec{r}} (-\tfrac{1}{2}\nabla^2_{\vec{r}} + V_{eA} + V_{eB} - \lambda_j) | \bar{\phi}^{B}_{j}(\vec{r}_B) \rangle \times \exp -i(\lambda_j - \varepsilon_K)t \qquad (3.4.28)$$

When the expressions (3.4.15) and (3.4.15a) for the appropriate pseudostates are substituted into expression (3.4.28) we obtain the following exact form for K

$$\bar{K}_{K_j}(t) = [A^{AB}_{K_j} + B^{AB}_{K_j} + C^{AB}_{K_j} + D^{AB}_{K_j} + E^{AB}_{K_j} + F^{AB}_{K_j} + G^{AB}_{K_j} + H^{AB}_{K_j}] \times \exp -i(\lambda_j - \varepsilon_K)t \qquad (3.4.29)$$

The individual terms in expression (3.4.29) are as follows

$$A^{AB}_{K_j} = \sum_{p=1}^{N^B_l} \sum_{q=1}^{N^A_{l'}} b_{nlp}\, a_{n'l'q} \{ \tfrac{1}{2}[l(l+1) - nb_{lp}(nb_{lp}+1)] \} \times \langle R^{A}_{l'q}(r_A) \bar{Y}_{l'm'}(\theta_A, \phi_A) | \frac{e^{-i\vec{v}.\vec{r}}}{r_B^2} | R^{B}_{lp}(r_B) \bar{Y}_{lm}(\theta_B, \phi_B) \rangle \qquad (3.4.30)$$

$$B^{AB}_{K_j} = \sum_{p=1}^{N^B_l} \sum_{q=1}^{N^A_{l'}} b_{nlp}\, a_{n'l'q} \{ \beta_{lp}(nb_{lp}+1) \} \times \langle R^{A}_{l'q}(r_A) Y_{l'm'}(\theta_A, \phi_A) | \frac{e^{-i\vec{v}.\vec{r}}}{r_B} | R^{B}_{lp}(r_B) \bar{Y}_{lm}(\theta_B, \phi_B) \rangle . \qquad (3.4.31)$$

$$C_{Kj}^{AB} = \sum_{p=1}^{N_l^B} \sum_{q=1}^{N_{l'}^A} b_{nlp}\, a_{n'l'q} \left\{ -\tfrac{1}{2} \beta_{lp}^2 \right\} \qquad (3.4.32)$$

$$\times \langle R_{l'q}^A(r_A)\, \bar{Y}_{l'm'}(\theta_A, \phi_A) \,|\, e^{-i\vec{v}\cdot\vec{r}} \,|\, R_{lp}^B(r_B)\, \bar{Y}_{lm}(\theta_B, \phi_B) \rangle$$

$$D_{Kj}^{AB} = \sum_{p=1}^{N_l^B} \sum_{q=1}^{N_{l'}^A} b_{nlp}\, a_{n'l'q} \left\{ Z_1^A \right\} \qquad (3.4.33)$$

$$\times \langle R_{l'q}^A(r_A)\, \bar{Y}_{l'm'}(\theta_A, \phi_A) \,|\, \frac{e^{-i\vec{v}\cdot\vec{r}}}{r_A} \,|\, R_{lp}^B(r_B)\, \bar{Y}_{lm}(\theta_B, \phi_B) \rangle$$

$$E_{Kj}^{AB} = \sum_{p=1}^{N_l^B} \sum_{q=1}^{N_{l'}^A} b_{nlp}\, a_{n'l'q} \left\{ Z_1^B \right\} \qquad (3.4.34)$$

$$\times \langle R_{l'q}^A(r_A)\, \bar{Y}_{l'm'}(\theta_A, \phi_A) \,|\, \frac{e^{-i\vec{v}\cdot\vec{r}}}{r_B} \,|\, R_{lp}^B(r_B)\, \bar{Y}_{lm}(\theta_B, \phi_B) \rangle$$

$$F_{Kj}^{AB} = \sum_{p=1}^{N_l^B} \sum_{q=1}^{N_{l'}^A} b_{nlp}\, a_{n'l'q} \left\{ Z_2^B \right\} \qquad (3.4.35)$$

$$\times \langle R_{l'q}^A(r_A)\, \bar{Y}_{l'm'}(\theta_A, \phi_A) \,|\, \frac{e^{-i\vec{v}\cdot\vec{r}}\, e^{-\gamma r_B}}{r_B} \,|\, R_{lp}^B(r_B)\, \bar{Y}_{lm}(\theta_B, \phi_B) \rangle$$

$$G_{Kj}^{AB} = \sum_{p=1}^{N_l^B} \sum_{q=1}^{N_{l'}^A} b_{nlp}\, a_{n'l'q} \left\{ Z_3^B \right\} \qquad (3.4.36)$$

$$\times \langle R_{l'q}^A(r_A)\, \bar{Y}_{l'm'}(\theta_A, \phi_A) \,|\, e^{-i\vec{v}\cdot\vec{r}}\, e^{-\gamma r_B} \,|\, R_{lp}^B(r_B)\, \bar{Y}_{lm}(\theta_B, \phi_B) \rangle$$

$$H_{Kj}^{AB} = \sum_{p=1}^{N_l^B} \sum_{q=1}^{N_{l'}^A} b_{nlp}\, a_{n'l'q} \left\{ -\lambda_j \right\} \qquad (3.4.37)$$

$$\times \langle R_{l'q}^A(r_A)\, \bar{Y}_{l'm'}(\theta_A, \phi_A) \,|\, e^{-i\vec{v}\cdot\vec{r}} \,|\, R_{lp}^B(r_B)\, \bar{Y}_{lm}(\theta_B, \phi_B) \rangle$$

Due to the suitable choice of the form of the effective potential in V_{eB} it is clear that the terms due to V_{eB} in the expressions for $\bar{K}_{kj}$ and K_{jk} can be evaluated in the same manner as the other terms in the expressions because the potential terms can be absorbed into the radial wavefunction on centre B. That is to say all of the integrals to be evaluated in expressions (3.4.18) to (3.4.25) and expressions (3.4.30) to (3.4.37) can be obtained from the following basic integral

$$\langle r_B^{n} e^{-\beta r_B} \bar{Y}_{lm}(\theta_B, \phi_B) | e^{i\vec{V}\cdot\vec{r}} \hat{O} | r_A^{n'} e^{-\alpha r_A} \bar{Y}_{l'm'}(\theta_A, \phi_A) \rangle \quad (3.4.38)$$

where $\hat{O}$ is one of the simpe radial operators $1/r_2$, $1/r_A$, 1, $1/r_B$ or $1/r_2$. The parameters n and n' are arbitrary integers and are greater than zero, and α and β have arbitrary positive values. These integrals are evaluated using the Fourier transform method of Sin Fai Lam, (1967). Noble (1980) produced a program which calculated these plane wave matrix elements which was used previously by Ermolaev (1983) and Bransden et al. (1983), for example. In the Fourier transform method the integrals of the type shown in expression (3.4.38) are analytically reduced to a one-dimensional integral which is evaluated numerically using Gauss-Legendre quadrature. The reduction of the

plane wave matrix elements to one-dimensional form is rather tedious and details can be found in Noble (1980).

This concludes the description of the direct and exchange matrix elements, and in the next section the solution of the close coupled equations will be considered.

3.5 The solution of the close-coupled differential equations.

3.5.1 Introduction.

In the previous parts of this chapter, we have discussed the form of the equations which have been derived in the impact parameter approximation (Section 3.1) and the method used in evaluating the direct and exchange matrix elements (Section 3.4). In this section, we shall describe the numerical methods used, in addition to the calculation of the matrix elements, in obtaining the solution of the close-coupled differential equations. In addition we shall also briefly describe the computer programs that we used in the present work.

3.5.2 The calculation of the cross sections and numerical methods.

The calculation of the cross sections is conveniently divided up into two stages. In the first stage the exchange matrix elements are calculated and stored on permanent disk files. Then in the second stage the direct matrix elements are calculated and the close-coupled differential equations are solved numerically. To begin with we shall describe the coordinate system to which we shall refer in the following discussion. The coordinate system has previously been given in Figure 3.1. The collision plane is defined by the z-axis and the impact parameter vector, $\vec{b}$. Hence the pair of values denoted by (z,b) defines a unique point and therefore we shall be referring to the (z,b) grid of points. We note that we have the following relationships for the case of straight-line nuclear trajectories

$$\vec{R} = \vec{b} + \vec{v}t \qquad (3.5.1)$$

$$R^2 = b^2 + (v\ t)^2 \qquad (3.5.2)$$

$$\vec{b}.\vec{v} = 0 \qquad (3.5.3)$$

$$z = vt \qquad (3.5.4)$$

where the quantities are defined in Figure 3.1.

We shall now describe the evaluation of the exchange matrix elements defined by either the exact forms as in expressions (3.2.7), (3.2.11) and (3.2.11a) or by the

approximate forms as in the expressions (3.2.14) and (3.2.15). We note that the explicitly time dependent exponential phases were not included in the exchange matrix elements in the first stage, but were included in the second stage of the calculation for convenience. It is necessary to choose a specific set of z and b points to form a grid at which to calculate the exchange matrix elements during the first stage. Subsequently in order to obtain the probability amplitudes the differential equations are integrated for fixed values of the impact parameter, b, by moving along the z-axis. Hence it is necessary to be able to obtain accurately the exchange matrix elements at any desired value of z and not just the initial set of points. In the previous calculations at Durham (c. 1981-1983) a maximum of nineteen states were used in the expansion basis and it was possible to solve the resulting close coupled equations by using four point Lagrange interpolation to interpolate the exchange matrix elements. However, increasing the number of states lead to problems of numerical instability and this was traced to the interpolation procedure. Subsequently Ermolaev (1984) introduced the familiar Chebyshev interpolation method into the problem and this apparently solved the problem of the numerical instability sufficiently well to allow larger basis sets to be used.

The Chebyshev system of interpolation is very effective because of its convergence propeties which are not shared by

equal interval Lagrangian interpolation (Fox and Parker, 1968). The numerical formulae used in the present work are given in Appendix 3. To employ the Chebyshev interpolation scheme it is necessary to divide the z-axis, for each different value of b, into adjacent sectors with a specified number of points in each sector. The Chebyshev interpolation is then applied independently in each sector. This results in a specific set of z points at which the exchange matrix elements have to be evaluated, which are chosen to be the same for each b value.

A substantial saving of computer time is made by using the fact that the exchange matrix elements at a negative z value are simply related to the exchange matrix elements at the positive z value corresponding to reflection through z = 0. This can be expressed in the following relation, where M_{jK} represents either N_{jK}, K_{jK} or $\bar{K}_{jK}$ as defined in Section 3.2

$$M_{jK}(-z) = M^{*}_{jK}(+z)\, T_j\, T_K \qquad (3.5.5)$$

where

$$T_j = (-1)^{\ell_j + m_j}, \quad T_K = (-1)^{\ell_K + m_K} \qquad (3.5.6)$$

ℓ_j and m_j are the angular and magnetic quantum numbers associated with the pseudostate denoted by index j. Thus the z-axis is divided up into sections between a large

negative z value and z = 0. Once the (z,b) grid has been established and the exchange matrix elements computed at all the grid points, the second stage of the solution can be started.

In the first part of the second stage of the solution the direct matrix elements are calcualted on a certain grid of points. However, this is not the same grid of points that we used for the exchange matrix elements. From Section (3.4) we remember that the direct matrix elements were calculated as a product of functions of R and θ_R (as in expression (3.4.13). The θ_R dependent function is the well known $Y_{lm}(\theta_R,0)$ function and can be found for any θ_R. The R dependent function is more complicated and to save time it is evaluated upon a specified R grid determined by the Chebyshev interpolation method, which can then be applied to obtain the direct matrix element values at any value of R. A maximum value of the parameter R is chosen, R_{Max}, and then it is subdivided into intervals between R_{max} and zero, with a specified number of points in each interval. Then Chebyshev interpolation is applied to each interval independently. Since a (z,b) grid point is defined by a corresponding (R,θ_R) then it is now possible to obtain both the exchange and direct matrix elements, for the initially specified b values, at any intermediate z values.

In the next stage of the solution the differential equations defined by equation (3.2.5) are solved. In practice we solve these equations in three distinct regions.

These regions correspond to four z values which we denote by z_I, z_{EX}, z_D and z_F.

In the first interval $z = z_I$ to $z = z_{EX}$, the exchange matrix elements are set to zero and as the exchange amplitudes are automatically zero (due to the boundary conditions) then only the target states are coupled.

Thus at $z = z_{EX}$ the target occupation amplitudes are in general non-zero whilst the exchange amplitudes are identically zero. The values of z_I and z_{EX} can be varied to check the dependence of the results. In the next interval from $z = z_{EX}$ to $z = z_D$ the full set of coupled equations are solved. That is the exchange matrix elements are included and consequently the exchange occupation amplitudes will begin to increase. In the final interval from $z = z_D$ to $z = z_F$, once again the exchange matrix elements are set to zero and only the direct matrix elements are computed. Thus there is no coupling between the direct and exchange channels and these both evolve independently for $z > z_D$. In practice z_I and z_{EX} are both large negative values whilst z_F and z_D are both large positive values. The close coupled equations defined by equation (2.3.54) are complex and must be recast into a different form before they can be integrated. Equation (2.3.54) can be rewritten as

$$\underset{\sim}{\dot{A}}(t) = -i \underset{\sim}{S}^{-1}(t) \underset{\sim}{M}(t) \underset{\sim}{A}(t) \qquad (3.5.7)$$

Thus $\underset{\sim}{\dot{A}}(t)$ can be separated into real and imaginary parts and

so also can the right hand side of equation (3.5.7) and so two real equations are obtained from each complex term. Hence the total number of coupled differential equations is double the number of elements of $\underset{\sim}{A}(t)$, which is therefore twice the total number of channels in the calculation. The real set of equations are of the following form

$$\dot{\underset{\sim}{y}} = F(z, \underset{\sim}{y}(z), \dot{\underset{\sim}{y}}(z)) \qquad (3.5.8)$$

and are solved using the integrator which is called DE (the name of a computer subroutine) as given by Shampine and Gordon, 1975. This is a very powerful Adams' method routine which incorporates automatic selection of order and step-size. The accuracy of the solution is determined by two parameters RELERR and ABSERR. Firstly RELERR controls the relative error and ABSERR is an absolute error control. At each internal step in the DE code the attempt is made to control the local error of each component of the solution, Y(L), so that

$$|\text{local error}|_L < \text{RELERR} * Y(L) + \text{ABSERR} \qquad (3.5.9)$$

The global error, namely the difference between the exact and computed solutions, should approximately satisfy this same criteria but is not guaranteed to do so. Another parameter controls the maximum number of steps which may be taken by the DE subroutine before it returns control to the user. This can be used to test whether the equations appear to be stiff or not. This means that the solution contains

both slow and rapidly varying components and the Adams' method is not the best approach to these problems. Using the DE routine the final amplitudes $\underset{\sim}{A}(z)$ are obtained at $z = z_F$.

The final step is to obtain the cross sections, and this is done in two ways. Firstly we give the definition of the cross section that is used in practice, for the excitation or charge exchange channels. From expression (2.3.72) or (2.3.73) we have in general the exact expression

$$\sigma_{Ki} = 2\pi \int_0^{b_{max}} db\, b\, |c_{K_i}(b)|^2 \qquad (3.5.10)$$

where $c_{K_i}(b)$ represents the occupation amplitude for excitation or charge exchange, at $z = z_F$.

In expression (3.5.10) b_{max} is a cut-off beyond which the contribution is negligible. We calculate $c_{K_i}(b)$ at a finite number of b values between 0 and b_{max}. We can then estimate σ_{K_i} by considering three adjacent b values at a time, fitting a parabola to the values of $b|c_{K_i}(b)|^2$ and integrating analytically over this interval to get the contribution to σ_{K_i}. In the second method the interval from $b = 0$ to $b = b_{max}$ is again broken up into adjacent sections containing three b values. Two separate parabola are fitted to the three real and three imaginary values of the amplitudes, $c_{K_i}(b)$ at the three b values. Interpolated values of the real and imaginary components of $c_{K_i}(b)$ are obtained at a specified number of equally spaced points in the section and finally Simpsons' rule is applied to the

interpolated values of $b|c_{ki}(b)|^2$ to get the contribution of the section to the total cross section. Both methods should agree closely provided the variation of $c_{ki}(b)$ with b is not too extreme.

The important unitarity relationship, as given in expression (2.3.68), is used throughout the integration procedure to monitor the progress of the calculation and its accuracy. We have found that satisfying the unitarity relationship does not guarantee that the coupled equations are solved correctly as it is possible to have certain errors in the computer codes which do not affect the conservation of unitarity. These problems will be discussed in the chapter containing the present results. We shall now describe the computer codes used in the present work.

3.5.3 The computer programs for calculating exchange matrix elements.

In Section (3.4) the method of evaluating the exchange matrix elements was described. Several computer programs were developed to calculate these matrix elements both in the exact form as defined by expressions (3.2.11) and (3.2.11a), and also in the form which is an approximation when pseudostates, which are not suitable eigenfunctions, are used as in expressions (3.2.14) and (3.2.15). The important feature of the pseudostate basis sets used in the present calculations is that for a particular value all

the pseudostates are formed from the same set of STO's, and as explained in Section (3.4) this results in some computational advantages. This feature was used in all the present programs to ensure that no matrix elements were evaluated more than once. A code called OQEX was used for calculating the approxiate form of the matrix elements (expresions (3.2.14) and (3.2.15)). For the case of the exact form of the matrix elements which use the potentials associated with both nuclear centres (expressions (3.2.11) and (3.2.11a)), three codes called SQOQEX, OQEX/F and OQEX/G were developed. In each of these codes pseudopotentials, with an arbitrary number of terms of the general form $zr^{n}e^{-\alpha r}$ (with $n \geq -1$), could be associated with both nuclear centres, although this feature was not fully utilised in the present work. The program SQOQEX was capable of calculating matrix elements between all combinations of pseudostates provided they were either s, p or d angular momentum pseudostates, on each centre. The program OQEX/F could calculate matrix elements between s states on one centre and either s, p, d or f states on the second centre. The programe OQEX/G could calculate matrix elements between s states on one centre and either s, p, d, f or g states on the second centre. Hence no program could calculate, for instance, the matrix elements between a p state on one centre and an f state on the second centre. This was because the necessary complicated expressions had not been obtained for the programming of these integrals in the

original work of Noble (1980), and were not therefore readily available. This was one of the limitations upon the calculations which could be made in the present work.

In Section (3.5.2) it was stated that the exchange matrix elements were reduced to one-dimensional integrals which were to be evaluated by numerical quadrature using the Gauss-Legendre method on the interval (0,1). This interval could be subdivided into a maximum of five subintervals and in each of these either 4, 8, 16, 32 or 64 quadrature points could be used. The choice of b and z grid points that were to be used was made prior to using the exchange codes. In almost all the calculations performed, thirteen impact parameters were used which covered the important region of space, up to a maximum value beyond which there was no contribution to the reaction cross sections. The z grid was typically chosen to consist of twelve intervals between $z = -70$ and $z = 0$ and on each interval eight point Chebyshev interpolation was used. This resulted in a total of eighty-five different z points at which the exchange matrix elements were to be found for each different b value. At each (z,b) grid point a complete set of exchange matrix elements were output onto a permanent file, consisting of the real and imaginary parts of the matrices $\underset{\sim}{N}(t)$, $\underset{\sim}{K}(t)$ and $\underset{\sim}{\bar{K}}(t)$ as defined in expressions (2.3.60), (2.3.63) and (2.3.64) respectively. The input to each matrix element code consisted of the collision energy and the atomic masses of the nuclei, the effective potentials and the

wavefunctions on each centre, the z and b grid data and various control parameters for testing the output. Once the complete set of exchange matrix elements were on a file, the calculation of the final cross sections could begin and this will be described in the next section.

3.5.4 The computer programs for calculating the cross sections

The calculation of the cross sections was performed using computer programs based upon an initial code written by Dr. C.J. Noble. This was used in the work of Bransden et al. (1980). Subsequently it was developed by Dr. A.M. Ermolaev (Ermolaev, 1983). In the present work two basic codes were constucted from the original code. Apart from numerous additions to the original code a few errors were also found and eliminated, although not until after some calculations had already been completed, which delayed progress for some time. The basic cross section code used in the present work was called MQ2/NEW. After the first stage of the calculation, described in Section (3.5.3), a data file containing the information to be used is constructed so that both the first and second stages are consistent. The collision energy, nuclear charges and masses and the effective potentials used are read in first. Then the wavefunctions and data controlling the z and b grids is read in, along with data to control the calculation

and interpolation of the direct matrix elements. Other data includes the parameters for controlling the integration of the coupled equations and calculating the final cross sections.

Data to control input and output is also read in. In the first part of the code all the information about the wavefunctions is set up. Then the z grid for Chebyshev interpolation is constructed. In the next part the geometrical factors needed for construction of the direct matrix elements are set up. These factors are those which are denoted by $g(\ell,m,\ell',m',\ell'',m'')$ in Appendix A.1. Then the radial integrals needed for the direct matrix elements are evaluated on a grid of points that are constructed for use with Chebyshev interpolation, as described in Section 3.5.2. The radial integrals are those denoted by $\bar{f}^1_\lambda(\alpha,n,R)$, $\bar{f}^2_\lambda(\alpha,\gamma,n,R)$ and $\bar{f}^3_\lambda(\alpha,\gamma,n,R)$ in Appendix A.1. At this point the data for evaluating the radial matrix elements at any z value, for a given b value, is complete.

A loop is now set up over all the b values. The next stage is to add to the exchange matrix elements, for the given b value, the remaining time dependent phase factors. All the exchange matrix elements for each z value are read in from a permanent file and multiplied by the energy dependent phase factors, $\exp(i(\lambda_j - \varepsilon_\kappa)t)$ and $\exp(i(\lambda_\kappa - \varepsilon_j)t)$ as in expressions (3.2.11) and (3.2.11a).

In the next stage the Chebyshev interpolation method is used to obtain the interpolation coefficients for each

exchange matrix element over the whole range of z values between $z = z_{EX}$ and $z = z_D$, and these coefficients are output onto a negative file. This means that the complete set of exchange matrix elements and direct matrix elements can now be determined for any z value between $z = z_I$ and $z = z_F$ and now integration of the coupled equations can begin. The initial conditions for the amplitudes are assumed to be such that at $z = z_I$ the initial state has an amplitude of unity and all other states have amplitudes equal to zero. The integration region between z_I and z_F is divided into three regions as described in the previous section, and the amplitudes obtained at the end of the first region are the initial amplitudes for the integration across the second region. Similarly the output amplitudes at the end of the second region are the initial amplitudes for integration over the third region. The important output from this part of the program is the value of the left hand side of the Greens unitarity relation in expression (2.3.68). This should be identically equal to unity but will differ from this due to the error in the integration procedure. Depending upon the input data, this quantity was output after every ten calls to the subroutine which evaluates the right hand side of equation (3.5.7).

One way in which the accuracy of the integration method could possibly be improved is to form the matrix $-i\underset{\sim}{S}^{-1}\underset{\sim}{M}$ in equation (3.5.7) and to interpolate upon this matrix as the integration proceeds (R. Shingal (1983)). In the present

code the separate matrices $\underset{\sim}{S}$ and $\underset{\sim}{M}$ are interpolated separately and then the right hand side of equation (3.5.7) is formed. However this did not seem to affect the integration except at the lowest collision velocities considered in the present work. At the end of the integration in the third z region the amplitudes at $z = z_F$ are stored and the next b value is considered

Finally after the amplitudes have been determined for all the b values, the cross sections are evaluated as described in the previous section. It is possible to extrapolate the amplitudes from the final z value z_F out to infinity. This had been discussed by Wilets and Gallaher (1966) and Cheshire (1968). However in the present work the value of z was chosen to be large enough so that the final cross sections had effectively converged. The details of numerical parameters such as the b grid and the z grid will be described in the chapter containing the present results, as they were varied for different calculations. Finally we note that two basic programs were constructed in the present work for integrating the coupled equations. The first, called MQ2, was for the case where the size of the expansion basis on each nuclear centre was similar and contained less than twenty-three states. A second program, called MOCF, was constructed which was used for the situation where less than ten states were on one centre with up to sixty five states on the second centre. Both programs used the same numerical methods. This concludes the description of the

coupled channel programs. In the next chapter we shall describe methods for representing the continuum by the use of wavefunctions which are not of the L^2 type but satisfy the Dirac delta function normalisation conditions.

CHAPTER FOUR

The First Born Approximation and the T-Matrix Method For Calculating Ionisation

4.1 Introduction

In the previous chapter a method for obtaining cross sections for positive expectation energy L^2 states was described, and to some extent these states represent the continuum during the collision process. However, the continuum can also be represented using the true continuum states for a given potential which are wavefunctions which are normalised to a Dirac delta function. Typically this is done using the First Born Approximation (FBA). A second method was developed in the present calculations and this will be referred to as the t-matrix method for ionisation. Both of these methods were investigated using similar computer programs and numerical methods, and hence they will be discussed together.

Firstly we shall describe the t-matrix method for calculating ionisation. This will be in the usual single active electron approximation during a collision between two heavy particles A and B in the impact parameter approximation. The numerical methods used in the evaluation of the cross sections will be considered in the final two

sections of this chapter.

4.1.1 The t-matrix for ionisation.

In order to obtain a t-matrix element for ionisation we shall begin by considering the electronic Hamiltonian in equation (2.3.6), which has the following form

$$H_{el} = -\frac{1}{2}\nabla^2_{\vec{r}} + V_{eA} + V_{eB} + W(\vec{R}) \qquad (4.1.1)$$

In the expression (4.1.1) V_{eA} and V_{eB} represent the usual projectile and target interaction potentials with the electron, and W(R) is a function of the internuclear distance, R, only. Then the time dependent Schrodinger equation in the usual impact parameter approach is given by

$$\left(-\frac{1}{2}\nabla^2_{\vec{r}} + V_{eA} + V_{eB} + W(\vec{R}) - i\frac{\partial}{\partial t}\right)_{\vec{r}_B} \Psi_i^+(\vec{r}_B, t) = 0 \qquad (4.1.2)$$

which is analogous to equation (2.3.18).

The (+) index attached to $\Psi_i^+(\vec{r}_B, t)$ indicates that outgoing boundary conditions are to be imposed upon the solution. The index (i) refers to the initial boundary conditions imposed upon the solution. The coordinate system which we shall use to describe the t-matrix formulation is shown in Figure 2.2.

In Figure 2.2 we have the usual relationship

$$\vec{R} = \vec{b} + \vec{v}t \qquad (4.1.3)$$

Since all of the present t-matrix calculations were made for the He^{2+} + Li(2s) system then we replace the potential V_{eA} by its correct form which is as follows

$$V_{eA}(\vec{r}_A) = -\frac{2}{r_A} \qquad (4.1.4)$$

Furthermore we shall consider the function W(R) to be restricted to the following form

$$\lim_{R\to\infty} R\, W(R) = 2 \qquad (4.1.5)$$

We shall now consider the final state of the electron which we will denote by $\Phi^{-}_{\vec{k}}(\vec{r}_B, t)$. The (-) subscript indicates that ingoing boundary conditions are to be imposed upon the wavefunction. The reason for this will be discussed later on in this section. The energy of the electron in this state is $\frac{k^2}{2}$ as $r_B \to \infty$.

The electron state $\Phi^{-}_{\vec{k}}(\vec{r}_B, t)$ represents a continuum state of the electron relative to nucleus B, and therefore corresponds to target ionisation. In the description of the ionisation process we can distinguish between various possibilities for the behaviour of the electronic wavefunction in the asymptotic region, which corresponds to $t \to \infty$. We begin by considering Figure 2.2 and in the asymptotic region after the collision we define a parameter α such that

$$\lim_{\substack{t \to \infty \\ r_A \to \infty}} \frac{r_B}{R} = \alpha \qquad (4.1.6)$$

The three regions of α given by $\alpha < 1$, $\alpha = 1$ and $\alpha > 1$ correspond to different asymptotic forms for the ejected electronic wavefunction, Salin (1969). For instance when $\alpha > 1$ and $k \to \infty$ the asymptotic form corresponds to an electron in the field of the combined charges of both nucleus A and nucleus B. This is the case when the ejected electron velocity, k, is much greater than the relative internuclear velocity, v. In the reverse situation, where $v >> k$ the ejected electron will effectively see only the target potential, and this corresponds to the case when $\alpha < 1$. This is obviously the case for direct excitation when the final state of the electron is a bound state, and it is physically reasonable to expect that ionisation into a final state with a small positive energy should be analagous to this.

In the calculations that are presented here, between He^{2+} and Li(2s), the lowest projectile velocity for He^{2+} which was considered was 0.63 (in a.u.) which corresponds to an incident energy of 40 keV.

We shall now construct the t-matrix expression for ionisation. Firstly, we consider the asymptotic form of equation (4.1.2), as $t \to \infty$, to obtain

$$\left(-\frac{1}{2}\nabla^2_{\vec{r}} + V_{eB}(\vec{r}_B) - i\frac{\partial}{\partial t}_{\vec{r}_B}\right)\Phi^-_{\vec{K}}(\vec{r}_B, t) \qquad (4.1.7)$$

In equation (4.1.7) terms of order $\frac{1}{K^2}$ have been neglected, and we have also used equation (4.1.6) with $\alpha < 1$, and equation (4.1.5).

The wavefunction $\Phi^-_{\vec{K}}(\vec{r}_B, t)$ represents the final state of the ejected electron satisfying incoming boundary conditions. This can be written as follows

$$\Phi^-_{\vec{K}}(\vec{r}, t) = \phi^-_{\vec{K}}(\vec{r}_B, t)\, e^{-iK^2t/2} \qquad (4.1.8)$$

where $\phi^-_{\vec{K}}(\vec{r}_B, t)$ satisfies the following equation

$$\left(-\frac{1}{2}\nabla^2_{\vec{r}} + V_{eB}(\vec{r}_B) - K^2/2\right)\phi^-_{\vec{K}}(\vec{r}_B, t) = 0 \qquad (4.1.9)$$

The t-matrix for ionisation can then be defined as follows

$$t_i(\vec{K}) = \lim_{t\to\infty} \langle \Phi^-_{\vec{K}}(\vec{r}_B, t) \mid \Psi^+_i(\vec{r}_B, t)\rangle \qquad (4.1.10)$$

where $\Psi^+_i(\vec{r}_B, t)$ is the complete wavefunction obtained from equation (4.1.2). We shall define the t-matrix element for some large finite time $t = t_b$, rather than at $t = \infty$ so that

$$t_i(\vec{K}) = \langle \Phi^-_{\vec{K}}(\vec{r}_B, t) \mid \Psi^+_i(\vec{r}_B, t)\rangle_{t=t_b} \qquad (4.1.11)$$

The initial boundary condition placed upon $\Psi_i^+(\vec{r}_B, t)$ is that

$$\lim_{t \to t_a} \Psi_i^+(\vec{r}_B, t) = \phi_i(\vec{r}_B)\, e^{-i\varepsilon_i t} \qquad (4.1.12)$$

where $\phi_i(\vec{r}_B)e^{-\varepsilon_i t}$ represents the initial state of the system and t_a is some large negative time. Then it follows that expression (4.1.11) can be rewritten as follows

$$\begin{aligned} \epsilon_i(\vec{k}) = & -i\int_{t_a}^{t_b} dt \left\langle -i\frac{\partial}{\partial t}\Phi_{\vec{k}}^-(\vec{r}_B, t) \,\middle|\, \Psi_i^+(\vec{r}_B, t)\right\rangle \\ & -i\int_{t_a}^{t_b} dt \left\langle \Phi_{\vec{k}}^-(\vec{r}_B, t) \,\middle|\, i\frac{\partial}{\partial t}\Psi_i^+(\vec{r}_B, t)\right\rangle \end{aligned} \qquad (4.1.13)$$

To obtain expression (4.1.13) we have used the fact that the following equation is assumed to be true

$$\left\langle \Phi_{\vec{k}}^-(\vec{r}_B, t) \,\middle|\, \phi_i(\vec{r}_B)\, e^{-i\varepsilon_i t}\right\rangle_{t=t_a} = 0 \qquad (4.1.14)$$

Then using equations (4.1.2) and (4.1.7) we can rewrite equation (4.1.13) as

$$\begin{aligned} \epsilon_i(\vec{k}) = & -i\int_{t_a}^{t_b} \left\langle \left(\tfrac{1}{2}\nabla^2 - V_{eB}\right)\Phi_{\vec{k}}^-(\vec{r}_B, t) \,\middle|\, \Psi_i^+(\vec{r}_B, t)\right\rangle \\ & -i\int_{t_a}^{t_b} \left\langle \Phi_{\vec{k}}^-(\vec{r}_B, t) \,\middle|\, \left(-\tfrac{1}{2}\nabla^2 + V_{eA} + V_{eB} + W(\vec{R})\right) \,\middle|\, \Psi_i^+(\vec{r}_B, t)\right\rangle \\ = & -i\int_{t_a}^{t_b} \left\langle \Phi_{\vec{k}}^-(\vec{r}_B, t) \,\middle|\, V_{eA} + W(\vec{R}) \,\middle|\, \Psi_i^+(\vec{r}_B, t)\right\rangle \end{aligned} \qquad (4.1.15)$$

In obtaining (4.1.15) we use the fact that $\Psi_i^+(\vec{r}_\beta, t)$ is on L^2 function and vanishes at $r_\beta \to \infty$, and integrate by parts to cancel the ∇^2 terms. It is possible to obtain a more general type of expression for the t-matrix in the spirit of the distorted wave method.

Firstly we define a wavefunction $\chi^-_{\vec{k}}(\vec{r}_\beta, t)$ so that

$$\left(-\frac{1}{2}\nabla^2_{\vec{r}} + V_{e\beta} + u(\vec{R}) - i\frac{\partial}{\partial t}_{\vec{r}_\beta}\right)\chi^-_{\vec{k}}(\vec{r}_\beta, t) = 0 \quad (4.1.16)$$

with the iniital boundary condition

$$\lim_{t \to t_a} \chi^-_{\vec{k}}(\vec{r}_\beta, t) = \Phi^-_{\vec{k}}(\vec{r}_\beta, t) \quad (4.1.17)$$

Then it is straightforward to show that (using (4.1.17))

$$\chi^-_{\vec{k}}(\vec{r}_\beta, t) = \Phi^-_{\vec{k}}(\vec{r}_\beta, t)\, e^{i\int_t^{t_b} u(\vec{R}')\, dt'} \quad (4.1.18)$$

is a solution of (4.1.16). The expression (4.1.11) for the t-matrix is now replaced by the equivalent expression

$$t_i(\vec{k}) = \langle \chi^-_{\vec{k}}(\vec{r}_\beta, t) \mid \Psi_i^+(\vec{r}_\beta, t) \rangle_{t=t_b} \quad (4.1.19)$$

It is then possible to rewrite expression (4.1.19) as

$$t_i(\vec{k}) = -i\int_{t_a}^{t_b} dt \left\langle -i\frac{\partial}{\partial t}\chi^-_{\vec{k}}(\vec{r}_\beta, t) \mid \Psi_i^+(\vec{r}_\beta, t)\right\rangle$$
$$-i\int_{t_a}^{t_b} dt \left\langle \chi^-_{\vec{k}}(\vec{r}_\beta, t) \mid i\frac{\partial}{\partial t}\Psi_i^+(\vec{r}_\beta, t)\right\rangle \quad (4.1.20)$$

where the following boundary condition is assumed

$$\langle \chi^{-}_{\vec{k}}(\vec{r}_B, t) \mid \Psi^{+}_{i}(\vec{r}_B, t) \rangle_{t=t_a} = 0 \qquad (4.1.21)$$

Equation (4.1.21) follows from equation (4.1.18) and (4.1.14). Then, by using equations (4.1.2) and (4.1.16), equation (4.1.20) can be written as

$$b_i(\vec{k}) =$$

$$-i \int_{t_a}^{t_b} dt \langle \chi^{-}_{\vec{k}}(\vec{r}_B, t) | V_{eA} + W(\vec{R}) - U(\vec{R}) | \Psi^{+}_{i}(\vec{r}_B, t) \rangle$$

$$= -i \int_{t_a}^{t_b} dt \; e^{-i \int_{t}^{t_b} U(\vec{R}')\, dt'}$$

$$\times \langle \Phi^{-}_{\vec{k}}(\vec{r}_B, t) | V_{eA} + W(\vec{R}) - U(\vec{R}) | \Psi^{+}_{i}(\vec{r}_B, t) \rangle \qquad (4.1.22)$$

A further transformation of the expression (4.1.22) is possible by removing the internuclear potential from equation (4.1.2), which is rewritten as

$$\left(-\frac{1}{2}\nabla^2_{\vec{r}} + V_{eA} + V_{eB} - i\frac{\partial}{\partial t}_{\vec{r}_B}\right) \Omega^{+}_{i}(\vec{r}_B, t) = 0 \qquad (4.1.23)$$

where

$$\Omega^{+}_{i}(\vec{r}_B, t) = \Psi^{+}_{i}(\vec{r}_B, t)\, e^{i \int_{t_a}^{t} W(\vec{R}')\, dt'} \qquad (4.1.24)$$

The boundary condition (4.1.12) is now replaced by

$$\lim_{t \to t_a} \Omega_i^+(\vec{r}_B, t) = \phi_i(\vec{r}_B) e^{-i\varepsilon_i t} \qquad (4.1.25)$$

Using expression (4.1.24) we can rewrite expression (4.1.22) as follows

$$t_i(\vec{K}) = -i \int_{t_a}^{t_b} dt \, \langle \Phi_{\vec{K}}^-(\vec{r}_B, t) | V_{eA} + W(\vec{R}) - U(\vec{R}) | \Omega_i^+(\vec{r}_B, t) \rangle$$

$$\times \exp\left[-i\left\{ \int_{t_a}^{t_b} U(\vec{R}') dt' + \int_{t_a}^{t} dt' (W(\vec{R}') - U(\vec{R}')) \right\}\right] \qquad (4.1.26)$$

The exponential phase factors have been rearranged for convenience in expression (4.1.26). If the function U(R) introduced into equation (4.1.16) is set equal to the internuclear potential function W(R), or set to be zero, the t-matrix element in expression (4.1.26) corresponds to the t-matrix elements defined by equations (11) and (6) respectively, as given by Salin (1969). The t-matrix element defined by expression (4.1.26) is exact and therefore $|t_i(\vec{K})|^2$ should be independent of the functions defined by W(R) and U(R), because U(R) is arbitrary and can therefore be used to remove the W(R) dependence. This can be used as a check upon the accuracy of the t-matrix and will be considered further in the next chapter containing the results.

The reason for applying the ingoing boundary conditions to the final continuum state, $\Phi_{\vec{K}}^-(\vec{r}_B, t)$, in expression (4.1.26) has been described by Rudge and Seaton (1964) and

is analagous to the time-independent formulation of the ionisation t-matrix element. So far we have only considered the transition amplitude for direct ionisation, where the final state of the electron is a target continuum state. A transition amplitude, corresponding to a continuum electronic state upon the projectile, can also be obtained in a similar manner. In the calculations to be presented only target ionisation was considered, because of limitations upon the available computing time.

We shall now describe how the ionisation cross sections are evaluated using the transition amplitude in expression (4.1.26). We begin by defining the final electron states defined by equation (4.1.9) to be normalized as follows

$$< \phi^{-}_{\vec{k}} \mid \phi^{-}_{\vec{k}'} > \; = K \, \delta (\vec{k} - \vec{k}') \qquad (4.1.27)$$

Then using expression (4.1.26) to define $t_i(\vec{k})$ means that the probability of ionisation is given by

$$P_{ion} = \int \frac{d\vec{k}}{K} \mid t_i(\vec{k}) \mid^2 \qquad (4.1.28)$$

This is the probability that the ejected electron is in a continuum state at the end of the collision. The $1/K$ factor is due to the normalization condition given in expression (4.1.27), and to the closure identity. To proceed we make a partial wave expansion of the final states, $\phi_{\vec{k}}(\vec{r}_B)$ and write (McDowell and Coleman (1970))

$$\phi_{\vec{K}}^{-}(\vec{r}_B) = \sum_{l=0}^{\infty} \frac{(2l+1)}{4\pi} (+i)^l e^{-i\delta_l^c} \frac{u_{Kl}(r)}{r} P_l(\cos \hat{K}.\hat{r}) \qquad (4.1.29)$$

where

$$\delta_l^c = \delta_l + \arg \Gamma(1 + l - i/K) \qquad (4.1.30)$$

In expression (4.1.30) δ_l represents the effect of the non-Coulomb part of the potential, $V_{eB}(\vec{r}_B)$, in equation (4.1.9), in the presence of the Coulomb potential. The second term is the appropriate Coulomb factor for a potential which has the asymptotic behaviour

$$\lim_{r_B \to \infty} V_{eB}(\vec{r}_B) \to -1/r_B \qquad (4.1.31)$$

The functions $u_{Kl}(r)_B$ are solutions of the radial Schrodinger equation

$$\left(-\frac{1}{2}\frac{d^2}{dr^2} - \frac{K^2}{2} + V_{eB}(r_B) + \frac{l(l+1)}{2r^2}\right) u_{Kl}(r)_B = 0 \qquad (4.1.32)$$

subject to the boundary condition

$$u_{Kl}(r_B) \underset{r_B \to \infty}{\to} \left(\frac{2}{\pi K}\right)^{1/2} \sin\left(Kr - l\frac{\pi}{2} + \delta_l^c + \frac{1}{K}\ln(2Kr)\right) \qquad (4.1.33)$$

We now consider the transition matrix element defined by

expression (4.1.26). By using the partial wave expansion method and the definition (4.1.28), it follows that the probability of ionisation is given by

$$P_{ion} = \int d\left(\frac{k^2}{2}\right) \sum_{l=0}^{\infty} \sum_{m=0}^{l} |t_{lm}(\vec{k})|^2 \qquad (4.1.34)$$

where

$$t_{lm}(k) = -i\int_{t_a}^{t_b} dt \left\langle \frac{u_{kl}(r_B)}{r_B} \bar{Y}_{lm}(\theta_B, \phi_B) e^{-i\frac{k^2}{2}t} |V_{eA} + W(\vec{R}) - U(\vec{R})| \Omega_i^+(\vec{r}_B, t) \right\rangle \qquad (4.1.35)$$

$$\times \exp\left[-i\int_{t_a}^{t} (W(\vec{R}') - U(\vec{R}'))\, dt'\right]$$

The second phase factor, denoted by $\exp[-i\int_{t_a}^{t_b} U(\vec{R}')\, dt']$, in expression (4.1.26), can be omitted from expression (4.1.35) as it cannot alter P_{ion} as defined by expression (4.1.34). We can rewrite expression (4.1.35) as follows

$$t_{lm}(k) = -i\int_{t_a}^{t_b} dt \exp\left[-i\int_{t_a}^{t} (W(\vec{R}') - U(\vec{R}'))\, dt'\right]$$

$$\times I_{klm}(t) \exp(i k^2 t/2) \qquad (4.1.36)$$

where

$$I_{klm}(t) = \left\langle \frac{u_{kl}(r_B)}{r_B} \bar{Y}_{lm}(\theta_B, \phi_B) |V_{eA} + W(R) - U(R)| \Omega_i^+(\vec{r}_B, t) \right\rangle \qquad (4.1.37)$$

The evaluation of the matrix elements, $I_{klm}(t)$, will be described in the next section.

Because the integration over $\vec{r}_B$ is independent of R, the (W(R) - U(R)) term can be removed so that $I_{Klm}(t)$ can be written as

$$I_{Klm}(t) = \left\langle \frac{u_{Kl}(r_B)}{r_B} \bar{Y}_{lm}(\theta_B, \phi_B) \middle| V_{eA} \middle| \Omega_i^+(\vec{r}_B, t) \right\rangle$$

$$+ (W(\vec{R}) - U(\vec{R})) \left\langle \frac{u_{Kl}(\vec{r}_B)}{r_B} \bar{Y}_{lm}(\theta_B, \phi_B) \middle| \Omega_i^+(\vec{r}_B, t) \right\rangle \quad (4.1.38)$$

Because the wavefunction $\Omega_i^+(\vec{r}_B, t)$ is determined for a particular impact parameter and because of symmetry about the collision plane we can write the total ionisation cross section, using expression (4.1.34), in a similar manner to expression (2.3.72), and obtain

$$\sigma_{ion} = \sum_{l=0}^{\infty} \sum_{m=0}^{l} 2\pi \int db\, b \int d\left(\frac{K^2}{2}\right) \left| t_{lm}(b, K) \right|^2 \quad (4.1.39)$$

where the explicit dependence of the t-matrix element upon b is shown. For convenience we shall often refer to the partial cross sections which are defined as follows

$$\sigma_{ion}^{l} = \sum_{m=0}^{l} 2\pi \int db\, b \int d\left(\frac{K^2}{2}\right) \left| t_{lm}(b, K) \right|^2 \quad (4.1.40)$$

To conclude this section we shall briefly discuss the motivation behind the t-matrix ionisation calculations. The first reason for using the expression (4.1.26) for the transition amplitude is that properly normalized continuum

functions can be used to represent the ionisation channels instead of an L^2 representation. Therefore the ionisation process should be more accurately accounted for, at least over a certain range of impact energies. Another motive is that in principle information can be extracted from the t-matrix which is not in the wavefunction represented by $\Psi_i^+(\vec{r}_\beta,t)$, in expression (4.1.22), when $\Psi_i^+(\vec{r}_\beta,t)$ represents an approximate solution to equation (4.1.2). This means that the t-matrix elements in expression (4.1.11) and (4.1.22) are equal provided $\Psi_i^+(\vec{r}_\beta,t)$ is the solution of equation (4.1.2, but if any approximations used in $\Psi_i^+(\vec{r}_\beta,t)$ then the t-matrix elements will not be equal in general. The most obvious case is in the Born approximation where $\Psi_i^+(\vec{r}_\beta,t)$ is replaced by the initial boundary condition in expression (4.1.12), which is $\phi_i(\vec{r}_\beta)e^{-i\varepsilon_i t}$. Then the ionisation transition amplitudes obtained from expression (4.1.15) will not be zero as opposed to those obtained from expression (4.1.11). Thus we may expect that for a reasonable approximation to $\Psi_i^+(\vec{r}_\beta,t)$, which includes some L representation of the continuum, the expression (4.1.15) should provide a more accurate ionisation amplitude.

We shall now consider how the approximation to $\Psi_i^+(\vec{r}_\beta,t)$ was obtained in the present work. The method consisted of performing a large close-coupled calculation as described in Chapter 3. The basis set was chosen to provide an effective representation of the continuum using a

completely L^2 basis. During the solution of the close-coupled equations, the time dependent amplitudes a_K and b_J in expression (3.2.2), were stored at a large number of intermediate t points. This meant that the approximate trial solution, defined by expression (3.2.2) could be exactly reconstructed at each intermediate time. This provided the approximate solution of equation (4.1.23) which was used subsequently in the t-matrix expression (4.1.26). We shall now consider the numerical evaluation of the matrix elements defined in expression (4.1.37).

4.2 The calculation of the t-matrix matrix elements in prolate spheroidal co-ordinates

In this section we shall consider how the matrix elements needed for the t-matrix calculation are calculated. The matrix elements have the following form

$$M_{K\ell m}(t) = \left\langle \frac{u_{K\ell}(r_B)}{r_B} \bar{Y}_{\ell m}(\theta_B, \phi_B) \middle| m(r_A) \middle| \Omega_i^+(\vec{r}_B, t) \right\rangle \quad (4.2.1)$$

where $m(r_A)$ represents either the potential operator $V_{\in A}$ as defined in Section (2.2) or is the unity operator. The matrix elements are to be found in the space fixed frame as this was the frame in which the t-matrix equations were derived. The problem of evaluating the integrals in expression (4.2.1) is due to the fact that the function $u_{K\ell}(r_B)$ is constructed numerically and not in the form of a

set of STO's. Hence the methods used in the close coupling calculations for evaluating the direct matrix elements cannot be applied to this case. However, the fact that both the $\mathcal{L}_i^{+}(\vec{r}_B, t)$ functions and the final state function are a combination of angular momentum eigenfunctions multiplied by radial functions can be used to reduce the three dimensional integral into a two dimensional numerical integration. The third integration can be performed analytically. The two dimensional integration method was used in the present work because it had been used extensively in other atomic collision problems. However, it is not claimed that it is the most efficient method as other integration methods were not used for comparison due to lack of time. To describe the evaluation of the integral in 4.2.1 we shall write it in full as follows,

$$M_{klm}(t) = \int d\vec{r}_B \left[\frac{u_{kl}(r_B)}{r_B} \bar{Y}_{lm}(\theta_B, \phi_B) \right]^{SF} m(r_A) \times \sum_{j=1}^{M} b_j(t) \left[R_{(n_B)_j (l_B)_j} (r_B) \bar{Y}_{(l_B)_j (m_B)_j} (\theta_B, \phi_B) \right]^{SF} e^{-i\lambda_j t} \quad (4.2.2)$$

In expression (4.2.2) the index SF denotes the fact that the angular functions are defined in the space-fixed frame. (The radial functions are invariant under rotation). The summation over j in expression (4.2.2) is over all the target expansion basis states used in the close coupled equations. We now rearrange the summation over j to collect all the terms with the same values of the quantities $(l_B)_j$, $(m_B)_j$ together, followed by a further summation over all the

different combinations of $(\ell_B)_j, (m_B)_j$ which are included in the basis. This means that we obtain the following relationship

$$\sum_{j=1}^{M} b_j(t) \, R^{(r_B)}_{(n_B)_j (\ell_B)_j} \left[\bar{Y}^{(\theta_B, \phi_B)}_{(\ell_B)_j (m_B)_j} \right]^{SF} e^{-i\lambda_j t}$$

$$= \sum_{(\ell_q)(m_q)} \left[\bar{Y}^{(\theta_B, \phi_B)}_{(\ell_q)(m_q)} \right]^{SF} \sum_{w(q)} R^{(r_B)}_{(n_{w(q)})(\ell_q)} \cdot b_{n_{w(q)} \ell_q m_q}(t) \cdot e^{-i\lambda_{w(q)} t} \quad (4.2.3)$$

In expression (4.2.3) the summation over $\ell_q m_q$ is over all different combinations of the quantities $(\ell_q)(m_q)$ which replace the previous labels $(\ell_B)_j, (m_B)_j$. Also the summation over w(q) is over all the values of $(n_B)_j$ which are associated with the combination $(\ell_q)(m_q)$. It is important to remember that the time dependent coefficients $(b_j(t))$ depend upon all three of the quantum numbers which define a state and this will be an important fact in the following discussion. Now since the matrix elements, $M_{klm}(t)$ are evaluated at a given value of the time parameter, t, we can replace the summation over w(q) by a function which has to be evaluated at each time t. That is to say we have the following relationship

$$\sum_{w(q)} R^{(r_B)}_{(n_{w(q)})(\ell_q)} \, b^{(t)}_{(n_{w(q)})(\ell_q)(m_q)} \exp(-i\lambda_{w(q)} t)$$

$$= F_q(r_B, t). \quad (4.2.4)$$

The function ($F_q(r_B,t)$) has no explicit angular dependence and is a function of r_B with real and imaginary components. Hence we have now replaced the integral in expression (4.2.2) by the following

$$M_{k1m}(E) = \int d\vec{r}_B \frac{u_{k1}(r_B)}{r_B} \left[Y_{lm}(\theta_B,\phi_B) \right]^{SF} m(r_A) \times \sum_{l_q m_q} \left[Y_{l_q m_q}(\theta_B,\phi_B) \right]^{SF} F_q(r_B,E) \qquad (4.2.5)$$

For example if the initial expansion basis upon the target, represented by the summation over j in expression (4.2.2), contained s, p and d states then the summation over q in expression (4.2.5) would contain six terms with the following combinations of the quantities $(l_q m_q)$; (0,0), (1,0), (1,1), (2,0), (2,1) and (2,2).

In order to evaluate the integral in expression (4.2.5) we must discuss the relation between the space-fixed and body-fixed frames of reference. The coordinate system to be used is shown in Figure 4.2.

In Figure 4.2, the position of the nuclei are shown for some time $t > 0$. The body fixed coordinates (x',y',z') rotate with the internuclear vector, R, during the collision. For $t \rightarrow -\infty$ the (x,y,z) and (x',y',z') coordinate systems coincide. In the integral defined in expression (4.2.5) the operator $m(r_A)$ is a function of r_A only as it represents either a Coulomb potential or is equal to unity and is invariant under rotation. We therefore need to consider the relationship between the spherical harmonics in the

Figure 4.2

Space fixed (x , y , z) and body fixed (x′, y′, z′) frames. The y and y′ axis are out of the paper.

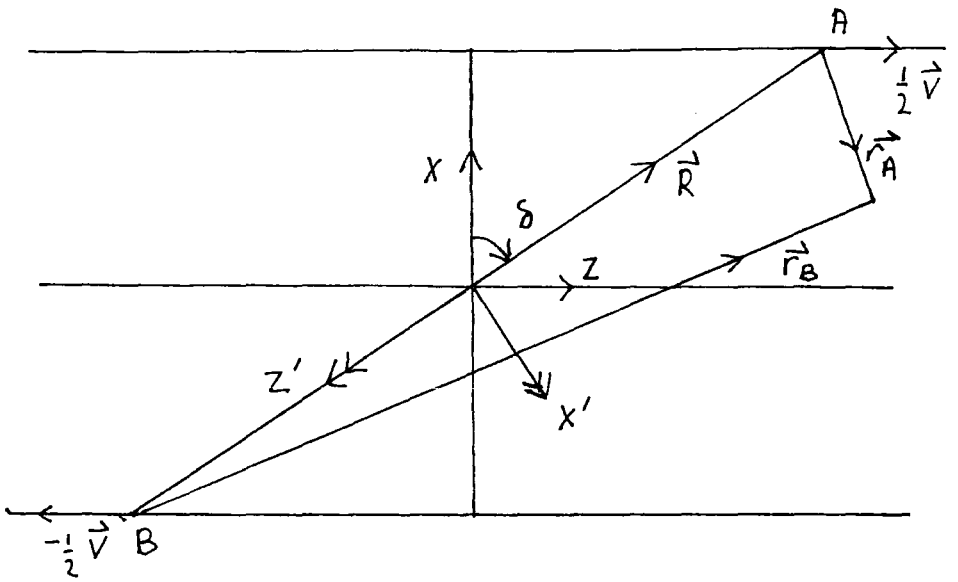

Figure 4.3

Relationship between rotated coordinate systems and the Euler angles α and β . (γ = 0).

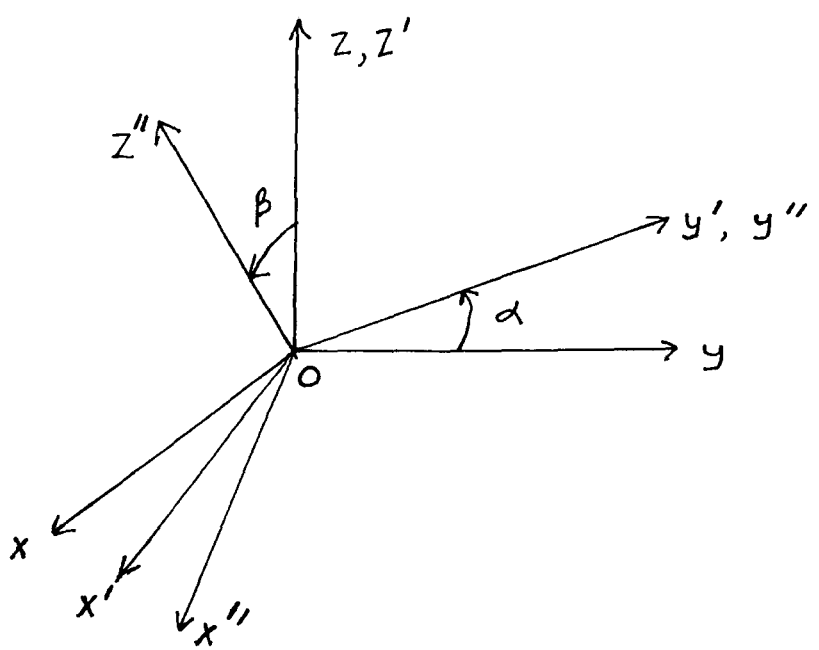

space-fixed and body-fixed frames. In Figure 4.3 the rotation of one co-ordinate frame with respect to another defined by the two Euler angles α and β is shown. The relationship between the spherical harmonics in the primed frame and the unprimed frame is given by

$$Y_{lm}(\theta,\phi) = \sum_{m'=-l}^{m'=l} D^{l}_{m'm}(\alpha,\beta,0)\, Y_{lm'}(\theta',\phi') \qquad (4.2.6)$$

$D^{l}_{m'm}(\alpha,\beta,0)$ are elements of the rotation matrix $\underset{\sim}{D}^{l}$ (Rose 1957). The point (θ,ϕ) is the same point in space as (θ',ϕ') but is measured in the new unprimed coordinate system. By considering Figure 4.2 and Figure 4.3 the Euler angles for the system in Figure 4.2 are $\alpha = 0$ and $\beta = \delta + \frac{\eta}{2}$, where the $\eta/_2$ term is needed to obtain the correct sense of rotation. Using equation (4.2.6) we can relate the space fixed and body fixed spherical harmonics as follows

$$Y^{SF}_{lm}(\theta,\phi) = \sum_{m'=-l}^{m'=l} D^{l}_{m'm}(0,\beta,0)\, Y^{BF}_{lm'}(\theta',\phi') \qquad (4.2.6a)$$

The angular variables (θ,ϕ) are used instead of (θ_B,ϕ_B) for convenience, in the space fixed frame. In order to relate the real spherical harmonics, which are used in the integral in expression (4.2.5), in the space fixed and body fixed frames we shall use the relation (Newby, 1983)

$$\bar{Y}^{SF}_{lm}(\theta,\phi) = \sum_{m'=0}^{m'=l} D^{l}_{m'm}(\beta)\, \bar{Y}^{BF}_{lm'}(\theta',\phi') \qquad (4.2.7)$$

where

$$\mathcal{D}^{\ell}_{m'm} = \frac{N_m}{N_{m'}} \left[d^{\ell}_{m'm}(\beta) + (-1)^m d^{\ell}_{-m'm}(\beta) \right] \frac{1}{\delta_{m'0}+1} \qquad (4.2.8)$$

The N_m and $N_{m'}$ factors have been defined in Section (3.2). The quantities $d^{\ell}_{m'm}(\beta)$ and $d^{\ell}_{-m'm}(\beta)$ are terms from the Wigner reduced rotation matrices, $\underset{\sim}{d}^{\ell}(\beta)$ (Rose 1957). We can now write the matrix element in expression (4.2.5) as follows

$$M_{k\ell m}(t) = \int d\vec{r}_B \; \frac{u_{k\ell}(r_B)}{r_B} \left[\sum_{m'=0}^{m'=\ell} \mathcal{D}^{\ell}_{m'm}(\beta) \, \bar{Y}^{BF}_{\ell m'}(\theta',\phi') \right] n(r_A)$$

$$\times \sum_{\ell_q m_q} F_q(r_B,t) \left[\sum_{m''=0}^{m''=\ell} \mathcal{D}^{\ell_q}_{m''m_q}(\beta) \, \bar{Y}^{BF}_{\ell_q m''}(\theta',\phi') \right] \qquad (4.2.9)$$

We can write this matrix element more conveniently as

$$M_{k\ell m}(t) = \sum_{\ell_q m_q} \sum_{m'=0}^{m'=\ell} \sum_{m''=0}^{m''=\ell_q} \mathcal{D}^{\ell}_{m'm}(\beta) \, \mathcal{D}^{\ell_q}_{m''m_q}(\beta) \, M^{BF}_{\ell_q m_q}(k,t:\ell,m'|\ell_q,m'') \qquad (4.2.10)$$

where the quantity $M^{BF}_{\ell_q m_q}(k\ t; \ell, m' | \ell_q, m'')$ is defined as

$$M^{BF}_{\ell_q m_q}(k, t : \ell, m' | \ell_q, m'') = \int d\vec{r}_B \frac{u_{k\ell}(r_B)}{r_B} \bar{Y}^{BF}_{\ell m'}(\theta', \phi') m(r_A) F_q(r_B, t) \bar{Y}^{BF}_{\ell_q m''}(\theta', \phi') \quad (4.2.11)$$

Thus from expression (4.2.10) we see that in order to obtain the space fixed frame matrix elements it is necessary to obtain the body fixed matrix elements, from expression (4.2.11), for all magnetic substates for given values of ℓ and ℓ_q. In order to illustrate this we consider the case where the target centre expansion consists of an s and a p state and the final continuum state is an s state. Then we can write expression (4.2.5) as follows (where the notation should be clear)

$$M^{SF}_{K00}(t) = \int d\vec{r}_B \frac{u_{k\ell}(r_B)}{r_B} \bar{Y}^{SF}_{00} m(r_A) \times \left[F_{00}(r_B, t) \bar{Y}^{SF}_{00} + F_{10}(r_B, t) \bar{Y}^{SF}_{10} + F_{11}(r_B, t) \bar{Y}^{SF}_{11} \right] \quad (4.2.12)$$

Then using expression (4.2.7) we obtain

$$
\begin{aligned}
M^{SF}_{K00}(t) &= \mathcal{D}^{0}_{00}(\beta)\,\mathcal{D}^{0}_{00}(\beta)\,M^{BF}_{00}(K,t:0,0\,|\,0,0) \\
&+ \mathcal{D}^{0}_{00}(\beta)\,\mathcal{D}^{1}_{00}(\beta)\,M^{BF}_{10}(K,t:0,0\,|\,1,0) \\
&+ \mathcal{D}^{0}_{00}(\beta)\,\mathcal{D}^{1}_{10}(\beta)\,M^{BF}_{10}(K,t;0,0\,|\,1,1) \\
&+ \mathcal{D}^{0}_{00}(\beta)\,\mathcal{D}^{1}_{01}(\beta)\,M^{BF}_{11}(K,t:0,0\,|\,1,0) \\
&+ \mathcal{D}^{0}_{00}(\beta)\,\mathcal{D}^{1}_{11}(\beta)\,M^{BF}_{11}(K,t:0,0\,|\,1,1)\,.
\end{aligned}
\qquad (4.2.13)
$$

where we have used the notation in expression (4.2.11), and where the label q is replaced by the quantities $(\ell_q\, m_q)$ which it represents. Therefore, in order to evaluate the space fixed matrix elements $M^{\ell}_{K\ell M}(t)$ we require the rotation matrix elements $D^{\ell}_{m'm}(\beta)$ and the body fixed matrix elements of the form in expression (4.2.11). To evaluate $D^{\ell}_{m'm}(\beta)$ we need the angle β which can be found using the relation $\beta = \delta + \frac{\pi}{2}$ where δ is defined as (Figure 4.4)

$$
\delta = \tan^{-1}(z/b) \qquad (4.2.14)
$$

This defines δ for both positive and negative z values. We shall now consider how the matrix elements in the body fixed frame in expression (4.2.11) are evaluated.

We shall begin by defining a new set of coordinates which will be used in the integration method. These coordinates are the prolate spheroidal coordinates which have been discussed by Morse and Feshbach (1953) and Arfken (1970). They are a set of orthogonal curvilinear co-ordinator defined by

Figure 4.4

definition of angle δ .

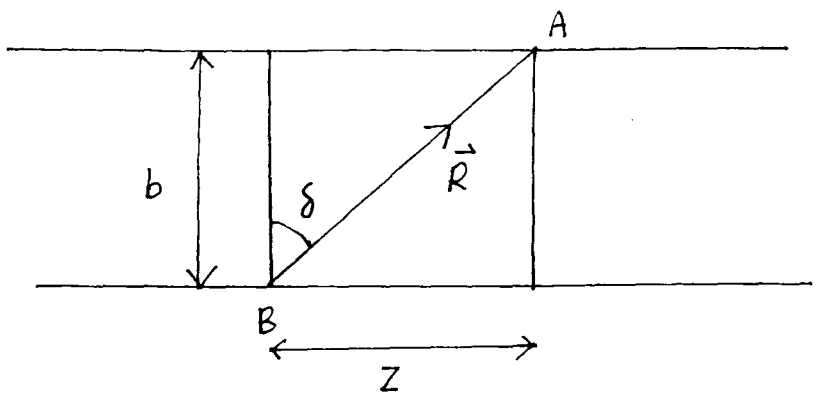

Figure 4.5

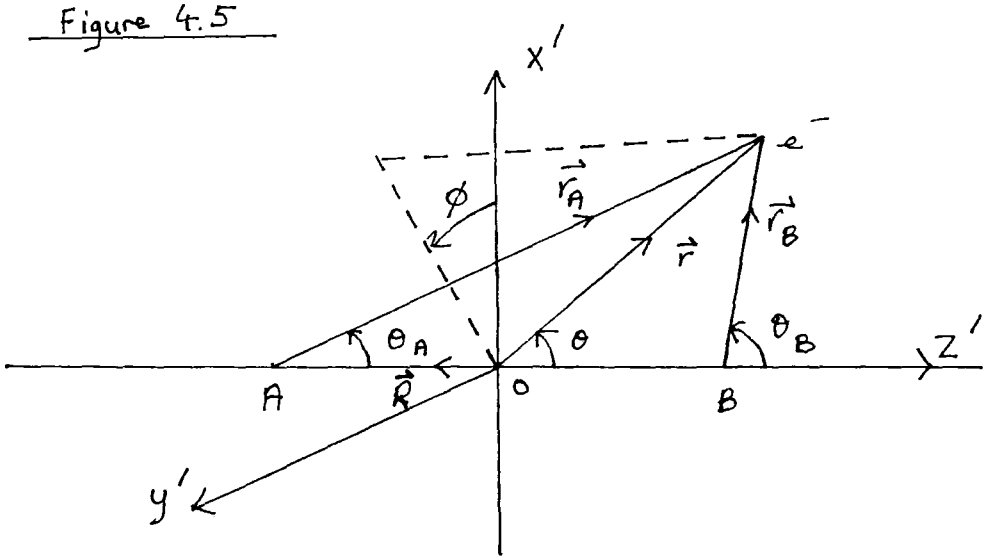

Figure 4.5

The electronic coordinates in the body fixed frame.

Angle ϕ is found by projecting $\vec{r}$ on the $x'y'$- plane.

$$\xi = \frac{1}{R}(r_A + r_B) \tag{4.2.15a}$$

$$\eta = \frac{1}{R}(r_A - r_B) \tag{4.2.15}$$

$$\phi = \phi \tag{4.2.16}$$

Figure 4.5 shows the vectors $\vec{r}_A$, $\vec{r}_B$ and $\vec{R}$ in the body fixed frame and also the azimuthal angle, ϕ.

In the body fixed frame the vectors $\vec{r}_A$, $\vec{r}_B$ and $\vec{R}$ have the same azimuthal angle, ϕ. For convenience we shall now use the angular variables (θ,ϕ), which were previously denoted by (θ',ϕ'), in the body fixed frame as shown in Figure 4.5. Thus the integral in expression (4.2.11) that is to be evaluated has the form

$$M^{BF}_{l_q m_q} = \int d\vec{r}_B \frac{u_{k_l}(r_B)}{r_B} \bar{Y}^{BF}_{lm'}(\theta,\phi)\, m(r_A) F_q(r_B,t) \bar{Y}^{BF}_{l_q m''}(\theta,\phi) \tag{4.2.17}$$

where for convenience the arguments of the symbol $M^{BF}_{l_q m_q}$ are dropped. We can rewrite expression (4.2.17) by using the formula from expression (3.2.24) to give the following

$$M^{BF}_{l_q m_q} = \int d\vec{r}_B \frac{u_{k_l}(r_B)}{r_B} N_{m'} C_{lm'} P^{m'}_{l}(\cos\theta)\cos m'\phi\, m(r_A) \times F_q(r_B,t) N_{m''} C_{l_q m''} P^{m''}_{l_q}(\cos\theta)\cos m''\phi. \tag{4.2.18}$$

We now define angular factors so that

$$\alpha_{\ell m'} = N_{m'} \, C_{\ell m'} \tag{4.2.19}$$

$$\alpha_{\ell_q m''} = N_{m''} \, C_{\ell_q m''} \tag{4.2.20}$$

We also use the formula for the volume element in the prolate spheroidal co-ordinates

$$d\vec{r}_B = \frac{R^3}{8} (\xi^2 - \eta^2) \, d\xi \, d\eta \, d\phi \tag{4.2.21}$$

Using expression 4.2.14 and 4.2.15 it follows that

$$d\vec{r}_B = r_A r_B \frac{R}{2} \, d\eta \, d\xi \, d\phi \, . \tag{4.2.22}$$

Thus we can write expression (4.2.18) as

$$M^{BF}_{\ell_q m_q} = \frac{R}{2} \alpha_{\ell m'} \alpha_{\ell_q m''} \int_1^\infty d\xi \int_{-1}^1 d\eta \int_0^{2\pi} d\phi \tag{4.2.23}$$
$$\times \left[r_A r_B \left[u_{k\ell}(r_B)/r_B \right] \right] F_q(r_B, t) \, M(r_A) \, P_\ell^{m'}(\cos\theta) \, P_{\ell_q}^{m''}(\cos\theta) \cos m'\phi \cos m''\phi \, .$$

The integral over ϕ in expression (4.2.23) has the simple form

$$I_\phi(m', m'') = \int_0^{2\pi} \cos m'\phi \, \cos m''\phi \, d\phi \, . \tag{4.2.24}$$

It is straightforward to show that

$$I_{\phi}(m', m'') = \begin{cases} 0 & \text{for} \quad m' \neq m'' \\ \pi & \text{for} \quad m' = m'' \neq 0 \\ 2\pi & \text{for} \quad m' = m'' = 0 \end{cases} \qquad (4.2.25)$$

The remaining double integration over the variables ξ and η is relatively straightforward. The integral over the variable ξ in the interval $(1,\infty)$ is transformed to the interval $(0,\infty)$ by the transformation

$$y = C(\xi - 1) \qquad (4.2.26)$$

where y is the new integration variable and C is a constant. The integration over the new variable uses Gauss-Laguerre integration while Gauss-Legendre integration is used for the integration over the variable η. Various relationships between the co-ordinates (r_A, r_B, ϕ) and the (ξ, η, ϕ) co-ordinates that are needed in the integrations are given in Appendix 4. We see that the evaluation of the matrix elements in expression (4.2.17) is therefore possible using two-dimensional numerical integration. In the next section we shall describe how the t-matrix cross sections were calculated.

4.3 The evaluation of the ionisation cross sections

In this section we shall describe how the approximation of the wavefunction, $\Omega_i^+(\vec{r}_B, t)$, in equation (4.1.35) is obtained. Next we shall describe the evaluation of the matrix elements $I_{klm}(t)$ in expression (4.1.37), and finally the evaluation of the t-matrix element in expression (4.1.35).

The wavefunction $\Omega_i^+(\vec{r}_B, t)$ was obtained using the standard formulation of the close-coupled equations as described in Chapter 3. The actual basis set used consisted of target centred states only, so that the expression (3.2.2) can be replaced by the following expression

$$\Omega_i^+(\vec{r}_B, t) = \sum_{j=1}^{M} b_j(t)\, \bar{\phi}_j^B(\vec{r}_B) \exp\left(-i\left(\lambda_j t + \tfrac{1}{2}\vec{v}\cdot\vec{r} + \tfrac{1}{8}v^2 t\right)\right) \quad (4.3.1)$$

When the coupled equations, analagous to equations (3.2.5), are solved, the internuclear potential is set to zero. This is why the wavefunction in expression (4.3.1) is denoted by $\Omega_i^+(\vec{r}_B, t)$, since it is the approximate solution of equation (4.1.23). The solution of the close-coupled equations proceeded in the same manner as described in section 3.5. However the subroutine DE, described in section (3.5.1) was changed so that the complex amplitudes, $b_j(t)$, in expression (4.3.1) were output onto permanent files at a predetermined

set of z points. These sets of z points were chosen by dividing the z axis into sub-intervals and calculating a Chebychev interpolation grid within each interval to provide the total z grid. The z points were clustered about the origin, which is at the target centre, where the amplitudes tend to change most rapidly, and were spaced farther apart at the beginning and end of the z integration range where the amplitudes, $b_j(t)$ change more slowly with time.

In order to calculate the matrix elements defined by $I_{K\ell m}(t)$ in expression (4.1.37), using the method described in Section (4.2), a program called 2DTMX was used. For convenience during a single run of the program matrix elements were evaluated for a range of k values and all values of m corresponding to a given value of ℓ. A separate calculation was needed to produce matrix elements for a different ℓ value. The program began by reading in data such as the impact energy of the projectile, the particle masses and the form of the potential V_{eA}. Data for a Chebychev interpolation procedure was also input, as well as the basis set data relating to the states $\bar{\phi}_j^B(\vec{r}_B)$ in expression (4.3.1). Finally data defining the final electron continuum states, including the ℓ value and the number of k values was input.

The functions $U_{K\ell}(r)$, in expression (4.1.33) were calculated previous to the matrix element calculation and subsequently read off a permanent file. For a given K and ℓ value $U_{K\ell}(r)$ was evaluated at 2900 r values between r = 0

and r = 113, as described in Appendix (A2). Subsequently any intermediate values of $u_{kl}(r)$ were determined by 5 point Lagrangian interpolation. The calculation of $\mathcal{L}_i^+(\vec{r}_\beta, t)$ as previously described meant that the $b_j(t)$ amplitudes were output on a specific grid of (b,Z) points and loops were set up over the same grid of points in the matrix element program. At each grid point the correct set of $b_j(t)$ amplitudes were read in from a file. In the next section of code the body-fixed matrix elements were evaluated as described in Section (4.2), in a subroutine called DIRECT. The function $F(r_{q\beta}, t)$ defined in expression (4.2.4), which was needed in the body-fixed calculation was conveniently determined by employing a Chebychev interpolation procedure, rather than explicitly calculating the function for every value of r that was needed. In both the numerical integrations, over the variables ξ and η, in expression (4.2.23), an arbitrary number of quadrature points could be used to enable numerical checks of convergence to be made.

A subroutine called ROTATE was entered next and the body-fixed matrix elements were rotated into the space-fixed frame as in expression (4.2.10).

Finally the matrix elements are output onto a permanent file, prior to the cross section calculation. We shall now describe how the partial cross sections defined in expression (4.1.40) were obtained, using a program called TMX. In the first part of the program the impact energy, and data for performing the integration over the three

variables, b, K and t is input (see expressions (4.1.38) and (4.1.26) which contain the integrals). The matrix elements read in from a file consisted of the two components of the $I_{K\ell m}(t)$ matrix element defined in expression (4.1.38), which we shall rewrite as follows

$$I_{K\ell m}(t) = D_{K\ell m}(t) + (W(R) - U(R)) S_{K\ell m}(t) \qquad (4.3.2)$$

where

$$D_{K\ell m}(t) = \left\langle \frac{u_{K\ell}(r_B)}{r_B} \bar{Y}_{\ell m}(\theta_B, \phi_B) \middle| V_{eA}(r_A) \middle| \Omega_i^+(\vec{r}_B, t) \right\rangle \qquad (4.3.3)$$

and

$$S_{K\ell m}(t) = \left\langle \frac{u_{K\ell}(r_B)}{r_B} \bar{Y}_{\ell m}(\theta_B, \phi_B) \middle| \Omega_i^+(\vec{r}_B, t) \right\rangle \qquad (4.3.4)$$

$D_{K\ell m}(t)$ and $S_{K\ell m}(t)$ are the matrix elements read into the cross section program. The functions W(R) and U(R) are controlled by data read in by the next part of the program. Only matrix elements for a single ℓ value are used in each calculation, and a loop over all the different m values is set up. The b and k values are also set up and then the first integration over the t variable, in expression (4.1.35) can begin. A subroutine WPHASE is called to numerically evaluate the time dependent phase factor in the integrand, which is given by

$$\gamma(t) = \int_{t_a}^{t} (W(R') - U(R'))\, dt' \qquad (4.3.5)$$

t_a is the initial time value as defined by expression (4.1.25). The variable t corresponds to one of the Chebychev grid points at which the matrix elements in expression (4.3.2) have been evaluated. We also note that as usual

$$R'^2 = b^2 + v^2 t'^2 \qquad (4.3.6)$$

The integrand in expression (4.1.35) can now be written as

$$y(t) = e^{iK^2 t/2} F(t) \qquad (4.3.7)$$

where

$$F(t) = e^{-i\gamma(t)} \left(D_{Klm}(t) + (W(R) - U(R)) S_{Klm}(t) \right) \qquad (4.3.8)$$

Y(t) and F(t) are evaluated at all the t points where the matrix elements have been evaluated. Two different methods were then used to perform the integration over t. In the first a third-order finite difference method due to Gill and Miller (1972) was used to integrate Y(t) between the two

limits t_a and t_b. This was available as a NAG subroutine.

In the second method, the function defined by F(t) in expression (4.3.7) was divided into adjacent intervals containing a fixed number of t points. In each interval F(t) was fitted to a polynomial (for both real and imaginary parts) and then the final integrations in each interval were performed analytically as they had the following form

$$\int_{t_1}^{t_2} e^{ik^2t/2} (c_1 + c_2 t + c_3 t^2 + \ldots) \qquad (4.3.9)$$

In the present calculations a third or fourth order polynomial was used to represent F(t). This method was mainly used at the lowest impact energies where the oscillatory factor $e^{ik^2t/2}$ in the integrand was varying most rapidly, and also to check the accuracy of the first method. All the values of $t_{lm}(b,k)$ needed in expression (4.1.39) were obtained in this manner. The final two integrations over the variables b and k in expression (4.1.39) were subsequently performed using the method of Gill and Miller previously referred to. In order to check the results a cubic spline interpolation method due to McCarthy and Stelbovics (1986) was used to interpolate the quantity $t_{lm}(b,k)$ prior to the integrations over b and k in expression (4.1.39) allowing a larger number of points to be used in the integration procedures. The same interpolation method was also applied to the integrand defined by Y(t) in

expression (4.3.7) to check how stable the initial integration over t was. The method of Gill and Miller was very useful as it provided an estimate of the error in each integral it was used for.

We have now described all the methods for obtaining cross sections that were used in the present work and in the next chapter we shall discuss the results that have been obtained.

CHAPTER FIVE

The Present Calculations and Results

5.1 Introduction

In the preceeding chapters the semi-classical impact parameter method was described in the form in which it was used in the present work. A new method for calculating ionisation using exact continuum states was also described in Chapter 4. In this chapter we shall describe the theoretical models used in the calculation of charge transfer, direct excitation and ionisation in the He^{2+} + Li(2s) collision system. We shall begin by describing the model used to calculate capture from the L shell of Li(2s). This is followed by a discussion of capture from the K shell of Li(2s) which is based upon the independent-electron model (IEM) of McGuire and Weaver (1977). Finally direct excitation and ionisation of the L shell of Li(2s) will be considered, using a different model to that for capture. In the case of ionisation results have also been obtained using the new t-matrix method. The possible relationship between the different types of basis set expansions used in investigating charge transfer and the direct reactions will be considered also.

The present results will be compared to existing calculations and experimental data where available. A

comparison with recent detailed classical results from the CTMC method, which have been made over a similar range of energies to the present calculations, will also be undertaken.

5.2 A description of the charge transfer models.

5.2.1 The basis sets and pseudopotentials for capture from the L shell.

In this section we shall describe the pseudopotential and the basis sets designed to investigate the following reaction

$$He^{2+} + Li(1s^2 2s) \rightarrow He^{+*}(nl) + Li(1s^2) \qquad (5.2.1)$$

Ermolaev and Bransden (1984) had considered the same reaction using the semi-classical methods as described in Chapter 3. They included only physical bound states in their expansion basis (see expression 3.2.2). The conclusion was that such a basis could not reproduce the total charge exchange cross section in the range of impact energies between 30 kev and 200 kev. For instance at 100.2 kev (lab) Ermolaev and Bransden obtained a total charge transfer cross section of 26.9×10^{-16} cm^2 compared to the experimental result of McCullough et al. (1982) which is $10.2 \pm 0.4 \times 10^{-16}$ cm^2. The conclusion was that an extended basis set containing some representation of the continuum

states about one or either atomic centre was needed to improve the agreement with experiment. This was the motivation behind the present calculations. We shall now describe the basis set choice in more detail.

The basis set used by Ermolaev and Bransden consisted of the n = 2 and 3 states on Li^{+} and the n = 2, 3 and 4 states on He^{2+} (with the l = 3 states omitted). They obtained results which showed that the basis contains the bound states which are the most important over a large range of impact energies and therefore made a suitable initial basis for the present calculations. To extend the previous calculations the decision was made to add positive energy pseudostates to the He^{2+} centre, in addition to retaining the important physical bound states about each centre in the expansion basis. This was for the following reasons. Firstly, such pseudostates could be used to extract information about capture into the high n states of He^{+} after the collision. This could not be done if pseudostates were added to the Li^{+} expansion centre. This meant that additional approximate methods for estimating the high n capture contribution could be avoided. A second consideration was one of computational convenience. It is more efficient (in computer time) to have a basis set distributed unequally between the expansion centres rather than one which is more equally distributed. We shall now describe how the basis sets were constructed upon each centre.

For the case of the Li^+ centre the pseudopotential used to represent the Li^+ nucleus and $1s^2$ core electrons was the same as in the calculations of Bransden and Ermolaev and was originally derived by Danielle (1979). The pseudopotential method has previously been described in section (3.3). The form of the Danielle pseudopotential was as follows

$$V_L = -\frac{1}{r} - e^{-\gamma r}(2 + \gamma r) \qquad (5.2.2)$$

where $\gamma = 2.92$.

The potential V_L was derived using a Restricted Ritz Principle (RRP) in the following manner. By choosing an initial 1s state of the form $\psi_{1s} = e^{-\alpha r}$ a 2s state, ψ_{2s}, is formed which is orthogonal to it but contains underdetermined parameters. The potential is chosen to have the form shown in expression (5.2.2) with the parameter γ undetermined. The expectation energy of the 2s state is then minimized by varying the parameters in both the wavefunction and the potential to obtain the best agreement with the experimental energy. A similar procedure is used for constructing p and d states except that the potential is fixed as the one obtained from the ψ_{2s} minimization. Higher s states can also be found in a similar manner. The Li(2s) and Li(2p) states obtained by Danielle using the RRP were included in the basis set. Two d states were also included in the basis set and were obtained in the usual manner by diagonalizing a two STO

basis using the Danielle potential to produce one state with the Li(3d) experimental energy and a positive energy state. A d state was used to represent the continuum because Born calculations (to be described in section (5.5)) had shown them to be more important than p or s continuum states in the energy range of interest. The basis set parameters used are shown in Table 5.1. The calculated bound state energies agree with the corresponding experimental energies to better than 0.8%. The calculated oscillator strength for the Li(2s -> 2p) transition is 0.625 compared to 0.788 given by Cowan (1981) for the same transition. The oscillator strength sum for transitions from the 2p state into all d states was found to be 1.08 which is close to the corresponding value of 1.16 given by Cowan, although the calculated Li (2p --> 3d) oscillator strength is only 0.536 compred to 0.696 from Cowan.

The continuum probabilities (described in section (2.4.6)) shown in table 5.1 indicate that in fact the positive energy d state represents both the continuum and the higher bound d states as it overlaps both significantly. We shall now consider the He^{2+} basis set used for capture from the L shell.

The He^{2+} basis set was constructed so that it represented the most important bound states and also satisfied certain oscillator strength sum rules. The basis was constructed by diagonalizing various s, p and d basis sets and then computing various oscillator strength sums to

Table 5.1

Radial wavefunctions of the 32-state basis employed in the present L-shell capture calculations.

Target centre (Li^{+}).

State $(\overline{nl})$ [a]	$\lambda(\overline{nl})$ [a]	$q(\overline{nl})$ [b]	STO basis n_i	STO basis β_i
$\overline{2s}$	- 0.19762	0.00	0	0.80864
			1	0.80864
$\overline{2p}$	- 0.13131	0.00	1	0.55179
$\overline{3d}$	- 0.05559	0.00	2	0.33388
$\overline{4d}$	+ 0.01889	0.55	3	0.40200

a) The $\overline{2s}$ and $\overline{2p}$ states are from Danielle (1979). The $\overline{3d}$ and $\overline{4d}$ states and energies $\lambda(\overline{nl})$ are obtained by diagonalizing the Hamiltonian $-\frac{1}{2}\nabla^2 + V_L$ with V_L from formula (5.2.2). using the STO basis sets given in the the last two columns of the table.

b) The quantities $q(\overline{nl})$ are determined according to expression (2.4.32) by the overlaps between the pseudostates $(\overline{nl})$ and the continuum of the Hamiltonian $-\frac{1}{2}\nabla^2 + V_L$ with V_L from eqn (5.2.2).

produce a final basis set which was consistent with these conditions. The parameters of the basis set are given in Table 5.2 along with the overlap of the basis with the exact n = 4 states which will be used in the results section. The oscillator strength sums are given in Table 5.3. Firstly, we note that the diagonalization of the s state basis produced a 1s state which was retained for convenience in the oscillator sum calculations but was not used in the close-coupled calculations. This was because it had an energy of -2.0 a.u. and this is far below the energy of the initial Li(2s) state, -0.1976 a.u. so that the coupling of this state to the target states is very small compared to higher n states on the projectile. Ermolaev and Bransden had shown it was not important in the charge exchange process in the impact energy range being considered. A comparison of the calculated and exact oscillator strength sums in Table 5.3 shows that for each l value the basis closely reproduces the total sum for bound and continuum transitions (denoted by row (e)). The sums over the negative and positive energy states are also shown (rows (c) and (d)). In the s state basis the $\overline{4s}$ state only has a $q(\overline{4s})$ value of 0.26 and does not represent the continuum very well but since the exact 4s state contribution is only 8% of the total oscillator sum it is not considered that the optimization of its calculated oscillator strength would be as important as the fact that it represented both the continuum and high n states to some extent. The p state

Table 5.2

Radial wavefunctions of the 32-state basis employed in the present L-shell capture calculations.

Projectile centre (He^{+})

State $(\overline{nl})$ [a]	$\mathcal{E}(\overline{nl})$ [a]	$q(\overline{nl})$ [b]	$\langle 4l \mid \overline{nl} \rangle$ [c]	STO basis n_i	STO basis α_i
$\overline{2s}$	- 0.50000	0.00	0.00	0	0.60000
$\overline{3s}$	- 0.22112	0.00	0.00	0	1.00000
$\overline{4s}$	+ 0.17698	0.26	0.72	1	1.00000
				1	0.50000
$\overline{2p}$	- 0.50000	0.00	0.00	1	1.00000
$\overline{3p}$	- 0.22222	0.00	0.00	1	0.66667
$\overline{4p}$	- 0.11255	0.01	0.91	2	0.66667
$\overline{5p}$	+ 0.28752	0.83	0.19	2	0.88270
$\overline{3d}$	- 0.22222	0.00	0.00	2	0.66667
$\overline{4d}$	- 0.12467	0.00	1.00	3	0.50000
$\overline{5d}$	+ 0.01054	0.18	-0.05	3	0.90000
$\overline{6d}$	+ 0.41104	0.92	-0.01	3	1.70000

a) States $(\overline{nl})$ and energies $\mathcal{E}(\overline{nl})$ are obtained by diagonalizing the Hamiltonian $-\frac{1}{2}\nabla^2 + V$ with $V = -2/r$ using the STO basis sets given in the last two columns of the table.

b) The quantities $q(\overline{nl})$ are determined according to eqn (2.4.35) by the overlaps between the pseudostates $(\overline{nl})$ and the continuum of the Hamiltonian $-\frac{1}{2}\nabla^2 + V$ with $V = -2/r$

c) $|4l\rangle$ is the exact $He^{+}(4l)$ state.

Table 5.3 Oscillator strengths for some transitions in He^+ computed using the 32-pseudostate basis (A032). Comparison is made with the exact hydrogenic values from Cowan (1981).

Initial state	2p $\overline{ns}$		2s $\overline{np}$		2p $\overline{nd}$	
Final state	a	b	a	b	a	b
n = 1	-0.135	-0.139	-	-	-	-
n = 2	0.000	0.000	0.000	0.000	-	-
n = 3	0.013	0.014	0.435	0.435	0.696	0.696
n = 4	—	—	0.188	0.103	0.132	0.122
c	-0.1220	-0.1199	0.623	0.649	0.828	0.928
d	0.0130	0.0088	0.351	0.351	0.286	0.183
e	-0.1090	-0.1111	0.975	1.000	1.114	1.111

a: present calculations.

b: hydrogenic oscillator strengths from Cowan (1981).

c: sum over negative-energy states of He^+ of the 32-state basis.

d: sum over positive-energy states of He^+ of the 32-state basis.

e: total of negative- and positive-energy states of the 32-state basis.

basis has a positive energy oscillator sum equal to the exact values and as the $\bar{5p}$ state has a $q(\bar{5p})$ value of 0.83 this suggests that it is a good representation of the p continuum. Finally the d state basis underestimates the negative state sum while the positive state sum is too big. However, since the positive 5d state overlaps strongly with the bound states its contribution to the positive energy sum includes a bound state contribution also which explains this effect. The basis set described above should therefore contain a reasonable representation of the important continuum states of He^{2+} in terms of their oscillator strength sums. The n = 2 and n = 3 states are also well represented in terms of their oscillator strengths. Since the total oscillator sums are also almost exact then it follows that the higher n states are also well represented in terms of their oscillator sums. This was important because it implied that the contribution of these states to the charge exchange cross section could be extracted from the final cross sections witin a single calculation, rather than by some additional approximation, using the methods described in Section (2.4). This completes the description of how the L shell charge exchange basis was selected. A basis set contining twenty-three states on He^{2+} and ten states on Li^{+} was also constructed in a similar manner with the main differences being that it contained p states with two positive energies and only a single positive energy d state on He^{2+}. The results for this basis set will be only

briefly discussed in the next section and therefore it will not be considered any further. In the next section we shall describe the basis sets used to model capture from the K shell of Li(2s).

5.2.2 K shell capture from Li and the Independent Electron Model.

In this section we shall consider how capture from the K shell of Li ($1s^2 2s$) was calcuated within the framework of the Independent Electron Model (IEM). We begin by noting that the energy needed to remove the 2s electron from neutral Lithium is 0.1982 a.u. while the corresponding energy needed to remove a 1s electron is 2.385 a.u. Therefore the core electrons in Li are very tightly bound compared to the valence electron and we shall ignore its effect upon the core. We then considered a one-active-electron model for the following process

$$He^{2+} + Li^{+}(1s^2) \rightarrow He^{+}(n\ell) + Li^{2+}(1s) \qquad (5.2.3)$$

In this model a pseudopotential with the following form was used to represent the interaction between the active electron and the Li^{+} (1s) core

$$V_K = -\frac{2}{r} - \frac{e^{-3.55r}}{r}(1 + 0.25r) \qquad (5.2.4)$$

This potential was constructed by diagonalizing a basis of 6

STO's with l = 0 with the requirement that the lowest eigenvalues corresponded to the lowest energy levels for single excitation of Li ($1s^2$). The same pseudopotential was then used in the usual diagonalization procedure to produce a set of 7p radial functions and 6d radial functions. The basis sets are given in Table 5.4. The eigenvalues for each l value spanned both the negative and positive energy regions and thus included a continuum contribution.

The previous work of Ermolaev and Bransden had indicated that capture from the K shell of $Li^+(1s^2)$ was mainly into the He^+ (1s) state. Therefore a basis consisting of the $He^+(1s)$, $He^+(2s)$ and $He^+(2p)$ states and a single positive energy s state was used on the He centre to represent the electron capture channels from the target represented by the pseudopotential in expression (5.2.4). Summing over all magnetic substates a total of thirty-eight target states and five projectile states were in the basis set. The parameters used in the construction of the basis are given in Table 5.4 and Table 5.5. Table 5.6 compares the energy levels of the lowest singly excited states of Li^+(1s nl) with experimental values. The 1s state obtained by using the potential (5.2.4) was in good agreement with the data of Herman and Skillman (1963) for the 1s state in Li($1s^2$2s) obtained using the modified Hartree-Fock-Slater method which includes a local exchange approximation in the potential. This is shown in figure 5.1. Because of the asymptotic form of the potential as r --> ∞ corresponding to

Table 5.4

Radial wavefunctions of the 43-state basis employed in the present K-shell capture calculations.

Target centre (Li^{2+}).

State $(\overline{nl})^a$	$\lambda(\overline{nl})^a$	$q(\overline{nl})^b$	STO basis	
			n_i	β_i
$\overline{1s}$	- 2.79869	0.00	0	2.66667
$\overline{2s}$	- 0.57216	0.00	1	2.66667
$\overline{3s}$	- 0.12089	0.18	0	2.00000
$\overline{4s}$	+ 0.81270	0.94	1	2.00000
$\overline{5s}$	+ 3.96233	0.97	0	1.50000
$\overline{6s}$	+22.55621	1.00	1	1.50000
$\overline{2p}$	- 0.51097	0.00	1	1.33000
$\overline{3p}$	- 0.22556	0.00	2	1.33000
$\overline{4p}$	- 0.10258	0.04	1	0.88500
$\overline{5p}$	+ 0.10944	0.88	1	1.70000
$\overline{6p}$	+ 0.62460	0.96	2	1.77000
$\overline{7p}$	+ 2.08186	0.97	1	1.00000
$\overline{8p}$	+ 8.15504	1.00	2	1.00000

Table 5.4 (continued)

State $(\overline{nl})^a$	$\lambda(\overline{nl})^a$	$q(\overline{nl})^b$	STO basis	
			n_i	β_i
$\overline{3d}$	- 0.22234	0.00	2	0.66667
$\overline{4d}$	- 0.12507	0.00	2	0.50000
$\overline{5d}$	- 0.06624	0.05	3	0.50000
$\overline{6d}$	+ 0.13274	0.93	2	1.33333
$\overline{7d}$	+ 0.93381	0.98	3	1.33333
$\overline{8d}$	+ 4.77532	0.98	3	2.00000

a) States $(\overline{nl})$ and energies $\lambda(\overline{nl})$ are obtained by diagonalizing the Hamiltonian $-\frac{1}{2}\nabla^2+V_K$ with V_K from eqn (5.2.4) using the STO basis sets in the last two columns of the table.

b) The quantities $q(\overline{nl})$ are determined according to eqn (2.4.32) by the overlaps between the pseudostates $(\overline{nl})$ and the continuum of the Hamiltonian $-\frac{1}{2}\nabla^2+V_K$ with V_K from eqn (5.2.4).

Table 5.5

Radial wavefunctions of the 43-state basis employed in the present K-shell capture calculations.

Projectile centre (He^{+}).

State $(\overline{nl})^{a}$	$\varepsilon(\overline{nl})^{a}$	$q(\overline{nl})^{b}$	STO basis	
			n_i	α_i
$\overline{1s}$	- 2.00000	0.00	0	2.00000
$\overline{2s}$	- 0.50000	0.00	0	1.00000
$\overline{3s}$	+ 0.62230	0.56	1	1.00000
$\overline{2p}$	- 0.50000	0.00	1	1.00000

a) States $(\overline{nl})$ and energies $\varepsilon(\overline{nl})$ are obtained by diagonalizing the Hamiltonian $-\frac{1}{2}\nabla^2 + V$ with $V = -2/r$ using the STO basis sets given in the last two columns of the tables.

b) The quantities $q(\overline{nl})$ are determined from eqn (2.4.32) by the overlaps between the pseudostates $(\overline{nl})$ and the continuum of the Hamiltonian $-\frac{1}{2}\nabla^2 + V$ with $V = -2/r$.

Table 5.6

A comparison of the experimental and calculated ionisation energies (IE) of Li^{+} (1snl) singlet states. The calculated values were obtained by diagonalizing the Hamiltonian $-\frac{1}{2}\nabla^2 + V_K$ using V_K from (5.2.4) in the finite STO basis sets in table 5.4 .

Singlet State	Experimental IE[a]	Calculated IE[b]
$1s^2$	2.779	2.799
1s2s	0.5468	0.5722
1s3s	0.2337	0.1209
1s2p	0.4933	0.5110
1s3p	0.2202	0.2256
1s4p	0.1241	0.1026
1s3d	0.2224	0.2223
1s4d	0.1251	0.1251
1s5d	0.0800	0.0662

a) Experimental data from Ford et al. (1982)

b) Calculated energies from Table 5.4.

Fig. 5.1 Comparison of K-shell wavefunctions

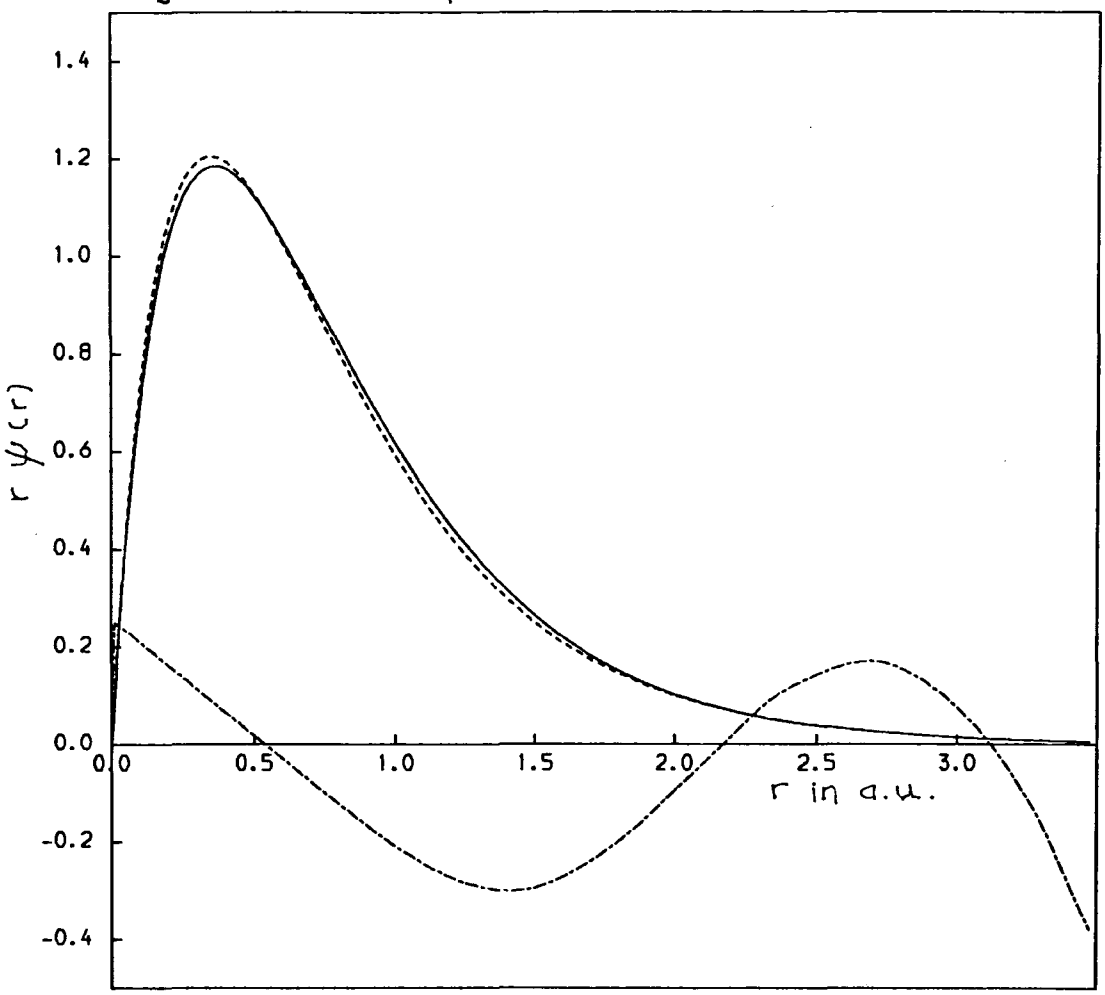

Key to Figure 5.1

Comparison of present Li^{+} (1s) wavefunction and Herman Skillman Li (1s) wavefunction.

———, represents $r\,\psi_{\overline{1s}}(r)$ where $\psi_{\overline{1s}}(r)$ is the $\overline{1s}$ state from the AO43 basis (Table 5.4)

- - - - - - -, represents $r\,\psi_{HF}(r)$ where $\psi_{HF}(r)$ is given by Herman and Skillman (1963).

—.—.—., represents $5 * (1 - \psi_{1s} / \psi_{HF})$. The factor of 5 is for convenience.

an electron in the field of Li^{2+} this potential will only be close to the local Hartree-Fock potential for the 1s state in Li($1s^2$ 2s) over a limited region of r. This model of the K shell is only expected to be valid for low impact energies where the second K shell electron is not active. As the impact energy increases into the Mev region this electron must be taken into account and in our model this is represented by the reaction

$$He^{2+} + Li^{2+}(1s) \rightarrow He^{+}(n\ell) + Li^{3+} \qquad (5.2.5)$$

In this case the electron on the target experiences a purely coulombic potential due to the target nucleus which is

$$V_{k'} = -\frac{3}{r} \qquad (5.2.6)$$

The basis states for electron capture from the K shell corresponding to the potential (5.2.6) consisted of the exact bound states on He^{2+} with $n <= 3$ or $n <= 2$ and the only target state was Li^{2+}(1s). This gave a total of eleven states or five states respectively. Only the Li^{2+}(1s) was included because of the large energy difference between the Li^{2+}(1s) and Li^{2+}(n = 2) states which means they are not

very important. The model which we have considered is essentially that obtained by writing the full Hamiltonian for the two electron system $Li^{+}(1s^2)$ in the approximate form

$$H = -\frac{1}{2}\nabla^2_{\vec{r}} + V_K - \frac{1}{2}\nabla^2_{\vec{r}} + V_{K'} \qquad (5.2.7)$$

and also using a Hartree (unsymmetrised product) approximation to represent the target two-electron wavefunction, ψ_{Har}, as follows

$$\psi_{Har}(\vec{r},\vec{r}') = \phi_a(\vec{r})\,\phi'_b(\vec{r}') \qquad (5.2.8)$$

We then performed two sets of calculations to obtain probability amplitudes corresponding to the choice of either (5.2.4) or (5.2.6) to represent the electron-target centre interaction. In order to obtain an estimate of single-electron capture in this model the transition probabilities obtained from the separate close-coupled calculations must be correctly combined (McGuire and Weaver (1977), Hansteen and Mosebekk (1972)). We write p^{C}_{1s} and $p^{I}_{1s'}$ to represent the transition probabilities (at a given impact parameter value, b) for the 1s electron for capture into any state and for ionisation respectively, obtained with the target potential in (5.2.4). In the same way we have the corresponding probabilities $p^{C}_{1s'}$, and $p^{I}_{1s'}$ for the 1s'

electron in the K shell, obtained with the target potential in (5.2.6). Then after integrating over all impact parameters and neglecting capture from the L shell the one-electron capture cross section is given by

$$\sigma_c = 2\pi \int_0^\infty b\, db \left[P_{1S}^c \left(1 - P_{1S'}^c - P_{1S'}^I \right) \right] \qquad (5.2.9)$$

$$+ 2\pi \int_0^\infty b\, db \left[P_{1S'}^c \left(1 - P_{1S}^c - P_{1S}^I \right) \right]$$

In the case where $p_{1s}^c \ll 1$, $p_{1s}^I \ll 1$, $p_{1S'}^c \ll 1$ and $p_{1S'}^I \ll 1$ then expression (5.3.7) reduces to

$$\sigma_c = 2\pi \int_0^\infty db\; b \left[P_{1S}^c + P_{1S'}^c \right] \qquad (5.2.10)$$

$$= \sigma_{1S}^c + \sigma_{1S'}^c \,.$$

where σ_{1S} and $\sigma_{1S'}$ are the single capture cross sections for the two distinguishable K shell electrons. In this approximation the second electron is allowed to undergo any transition and consequently the cross section (5.2.10) overestimates single-electron capture. This type of model has been successfully applied to collisions between He^{2+} and Mg by Ermolaev (1987). In the IEM it is possible to estimate double-electron capture using the transition probabilities defined above. However, the experimental results of McCullough et al. (1982) and Sasao et al. (1983)

show this process is negligible compared to single-electron capture in the energy range that we have considered and we did not estimate it in the present model. Furthermore the work of Ghosh, Mandal and Mukherjee (1985) concerning double-electron capture in the same system suggests that electron correlation effects must be included explicitly in order to obtain agreement with experiment. These effects are not included in the model we have considered. This concludes the description of the basis sets used for charge transfer and we shall now describe the results obtained in the calculations.

5.2.3 Numerical methods used in the capture calculations

In the calculations made using the basis sets described in Section 5.2.2 there are several numerical problems to investigate. Firstly a suitable grid of z and b points must be chosen as described in Section 3.5.2. In the present calculations it was found that using thirteen impact parameter values, with 0.05 a.u. < b < 24 a.u., was sufficient for L-shell capture. All cross sections except the Li(2p) cross section had converged in this interval. A small correction was added to the Li(2p) result to allow for this, by fitting the Li(2p) transition probabilities to a simple exponential form for large b. The z grid for Chebyshev interpolation of the exchange matrix elements had been investigated previously by Ermolaev (1984). It was found that a grid consisting of twelve intervals between -55.0 a.u. and 0 a.u. with eight points in each interval was

satisfactory. A similar grid with up to fifteen intervals with eight point interpolation was used for the interpolation over R for the direct matrix elements, as discussed in Section 3.5.2. Using more interpolation points did not seem to greatly improve the results, while using much more computer time in the calculations. Tests were also made of the 1-dimensional integration method for evaluating the exchange matrix elements as described in Section 3.5.3. Using more than sixty-four Gauss-Legendre points did not change the test results significantly and in general in the calculations sixty-four quadrature points were used in four intervals of sixteen points. For example for an impact energy of 125 keV lab. the total capture cross section (summed over all energies) computed using 64 and 128 quadrature points were 16.626×10^{-16} cm^2 and 16.919×10^{-16} cm^2 respectively.

In the case of the K-shell capture the impact parameter grid was reduced to the interval 0.04 a.u. < b < 6.75 a.u. and the exchange matrix elements were only calculated for values of z in the range -30 a.u. < z < 0 a.u. As described in section 2.3.3 the quantity defined in expression (2.3.68) was monitored during the calculation. It was generally found that unitarity could be conserved to within 0.001 or better. It was more difficult to satisfy unitarity at low energies or for small impact parameters, or when large basis sets were used on a single centre. However, by trial and error it was found that even when unitarity was well

conserved errors could be present in the computer programs. A better test of the present methods is provided by the time reversal properties of the impact parameter equations as described in Section 2.3.3. For one energy the complete set of amplitudes obtained by setting the initial channel to be each of the target states in turn was calculated. The relation defined by expression (2.3.71) was investigated using the 32 state L-shell basis for an impact energy of 65 keV lab. For the case of the Li(2s -> 2p) transition the values of $|a_{2s,2p_1}|^2$ and $|a_{2p_1,2s}|^2$ are 0.31767 and 0.31708, for an impact parameter value of 10 a.u. The corresponding values of $|a_{2s,3d_0}|^2$ and $|a_{3d_0,2s}|^2$ are 0.022691 and 0.022689. These results suggest that the coupled equations are solved accurately. We have also investigated the effect of changing the tolerances RELERR and ABSERR defined in section 3.5.2 (see expression (3.5.9)). For the 32 state basis the total capture cross section (summed over all states) and the total direct reaction cross section (summed over all states) at 65 keV lab. were 25.128×10^{-16} cm^2 and 46.788×10^{-16} cm^2 respectively, for RELERR = 10^{-5} and ABSERR = 10^{-5}. The corresponding values obtained for RELERR = 10^{-6} and ABSERR = 10^{-6} were 25.126 and 46.791×10^{-16} cm^2. We also investigated the effect of including an internuclear potential function in the Hamiltonian defined in expression (3.2.1) in a consistent manner. Two different functions were used, namely W(R) = 2/R and W(R) = 0. The results were obtained using the 33-state basis set mentioned

in Section 5.2.1 using the exact exchange matrix element method. For an impact energy of 35 keV lab. the total capture cross section, summed over all states, for W(R) = 2/R and W(R) = 0, was 73.286 x 10^{-16} cm^2 and 73.284 x 10^{-16} cm^2 respectively.

Some of these tests of the computer programs were made for most of the impact energies used and allowed several errors in the original programs to be eliminated. They were also made for several of the basis sets used and not just the 32-state basis. They also suggest that the changes made to the original programs to allow for the inclusion of the pseudostate basis sets in an efficient manner were also correctly done. Overall we feel that the present results should be accurate to better than 5 per cent maximum. We shall now consider the results obtained for L-shell capture.

5.3 Present Results for L-shell Capture.

In this section we shall present the results obtained for single-electron capture from the L-shell of Li using the basis set discussed in Section (5.2) in the energy range 8-400 keV lab. Below 8 keV. numerical problems were encountered in the solution of the coupled equations with a large basis set. Above 400 keV. the L-shell gave a negligible contribution as compared to the K-shell, and was ignorred. In the energy region 1-64 keV. lab. previous quantal calculations exist for comparison. Quantal

calculations have been made with a molecular orbital (MO) basis expansion (Sato and Kimura (1983)) and also with a united-atom atomic orbital (AO+) basis (Fritsch and Lin (1983b)).

The present calculations were designed to investigate the importance of the continuum in the charge transfer process and were an extended version of the work of Ermolaev and Bransden (1984) previously mentioned. Initially a 33-state basis which included positive energy pseudostates, mentioned in Section (5.2), was used to compute charge transfer over the energy region 8-600 kev. lab In these calculations the exchange matrix elements were evaluated using the approximate method described in Section (3.3) (equations (3.3.14) and (3.3.15)). The results were disappointing because reasonable agreement with experiment was not achieved for energies above 65 kev. lab although an improvement over the results of Ermolaev and Bransden (who did not include the continuum) was obtained (Ermolaev and Hewitt,1985). It was though that a different representation of the continuum could improve the results, and that was the reason for introducing the thirty-two state basis set described in Section (5.2). Subsequently an error was found and corrected in the computer program used to integrate the coupled equations (Section (3.5.4)) and the new 33-state results were less in agreement with experiment than the old results (with the program error). This result was found to be due to the approximations used in computing the exchange

matrix elements. Therefore the 32-state basis set results were obtained with the exact exchange matrix elements. The error in the computer program caused doubt about the results of Ermolaev and Bransden (1984) and Ermolaev and Hewitt (1985) and therefore we shall not discuss them explicitly.

However, we essentially repeated the calculations of Bransden and Ermolaev by removing the positive energy states in the 32-state basis set to obtain a 20-state basis set containing only bound states and the results obtained will be discussed presently. We begin with the results obtained for capture from the L-shell. A complete set of partial cross sections for single-electron charge transfer computed using the 32-state expansion basis, is given in Table 5.7. All entries of Table 5.7 correspond to transitions between the basis states defined as in Table 5.1 and Table 5.2 rather than to those between exact (physical) states of He^{+}. Therefore a subsequent projection of the data onto the physical states is required as described in Section (2.4.6). The projected results were obtained in the following manner. $\sigma(\bar{n}l)$ denotes the cross section for a state defined in Table 5.2. Therefore the total bound state cross section is

$$\sigma_{tot}^{cap} = \sum_{\substack{all\ (\bar{n}l) \\ on\ projectile}} \sigma(\bar{n}l)(1-q(\bar{n}l)) \qquad (5.3.1)$$

where $q(\bar{n}l)$ are defined in Table 5.2.

The total projected cross section for capture into the

Table 5.7

Computed partial capture cross sections for $He^{2+} + Li(\overline{2s}) \rightarrow He^{+}(\overline{nT}) + Li^{+}$ (in units of 10^{-16} cm^2) obtained using the 32-pseudostate basis (AO32).

State ($\overline{nT}$)	E keV lab 8.0	15.0	22.0	35.0	50.0	65.0	100.0	125.0	200.0	400.0
$\overline{2s}$	1.50	1.75	3.12	1.84	1.05	0.505	0.370	0.241	0.0576	0.00480
$\overline{3s}$	12.6	5.46	4.52	3.20	1.06	0.395	0.215	0.102	0.0270	0.00197
$\overline{4s}$	0.808	0.599	0.784	0.839	1.56	1.49	0.565	0.250	0.0423	0.00894
$\overline{2p}$	7.05	4.45	5.18	5.07	4.10	3.38	2.47	1.36	0.225	0.0234
$\overline{3p}$	26.3	20.7	17.2	10.2	3.74	2.07	0.839	0.414	0.0741	0.00689
$\overline{4p}$	1.56	3.00	3.09	4.51	5.17	4.34	1.61	0.703	0.134	0.0108
$\overline{5p}$	0.031	0.056	0.171	0.202	0.720	2.73	5.25	4.26	1.24	0.0564
$\overline{3d}$	52.4	65.7	57.6	37.7	17.2	7.69	1.44	0.515	0.0555	0.0027
$\overline{4d}$	2.93	6.24	8.02	7.63	5.37	3.06	0.750	0.295	0.0528	0.0020
$\overline{5d}$	0.850	0.548	1.11	3.97	6.70	7.92	3.77	1.73	0.240	0.0106
$\overline{6d}$	0.033	0.031	0.0924	0.149	0.295	1.00	4.18	6.75	2.53	0.037

continuum states (CTTC) is the difference between the total for all $\sigma(\bar{n}l)$ and $\bar{\sigma}_{tot}^{cap}$ so that

$$\bar{\sigma}_{tot}^{ion} = \sum_{\substack{all\ (\bar{n}\bar{l}) \\ on\ projectile}} \sigma(\bar{n}\bar{l})\ q(\bar{n}\bar{l}) \qquad (5.3.2)$$

Expression (5.3.2) corresponds to expression (2.4.34). The corresponding unprojected totals for capture and CTTC are obtained by using

$$\sigma_{tot}^{cap} = \sum_{\substack{all\ (\bar{n}\bar{l}), \\ \mathcal{E}(\bar{n}\bar{l}) < 0}} \sigma(\bar{n}\bar{l}) \qquad (5.3.3)$$

and

$$\sigma_{tot}^{ion} = \sum_{\substack{all\ (\bar{n}\bar{l}), \\ \mathcal{E}(\bar{n}\bar{l}) > 0}} \sigma(\bar{n}\bar{l}) \qquad (5.3.4)$$

$\mathcal{E}(\bar{n}l)$ are defined in Table 5.2. Table 5.2 shows that the states with $\mathcal{E}(\bar{n}l) < 0$ have very small or no overlap with the continuum and therefore σ_{tot}^{cap} in (5.3.3) closely represents capture into a set of physical states but spanning a smaller Hilbert space than those represented by $\bar{\sigma}_{tot}^{cap}$. The projected and unprojected cross section sums are shown in Table 5.8. The 20-state basis set obtained by deleting all the positive energy states in Table 5.2 was also used in the same energy region and the results obtained are shown in table 5.9. This enables the effect of including the positive energy

Table 5.8

Comparison of the unprojected and projected total capture cross sections (in units of 10^{-16} cm^2) obtained using the 32-pseudostate basis set.

	E keV lab									
	8.0	15.0	22.0	35.0	50.0	65.0	100.0	125.0	200.0	400.0
a	104.3	107.3	98.7	70.1	37.7	21.4	7.69	3.63	0.626	0.0525
b	1.72	1.23	2.16	5.16	9.27	13.1	13.8	13.0	4.05	0.1132
c	105.6	108.2	100.2	74.0	44.4	29.5	12.4	6.49	1.26	0.0803
d	0.44	0.37	0.67	1.30	2.55	5.06	9.05	10.1	3.41	0.0855

a : Total capture cross sections computed as a sum of all the negative-energy state contributions (see formula (5.3.3)).

b : Capture cross sections into the projectile continuum computed as the sum of all the positive-energy state contributions (see (5.3.4)).

c : Total cross sections computed using equation (5.3.1) by projecting the projectile-centred part of the 32-state basis onto all bound states.

d : Capture into the projectile continuum computed as a + b - c (see formula (5.3.2)).

Table 5.9

Partial cross sections for single capture into final n states for He^{2+} + Li collisions (in units of 10^{-16} cm^2) ,computed using the 20-pseudostate basis set (AO20).Comparison with the projected capture cross sections ,from Table 5.8, obtained with the 32-pseudostate basis set (AO32).

	E keV lab									
	8.0	15.0	22.0	35.0	50.0	65.0	100.0	125.0	200.0	400.0
n										
2	1.3	3.6	5.0	6.5	6.3	4.7	0.85	0.41	0.13	0.034
3	94.4	96.5	83.7	48.8	24.4	12.2	2.9	1.25	0.19	0.075
4	5.0	6.8	8.9	13.4	11.2	7.8	2.9	1.51	0.27	0.022
a:	100.4	106.5	97.1	67.3	41.2	23.9	6.39	3.04	0.569	0.0696
b:	104.3	107.3	98.7	70.1	37.7	21.4	7.69	3.63	0.626	0.0525
c:	105.6	108.2	100.2	74.0	44.4	29.5	12.4	6.49	1.26	0.0803
d:	0.951	0.984	0.969	0.909	0.928	0.810	0.515	0.468	0.451	0.867
e:	0.963	0.992	0.984	0.960	1.093	1.117	0.831	0.837	0.909	1.328

a: Total capture cross sections computed from the 20-state basis set as the sum of all the negative-energy state contributions.

b: Total capture cross sections computed from the 32-state basis set as the sum of all the negative-energy state contributions(row(a) in Table 5.8).

c: Total capture cross sections as estimated by projecting the 32-state basis onto all bound states centred on the projectile(row(c) in Table 5.8)

d: Ratio of (a) to (c).

e: Ratio of (a) to (b)

states in the basis to be explicitly investigated.

We shall now compare the present results with those of Fritsch and Lin (1983b) who considered impact energies in the range 8-64 keV lab. Fritsch and Lin used a basis set consisting of all 19 n = 2, 3 and 4 He^+ states and 21 states on the Li centre including 10 positive energy states. They estimated capture into states with n > 4 by close coupled calculations with a basis set contining the Li(2s) and Li(2p) states along with the He^+ n shell states. Only n = 5 and separately n = 6 states were considered. Figure 5.2 shows good agreement between their results and the present results corrected using the projection method (equation 5.3.1) except at the high energy end of the interval. Data for their highest energy E = 64 keV. lab. can be compared with our cross sections at 65 keV. lab.

They give the total cross section for capture into n = 2, 3, and 4 as 27.2 x 10^{-16} cm^2 and a correction to account for omitted n > 4 states, as 11.6 x 10^{-16} cm^2, the total being 38.8 x 10^{-16} cm^2. Our values from Table 5.7 are 21.6, 7.9, and 29.5 x 10^{-16} cm^2, respectively, and they compare well, within a probable uncertainty of 20 per cent, with the experimental value of 24.0 $\pm$ 1 10^{-16} cm^2 measured at E = 66.7 keV. lab. (McCullough et al. 1982). At the lowest energy of 8 keV. lab. Fritsch and Lin obtained the cross section for capture into all states with n = 2, 3 and 4 as 108.9 x 10^{-16} cm^2 compared to our corresponding value of 104.6 x 10^{-16} cm^2.

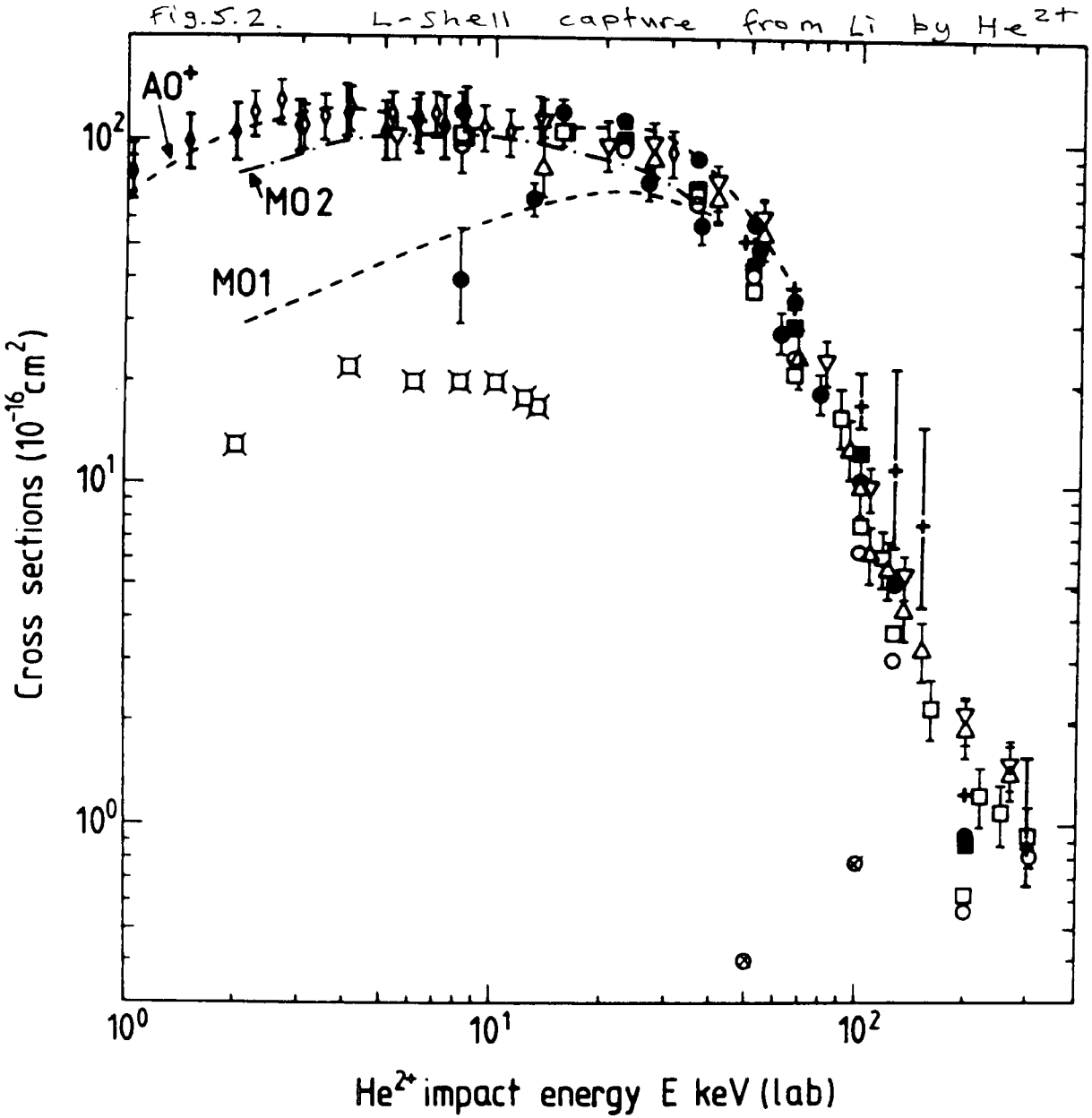
Fig.5.2. L-Shell capture from Li by He^{2+}
$A0^+$
M02
M01
10^2
10^1
10^0
Cross sections ($10^{-16}cm^2$)
10^0
10^1
10^2
He^{2+} impact energy E keV (lab)

Key to Figure 5.2

Cross sections for capture from the L-shell of Li due to He^{2+} impact .

Theoretical cross sections

MO1 , Perturbed-Stationary State results of Shipsey et al. (1978).

MO2 , 11-state molecular orbital expansion, Sato and Kimura (1983).

AO+ , 40 state United Atomic orbital expansion of Fritsch and Lin (1983).

○ , 20-state expansion , present work.

● , 20-state expansion with $1/n^3$ correction , present work

□ , 32-state expansion without applying projection method , present work.

■ , 32-state expansion with projection correction applied , present work.

\+ , Classical Trajectory Monte Carlo (CTMC) results (Ermolaev, Hewitt and McDowell ,1987).

⊗ , capture from K-shell obtained using 23-state expansion , present work.

Experimental cross sections

⋈ , optical data of Barrett and Leventhal (1981), for production of He^+ (n=3) only.

◇ , optical data of Kadota et al. (1982a).

Key to Figure 5.2 continued.

 , charge state selection data of Murray et al. (1982),(from a graph in their paper).

 , charge state selection data of McCullough et al. (1982).

 , charge state selection data of Varghese et al. (1985).

 , charge state selection data of DuBois and Toburen (1985).

 , charge state selection data of Shah et al. (1985).

As was noted before the capture cross sections of Fritsch and Lin (1983b) include an AO+ coupled-state contribution due to capture into 4f states of He^+. We estimated capture into 4f states by carrying out coupled state calculations with a basis set initially consisting of the Li(2s) state and the 4f states of He^+ only. Then we added the He^+(3d) states to the basis. For capture into the 4f states Fritsch and Lin obtained the values 7.88, 5.74, and 1.60×10^{-16} cm^2 for E = 24, 32 and 64 keV. lab. respectively. Retaining only the (4f) basis on He^+ we found the corresponding values to be 12.1, 15.3, and 7.76×10^{-16} cm^2 which are larger, especially at the highest impact energy. Using a (3d+4f) basis on He^+ we obtained 4f capture cross section values of 11.5 and 6.89×10^{-16} cm^2 at 32 and 64 keV. lab., which are smaller than the corresponding (4f) basis values. The (3d + 4f) basis also produced 3d capture cross sections of 48.6, 14.5 and 1.83×10^{-16} cm^2 compared to the corresponding 32 pseudostate results of 57.7, 7.69 and 0.515×10^{-16} cm^2 at energies of 35, 65 and 125 keV. lab. We also note that Fritsch and Lin obtain a 4f capture cross section of 3.55×10^{-16} cm^2 at 8 keV. lab. compared to our (3d + 4f) result of 2.52×10^{-16} cm^2. These results suggest that for energies in the range 8 - 40 keV. a basis contining the (4f) or (3d + 4f) states and the Li(2s) state is adequate to provide the 4f capture cross sections. However, above 40 keV. lab. this may fail because of neglect of coupling to the target

channels which have the largest cross sections. We estimate the actual 4f capture correction to be less than 10 per cent of the total capture cross section over the energy range 8 - 40 keV. This has not been included in our present tables and graph however. With this uncertainty in mind Figure 2 shows that there is excellent agreement between the present 32 state results corrected using the projection method (expression (5.3.1)) and the recent data from several experimental groups. In the following discussion we shall suggest that the importance of pseudostates in the basis may be chiefly limited to a particular energy interval. Table 5.9 compares capture computed using 32-pseudostate and 20-bound-state bases. It shows that both 32- and 20-state expansions agree remarkably well between 8 and 65 keV lab and reasonably for E > 200 keV lab. Earlier it was suggested (Ermolaev and Bransden 1984, Ermolaev and Hewitt 1985) that the practical usefulness of the bound-state expansions was limited by the presence of the ionisation chanel. Table 5.9 shows that predictions of both expansions are significantly different in the specific energy range 65-200 keV lab. It will be shown in section (5.6) of the present work that this interval coincides with the energy region where ionisation of lithium by the He^{2+} impact is particularly prominent (the ionisation maximum is positioned at approximately 80 - 100 keV lab). Firstly we shall examine how estimates of cross sections for basis states not included explicitly in the calculations were obtained.

A simple way of obtaining such corrections is to use the $1/n^3$ rule (Oppenheimer, 1928) as was suggested, for instance, by Bransden et al. (1980). Assuming that the highest bound states present in the basis, have the principal quantum number n , then the correction for all states with $n > n_0$ is written in the form

$$\Delta\sigma(n > n_0) = \sigma(n_0)\left[\zeta(3)\, n_0^3 - \sum_{K=1}^{n_0}\left(\frac{n_0}{K}\right)^3\right] \quad (5.3.5)$$

where $\zeta(3) = 1.202$ is the Riemann zeta function. Another method is to use the two-state approximation (Fritsch and Lin (1983b). Alternatively we can use the projection method which gives

$$\Delta\sigma(n > n_0) = \bar{\sigma}_{tot}^{exp} - \sum_{n \le n_0} \bar{\sigma}(n) \quad (5.3.6)$$

where

$$\bar{\sigma}(n) = \sum_{all\ (\bar{n}\bar{l})} \sigma(\bar{n}\bar{l})\, |\langle \bar{n}\bar{l} | n \rangle|^2 \quad (5.3.7)$$

is the projected cross section for the exact state $|n\rangle$ (equation (2.4.26b)).

In the present work, the high-n corrections have been obtained in two different ways. Firstly we apply (5.3.5) to

the 20-state basis with n = 4. We use the following $(1/n)^3$ approximation

$$\sigma(4S) \lesssim (3/4)^3 \sigma(\bar{3}S) \qquad (5.3.8)$$

and also (using equation (5.3.7))

$$\bar{\sigma}(4p) \lesssim 0.91^2 \sigma(\bar{4}p) \qquad (5.3.9)$$

which gives

$$\begin{aligned}\Delta\sigma' &= \sigma(4S) + \Delta\sigma(n>4) \\ &\quad - (1 - 0.91^2 - 0.01)\,\sigma(\bar{4}p) \\ &= 1.079\,\sigma(\bar{3}S) \\ &\quad + 1.558\,(0.91^2\sigma(\bar{4}p) + \sigma(\bar{4}d)) \\ &\quad - 0.162\,\sigma(\bar{4}p).\end{aligned} \qquad (5.3.10)$$

The term, $-0.162\,\sigma(\bar{4}p)$, takes into account the fact that the $\sigma(\bar{4}p)$ cross section includes a contribution to $\Delta\sigma(n>4)$ and this must not be counted twice. To calculate the high-n correction to the 32-state results we use the fact that this must be the difference between σ_{tot}^{cap} and $\bar{\sigma}_{tot}^{cap}$ (from (5.3.3) and (5.3.1)) which can be written as

$$\Delta\sigma'' = 0.74\,\sigma(4\bar{s}) + 0.17\,\sigma(5\bar{p}) \qquad (5.3.11)$$
$$+ 0.82\,\sigma(5\bar{d}) + 0.085\,\sigma(6\bar{d})$$
$$- 0.01\,\sigma(4\bar{p})$$

As shown in Table 5.10, at low E, formulae (5.3.10) and (5.3.11) produce corrections which may differ from each other by a factor of ten or more. For E = 8 - 25 keV lab. (the region of a plateau in Figure 5.2, the n = 3 contributions are particularly large and the principal assumption of the use of 5.3.10 is evidently violated. In the same energy region, as will be seen, the pseudostate basis where the n > 5 states are not represented accurately enough, underestimates, within the formula (5.3.11), the high-n correction to the total capture. This will be discussed in more detail presently when a comparison with optical data of de Heer and co-workers is made.

For higher energies, E > 40 keV lab., the use of both (5.3.10) and (5.3.11) is more justified and both estimates agree well with each other. As Table 5.10 shows, the significance of this correction increases with energy and constitutes some 30 per cent of the total capture at E > 100 keV. lab. It is interesting to see in figure 5.2 that the present data is very consistent: uncorrected (or un-projected) data for both 20- and 32-state bases, underestimates experimental cross sections whereas the corrected data brings theory and experiment together within a probable experimental error within the whole energy interval 8 - 400 keV lab. (an apparent disagreement at the

Table 5.10
High-n corrections $\Delta\sigma$ to computed capture cross sections (in units of 10^{-16} cm^2) obtained using the 20- and 32-state basis sets.

E (keV lab)	High-n corrections			Total cross sections	
	a	b	c	d	e
8.0	20.7	19.9	1.12	120.7	105.6
15.0	15.8	19.0	1.05	122.1	108.2
22.0	18.1	20.9	1.59	114.9	100.2
35.0	22.3	20.5	4.18	99.9	74.0
50.0	16.0	15.4	6.75	56.4	44.4
65.0	10.3	10.3	7.94	33.6	29.5
100.0	3.66	3.52	4.50	9.77	12.4
125.0	1.88	1.60	2.69	4.76	6.49
200.0	0.337	0.332	0.596	0.875	1.265
400.0	0.0246	0.0206	0.0229	0.0919	0.0803

a: Equation (5.3.10) with partial cross sections computed using the 20-state basis.

b: Equation (5.3.10) with partial cross sections computed using the 32-state basis.

c: Equation (5.3.11) with partial cross sections computed using the 32-state basis.

d: The sum of the 20-state total cross sections (row (a) of Table 5.9) plus the high-n correction (a) given above.

e: The total capture cross section obtained by projecting the 32-state basis onto all the projectile bound states (row (c) in Table 5.9).

high energy end of the graph i.e. for E > 200 keV lab., is entirely due to the K-shell effect which will be discussed in the next section).

Quantal partial cross sections $\sigma(\overline{n,1})$ for reaction (5.2.1) presented in Table 5.7 can be compared with the experimental data obtained using optical methods. For He^{2+} + Li, relevant results in the energy region of 12-150 keV lab. have been obtained by de Heer and collaborators (Kadota et al. 1982a, 1982b, Boellard 1984). Capture cross sections $\sigma(n,1)$ are related to the observed line intensities $\sigma_{em}(nl \rightarrow n'l')$ according to

$$\sigma(n,l) = \frac{\sigma_{em}(nl \rightarrow n'l')}{A_{nl\,n'l'}\,\tau_{nl}} - \sum_{n''>n} \sigma_{em}(n''l'' \rightarrow nl) \quad (5.3.12)$$

where $A_{nln'l'}$ is the probability for an (nl→n'l') transition per second and τ_{nl} is the life-time of the nl state. For electrical dipole transitions in one-electron ions these parameters are known and can be used in (5.3.12) to predict experimental capture cross sectins as derived from the observed emission. The first term in this equation contains the branching factor for transitions from the initial state (nl) and the sum gives the cascade correction to the observed intensity of the emission line.

Equation 5.3.12 can be inverted thus giving emission $\sigma_{em}(nl \rightarrow n'l')$ in terms of the capture cross sections. For

instance,

$$\sigma_{em}(2p \rightarrow 1s) = \sigma(2p) + \sigma(3s) + \sigma(3d) + 0.66\,(\sigma(4s) + \sigma(4d)) \qquad (5.3.13)$$

where the coefficient 0.66 accounts for branching into the 2p and 3p states from the higher-lying 4s and 4d states and the population of the $n > 4$ levels of the He^{2+} ion is assumed to be zero.

Kadota et al. (1982a) give equations (5.3.12) with numerical branching coefficients for specific capture cross sections and obtain, by using observed emission intensities, experimental values for partial capture cross sections $\sigma(nl)$, with nl = 2p, 3p, and 4p as well as (3s + 3d), (4s + 4d), and $n > 4$.

The experimental partial capture cross sections should be compared with the theoretical data of table 5.7 only after the projection method has been applied to the theoretical data. The cross sections for capture into the $\bar{2}s$, $\bar{3}s$, $\bar{2}p$, $\bar{3}p$, $\bar{3}d$ and $\bar{4}d$ He^{+} states are taken from Table 5.7 without correction. The capture cross sections into the $\bar{4}s$ and $\bar{4}p$ states are calculated using the data from Table 5.2 and expression (5.3.7). We therefore obtained the following expressions for capture using the projection method:

$$\sigma(4p) \simeq 0.91^2\,\sigma(\bar{4}p) + 0.19^2\,\sigma(\bar{5}p) \qquad (5.3.14)$$

$$\sigma(4s) + \sigma(4d) \simeq 0.72^2\,\sigma(\bar{4}s) + \sigma(\bar{4}d) \qquad (5.3.15)$$

$\sigma_{em}(2p \longrightarrow 1s)$ is obtained from the 32-pseudostate basis, using expression (5.3.13), which gives

$$\begin{aligned}\sigma_{em}(2p \to 1s) = {} & \sigma(\bar{2}p) + \sigma(\bar{3}s) \\ & + \sigma(\bar{3}d) \\ & + 0.66\left(0.72^2\,\sigma(\bar{4}s) + \sigma(\bar{4}d)\right)\end{aligned} \qquad (5.3.16)$$

Using the 20-pseudostate basis and assuming that $\sigma(\bar{4}s)$ is negligible (Table 5.7 shows this to be justified) we obtain the corresponding expression

$$\begin{aligned}\sigma_{em}(2p \to 1s) = {} & \sigma(\bar{2}p) + \sigma(\bar{3}s) \\ & + \sigma(\bar{3}d) \\ & + 0.66\,\sigma(\bar{4}d)\end{aligned} \qquad (5.3.17)$$

The case of $n >= 5$ was considered by using either the $1/n^3$

method or the projection method. From expressions (5.3.8) and (5.3.10) we obtain, for the 20-pseudostate basis,

$$\begin{aligned}\sigma(n \geq 5) &= \Delta\sigma' - \sigma(4\bar{5}) \\ &= 0.657\,\sigma(\bar{3}\bar{5}) \\ &\quad + 1.558\,(0.91^2\,\sigma(4\bar{p}) + \sigma(4\bar{d}))\end{aligned} \tag{5.3.18}$$

For the 32-pseudostate basis we use expression (5.3.16) and (5.3.17) with n = 4 to obtain

$$\begin{aligned}\sigma(n \geq 5) &= 0.74\,\sigma(4\bar{5}) - 0.72^2\,\sigma(4\bar{5}) \\ &\quad + 0.99\,\sigma(4\bar{p}) - 0.91^2\,\sigma(4\bar{p}) \\ &\quad + 0.17\,\sigma(4\bar{p}) - 0.195\,\sigma(\bar{5}\bar{p}) \\ &\quad + 0.82\,\sigma(4\bar{d}) \\ &\quad + 0.86\,\sigma(\bar{5}\bar{d}) - 0.05^2\,\sigma(\bar{5}\bar{d}) \\ &\quad - 0.01^2\,\sigma(\bar{6}\bar{d}).\end{aligned} \tag{5.3.19}$$

The present results for the partial capture cross sections are given in tables 5.11, 5.12, 5.13 and 5.14. Table 5.15 shows the normalised distribution for capture in the n shells of He^+. σ (n = 4) was computed from expressions (5.3.14) and (5.3.15), while σ (n > 4) was computed from expression (5.3.19).

We begin by considering the n shell distribution in table 5.15. This shows the n = 3 shell is the most

Table 5.11

Computed cross sections for the emission $He^+(2p \rightarrow 1s)$ and for capture into $He^+(\overline{4p})$ (in units of 10^{-16} cm^2).

	$\sigma_{em}(2p \rightarrow 1s)$		$(\overline{4p})$
E (keV lab)	a	b	c
8.0	74.3	73.5	1.30
15.0	79.9	81.1	2.50
22.0	72.9	73.5	2.58
35.0	51.3	49.6	3.76
50.0	26.4	28.2	4.33
65.0	14.0	15.3	3.71
100.0	4.81	3.26	1.53
125.0	2.26	1.37	0.737
200.0	0.357	0.245	0.156
400.0	0.0324	0.0362	0.0110

a: Calculated from formula (5.3.16) using the 32-state partial cross sections .

b: Calculated from formula (5.3.17) using the 20-state partial cross sections .

c: Calculated from formula (5.3.14) using the 32-state partial cross sections.

Table 5.12

Computed capture into $He^+(3s) + He^+(3d)$ and into $He^+(4s) + He^+(4d)$ (in units of 10^{-16} cm^2).

	3s + 3d		4s + 4d
E (kev lab)	a	b	c
8.0	67.2	65.0	3.35
15.0	74.5	71.2	6.55
22.0	64.6	62.1	8.43
35.0	37.9	40.9	8.06
50.0	18.9	18.3	6.18
65.0	9.13	8.08	3.83
100.0	1.88	1.65	1.04
125.0	0.721	0.617	0.425
200.0	0.090	0.083	0.075
400.0	0.0068	0.0047	0.0066

a: Computed using the 20-state partial cross sections.

b: Computed using the 32-state partial cross sections.

c: Computed from formula (5.3.15) using the 32-state partial cross sections.

Table 5.13

Computed total capture cross sections into all $n > 4$ states (in units of 10^{-16} cm^2) using the 20- and 32- state basis sets.

E (keV lab)	a	b
8.0	15.1	1.12
15.0	13.3	1.05
22.0	15.9	1.59
35.0	20.7	4.18
50.0	15.3	6.75
65.0	9.97	7.94
100.0	3.57	4.50
125.0	1.83	2.69
200.0	0.325	0.596
400.0	0.0232	0.0229

a: Computed from formula (5.3.18) using the 20-state partial cross sections.

b: Computed from formula (5.3.19) using the 32-state partial cross sections.

Table 5.14

Partial cross sections for capture into n = 3 of He^{+} in collisions between He^{2+} and Li (obtained using the 32-pseudostate basis). The distribution in l.

All corrections are in units of 10^{-16} cm^{2}.

E (keV lab)	l = 0	l = 1	l = 2	Total
8.0	12.6	26.3	52.4	91.3
15.0	5.46	20.7	65.7	91.9
22.0	4.52	17.2	57.6	79.3
35.0	3.20	10.2	37.7	51.1
50.0	1.06	3.74	17.2	22.0
65.0	0.395	2.07	7.69	10.1
100.0	0.215	0.839	1.44	2.49
125.0	0.108	0.414	0.515	1.04
200.0	0.0270	0.0741	0.0555	0.157
400.0	0.00197	0.00689	0.0027	0.0116

Table 5.15

The normalized n-shell distribution for single electron capture cross sections in He^{2+} + Li(2s) collsions computed using the 32-state basis , AO32.

n-shell	2	3	4	>4
E keV lab.				
8	0.0809	0.864	0.044	0.0106
15	0.0573	0.849	0.0836	0.00975
22	0.0828	0.791	0.110	0.0159
35	0.0934	0.690	0.160	0.0564
50	0.116	0.495	0.236	0.152
65	0.132	0.344	0.255	0.269
100	0.229	0.201	0.207	0.363
125	0.247	0.159	0.179	0.415
200	0.223	0.124	0.182	0.471
400	0.351	0.144	0.219	0.285

The normalized distribution is obtained as $\sigma(n)/\bar{\sigma}^{cap}_{tot}$.

$\sigma(2)$ and $\sigma(3)$ are computed directly from Table 5.7 .

$\sigma(4)$ is computed using formulas (5.3.14) and (5.3.15).

$\sigma(n>4)$ is computed using formula (5.3.19).

important up to an energy of 65 keV lab. Preferential capture into the n = 3 state of He^{+} was first predicted for E < 8 keV lab, by Shipsey et al. (1978) using a MO model and, for higher impact energies E = 8 - 40 keV lab, by Bransden and Ermolaev (1981) using a two-state AO model. The present close-coupled calculations show that even at E = 65 keV lab, the n = 3 contribution is expected to give almost 35 per cent of the total capture. For this dominant transition, the computed distribution, in 1, of partial capture cross sections is given in Table 5.14. As this table shows, with an exception of the lowest energy E = 8 keV lab, the computed l-distribution, for n = 3, is never close to the statistical (21 + 1) distribution. For energies E = 35, 50, 65, and 100 keV lab, the computed ratios $\sigma_{30} : \sigma_{31} : \sigma_{32}$ are 1:3.2:11.8;, 1:3.5:16.2; 1:5.2:19.5; and 1:3.9:6.7, respectively. It is also interesting to compare the present quantal results with those obtained using the CTMC method described Ermolaev, Hewitt and McDowell (1987). The total capture results obtained from the CTMC method are shown in figure 5.2 and agree with the present results to within 30% in the energy range 50-200 keV lab. In the energy range 50 - 100 keV lab. the CTMC results for capture into states with n = 2,3,4 and n > 4 states also agrees with the corresponding quantal results to within $\pm$ 30%. Similar behaviour has also been found for other systems (McDowell 1985).

Figures 5.3 to 5.8 show an overall comparison of the

present quantal partial cross sections with the experimental data of Boellard (1984) and Kadota et al. (1982a). We have also included in the graphs the theoretical cross sections computed using the AO^+ data of Fritsch and Lin (1983b). In Figure 5.3, both the partial 2p and the 2p emission cross sections are compared with the corresponding theoretical results. There is excellent agreement between the present data, the AO^+ data of Fritsch and Lin, and both experiments in the whole energy range considered. The population of the 2p level is largely due to cascade from n > 2, and this agreement indicates good accuracy of the n > 2 theoretical data

For 2p capture, agreement with experiment is very good for E > 50 keV lab. At the high energy end of the interval considered by Fritsch and Lin, their data is in good agreement with the present results but for energies E < 50 keV lab. their data lies below our cross sections with the experimental capture lying in between. It is worth pointing out that the small magnitude of the 2p capture makes it difficult to obtain with high accuracy both theoretically and experimentally. In fact below 50 keV lab. Kadota et al. can only estimate an upper limit of 5×10^{-16} cm^2 for 2p capture and the actual values they quote are probably not very accurate. The theoretical problems can be demonstrated by considering the 32- and 20-pseudostate results which show the effect of the positive energy pseudostates upon the 2p capture. At 50, 65, 100 and 200 keV. lab the 32-pseudostate

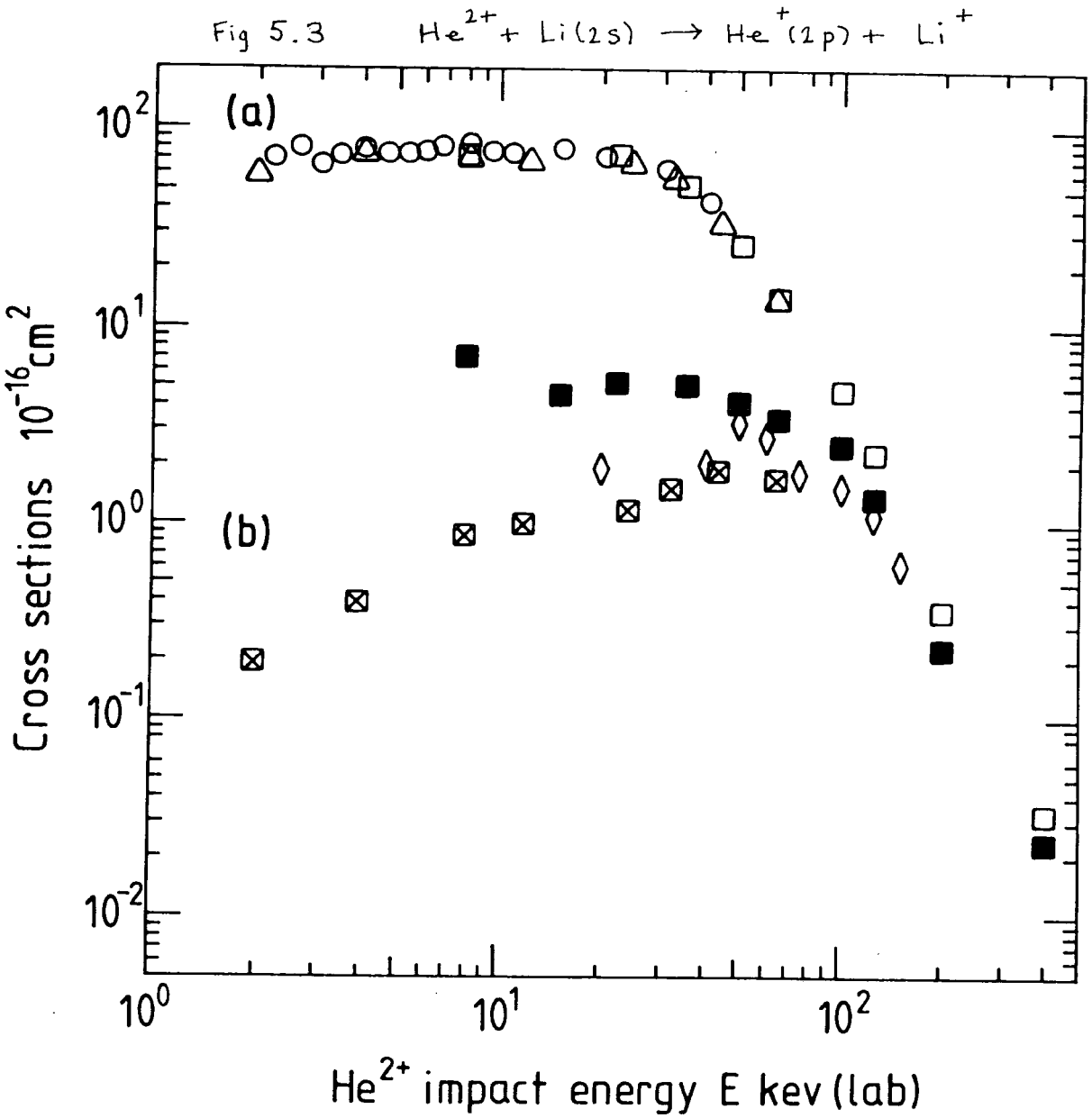
Fig 5.3 $He^{2+} + Li(2s) \rightarrow He^{+}(2p) + Li^{+}$
(a)
(b)
Cross sections $10^{-16} cm^2$
10^2
10^1
10^0
10^{-1}
10^{-2}
10^0
10^1
10^2
He^{2+} impact energy E kev (lab)

Key to Figure 5.3

Theoretical cross sections for 2p -> 1s emission cross section from He^{+}(2p).

□ , 32-state expansion data , using formula (5.3.16) , present work.

△ , 40-state AO+ expansion data of Fritsch and Lin (1983), using formula (5.3.13).

Experimental cross sections for 2p -> 1s emission cross section from He^{+}(2p).

○ , optical data of Boellard (1984).

Cross sections for capture into He^{+}(2p).

Theoretical

■ , 32-state expansion , present work.

⊠ , 40-state United Atom expansion of Fritsh and Lin (1983).

Experimental results

◇ , optical data of Kadota et al. (1982).

Fig. 5.4. $He^{2+} + Li(2S) \rightarrow He^{+}(3p) + Li$

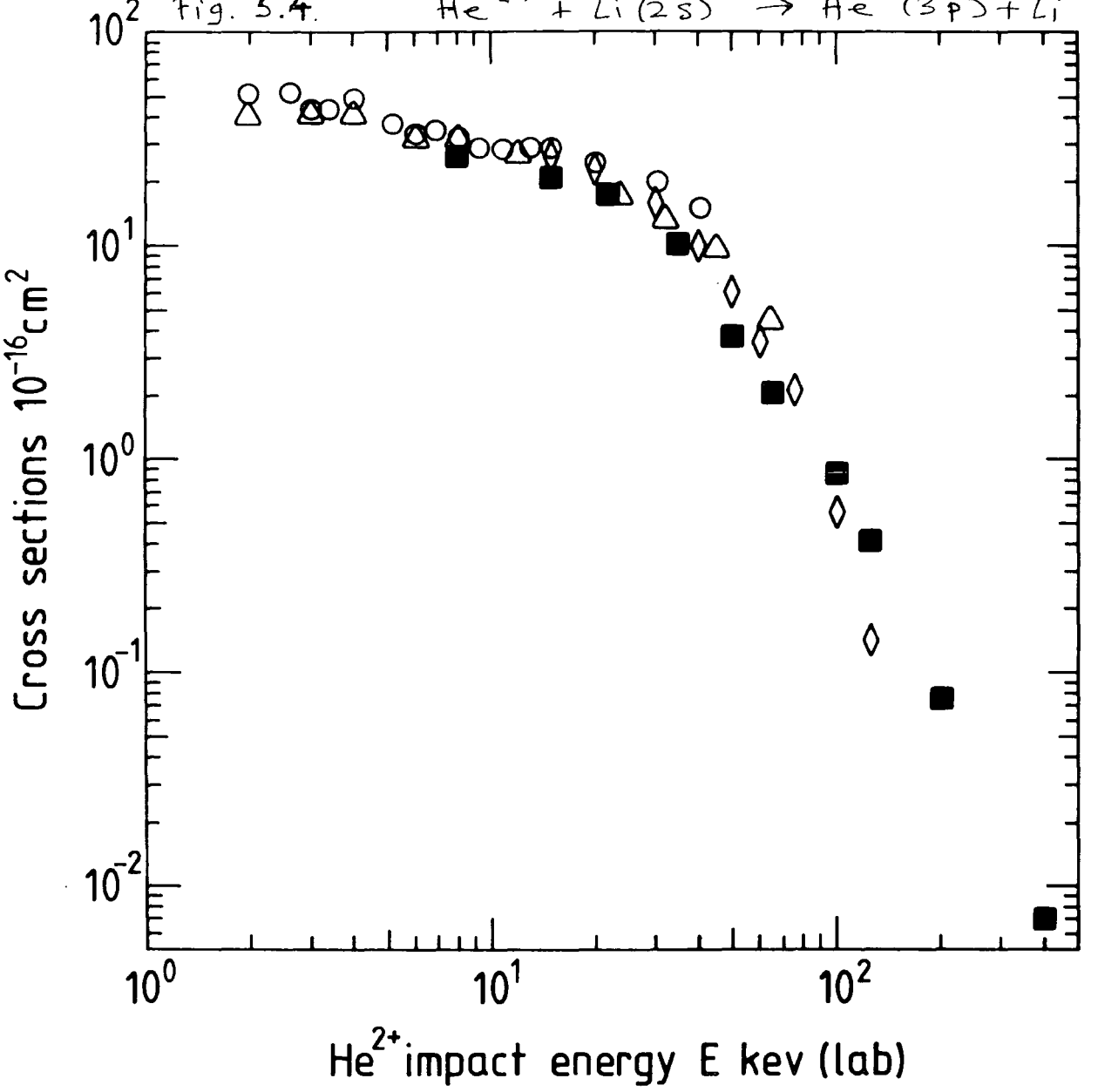

Key to Figure 5.4.

Cross sections for $He^{+}(3p)$ capture.

Theoretical cross sections

■ , 32-state expansion , present work.

△ , 40-state United Atom expansion of Fritsch and Lin (1983).

Experimental cross sections

○ , optical data of Boellard (1984).

◇ , optical data of Kadota et al. (1982a)

Fig 5.5 $H\text{-}e^{2+} + Li(2s) \rightarrow He^{+}(4p) + Li^{+}$

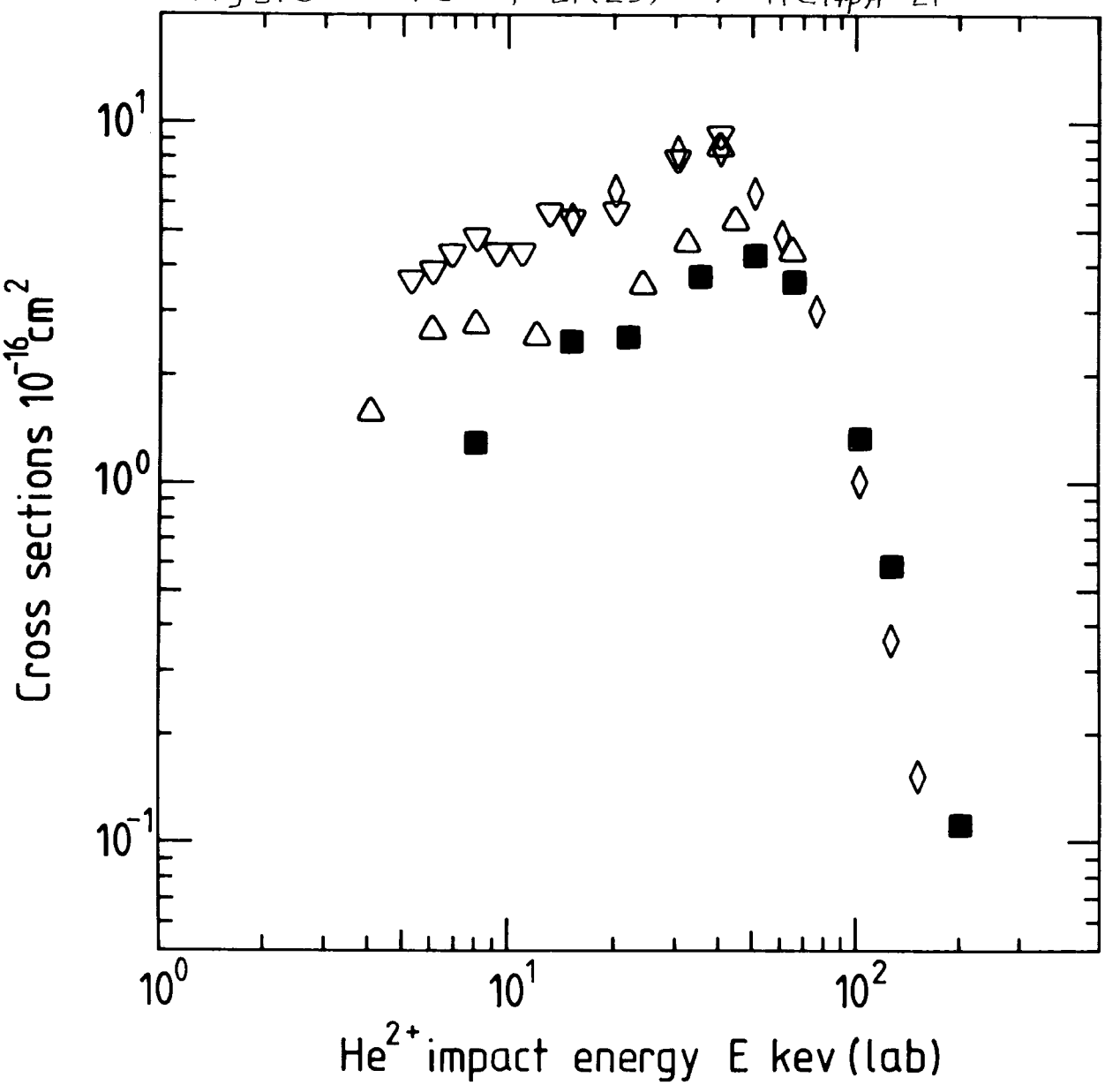

Key to Figure 5.5.

Cross sections for $He^{+}(4p)$ capture.

Theoretical cross sections

■ , 32-state expansion , formula (5.3.14), present work.

△ , 40-state United Atom expansion of Fritsch and Lin (1983).

Experimental cross sections

◇ , optical data of Kadota et al (1982a).

▽ , optical data of Boellard (1984).

Fig. 5.6 $He^+(3s) + He^+(3d)$ capture

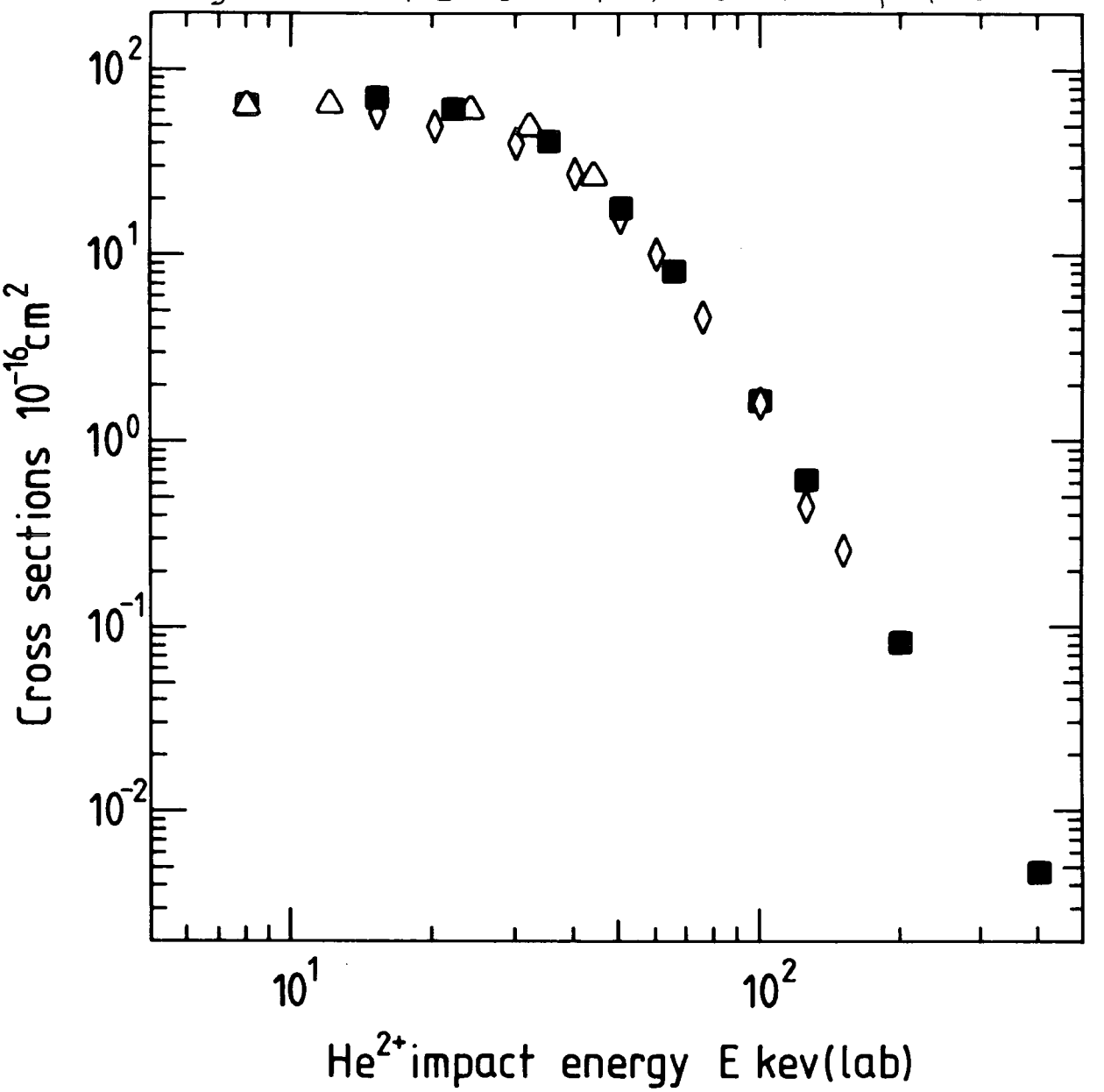

Key to Figure 5.6.

Cross sections for $He^+(3s) + He^+(3d)$ capture.

Theoretical cross sections

■ , 32-state expansion , present work.

△ , 40-state United Atom expansion of Fritsch and Lin (1983).

Experimental cross sections

◇ , optical data of Kadota et al (1982a).

Fig. 5.7 $He^+(4s)$ and $He^+(4d)$ capture

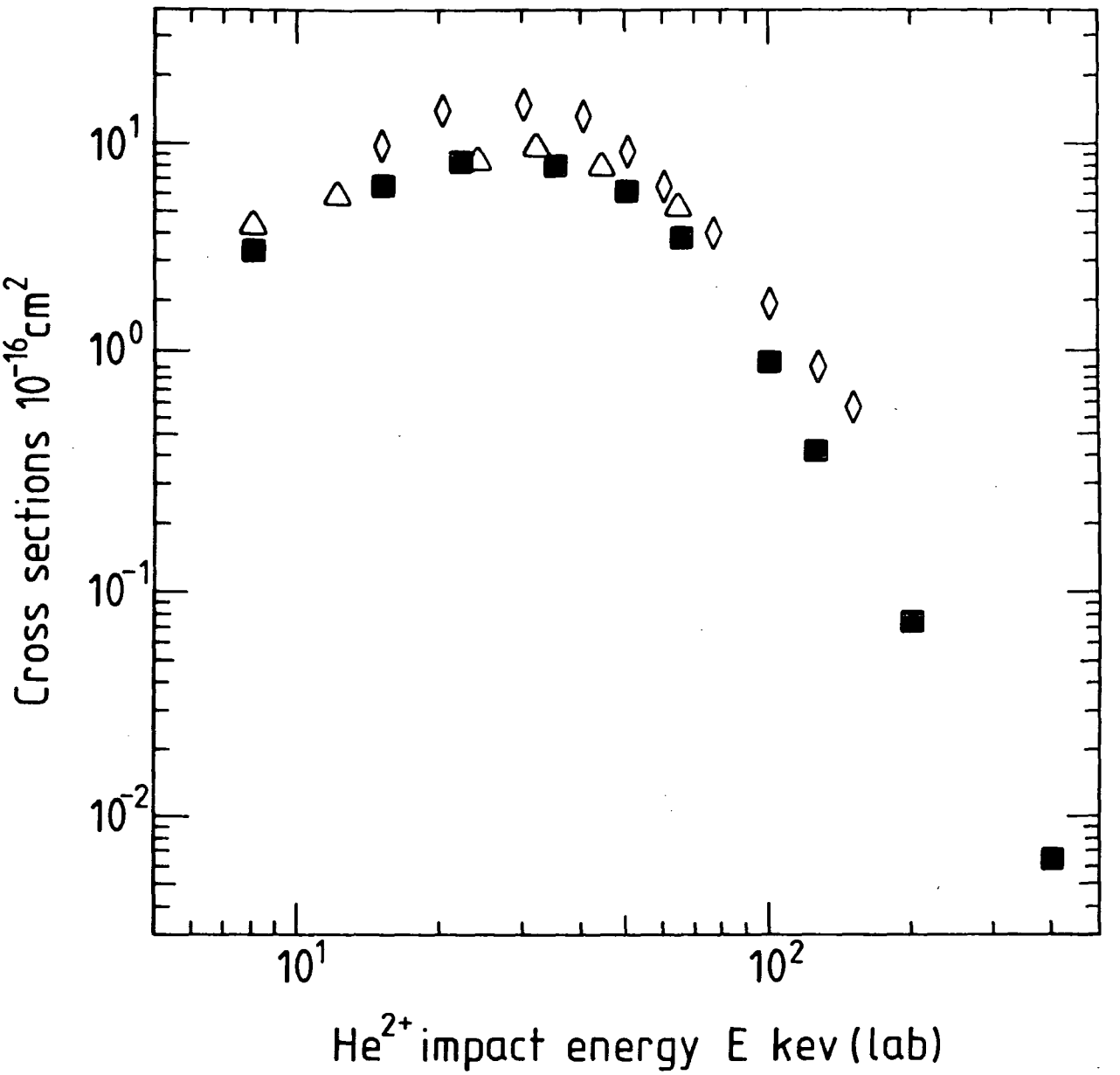

Key to Figure 5.7.

Cross sections for $He^+(4s) + He^+(4d)$ capture.

Theoretical cross sections

■ , 32-state expansion , formula (5.3.15), present work.

△ , 40-state United Atom expansion of Fritsch and Lin (1983).

Experimental cross sections

◇ , optical data of Kadota et al (1982a).

Fig. 5.8 $He^{2+} + Li(2s) \rightarrow He^{+}(n>4) + Li^{+}$

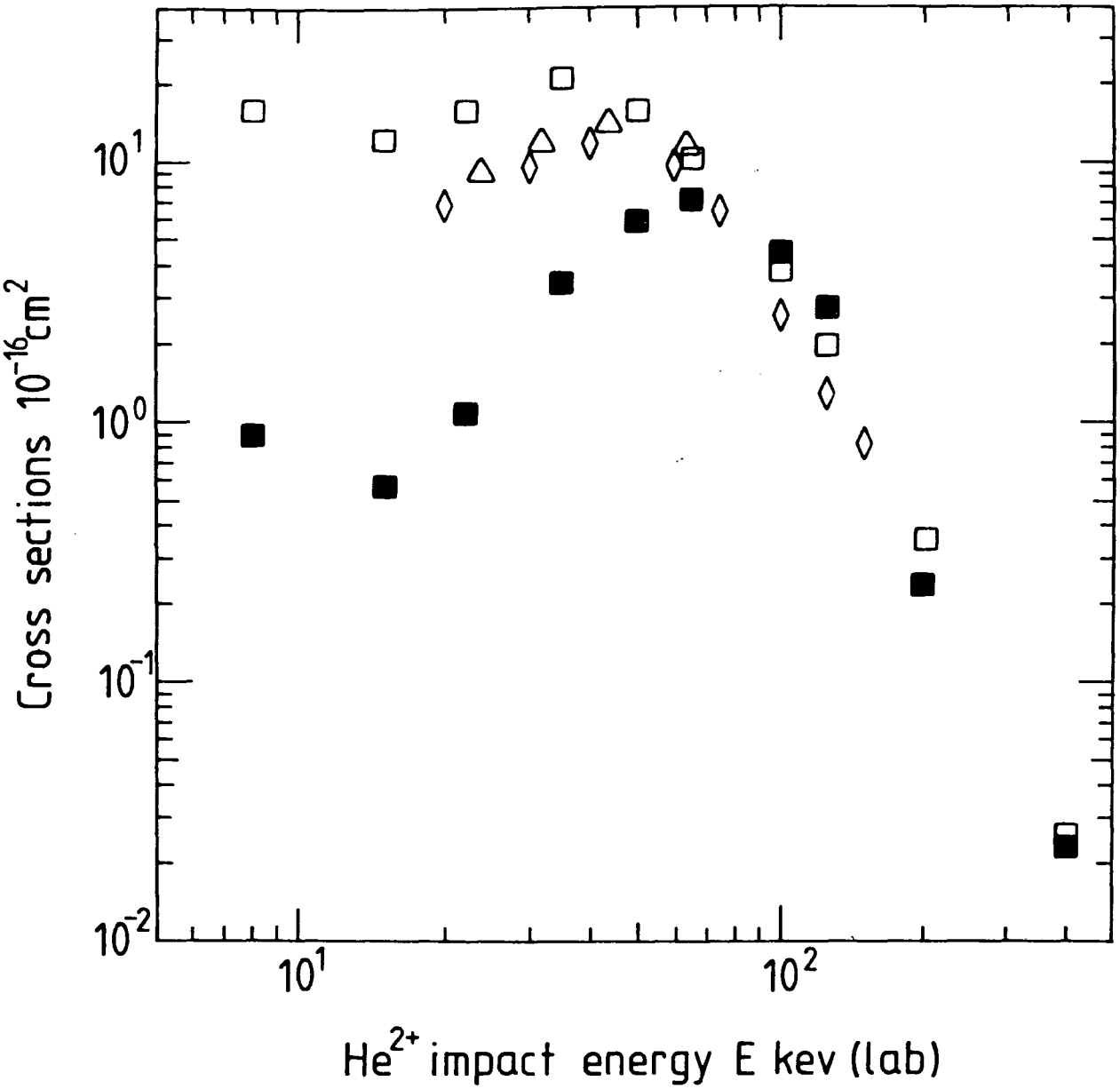

Key to Figure 5.8.

Cross section contributions for capture into $He^{+}(n)$, $n > 4$.

Theoretical cross sections

□ , 20-state expansion , with $1/n^3$ correction from formula (5.3.18), present work.

■ , 32-state expansion , projected total using formula (5.3.19), present work.

△ , sum of n=5 and n=6 estimates of Fritsch and Lin (1983).

Experimental cross sections

◇ , optical data of Kadota et al (1982a).

results are 4.10, 3.38, 2.47 and 0.225 x 10^{-16} cm^2 respectively. The corresponding 20-pseudostate results are 5.19, 3.73, 0.675 and 0.108 x 10^{-16} cm^2 This shows, in the energy region near 100 keV. lab, the effect of introducing the positive energy states in increasing the 2p capture.

For the partial 3p capture, shown in Figure 5.4, the agreement between our results and experiment is good for energies up to E = 100 keV. lab but may show some divergence from the experiment at higher energies. The partial 4p cross sections (see Figure 5.5) agree in the interval 50 - 100 keV. lab within an experimental uncertainty but differ outside the interval. It is interesting to notice that, for E < 50 keV. lab both experiments tend to group together. A similar tendency is also shown, at low energies, by the theoretical data though the latter are a factor of two to three lower than experiment. The agreement of the present data with the other results is satisfactory considering it is obtained from the projection method as in expression (5.3.14).

The present 3s + 3d results (a dominant part of the total capture) and AO^+ data are shown in Figure 5.6. They are in excellent agreement with experiment over the full energy range considered. For the 4s + 4d (see Figure 7), both theoretical sets agree with each other, but experimental data is higher by some 30 per cent than theory at the maximum and this discrepancy increases for energies E > 100 keV. lab. This could be because the He^+(4s) cross

section is obtained by the projection method which presumably underestimates the true cross section at high energies.

Figure 5.8 presents estimates for the sum of all contributions to the total capture for n > 4 states. For E > 50 keV. lab theoretical and experimental data, including 20-state capture cross sections, agree well. However, for lower impact energies, the theoretical data shows striking diversions. The 20-state data overestimate experiment, due to the overestimation, at low energies, of the high-n correction by the $1/n^3$ rule. On the other hand, in our 32-state basis, the pseudostate 4s (with $\mathcal{E}(\bar{4}s)$ = 0.17698 a.u.) gives a reasonable estimate of the 4s contribution, using $\sigma(4s) = 0.72^2\ \sigma(\bar{4}s)$, but fails to accurately represent the 5s and 6s states omitted from the basis. Similarly the $\bar{4}p$ and $\bar{5}p$ states only have a small overlap with higher p states and also the $\bar{6}d$ state lies almost entirely in the continuum. However, the $\bar{5}d$ state does have a large overlap with the d states with n > 4. These conclusions are evident in expression (5.3.19) which shows that of the d states the $\bar{5}d$ state has the largest coefficient. It is therefore not surprising that, since the positive energy He^+ states do not give any significant contribution at the lowest energies (as shown in table 5.8), the projected $\sigma(n > 4)$ sum (expression 5.3.19) is underestimated here. However, at higher energies their contribution increases and therefore the corresponding

projected σ (n > 4) sum increases.

The two-state estimates of these terms by Fritsch and Lin (1983b) show that the corresponding contributions are relatively large at energies where the positive energy states in the 32-pseudostate basis give a much smaller contribution. The present results suggest that the extraction of the σ (n > 4) capture total using the projection method, as in expression (5.3.14), can be unreliable at impact energies where the continuum does not play an important role.

The previous comparison with theory made by Kadota et al. (1982b) used the two-state (TS) capture cross sections of Bransden and Ermolaev (1981). Bransden and Ermolaev suggested that TS data would be accurate for $E > E_c = 40$ keV. lab but overestimate cross sections for lower energies. The estimate of E_c was made using the Massey criterium $V_e = V_c$, where V_e was the velocity of the valence electron in the target atom, for the velocities V_c of the projectile favoured by capture. In fact, within the interval 8 - 100 keV. lab. considered by Bransden and Ermolaev (1981), two-state calculations produced partial cross sections which were close to the experimental capture at the low-energy end but could be out as much as by factor of two at the high-energy end of the interval. This cannot be readily explained on the strength of simple energetics.

The present results allow us to give a more precise analysis of the situation arising in the He^{2+} + Li system at

intermediate energies. First we shall recall a discussion (Ermolaev 1984) of two-state (TS) and multi-state (MS) expansions for p + H. The earlier coupled-state MS calculations of capture (Shakeshaft 1976, 1978) had provided an accurate basis for a comparison of the two models. It turns out that for p + H both methods produce main partial capture cross sections which are very close to each other numerically at E < 100-200 keV. lab. For instance, at incident proton energies E = 15, 25, and 40 keV lab, in units of 10^{-16} cm^2, the TS capture into H(1s) is 56.0, 27.6, and 11.2, respectively, to be compared with the MS values 58.4, 30.4, and 11.9 of Shakeshaft (1978). For n = 2 agreement is also good but it worsens more rapidly with increasing incident energy than for n = 1. In the latter case, TS gives 3.4, 2.7, and 1.95 for capture into H(2s) and 2.2, 2.5, and 1.52 for capture into H(2p), at the same energies, whereas the MS values for H(2s) are 3.4, 4.22 and 2.47 and those for H(2p) are 3.1, 1.74 and 0.72. Therefore, the main capture channels in p + H are not strongly coupled at intermediate impact energies. It was suggested by Ermolaev (1984) that a similar situation may exist in other systems.

The present work confirms that this is also the case for He^{2+} + Li. In both systems, the TS and MS results for the dominant transitions agree well with each other within a wide range of intermediate energies where capture is large and ionisation is not very significant. For He^{2+} + Li, it is

particularly so for capture into the n = 3 shell. However, for higher energies where the ionisation channel becomes important, this agreement between the two-state and multi-state models is less good.

Similarly, we have found, for the dominant n = 3 transition, that the l-distributions of partial cross sections obtained earlier by Bransden and Ermolaev (1981) for He^{2+} + Li, are in a good correspondence with the present multi-state results for energies well below the ionisation maximum at 80 keV. lab. For instance, at E = 8 keV. lab the two-state l-distribution, in units of 10^{-16} cm^2, is 9.1, 31.8 and 59.7 for l = 0, 1, and 2, respectively, to be compared with 12.6, 27.3 and 52.4 of the 32-state calculation. For E = 22.0 keV. lab the two-state distribution is 5.60, 18.1 and 47.7 to be compared with the 32-state result: 4.52, 17.2 and 57.6 respectively. This seems to lend some additional support to the suggestion of Kadota et al. (1982b) that, at E = 20 keV. lab the population of the n = 3 level is even more selective than that predicted by the TS model. For higher energies, this correspondence between the TS and MS models becomes poorer, particularly for l = 2. AT E = 100 keV. lab, the two-state distribution is 0.35, 0.80, and 4.20 to be comapred with 0.22, 0.84 and 1.44, respectively, of the 32-state calculation.

We can make some further comments upon the effect of incuding the continuum in the calculations upon the charge exchange cross sections by examining the impact parameter

distribution of the impact parameter weighted transition probabilities denoted by $bP(b)$. Figure 5.10 shows the distribution of the partial wave contributions to capture into bound states and to ionisation on the projectile. The bound state sums are calculated using the following expression

$$t_N^C(b) = \sum_{(n\bar{l})} b\, P_{(n\bar{l})}(b)\,(1 - q(n\bar{l})) \qquad (5.3.20)$$

where N denotes that the probabilities $pP_{(n\bar{l})}(b)$ are obtained from either the 20- or 32-pseudostate calculations. The ionisation probability sums are obtained by using the expression

$$t_N^I(b) = \sum_{(n\bar{l})} b\, P_{(n\bar{l})}(b)\, q(n\bar{l}) \qquad (5.3.21)$$

In (5.3.20) and (5.3.21) the summations over $(n\bar{l})$ include all the terms corresponding to the angular momentum $\mathbf{l}$. In Figure (5.9) the sums of the separate partial wave contributions to capture and ionisation are shown at E = 100 keV. lab. Figure (5.10) show the result of including the pseudostates upon the capture probabilities. The p-state capture distribution is pulled in towards the origin and its maximum is increased in size, while the d-state capture distribution is increased in magnitude everywhere. Figure (5.9) shows that the total ionisation distribution has a maximum in the region where the

Fig 5.9. $He^{2+} + Li(2s) \rightarrow He^{+}(n) + Li^{+}$

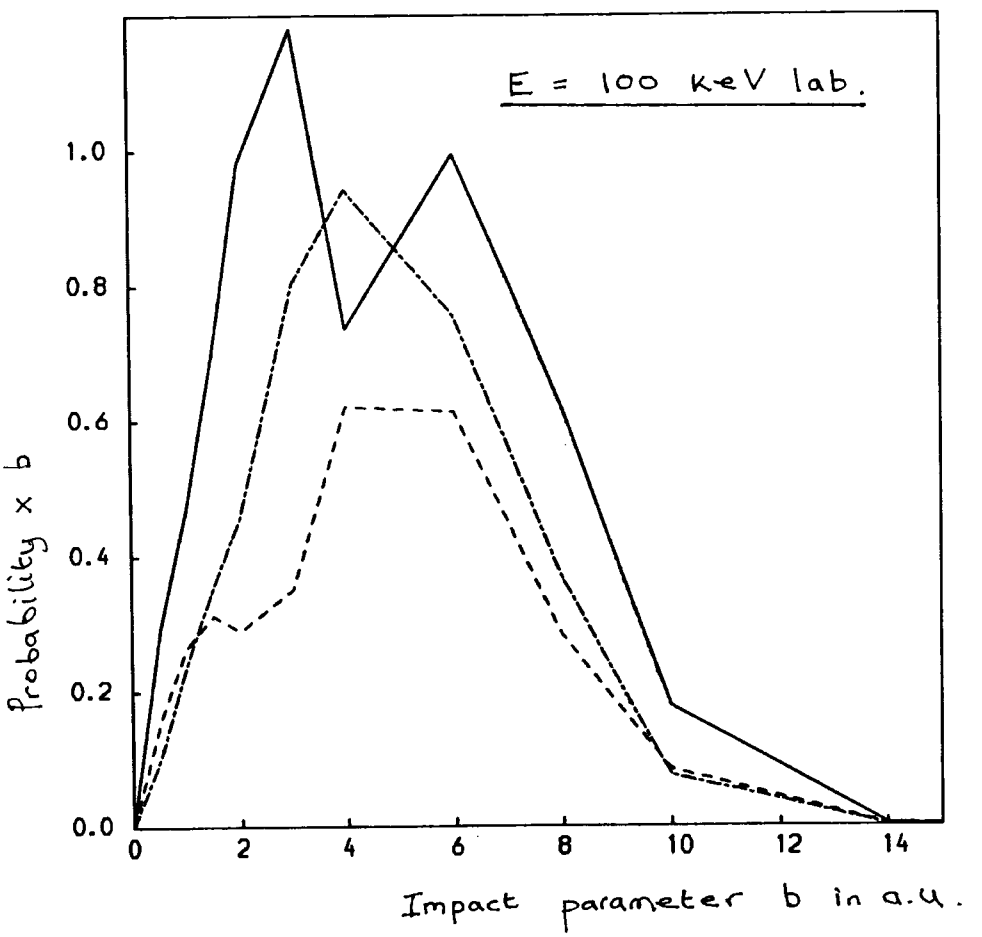

Key to Figure 5.9:

Impact parameter weighted distribution of the total probabilities for capture into bound and continuum states of He^{2+} (i.e. summed over all projectile states after projection).

- - - - - -, 20-state capture probability * b

————, 32-state capture probability * b

—·—·—, 32-state capture into continuum probability * b.

Fig. 5.10 $He^{2+} + Li(2s) \rightarrow He^{+}(n) + Li^{+}$

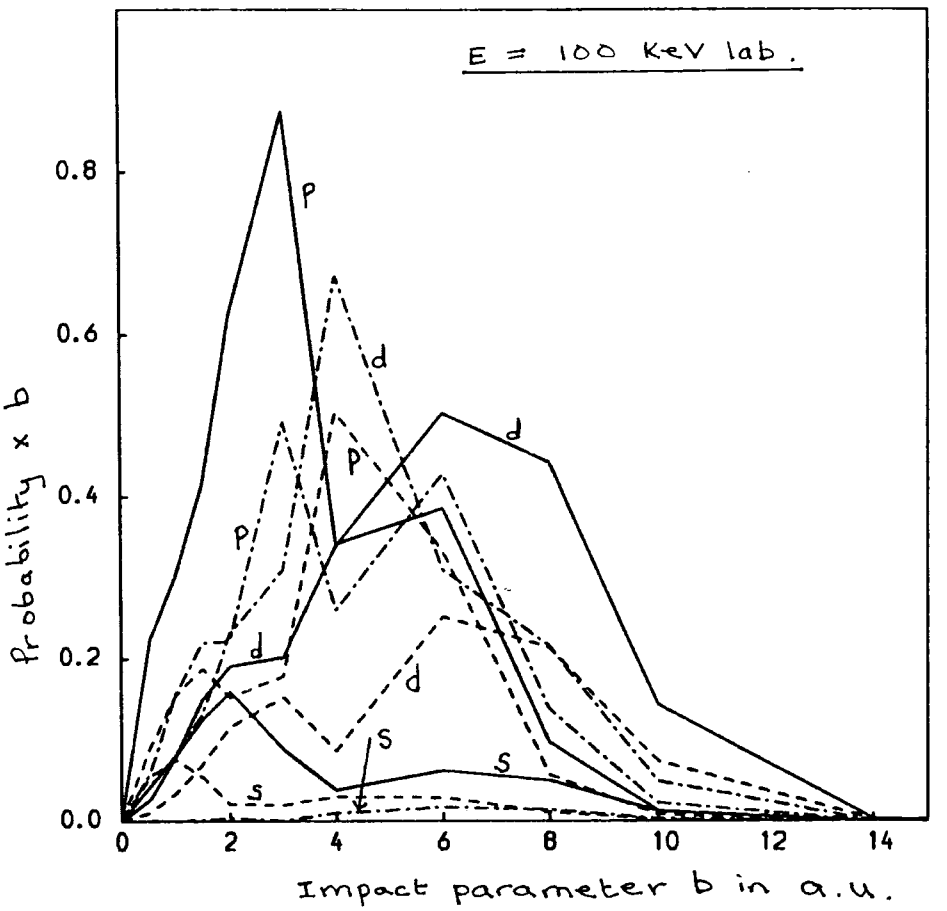

Key to Figure 5.10

Impact parameter weighted distributions of the partial wave probabilities for capture into the bound and continuum states of He^{2+}. The symbols have been described in the text, eqns (5.3.20) and (5.3.21)).

– – – – – , ℓ^{c}_{20}

——— , ℓ^{c}_{32}

– – – – , ℓ^{I}_{32}

Only the ℓ values are indicated in Fig. 5.10.

32-pseudostate capture distribution has a minimum which is not present in the 20-pseudostate capture distribution. Similar conclusions can be made about the corresponding distributions at E = 125 keV. lab. The 32-pseudostate total capture probability shows a minimum due to the p-state distribution being pulled in towards the origin and this is not reflected in the 20-pseudostate data. A similar effect is present at higher energies but at lower energies the pseudostates on the projectile are less important and do not cause a significant redistribution of the probabilities. The result is very interesting because the impact parameter distribution provides a much more sensitive test of the theory than the total integrated cross sections. The effect of adding f-states to the projectile basis is not known, as far as the impact parameter distribution is concerned and would be interesting to investigate.

5.4 Present Results for K-shell Capture

We shall now discuss the single-electron capture from the K-shell of Lithium using the model described in section 5.2.2.

The present calculations of single-electron capture using expression (5.2.10) have been carried out in the energy range from 50 keV. lab up to 2 MeV lab. The various expansion basis sets used to obtain the separate transition probabilities have been described in Section 5.2 and the

results are presented in tables 5.16 and 5.17. Capture cross sections σ_1^c, which represent capture of the outer electron in the model, were obtained using the 23-pseudostate expansion at all energies, while the 43-pseudostate expansion was used only for energies $E > 300$ keV. lab This was because of numerical problems at lower energies which caused a violation of unitarity. Capture cross sections $\sigma_{1'}^c$ which represent capture of the inner electron of the model, were obtained using the 5-state basis at 50 and 100 keV. lab and then wth the 11-state basis at the remaining energies. It can be seen that a low E, $\sigma_{1'}^c$ constitutes only a small fraction of σ_1^c, due to the difference in the binding energies for the two electrons in the model (-4.5 and -2.8 a.u. respectively). As the collision energy increases, both electrons in the model become energetically more equivalent, and at E = 2 MeV. lab the capture cross sections for electrons 1 and 1′ are practically the same.

Table 5.17 confirms that capture into $He^+(1s)$ is by far the dominant process. For E = 300 keV. lab the capture of either electron 1 or 1 into $He^+(nl)$, with nl = 1s, 2p and 2p, represents 95.5, 1.8, and 2.2 per cent of the total respectively. With impact energy E increasing, capture into n = 2 becomes more significant. Still, for the highest energy considered, E = 2 MeV lab, the corresponding values are 70.3, 12.3, and 1.9 per cent, respectively. We shall now consider the capture of the outer electron in the model,

Table 5.16

Quantal cross sections for single-electron capture by He^{2+} from the K-shell of the lithium ion $Li^{+}(1s^{2})$ using the basis set in Tables 5.4 and 5.5 with the effective potential in (5.2.4).

E (keV lab)		1s	2s	2p	Sum of partial cross sections
50.0	(a)	0.396	0.00031	0.000034	0.396
	(b)	0.395	0.00183	0.00531	0.402
100.0	(a)	0.733	0.0009	0.0017	0.736
	(b)	0.768	0.0028	0.0148	0.786
300.0	(a)	0.728	0.0156	0.0081	0.752
	(b)	0.746	0.0170	0.0302	0.793
	(c)	0.780	0.0189	0.0232	0.822
600.0	(a)	0.308	0.0252	0.0124	0.346
	(b)	0.335	0.0411	0.0080	0.384
	(c)	0.331	0.0399	0.0086	0.379
1000.0	(a)	0.114	0.0156	0.0073	0.137
	(b)	0.117	0.0233	0.0024	0.143
	(c)	0.115	0.0231	0.0035	0.142
2000.0	(a)	0.0187	0.00349	0.00122	0.0234
	(b)	0.0164	0.00370	0.00038	0.0205
	(c)	0.0149	0.00324	0.00051	0.0186

a: Partial cross sections obtained from two-state (TS) calculations.

b: Partial cross sections obtained from 23-state calculations.

c: Partial cross sections obtained from 43-state calculations.

Table 5.17

Partial cross sections (in units of 10^{-16} cm^2) for single-electron capture by He^{2+} from the K-shell of $Li^+(1s^2)$ in the Independent Electron Model.

E (keV lab)		$\overline{1s}$	$\overline{2s}$	$\overline{3s}$	$\overline{2p}$	Sum of partial cross sections d	Sum of partial cross sections e	Total [f]
50.0	(a)	0.395	0.00183	0.00115	0.00531	0.402	0.403	0.417
	(c)	0.0127	0.00003	---	0.00083	0.0138	0.0138	
100.0	(a)	0.768	0.0028	0.0012	0.0148	0.786	0.786	0.859
	(c)	0.069	0.0031	---	0.0033	0.073	0.073	
300.0	(a)	0.746	0.0170	0.0168	0.0302	0.793	0.801	
	(b)	0.780	0.0189	0.0088	0.0232	0.822	0.826	1.119
	(c)	0.289	0.0014	0.0005	0.0019	0.293	0.293	
600.0	(a)	0.335	0.0411	0.0890	0.0080	0.384	0.423	
	(b)	0.331	0.0399	0.0517	0.0086	0.379	0.402	0.634
	(c)	0.225	0.0062	0.0005	0.00079	0.232	0.232	
1000.0	(a)	0.117	0.0233	0.0816	0.0024	0.143	0.179	
	(b)	0.115	0.0231	0.0713	0.0035	0.142	0.173	0.289
	(c)	0.106	0.0081	0.0014	0.00062	0.116	0.116	
2000.0	(a)	0.0164	0.00370	0.0191	0.00038	0.0205	0.0289	
	(b)	0.0149	0.00324	0.0161	0.00051	0.0186	0.0257	0.0507
	(c)	0.0208	0.0030	0.0008	0.00043	0.0250	0.0250	

a: Partial capture cross sections σ^c for $He^{2+} + Li^+$ obtained with the 23-state basis.

b: Partial capture cross sections σ^c_{1s} for $He^{2+} + Li^+$ obtained with the 43-state basis.

c: Partial capture cross sections $\sigma^c_{1s'}$ for $He^{2+} + Li^{2+}$ using 4- and 11- state basis sets.

d: Sum of negative-energy state contributions to total capture.

e: Projected total capture cross section (using formula (5.3.1)).

f: Sum of σ^c_{1s} and $\sigma^c_{1s'}$ (from 43- and 11-state results except for E= 50 and 100 keV lab.)

which corresponds to using the potential (5.2.4) to represent the target centre. This was investigated using various basis sets to find if the continuum played an important role during the collision. The dominant 1s transition is described quite well by the TS model, as Table 5.16 shows.

The TS model gives also a very good 2s capture but the TS cross sections for the 2p capture are much more variable. Table 5.16 also shows the effect on the capture channels of including the positive energy pseudostates on the target. In general although the partial capture cross sections from the 23- and 43-pseudostate calculations are altered, the combined sum is very stable with a maximum change of 10 per cent at the highest energy, E = 2 MeV. Since the total positive energy cross section obtained from the 43-pseudostate basis (for target states only) at E = 2 MeV lab is 0.127×10^{-16} cm^2 compared to the total electron capture value of 0.0186×10^{-16} cm^2 this suggests that the coupling between the charge exchange channels and the continuum is rather small even when ionisation is the dominant process.

It also appears that capture into n > 2 states of $He^+(n)$ is negligibly small at low energies but increases with E and at E = 2 MeV lab partial cross sections for capture into n = 1, 2, and n > 2 are 0.0149, 0.0038, and 0.0071×10^{-16} cm^2 where the projection method has been applied to the $He^+(3s)$ cross section. If we apply the $1/n^3$

correction from formula (5.3.5) at this energy with n = 2, the total obtained for $\Delta\sigma(n > 2)$ is 0.616 σ (n = 2) = 0.0023×10^{-16} cm^2, which considerably underestimates the total from the projection method.

Figure 5.11 gives the overall comparison of the present calculations with the experimental data of McCullough et al. (1982), Shah et al. (1985) Sasao et al. (1986a) and Dubois and Toburen (1985). The agreement with Shah et al. (1985) appears to be very good in the interval considered, particularly for low collision energies.

For E = 300 keV. lab, the computed total capture is 1.12×10^{-16} cm^2 to be compared with the experimental value of $0.939 \pm 0.062 \times 10^{-16}$ cm^2. However at the highest energy of E = 2 MeV. lab considered, the computed capture is 0.051×10^{-16} cm^2 to compare with the experimental value of $0.030 \pm 0.003 \times 10^{-16}$ cm^2 (interpolated using experimental values at E = 1892.0 and 2188.0 keV. lab). It appears that the experimental capture of Shah et al. (1985) lies consistently lower than the computed cross sections, the difference being particularly marked at the highest energies. Some of this difference can be traced to the use of expression (5.2.10). In Table 5.17 the total capture from the K-shell has been computed as the sum of the capture cross sections for the outer and inner electron according to (5.2.10). Ford et al. (1982) discuss, in the case of capture by protons from the K-shell of ionic lithium Li^+, the difference between using expression (5.2.9) and (5.2.10). They find that in the

Fig. 5.11 K-shell capture from Li by He^{2+}

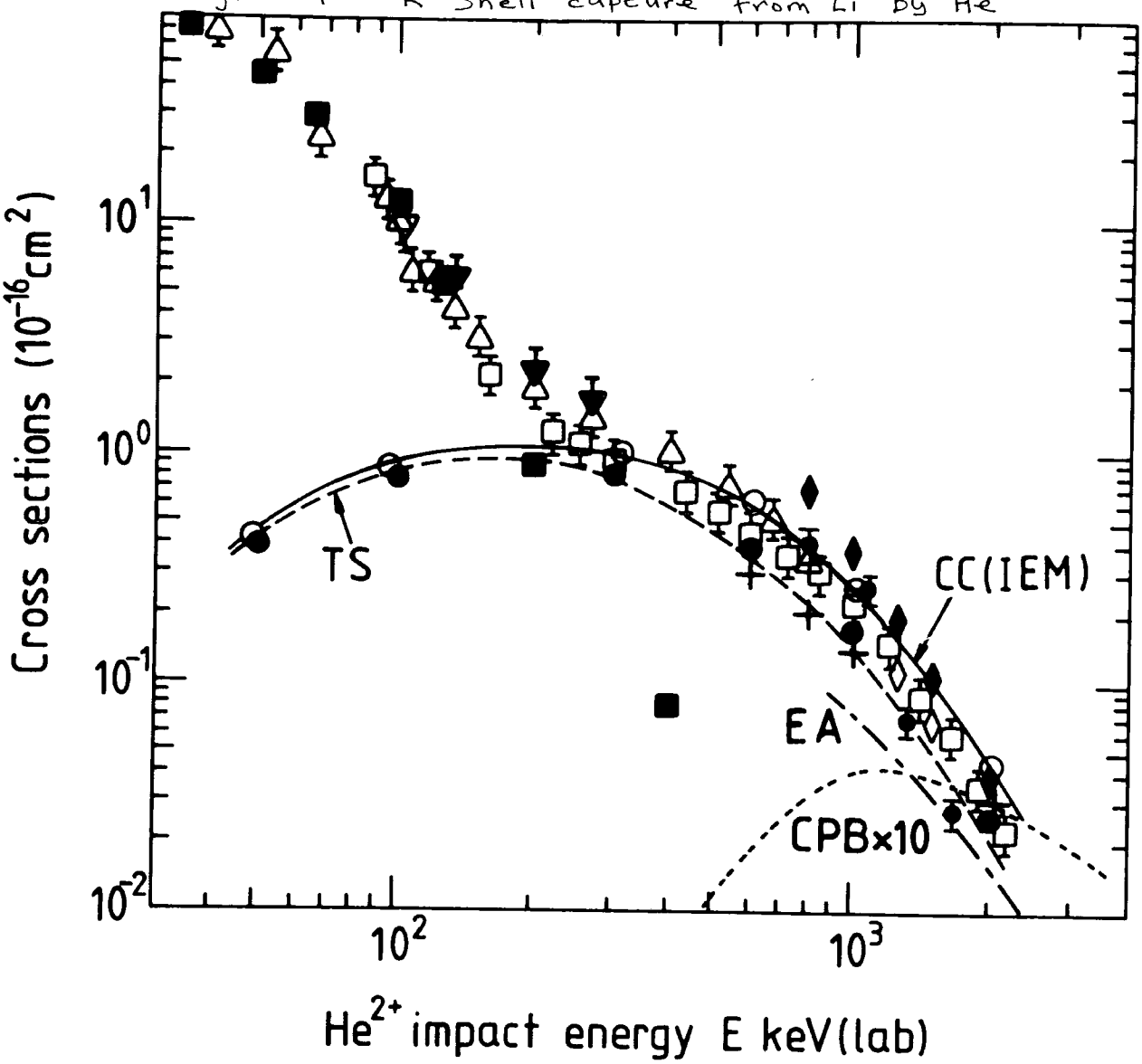

Key to Figure 5.11.

Single-electron capture from the K-shell of Li^{2+} in He^{2+} + Li collisions.

Theoretical cross sections.

– – – TS , one-active electron approximation using the two-state expansion ,projected total from present work (Table 5.16).

● , 23-state expansion for E < 300 keV lab. and 43-state expansion for E >= 300 keV lab., (projected totals) , present work(Table 5.17).

■ , 32-state projected total L-shell capture for comparison , present work.

—— ○ , IEM total for two active electrons obtained using (5.2.10) , (Column (f) , Table 5.17).

\+ , Classical Trajectory Monte Carlo method from Ermolaev, Hewitt and McDowell (1987).

◇ , CDW data of Ghosh et al. (1985) , n <= 3 total.

◆ , CDW data of Ghosh et al. (1985) , with $1/n^3$ correction.

—·—·—, EA, eikonal approximation , Eichler and Chan (1979).

– – – – , CPB, Coulomb Projected Born approximation , Lal et al. (1982).

Experimental cross sections for single electron capture from Li by He^{2+} .

 , McCullough et al. (1982).

 , DuBois and Toburen (1985).

 , Shah et al. (1985)

 , Sasao et al. (1986a)

energy range from 70 to 400 keV. amu^{-1} expression (5.2.10) may overestimate capture by up to 15 per cent. In the present case it appears that a similar correction improves the agreement of the present results with the available experimental data other than those of Sasao et al. (1986a). We have obtained an estimate of this correction using the AO43 basis set for the outer electron probabilities, and a basis set consisting of 49 states for the inner electron proabilities, described in the next section. This basis contained only a single projectile centre state, $He^{+}(1s)$. For the He^{2+} impact energy of 2 MeV lab. the capture cross section for the inner electron obtained using the 11-state basis and the 49-state basis are 0.0208×10^{-16} cm^{2} and 0.0182×10^{-16} cm^{2} respectively. This shows that the inclusion of 47 target centres states only decreases the capture cross section by some 12 per cent. At 600 keV lab. the same capture cross section computed using the 11- and 49-state basis sets in units of 10^{-16} cm^{2} has the values of 0.225 and 0.217 respectively. This shows the projectile and target excited states are not coupled very strongly. Using AO43 and the 49-state basis set and the expression (5.2.9) for combining the probabilities, rather than (5.2.10) we find that, at 2 MeV lab., the outer electron capture cross section is reduced from 0.0257 to 0.0230×10^{-16} cm^{2}, while for the inner electron the capture is reduced from 0.0182 to 0.0156×10^{-16} cm^{2}. Therefore the total capture cross section is reduced by some 12 per cent from 0.0439 to

0.0386×10^{-16} cm^2, compared to the interpolated Shah et al. experimental results of $0.030 \pm 0.003 \times 10^{-16}$ cm^2. The calculated value should also include a small contribution from capture into higher projectile states from the inner electron and this is about 0.0042×10^{-16} cm^2 (from the 11-state basis). Hence the best theoretical result is still about 30 per cent too high at 2 MeV lab. At 300 keV lab. the theoretical results obtained from the 43- and 11-state basis sets, using expression (5.3.10), overestimates the experimental value by some 16 per cent. It appears that the IEM model we have used may in general overestimate the experimental results, but these are subject to the possibility of a 20 per cent renormalization factor due to the uncertainty in the Lithium vapour density. Therefore any final conclusion is difficult. Sasao et al. agree qualitatively with Shah et al. at lower energies but generally, for single capture, their results appear to display a difference dependence upon E as E increases, and at E = 1640 keV. their result is only 50% of that obtained by Shah et al.

Figure 5.11 also shows the eikonal approximation (EA) of Eichler and Chan (1979), the Coulomb projected Born approximation (CPB) of Lal et al. (1982), and the data of Ghosh et al. (1985), who used the continuum distorted-wave approximation (CDW). (Numerical data for the EA and CPB curves shown in Figure 5.11 have been taken from figure 1 of Sasao et al. 1986b). Ghosh et al. (1985) computed both

single-electron and two-electron capture for the energies E = 800 to 2000 keV. lab, using the CDW model and electron transfer probabilities obtaind from the independent-electron model of McGuire and Weaver (1977). For single-electron capture, Ghosh et al. directly computed partial cross sections, with n = 1,2, and 3, and corrected them by using the $1/n^3$ rule. There is a good correspondence between the present IEM results and the data of Ghosh et al. at E = 2 MeV. lab. They obtain the values of 0.0252 and 0.0386×10^{-16} cm^2 for capture into He^+(1s) and for capture into all states respectively. The present values, from table 5.17, are 0.0357 and 0.0507×10^{-16} cm^2 respectively, subject to the use of expression (5.2.10). The present computed value obtained for He^+(1s) capture, using the 43- and 49-state basis sets and expression (5.3.9), is 0.0289×10^{-16} cm^2 and this compares very well with the CDW value of Ghosh et al. of 0.0257×10^{-16} cm^2. This agreement worsens rapidly as the impact energy E decreases and, for example, at E = 1 MeV lab the CDW capture is 0.370×10^{-16} cm^2 to be compared with the experimental value of $0.216 \pm 0.014 \times 10^{-16}$ cm^2 (Shah et al. 1985) and with the quantal vaue of 0.289×10^{-16} cm^2.

It also appears that estimates of Ghosh et al. (1985) for the n = 1 and n = 2 cross sections are much larger than those obtained in the present work, particularly at the lowest energy, E = 800 keV. lab.

5.5 The Calculation of the Ionisation of Li by He^{2+}

5.5.1 The ionisation basis sets.

We have now completed the discussion of single-electron capture from lithium and presently we shall consider ionisation of Li. Firstly it is necessary to describe the new model of Li(2s) that was constructed to describe this process and why it was different to that described in Section (5.2.1).

The two centre thirty-two state basis expansion, which has been described in Section (5.2.2) is only expected to be useful for calculating charge transfer cross sections in the He^{2+} + Li(2s) system. The cross sections for charge exchange into bound states can be calculated and the basis will also allow an estimate of the CTTC process referred to previously in Section (2.4), because of the positive energy pseudostates on the He^{2+} centre, which overlap with the continuum states. However direct ionisation will be very poorly represented because there is only a single positive energy d state on the Li centre. A comparison of the 32 state ionisation cross section with those from the CTMC calculations of McDowell (1985p) revealed that the classical results for ionisation were substantially larger than the quantum mechanical values for energies less than 100 keV. lab.

This suggests that direct ionisation is important in this energy range as well as at higher energies when the

Born approximation is valid. We also expect that the direct excitation cross sections of the bound states in the 32-pseudostate basis are likely to be inaccurate at low energies because of the neglect of couplings to the target states omitted from the 32-state expansions.

The problem of the calculation of ionisation can be approached from two different viewpoints. Firstly one can add more states which represent the continuum about both centres, to the original 32 state basis. This would result in a very complete description of the collision process and should provide accurate cross sections for both the direct and CTTC ionisation channels. This method is justifiable a priori and the interpretation of the final cross sections is relatively straight forward. However it would result in an unreasonable amount of computational time being used to calculate the corresponding exchange matrix elements. There may also be numerical problems solving the larger set of coupled equations. For these reasons we decided upon a second approach, which is sufficient for large impact energies but is less justified at the lower impact energy range. In this approach we expanded the total wavefunction about the Li centre using a large basis containing positive and negative energy pseudostates, and use only a single state upon the He^{2+} centre. This single state will provide some approximation to the charge exchange channels and may have some effect on the direct channels. At large impact energies when the first Born approxiation is valid (and

where charge exchange is negligible compared to excitation) we expect this basis set to provide the correct cross sections for the direct channel processes with the only limitation being the accuracy with which the bound states and the continuum states of the Li atom are represented by the basis states in the expansion.

However, as the impact energy decreases and the charge exchange channels become important we suspect that the simplified model will become less accurate. This approach shall be called the Extended One Centre method (EOCM) as distinct from the previously described two centre basis set expansions. We can justify the EOCM a posteriori by comparison with other calculations and experimental data and this will be done in the next section. Firstly the EOCM basis expansion will be considered in detail.

5.5.2 Calculation of 54 state basis set

The calculation of the large basis set on the Li centre using the model potential of Danielle (1979) from expression (5.2.2) was not followed in the present work. We recall that the Danielle model potential was obtained simultaneously along with the corresponding wavefunctions to form a consistent model of the Li atom. We have modified this approach for several reasons to be given below. Firstly, in Chapter 2 it was shown that it is desirable to use basis sets which result from a single diagonalization (unrestricted Ritz principle) in order to retain the important second order characteristics of the coupled

equations solution. We also need the s type pseudostates to reproduce several negative and positive energy eigenvalues from this diagonalization procedure to span the bound and continuum states. However, if set of six s type STO's (for example) is diagonalized using the Danielle model potential given in (5.2.2), the second lowest eigenvalue corresponding to the energy of the Li(2s) state is usually found to be below the experimental value of -0.1982 a.u.

The STO parameters were selected to give reasonably small positive eigenvalues but were not optimized in any other manner. From the well known Hylleras-Undheim theorem (1930) this result implies that the upper bound to the second lowest eigenvalue of the Danielle model potential is lower than the experimental value and the corresponding state is unlikely to represent the Li(2s) state accurately. Therefore the model potential parameters were changed so that the second lowest eigenvalue was equal to the experimental value for a particular basis set, using the unrestricted Ritz method. In the same spirit as the Danielle approach the same form was retained for the model potential. The new potential is given below

$$V(r) = -\frac{1}{r} - e^{-3.2r}(2 + 3.2r) \qquad (5.5.1)$$

This potential was used to determine all other states for all values of l (i.e. no angular dependent model potentials were used in the calculations). The s basis STO's which

were used to construct the pseudostates are given in Table 5.18 with the corresponding eigenvalues. By construction the Li(2s) energy is reproduced. The energy of the Li(3s) pseudostate, -0.0731 a.u., is close to the exact value, -0.0742 a.u. However the last Li s pseudostate with a negative eigenvalue will represent the higher bound states and some of the continuum states because of its small negative energy. The lowest eigenvalue produced is -1.88 a.u. and this represents an unphysical fictitious state for the Li valence electron with an energy that is not physically observable. Because of its large negative energy this state would not be expected to couple strongly to any other states in the expansion in the ionisation calculation. Also it would not have any physical interpretation at large time values as its overlap with the continuum and physical bound states is zero. Therefore we have neglected this state in all subsequent calculations.

Once the model potential form has been established which produces an Li(2s) energy in agreement with experiment, a basis of seven p type STO's was diagonalized. The criteria for the choice of pseudostates was based on the previously discussed idea of obtaining the correct oscillator strengths for certain transitions. The oscillator strengths for all the p states were found using the previously determined Li(2s) state as the initial state. By adjusting the STO parameters a set of p type pseudostates was found which included one with an energy

Table 5.18

Radial wavefunctions of the 54-state basis employed in the present L-shell ionization calculations.

Target centre (Li^{+}).

State (nl)	$\lambda(\overline{nl})^{a}$	$\bar{\epsilon}(\overline{nl})^{b}$	$q(\overline{nl})^{c}$	STO basis n_i	STO basis β_i
$\overline{2s}$	- 0.1982	-	0.00	0	0.50462
$\overline{3s}$	- 0.073	-	0.00	1	0.50462
$\overline{4s}$	- 0.00034	-	0.37	0	0.80864
$\overline{5s}$	0.278	0.253	0.94	1	0.80864
$\overline{6s}$	1.342	0.818	0.95	0	1.05
				1	1.05
$\overline{2p}$	- 0.1306	-	0.00	1	0.635
$\overline{3p}$	- 0.0514	-	0.01	2	0.635
$\overline{5p}$	0.043	0.103	0.76	1	0.86164
$\overline{5p}$	0.281	0.955	0.95	2	0.86164
$\overline{6p}$	0.893	1.570	0.97	1	1.90
$\overline{7p}$	2.629	2.821	0.98	2	1.90
$\overline{8p}$	9.45	11.72	0.96	1	2.40

Table 5.18 continued.

Target centre (Li^+) continued .

State $(\overline{nl})$	$\lambda(\overline{nl})^a$	$\bar{\epsilon}(\overline{nl})^b$	$q(\overline{nl})^c$	STO basis n_i	STO basis β_i
$\overline{3d}$	- 0.0556	-	0.00	2	0.265
$\overline{4d}$	- 0.0312	-	0.00	3	0.265
$\overline{5d}$	- 0.0144	-	0.066	2	0.450
$\overline{6d}$	0.0385	0.057	0.91	3	0.450
$\overline{7d}$	0.239	0.285	0.96	2	1.0
$\overline{8d}$	1.009	1.174	0.98	3	1.0
$\overline{4f}$	- 0.0312	-	0.00	3	0.25
$\overline{5f}$	- 0.0129	-	0.10	4	0.60
$\overline{6f}$	0.0419	-	0.94	5	0.70
$\overline{7f}$	0.225	-	0.98	4	0.90

a) States $(\overline{nl})$ and energies $\lambda(\overline{nl})$ are obtained by diagonali-
-zing the Hamiltonian $-\frac{1}{2}\nabla^2+V$ with V from eqn (5.5.1)
usinh the STO basis sets in the last two columns of the table.

b) The energies are determined by the method of Reading et al (1979) using equations (5.5.4) .

c) The quantities $q(\overline{nl})$ are determined from eqn (2.4.32) by the overlaps between the pseudostates $(\overline{nl})$ and the continuum of the Hamiltonian $-\frac{1}{2}\nabla^2+V$,with V from eqn (5.5.1)

which is close to the experimental Li(2p) energy of -0.13025 a.u. The second restriction was that the oscillator strength sum for all transitions into positive energy p pseudostates, from the Li(2s) state, should be close to the value given by Cowan (1981) for the Li(2s-> p continuum) oscillator strength sum. The Li(2s -> 2p) oscillator strength was calculated and initially this was not satisfactorily close to the experimental value so the process of finding an s type basis and a p type basis as described above was repeated until a more reasonable agreement was found. Once the p pseudostates were determined a d type basis was diagonalized and the oscillator strengths from the Li(2p) state into all the d states were found, with the usual restriction that the lowest eigenvalue be close to the correpsonding experimental value and also that the positive energy d psedostates have a total oscillator strength close to the value from Cowan (1981) for the Li(2p -> d continuum) oscillator strength. In the same manner an f state basis was constructed so that it reproduced the hydrogenic oscillator strength sum for transitions from the H(3d) state, when the oscillator strength from the Li(3d) state into the f states was calculated. This is justified because the Li states for high l are almost hydrogenic in character. Table 5.19 shows that there is a good correspondence between the present values and those from Cowan (1981), obtained by using the Hartree-Fock method, for the most important oscillator

Table 5.19 Oscillator strengths for some transitions in Li computed using the 54-pseudostate basis. Comparison with the values from Cowan (1981) obtained using the Hartree-Fock method.

Init. state	Li($\overline{2s}$)		Li($\overline{2p}$)		Li($\overline{2p}$)		Li($\overline{3d}$)	
Final state	Li($\overline{np}$)		Li($\overline{ns}$)		Li($\overline{nd}$)		Li($\overline{nf}$)	
	a	b	a	b	a	b	a	b *)
n = 2	0.817	0.788	-0.248	-0.263	-		-	
n = 3	0.020	0.003	0.116	0.120	0.628	0.693	-	
n = 4	-		0.030	0.013	0.129	0.128	1.018	1.016
n = 5	-		-		0.131	0.048	0.340	0.156
c	0.837	0.803	-0.102	-0.119	0.888	0.940	1.358	1.303
d	0.313	0.318	0.0097	0.023	0.222	0.222	0.049	0.098
e	1.15	1.12	-0.092	-0.09	1.11	1.16	1.41	1.40

a: Present calculation using the AO54 basis.
b: Computed using the Hartree-Fock method , from Cowan (1981).
c: Sum over negative energy states of the AO54 basis.
d: Sum over positive energy states of the AO54 basis.
e: Total of (c) + (d) .
*) Hydrogenic oscillator strengths.

strengths and oscillator sums in Li. We also find the lowest experimental energies for single excitation of Li(2s) are well reproduced as shown in Table 5.20.

Table 5.20 includes values of the energies $\bar{e}_{Kl}$ defined for the positive energy pseudostates only. The $\bar{e}_{Kl}$ were suggested by Reading et al. (1979) as a test of the accuracy of a basis set in representing the continuum. The $\bar{e}_{Kl}$ are associated with 'effective' widths which were computed using the method suggested by Reading et al. (1979) and were obtained from the formula

$$\Delta_{Kl} = \frac{\pi}{2 N_{Kl}^2} \tag{5.5.2}$$

where N_{Kl} was determined from

$$N_{Kl} = \frac{\left[\int_0^\infty j_l(kr)\, 2V(r)\, R_{Kl}(r)\, r^2\, dr \right]}{\int_0^\infty R_{Kl}^2(r)\, 2V(r)\, r^2 dr - \int_0^\infty \int_0^\infty R_{Kl}(r')\, 2V(r') \left(\frac{-1}{K} j_l(kr_<)\, \eta_l(kr_>)\right) R_{Kl}(r)\, 2V(r)\, r^2 r'^2 dr dr'} \tag{5.5.3}$$

where $j_l(kr)$ and $\eta_l(kr)$ are the usual spherical Bessel functions (Weissbluth (1978)). $R_{Kl}(r)$ is the radial wavefunction corresponding to the pseudostate with energy $\varepsilon_K(l)$ The success of this method is based upon the fact that, over a limited region of r , the pseudostate $R_{Kl}(r)$ and the exact continuum state with the same energy differ

Table 5.20

Comparison of the calculated and experimental energies for single excitation of Li(nl). Values of the Reading et al. parameters $\bar{e}_{k\ell}$ for the positive energy states are also given.

State $(\overline{n\ell})$	Experimental energy level [a]	Calculated energy [b]	$\bar{e}_{k\ell}$ [c]
$\overline{2s}$	-0.19814	-0.1982	--
$\overline{3s}$	-0.07418	-0.073	--
$\overline{5s}$	--	0.278	0.253
$\overline{6s}$	--	1.342	0.818
$\overline{2p}$	-0.1302	-0.1306	--
$\overline{3p}$	-0.0572	-0.0514	--
$\overline{4p}$	--	0.043	0.103
$\overline{5p}$	--	0.281	0.955
$\overline{6p}$	--	0.893	1.570
$\overline{7p}$	--	2.629	2.821
$\overline{8p}$	--	9.45	11.72
$\overline{3d}$	-0.0556	-0.0556	--
$\overline{6d}$	--	0.0385	0.057
$\overline{7d}$	--	0.239	0.285
$\overline{8d}$	--	1.009	1.174

a : Experimental energy levels .

b : Computed energies using the AO54 basis set.

c : Computed values of $\bar{e}_{k\ell}$ using eqn. (5.5.4).

only by a normalization factor N_{Kl} as shown by Reading et al. (1979). The $\bar{e}_{Kl}$ can be defined as follows

$$\bar{e}_{Kl} = \frac{1}{2}\left(\Delta_{Kl} + \Delta_{(K-1)l}\right) + \varepsilon^{(l)}_{K-1} \qquad (5.5.4)$$

For an ideal basis then we expect that

$$\bar{e}_{Kl} \approx \varepsilon_K(l) \qquad (5.5.5)$$

but this will be violated in the case of a finite L^2 basis. The results in table 5.20 show that the A054 basis does not satisfy the Reading et al. criteria (5.5.2) very closely ($\bar{e}_{Kl}$ was not computed for f states in A054).

The effectiveness of this basis set in representing ionisation will be described in connection with the Born approximation in the next section.

Ionisation of the K-shell was also considered using various basis sets. The 43-pseudostate basis used to study capture of the outer electron from the K-shell, as described in Section 5.2.2, included a total of 21 positive energy pseudostates which provided an estimate of ionisation from the same capture calculatins. Therefore no further pseudostate basis sets were constructed for the outer

electron. This basis set will be denoted by AO43. The basis sets used to study capture of the inner electron in the K-shell contained no continuum contribution and a new basis set was used for the ionisation calculations. According to the corresponding potential (5.3.4) the target states in this basis are purely hydrogenic in character. The basis STO parameters were chosen therefore so that certain exact oscillator strength sums were reproduced by the basis states. The basis parameters are given in Table 5.21. The oscillator strength sums for the transitions Li^{2+} (1s - > s continuum), Li^{2+} (2p - > p continuum) and Li^{2+} (2p - > d continuum) obtain with the basis were 0.448, 0.183 and 0.0095 respectively, compared to the exact values of 0.435, 0.183 and 0.008 (where the positive energy states represented the continuum).

The corresponding sums for transitions into all the s,p and d bound states (represented by the negative energy states) were -0.119, 0.551 and 0.928 to be compared with the exact values of -0119, 0.565 and 0.928 respectively. This basis contained a total of 49 states on the target and the important He^{+} (1s) capture channel was added to the projectile to improve the convergence of the basis, making a total of 49 states in all. This will be denoted by AO49. The total K-shell ionisation cross section, for single electron loss, represented by

Table 5.21

Radial wavefunctions of the 49-state basis employed in the present K-shell ionization calculations.

Target centre (Li^{2+}).

State $(\overline{nl})^a$	$\lambda(\overline{nl})^a$	$q(\overline{nl})^b$	STO basis	
			n_i	ζ_i
$\overline{1s}$	- 4.50000	0.00	0	3.00000
$\overline{2s}$	- 1.12500	0.00	0	1.50000
$\overline{3s}$	- 0.49992	0.00	1	1.50000
$\overline{4s}$	- 0.26475	0.01	0	1.95000
$\overline{5s}$	+ 0.09097	0.59	1	1.95000
$\overline{6s}$	+ 1.06088	0.93	2	1.95000
$\overline{7s}$	+ 4.48378	0.96	0	1.00000
$\overline{8s}$	+26.68722	0.97	1	1.00000
$\overline{2p}$	- 1.12500	0.00	1	1.50000
$\overline{3p}$	- 0.50000	0.00	1	1.00000
$\overline{4p}$	- 0.28080	0.00	2	1.00000
$\overline{5p}$	- 0.16886	0.01	1	0.87000
$\overline{6p}$	+ 0.06017	0.59	2	0.87000
$\overline{7p}$	+ 0.76235	0.92	3	0.87000
$\overline{8p}$	+ 3.43550	0.97	1	3.30000
$\overline{9p}$	+16.66553	0.98	2	3.30000

Table 5.21 (continued)

State $(\overline{nl})^a$	$\lambda(\overline{nl})^a$	$q(\overline{nl})^b$	STO basis n_i	STO basis i
$\overline{3d}$	- 0.50000	0.00	2	1.00000
$\overline{4d}$	- 0.28125	0.00	2	0.75000
$\overline{5d}$	- 0.17948	0.00	3	0.75000
$\overline{6d}$	- 0.08875	0.07	4	0.75000
$\overline{7d}$	+ 0.19129	0.89	5	0.75000
$\overline{8d}$	+ 1.25244	0.97	2	3.30000
$\overline{9d}$	+ 4.66288	0.99	3	3.30000
$\overline{10d}$	+17.44786	0.99	4	3.30000

a) States $(\overline{nl})$ and energies $\lambda(\overline{nl})$ are obtained by diagonali-
-zing the Hamiltonian $-\frac{1}{2}\nabla^2 + V_K$ with V_K from eqn (5.2.4)
using the STO basis sets in the last two columns of the tables.

b) The quantities $q(\overline{nl})$ are determined from eqn (2.4.32)
by the overlaps between the pseudostates $(\overline{nl})$ and the continuum
of the Hamiltonian $-\frac{1}{2}\nabla^2 + V_K$,with V_K from eqn (5.2.4).

Projectile centre (He^+)

State (nl)	(nl)	$q(nl)$	STO basis n_i	STO basis i
1s	-2.00000	0.00	0	2.00000

The $He^+(1s)$ state is the exact eigenfunction.

$$He^{2+} + Li^{+}(1s^2) \rightarrow He^{2+} + Li^{2+}(1S) + e^{-} \qquad (5.5.6)$$

was obtained using formula analagous to (5.3.8), with the cross sections obtained from AO43 and AO50.

In the final states of the present calculations a large basis set was constructed using the 32 state basis (from Section 5.2) designed for charge transfer, and AO54. This basis set consisted of the complete set of 23 projectile centred states (with the parameters in Table 5.2), together with a shortened form of AO54 obtained by deleting the 3s, 4s, 6s, 3p, 6p, 7p and 8p states in Table 5.18. Also the He^{+}(1s) state in AO54 was omitted from the final basis. The total number of target states used was 42 and hence this large basis set contained 65 states in total, and will be denoted by AO65. The resultant close-coupled calculations were made, for numerical reasons, using the code of Shingal (1987). The AO65 basis is expected to be superior to the AO54 basis at low energies where capture is an important process. The results from the AO32 basis show that at E = 300 keV. lab the total capture cross section, after projection, is 0.89×10^{-16} cm^2. The projected ionisation cross section obtained from a basis similar to AO54, but which contained 50 states with $0 <= 1 <= 3$, and used by Ermolaev and Hewitt (1985), was 21.9×10^{-16} cm^2. Therefore AO54 and AO65 should be almost equivalent as far as ionisation is concerned at this energy where capture is not

very important. This suggests that we can consider the impact energies to divide up into two regions, E > 200 keV. lab and E < 200 keV. lab, where a single centre expansion and a two centre expansion respectively are needed to obtain accurate ionisation results. We shall now describe the results for ionisation obtained with these basis sets.

5.6 Ionisation and Excitation Results

In this section we shall describe the results that have been obtained for single-electron ionisation and direct excitation in collisions between He^{2+} particles and the lithium target,

$$He^{2+} + Li(2s) \rightarrow He^{2+} + Li^{+} + e^{-} \qquad (5.6.1)$$

$$\rightarrow He^{2+} + Li^{*}(nl) \qquad (5.6.2)$$

using the various basis sets described in Section 5.5.

Ionisation of the L-shell was initially investigated in the First Born Approximation (FBA) using the pseudostate basis A054 and the exact continuum states of the potential (5.2.2). The FBA is obtained by replacing the wavefunction $\Psi_i^+(\vec{r}_B, t)$ in equation (4.1.24) by the initial state and by setting the distorting potential $U(R)$ to zero. Expression

(4.1.35) is then used to obtain the FBA transition amplitudes). The internuclear potential $\omega(R)$ does not contribute due to the orthogonality of the initial and final states. The final state of the ejected electron is represented by $\psi_{k\ell}(\vec{r}_B)$. For the case where the exact continuum states of the target potential are used as final states from (4.1.32), then equation (4.1.40) is used to obtain the final partial cross sections, denoted by σ_ℓ^{FBA}, correponding to different final angular momentum, .

In the case where the final states are the pseudostates of the AO54 basis, the integral over energy in expression (4.1.40) is replaced by a summation over the final states, weighted with the correct projection factors from Table 5.18, according to the second term in expression (2.4.37). Therefore the FBA partial cross section in this case can be written as

$$\bar{\sigma}_\ell^{FB} = \sum_{m=0}^{\ell} 2\pi \int_0^{b_{max}} db\, b \sum_j |c_{j\ell m}|^2 q(j\ell) \qquad (5.6.3)$$

where

$$c_{j\ell m} = -i \int_{-t_a}^{t_b} dt\, e^{-i(\varepsilon_i - \varepsilon_f)t} \langle \bar{\phi}^B_{j\ell m}(\vec{r}_B) | -\frac{2}{r_A} | \bar{\phi}^B_i(\vec{r}_B) \rangle \qquad (5.6.4)$$

where $\bar{\phi}^B_i(\vec{r}_B)$ is the initial state and $\bar{\phi}^B_{j\ell m}(\vec{r}_B)$ represents the pseudostates from the AO54 basis.

The FBA has been evaluated for the case of the exact

continuum wavefunctions for $0 = l < = 6$, and for the AO54 basis set as in expression (5.6.4) and the results are compared in Figure 5.12. There is very good agreement between both sets of results above E = 100 keV lab. Below this energy the smaller partial wave contributions show less agreement than the larger ones. At E = 40 keV lab. the sum over partial waves with $0 < = 1 < = 3$ gives $\sigma^{FBA}_{spdf} = 46.0 \times 10^{-16}$ cm^2 and $\bar{\sigma}^{FBA}_{spdf} = 42.5 \times 10^{-16}$ cm^2. However if the pseudostate basis set is used without using the projection method, as in (2.4.37), and ionisation is estimated by simply summing over the positive energy contributions, the corresponding FBA results is 43.1×10^{-16} cm^2. At E = 3000 keV lab. σ^{FBA}_{spdf} and $\bar{\sigma}^{FBA}_{spdf}$ have values of 1.33 and 1.14 x 10^{-16} cm^2 respectively, while the unprojected pseudostate sum is 1.22×10^{-16} cm^2. In general the result of projecting the AO54 basis onto the continuum is not very different to the unprojected method, in the FBA, and AO54 should provide a good representation of the target continuum over a wide range of impact energies when it is used in the close-coupled method, which we shall denote by CC.

The single-electron cross sections have been obtained using the CC method with AO54, for 22 < 10000 keV lab., and with AO65, for a shorter interval 22 < E < 1000 keV. We used two independent codes to calculate exchange matrix elements and solve the problems code CI (the recent codes) and code CII (Shingal 1987).

Calculations with AO54 were carried out using both CI

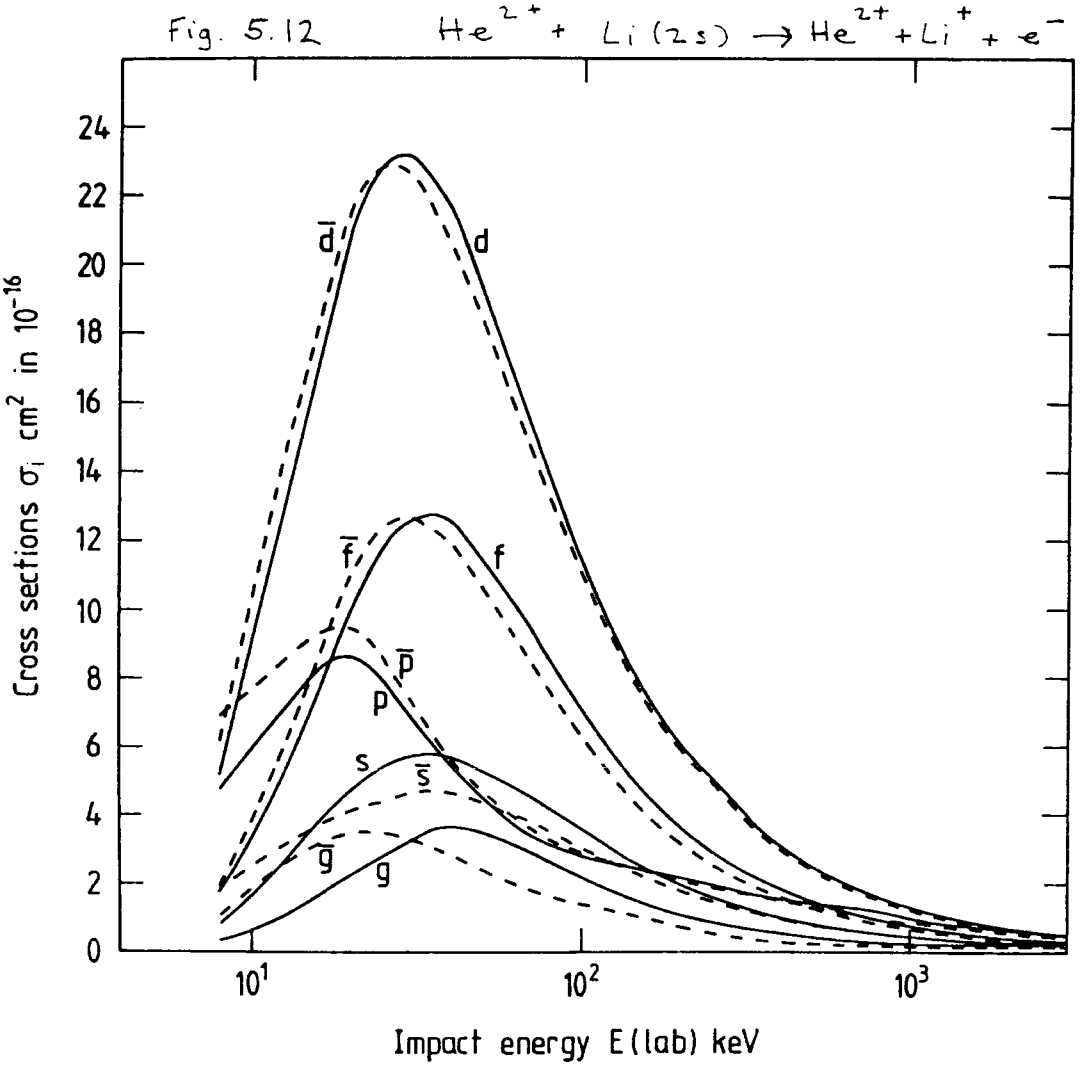

Key to Figure 5.12

Ionisation in He^{2+} + Li collisions.

First Born partial cross sections for Li(2s -> εl) transitions (l < = 4).

——— , FBA obtained by using exact continuum states and expression (4.1.40).

- - - - -, FBA obtained by using expression (5.6.3) and the L^2 pseudostate basis A054. The l=4 states were an additional set, not included in A054.

and CII to confirm the consistency of our numerical results. In the case of AO65, only CII was used.

Table 5.22 gives selected quantal results for two energy regions, (a) E < 200 keV. lab, and (b) E > 600 keV lab. The total ionisation cross sections were obtained as sums of the partial 1-wave contributions after projection onto the continuum, that is

$$\bar{\sigma}_{ion} = \sum_{\text{all } (\bar{n}\bar{l}) \text{ on } B} q_B(\bar{n}\bar{l})\, \sigma^B(\bar{n}\bar{l}) + \sum_{\text{all } (\bar{n}\bar{l}) \text{ on } A} q_A(\bar{n}\bar{l})\, \sigma^A(\bar{n}\bar{l}) \qquad (5.6.5)$$

$$= \sigma^B_{DI} + \sigma^A_{CTTC}$$

where σ^B_{DI} and σ^A_{CTTC} are contributions due to direct ionisation (DI) and capture into the projectile continuum (CTTC). In equation (5.6.5) the summations are extended to all states of the basis on each centre.

Figure 5.13 presents a set of ionisation curves in the form of a product $Q = E\,\sigma(E)$ against log E. Each curve has been obtained by summing the computed partial cross sections with $\bar{l} \leq 3$. In the range 20 < E < 200 keV. lab, the best result is given by AO65 : AO54 overestimates ionisation, particularly at low energies. This is due to neglect of the coupling to the charge exchange channels in AO54. For energies below E = 100 keV. lab, the FBA cross sections greatly exceed the values predicted by the coupled channel models. In the region E > 200 keV lab. the best result is generally given by AO54 because the 65-state basis contains only a truncated set of the target states. The difference between AO54 and AO65 is small if E < 300 keV. lab but it

Table 5.22 Close-coupled (CC) and First Born (FB) partial cross sections for L-shell ionization in He^{2+} + Li collisions (in units 10^{-16} cm^{**2}

	Close coupled				First Born						
		l				l					
E(keV lab)	0	1	2	3	0	1	2	3	4	5	6
				A. Low energy region[a]							
40.0	0.58	1.09	3.27	1.78	5.63	5.56	21.8	13.0	3.68	0.97	0.16
65.0	0.83	1.90	5.63	5.09	4.70	3.72	16.6	10.5	3.02	0.76	0.12
80.0	0.90	3.58	6.68	6.67	4.15	3.25	14.2	9.06	2.57	0.64	0.099
100.0	0.51	6.13	6.71	7.83	3.60	2.91	11.8	7.55	2.11	0.52	0.080
150.0	0.44	3.18	7.75	7.80	2.57	2.50	8.20	5.19	1.43	0.35	0.054
200.0	0.40	2.24	6.90	7.58	2.00	2.27	6.27	3.92	1.08	0.26	0.041
				B. High energy region[b]							
600.0	0.54	0.94	1.96	1.89	0.66	1.14	2.00	1.07	0.22		
1000.0	0.38	0.75	1.23	0.91	0.41	0.84	1.21	0.64	0.14		
2000.0	0.21	0.51	0.63	0.38	0.21	0.52	0.60	0.32	0.06		
3000.0	0.14	0.39	0.42	0.23	0.14	0.38	0.41	0.21	0.04		

a) CC cross sections computed using the AO65 basis ; FB cross sections computed with a numerical integration over the energies of the target continuum states (equation (4.1.40)).

b) $\tilde{CC}$ and $\tilde{FB}$ cross sections computed using the same 54-pseudostate basis. $\tilde{FB}$ results computed using expression (5.6.3).

Fig 5.13

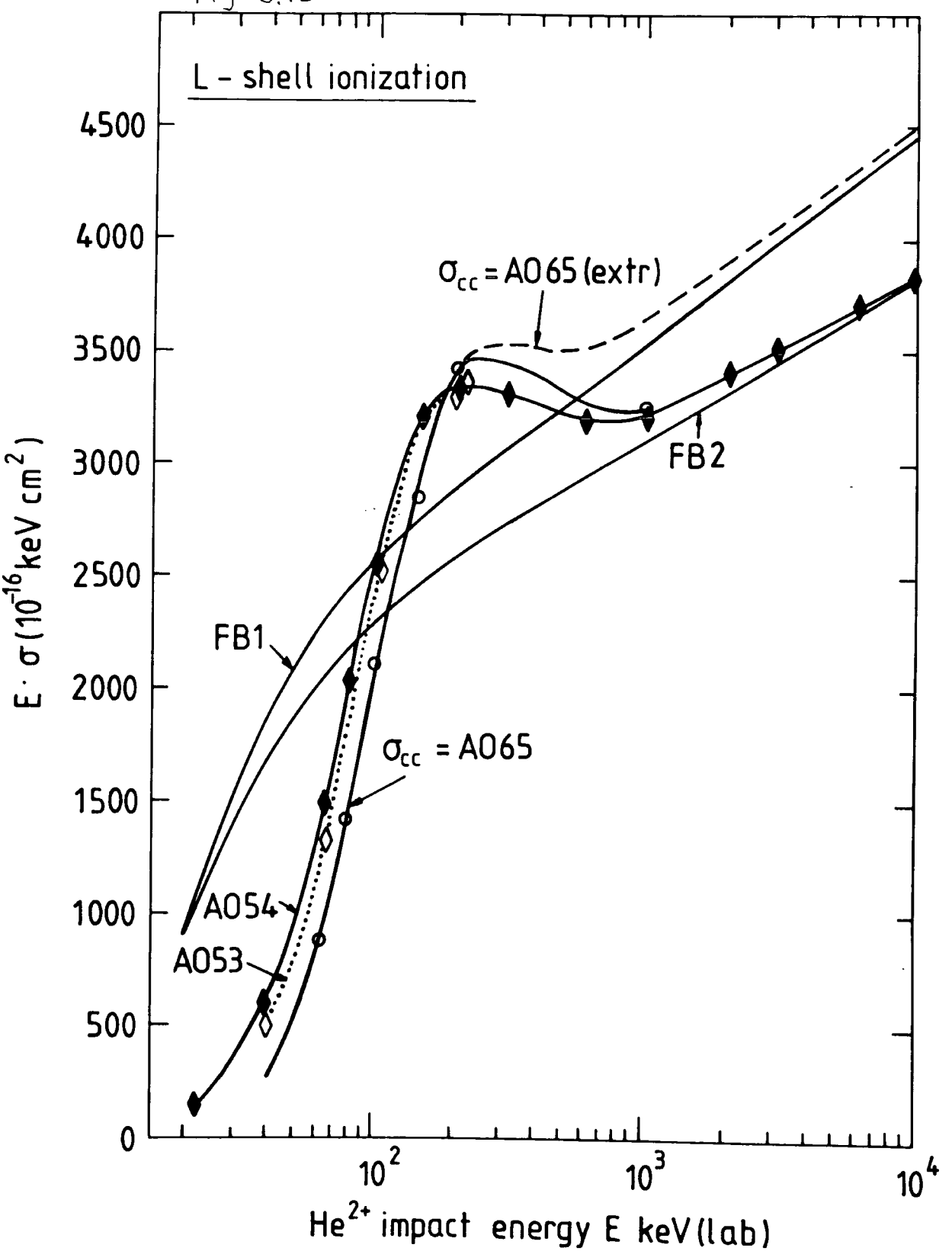
L - shell ionization
4500
4000
3500
3000
2500
2000
1500
1000
500
0
$E \cdot \sigma (10^{-16} keV\ cm^2)$
σ_{cc} = A065 (extr)
FB2
FB1
σ_{cc} = A065
A054
A053
10^2
10^3
10^4
He^{2+} impact energy E keV (lab)

Key to Figure 13

L-shell ionisation. Plots of the energy - cross section product , $Q = E\ \sigma(E)$, against log E for the sum of partial cross sections with $l <= 3$.

FB ——— , FB results obtained by summing σ_{ion}^{l} from (4.1.40), using exact continuum states.

$\widetilde{FB}$ ———→ , $\widetilde{FB}$ results obtained by summing $\bar{\sigma}_{l}^{FB}$ from (5.6.3) , using the AO54 basis.

——— o , two-centre AO65 expansion and formula (5.6.5).

——— ♦ , EOCM AO54 expansion and formula (5.6.5).

----- ◊ , SCE AO53 expansion and formula (5.6.5).

— — — — , extrapolation of AO65 results to higher values of E (E › 200 keV lab.) using (5.6.10).

increases with E and at 1 MeV lab. AO65 underestimates ionisation by some ten per cent (the part of the A65 curve for E > 200 keV. lab is not shown in figure 5.13). For E > 1 MeV lab, the AO54 curve approaches a first Born curve. We note that the high E limit of AO54 is $\overline{FB}$ and not the exact FB. This is because in both cases the same 53-state target-centred set has been used. Also shown in figure 5.13 is the result of using AO53 which is identical to AO54 except that the He^{+}(1s) state is omitted from the basis and this does not produce a significant change in the results. We shall now examine a semi-empirical method for combining the AO65 and FB results to produce a single ionisation curve at all energies. We shall begin by considering an approach which starts with a one-centre model instead of the exact two-centre problem. We note first that if E is large enough, the CC cross sections are close to the FB cross sections. In the latter case, we have to deal with a one-centre expansion which can be handled numerically with the required acuracy. In Figure 5.13, the 'exact' curve FB has been obtained using the exact continuum states for the target for $1 \leq 3$ and therefore its only defect is the omission of $1 > 3$ states at high energies (within the potential model method).

The second curve, $\overline{FB}$, has been obtained using equation (5.6.3) and the target centre states of the finite basis AO54 and therefore requires a correction. In the two-centre case, if E is not too high, we can treat AO65 as an exact

basis and AO54 as an approximate one which needs a correction. AO65 is exact in that it has a very good representation of the target continuum for $l <= 3$ for $E < 200$ keV. lab, and also includes the most important target bound states with $l <= 3$. Its only defect is the omission of states with $l > 3$ on the target. Therefore AO65 will ultimately need to be corrected to allow for this, but it should be a small correction. It includes the most important projectile states also with $l <= 2$.

We can consider the differences

$$\Delta_L^{I} = \sigma_L^{65} - \sigma_L^{FB}, \quad E < 200 \text{ keV. lab.} \quad (5.6.6)$$

$$\Delta_L^{II} = \sigma_L^{54} - \sigma_L^{FB}, \quad E > 200 \text{ keV. lab.} \quad (5.6.7)$$

where an 'infinitely' large and a finite bases are used, respectively. We may say that Δ_L^{I} and Δ_L^{II} do not vanish because of the coupling which exists between the channels, due to the difference between the close-coupling method and the First Born Approximation. Ideally the AO65 results should converge to FB at high energies but this does not happen because the basis is not complete. However at $E = 200$ keV lab. we can assume it is complete (for $l <= 3$ only on the target).

One can match Δ_L' and Δ_L'' at E = 200 keV. lab by writing

$$\Delta\sigma'_{spdf} = c_0 \, \Delta\sigma''_{spdf} \qquad (5.6.8)$$

Using Table 3, one finds for E = 200 keV lab, that

$$c_0 = 0.793 \qquad (5.6.9)$$

The 'Best' CC ionisation curve ϵ_L^{∞} which includes the 'finite-basis' correction, is then obtained by extrapolating formula 5.6.8 to values of E higher than 200 keV. lab. In this manner we obtain the following

$$\sigma^{\infty}_{spdf} = \begin{cases} \sigma^{65}_{spdf} & , E < 200 \text{ keV lab.} \\ \sigma^{FB}_{spdf} + c_0 \, \Delta\sigma''_{spdf} & , E > 200 \text{ keV. lab} \end{cases} \qquad (5.6.10)$$

In equations (5.6.9) and (5.6.10) all data relate to the sum over the first four partial waves with $l \leq 3$.

The other correction we can apply to the data is due to the partial waves with $l > 3$.

This high-l correction has been obtained in the

following way. Let us write for a CC partial cross section with angular momentum l as follows

$$\sigma_l^{CC} = \mathcal{H}(E)\,\sigma_l^{FB} \quad , \quad l > 3 \tag{5.6.11}$$

In (5.6.11) the function $\mathcal{H}(E)$ represents an average account of including the coupling between the target centre states, and it is reasonable to estimate it by the following expression

$$\mathcal{H}(E) = \sigma_{spdf}^{CC} / \sigma_{spdf}^{FB} \tag{5.6.12}$$

The total ionisation cross section is then given by

$$\sigma_{tot}^{CC} = \sigma_{spdf}^{\infty} + \mathcal{H}(E) \sum_{l \geq 4} \sigma_l^{FB} \tag{5.6.13}$$

The relative importance of high-l contributions was discussed within the FB approximation, by McGuire (1971) who followed an earlier work by Merzbacher and Lewis (1958). Using a semi-classical criterion McGuire found that some 15 partial waves had to be retained in the expansion though only the

first seven waves were practically important in a wide range of energies. In the present calculations summarized in table 5.23, we have used a total of seven waves with $0 \leq l \leq 6$. Therefore, the corrective term in (5.6.13) contained only three high-l partial FB cross sections (for g-, h-, and i- waves). Above E = 150 keV. lab σ^{FB}_{ghi} is less than 10 per cent of σ^{FB}_{spdf} and the exact form of the correction term (5.5.11) is therefore not very important. We shall now consider the K-shell ionisation results. In the present CC calculations of single-electron ionisation from the K-shell of Li, we have used the independent-electron model (IEM) described in Section (5.2.2).

The AO bases which have been employed in these calculations were AO43, as described in Section (5.2.2), for the outer electron, and AO49, as specified in Section (5.6.1), for the inner electron. The final cross section was obtained by adding the separate cross sections according to formula (5.2.10). We note that there was a contribution to the AO43 ionisation total from the $He^{+}(\bar{3}s)$ pseudostate, after the projection method was used. We did not project the K-shell target ionisation cross sections onto the continuum because the projection factors were usually very close to the ideal values of 0 or 1, for the negative and positive energy states in both basis AO43 and AO49. Furthermore, the ionisation of the K-shell is far less important than that of the L-shell at all energies. We have also computed the FBA for ionisation of the outer electron

Table 5.23

The First Born (FB) and close-coupled (CC) calculations of single-electron ionization in collisions of He^{2+} ions with the Li target. All cross sections are given in units of 10^{-16} cm^2.

E_{lab} (keV)	First Born			Close Coupled				Total cross section[d]
	spdf	ghi	spdf	54 spdf	65 spdf	spdf[a]	$\mathcal{H}(E)$[b]	
20	45.25	2.97	46.48	7.45[c]	-	-	-	-
40	45.97	4.82	42.53	15.53	6.72	6.72	0.146	7.42
65	35.52	3.90	31.86	23.10	13.45	13.54	0.379	14.93
80	30.65	3.31	27.29	25.63	17.83	17.83	0.582	19.76
100	25.84	2.71	22.93	25.45	21.18	21.18	0.820	23.40
150	18.45	1.84	16.48	21.29	19.00	19.00	1.030	20.90
200	14.46	1.38	12.77	16.10	17.10	17.00	1.183	18.73
300	10.18	0.92	9.20	11.06	-	11.65	1.145	12.71
600	5.53	0.46	4.87	5.33	-	5.89	1.066	6.39
1000	3.53	0.27	3.10	3.26	-	3.65	1.036	3.94
2000	1.90	0.14	1.65	1.72	-	1.95	1.027	2.10
3000	1.33	0.094	1.14	1.18	-	1.36	1.024	1.45
6000	0.708	0.046	0.609	0.621	-	0.723	1.021	0.770
10000	0.425	0.028	0.379	0.381	-	0.427	1.005	0.453

a) Computed using equation (5.6.10)

b) Computed using equation (5.6.12)

c) For E = 22 keV lab.

d) Computed using equation (5.6.13)

in the K-shell, using the exact continuum states of the appropriate potential model (5.2.4). The FBA results were obtained for $0 <= l <= 3$. The f states contributed less than 3 per cent to the total for impact energies in the range 40 - 6000 keV lab. and higher l values were therefore neglected. The present results are shown in table 5.24. At the highest energy of E = 6 MeV, where the Born approximation is most valid, the values for the projected and unprojected AO43 target ionisation cross section are 0.0713 and 0.0688×10^{-16} cm^2 respectively. The FBA value using the exact continuum is 0.0535×10^{-16} cm^2. In contrast to the case for the L-shell the FBA results lie below the CC results at high energies. The CC results indicate that target continuum states with high energies contribute significantly to ionisation. At E = 6 MeV lab. the $(\overline{8p})$ and $(\overline{8d})$ states, which have energies of 8.1 and 4.8 a.u. respectively, contribute 9 and 10 per cent of the total target ionisation in AO43. A similar situation is also found in the case of the AO50 basis where the $(\overline{8p})$ and $(\overline{9d})$ states, with energies 3.4 and 4.7 a.u., contribute 24 and 10 per cent of the total ionisation cross section respectively at E = 6 MeV lab.

It is possible that, since such a large range of continuum energies contribute to the total ionisation, the use of only a small number of pseudostates to span these energies could lead to a larger error in the cross sections than in the L-shell calculations. The agreement between the

Table 5.24

A comparison of the K-shell ionization cross sections obtained using the close-coupled (CC) and First Born (FB) methods in the Independent Electron Model (in units of 10^{-16} cm^2).

	First Born[a]	Close-coupled[b]		
E(keV lab)	(1s)	(1s)	(1s')	Total[c]
300.0	0.163	0.0602	0.0158	0.0750
600.0	0.177	0.144*)	0.0463*)	0.190*)
800.0	0.164	0.149*)	0.0554*)	0.204*)
1000.0	0.159	0.150	0.0588	0.209
2000.0	0.111	0.137	0.0733	0.210
3000.0	0.0861	0.114	0.0627	0.177
6000.0	0.0535	0.0713	0.0402	0.111

*) Interpolated cross sections.

a) FB results are summed over l=0,1,2 and 3..

b) $|1s\rangle$ and $|1s'\rangle$ are states in the model which are occupied by the outer and inner K-shell electrons, with the binding energies -2.799 a.u. and -4.5 a.u., respectively.

c) Total cross section obtained as sum of $\sigma^c_{1s} + \sigma^c_{1s'}$, as in expression (5.2.10).

FBA and CC results is therefore quite reasonable.

In Figure 5.14, we compare our results with the available experimental cross sections (Shah et al. (1985), Sewell et al. (1980)). We shall note that the K-shell data of Shah et al. (1985) have been extracted from the measured total ionisation cross sections. The ionisation data of Sewell et al. (1980) shown in Figure 5.14 is that for $p + Li^{+}$, appropriately scaled to represent $He^{2+} + Li$. This invoves multiplying the cross sections by 4 and the corresponding proton impact energy by 4 also to allow for the different charge and mass ratios of p and He^{2+}.

Figure 5.15 gives an overall comparison of single-electron ionisation in $He^{2+} + Li$ collisons in terms of the product E (E) as a funcion of log E. A large part of the cross section, even in the MeV range, is due to the L-shell ionisation. The curve L is the 'best' ionisation curve obtained from formula (5.6.13) which includes the main CC contribution from the L-shell as well as corrections described earlier. The curve L + K is a sum of curve L and the total K-shell contribution obtained from table 5.24 (column c) which is curve CC in figure 5.14.

Figure 5.15 shows that for low energies, $E < 125$ keV. lab, there is a reasonable agreement between the quantal CC and CTMC results. In the same energy region, the FBA differs sharply from the CC and classical data and overestimates ionisation at $E < 100$ keV. lab. The present Born results from the L-shell lie somewhat lower than

Fig. 5.14

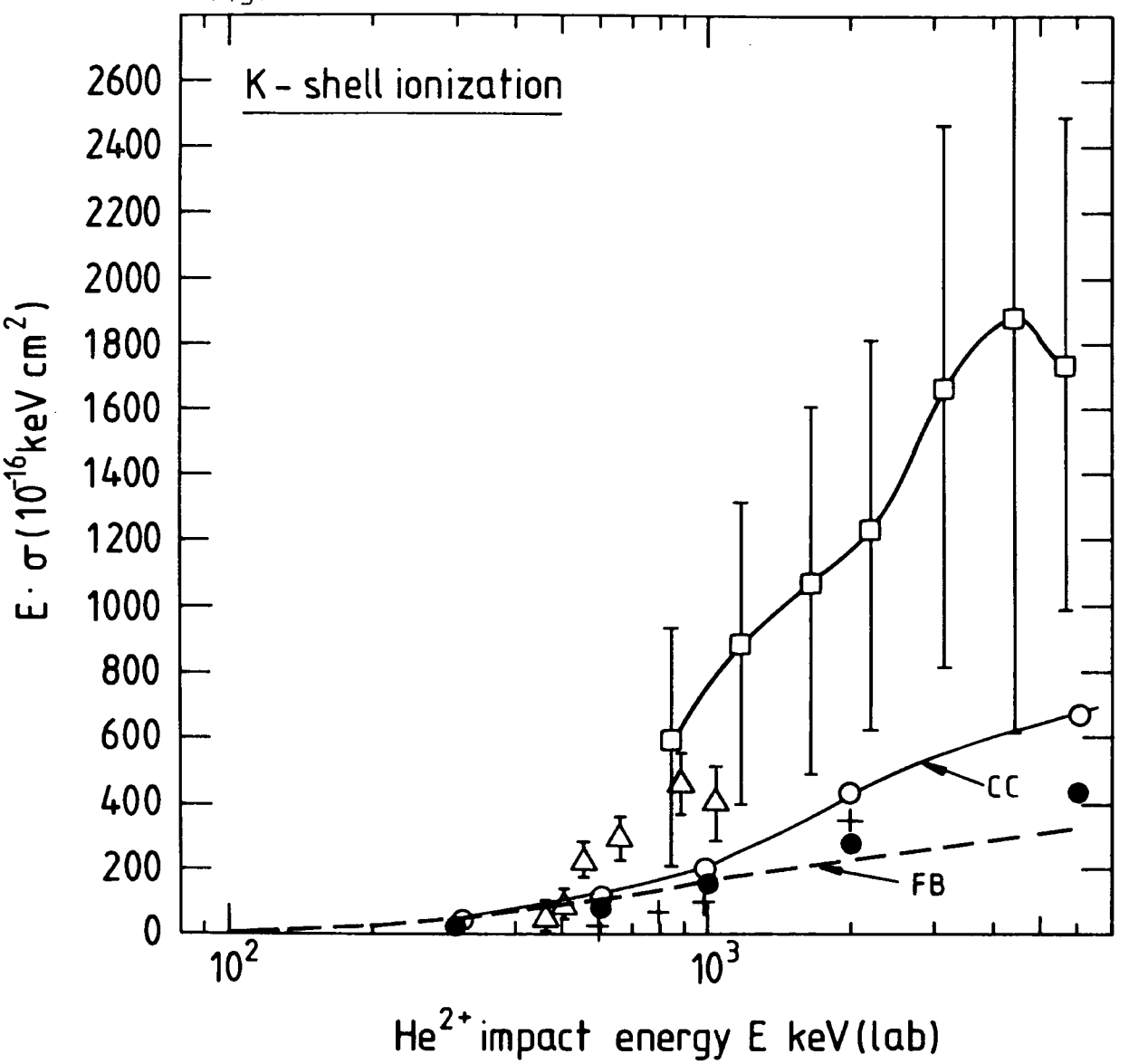
K - shell ionization
2600
2400
2200
2000
1800
1600
1400
1200
1000
800
600
400
200
0
$E \cdot \sigma (10^{-16} keV\,cm^2)$
10^2
10^3
He^{2+} impact energy E keV (lab)
CC
FB

Key to Figure 5.14.

K-shell ionisation. Plots of the energy - cross section product , $Q = E\,\sigma(E)$, against log E .

Theoretical results for K-shell ionisation .

● , AO43 expansion results with projected contribution from $He^{+}(\overline{3s})$ state.

– – – – –, sum over FB results , σ_{ion}^{t} , obtained for outer electron only , with exact continuum states for potential from (5.2.4).

\+ , Classical Trajectory Monte Carlo results for IEM model (Ermolaev , Hewitt, McDowell and Shingal 1987).

—○— , IEM total obtained from the AO43 expansion and the AO49 expansion , using (5.2.10).

Experimental data .

 , SEG , Shah et al. (1985) , extracted from total ionisation cross section.

 , scaled data of Sewell et al. (1980) for single ionisation of Li^{+} by H^{+}.

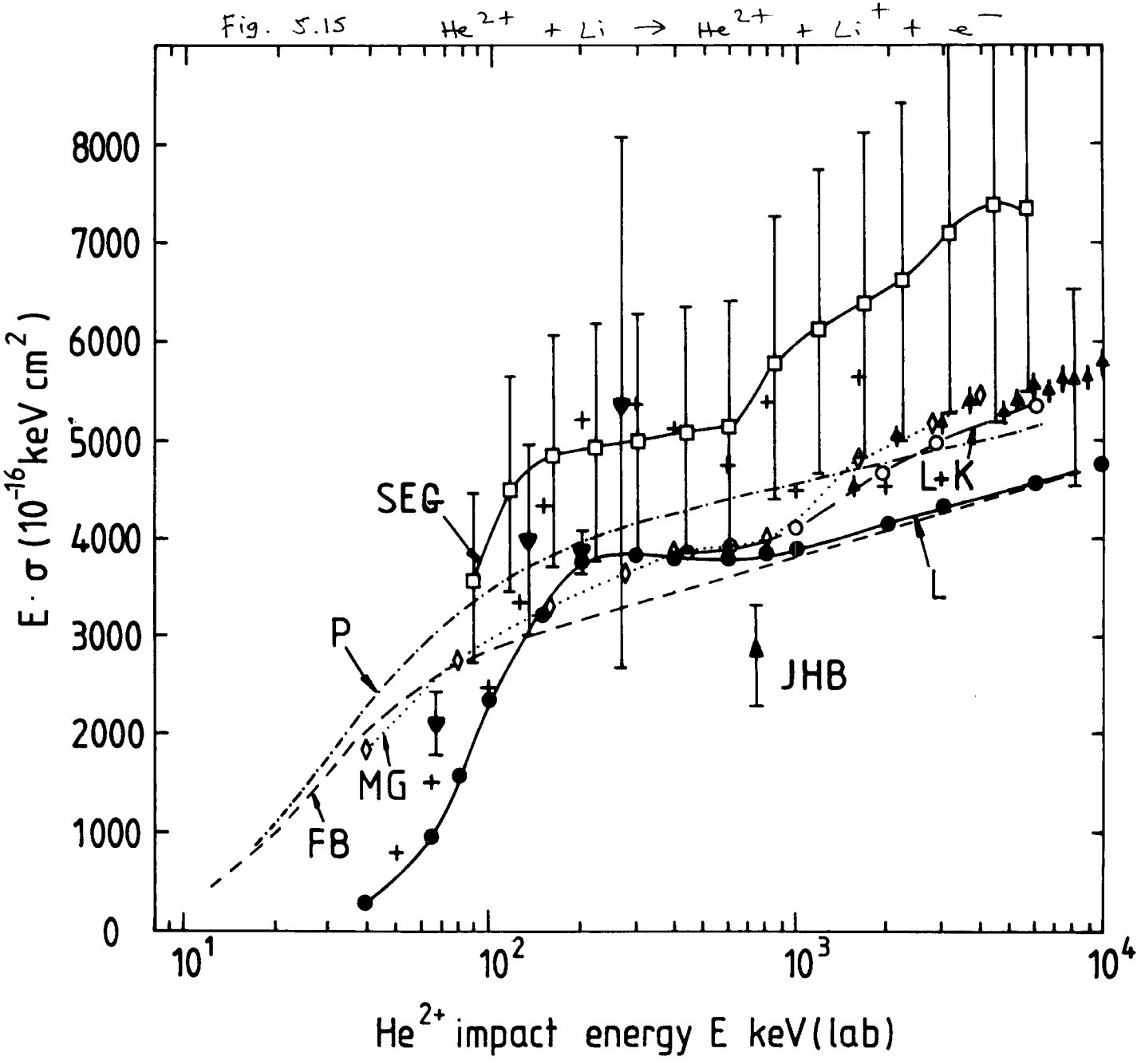
Fig. 5.15
$He^{2+} + Li \rightarrow He^{2+} + Li^{+} + e^{-}$
$E \cdot \sigma\ (10^{-16} keV\ cm^2)$
8000
7000
6000
5000
4000
3000
2000
1000
0
10^1
10^2
10^3
10^4
He^{2+} impact energy E keV(lab)
SEG
L+K
L
P
JHB
MG
FB

Key to figure 5.15

Single-electron ionisation in He^{2+} + Li collisions.

Comparison of theory and experiment in terms of the product $Q = E\,\sigma(E)$.

Theoretical results.

----, FB , FB results obtained by adding σ_{ion}^{1} for all $0 <= l <= 6$ for the L-shell , present work.

MG, ----◇---- , McGuire (1971) , FBA result, including the L- and K-shell contributions.

P, ... , Peach (1965) , FB results for the L-shell.

L, —●— , best L-shell curve obtained from the present work using expression (5.6.13).

L+K, ---○---, curve L corrected for the K-shell contribution from Table 5.24.

\+ , Classical Trajectory Monte Carlo results for IEM model (Ermolaev , Hewitt, McDowell and Shingal 1987).

Experimental results.

▼ , DuBois (1985)

⊟ , Shah et al. (1985)

▲ , scaled data for e^- + Li collisions from Jalin et al. (1973).

respective cross sections of Peach (1965) but agree better with her revised calculations (Peach 1986, private communication). The results of Peach are for the L-shell only. For higher energies, the classical cross sections are considerably larger than those of the quantal CC and FBA methods. In the MeV-range, our L + K curve agrees very well with earlier IEM First Born calculations of McGuire (1971). His cross sections as well as ours include the K-shell contribution. The numerical method of McGuire (1968) is closely related to the present exact FBA calculations rather than to the pseudostate expansion method. McGuire choose to obtain his effective potential for the single active electron model by approximating the Herman and Skillman potential by a sequence of straight lines (Herman and Skillman 1963). There is also a variation in the form of the independent electron model used in his calculation. This may explain the small difference between the cross sections obtained by us and by McGuire for high E.

The ionisation cross sections for reaction (5.6.1) were recently measured by DuBois (1985) in the energy interval $66.8 < E < 266.8$ keV. lab. (scaled for a projectile with a mass of 4 a.u.) and by Shah et al. (1985) in a wider interval $88 < E < 5800$ keV lab. Figure 5.15 shows that, except for the lowest energy E = 66.8 keV lab where the experimental cross section is larger than ours by a factor of two, there is an excellent agreement between our results and the data of DuBois (1985). However DuBois states that

his ionisation results may be uncertain to within a factor of two, although it is more probable that the accuracy is within 50 per cent. The error bars in figure 5.15 show experimental reproducibility only for the DuBois data.

The smallest experimental uncertainty of his data is for E = 200 keV. lab. where the experiment gives $19.3 \pm 1.1 \times 10^{-16}$ cm^2 to be compared with the quantal cross section of 18.7×10^{-16} cm^2. The shape of the ionisation curve reported by Shah et al. (1985) is very similar to that of the 'best' theoretical curve L + K, in the whole energy range, but the theoretical cross sections lie below the measured cross sections just outside the experimental uncertainty. The disagreement with the data of Shah et al. (1985) could be due to the normalization procedure they have applied to their measurements which produces an uncertainty of 20 per cent and this is shown in Figure 5.15 by the error bars. A slightly larger value would greatly increase the agreement with theory. Shah et al. suggested that the disagreement between their data and the FBA results of McGuire (1971), which agree rather well with the present results at high energies, was due to the use of the approximate Li(2s) wavefunction in his calculation. It is doubtful whether this is the case and also whether it could explain the low energy difference between L + K and the Shah et al. data. For example at 88 keV, which is near the maximum in our computed ionisation cross section, the present value

obtained by interpolation from the L + K curve is 21.3 x 10^{-16} cm^2 to be compared to 40.5 x 10^{-16} cm^2 as measured by Shah et al. The difference in the Born approximation between the exact results, FB, and the projected AO54 basis results, as discussed earlier in this section was only 8 percent at E = 40 keV. for the $1 <= 3$ total. It is considered unlikely that an average correction to allow for the pseudostate nature of the AO65 basis will increase the present CC result by more than 10-15 per cent therefore. At E = 40 keV lab. the projected partial cross sections for the CTTC contribution to expression (5.6.5), corresponding to 1 = 0,1 and 2 (obtained from the AO65 basis) are 0.304, 4.84 and 2.54 x 10^{-16} cm^2 respectively. This suggests that if f pseudostates were included in the projectile centre basis they would not contribute significantly to the ionisation total. However we have not been able to carry out extensive calculations involving larger projectile basis sets. Figure 5.16 summarises the present cross sections. it is seen that the CTTC contribution closely follows the shape of the target ionisation contribution but is reduced in magnitude. This is not the case in, for example, the resonant p+H(1s) system as shown by Shakeshaft (1978). In that case the CTTC and target ionisation contributions have well defined separate maxima at impact energies of 45 and 70 keV lab. It is possible that the distinction between these two processes in the non-resonant system of He^{2+} + Li is not so clear. It is also seen that the total $n >= 4$ excitation cross section

Fig. 5.16

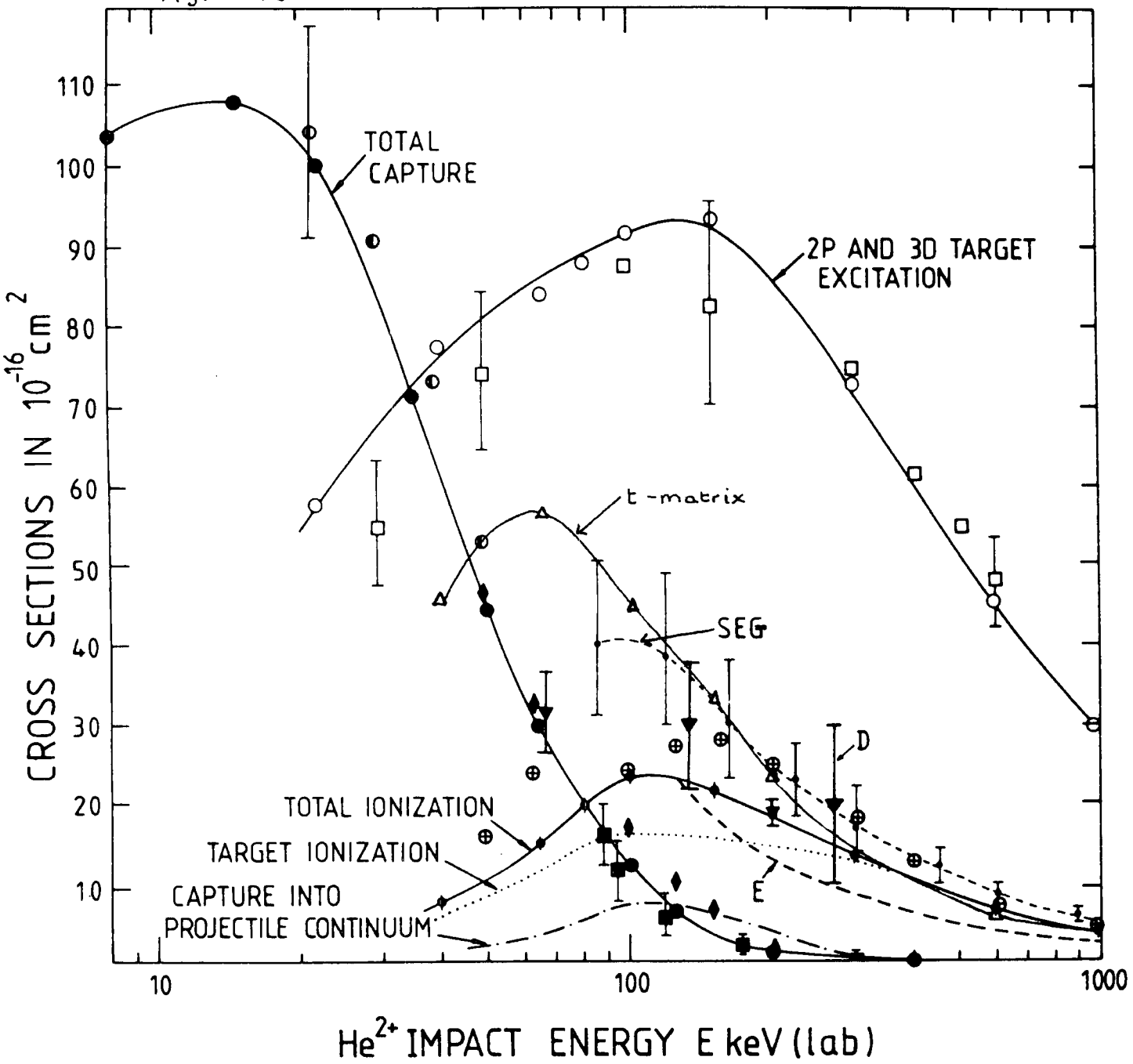
TOTAL CAPTURE
2P AND 3D TARGET EXCITATION
t-matrix
SEG
D
E
TOTAL IONIZATION
TARGET IONIZATION
CAPTURE INTO PROJECTILE CONTINUUM
CROSS SECTIONS IN 10^{-16} cm^2
He^{2+} IMPACT ENERGY E keV (lab)
10
100
1000
110
100
90
80
70
60
50
40
30
20
10

Key to figure 5.16

Comparison of theory and experiment for He^{2+} + Li collisions.

Theoretical results for total capture.

—●— , 32-state projected total charge transfer.

♦ , Classical Trajectory Monte Carlo total charge transfer (Ermolaev, Hewitt and McDowell 1987).

Experimental results for total capture.

 , Kadota et al. (1982a)

 , Shah et al. (1985)

Theoretical results for direct excitation.

○ , present results for sum of Li(2p) and Li(3d) excitation cross sections

E, - - - -, present results for sum of Li(n=4) and Li(n=5) excitation from AO65 expansion.

Experimental results for direct excitation.

 , sum of Li(2p) and Li(3d) cross sections from Kadota et al. (1982c).

Theoretical results for ionisation.

♦ , total ionisation from curve L+K in Figure 5.15 , present results.

— · — · — , capture into projectile continuum obtained from AO65 expansion .

- - - - - - - , target ionisation obtained as difference between total ionisation and capture into projectile continuum .

⊕ , Classical Trajectory Monte Carlo results (Ermolaev, Hewitt and McDowell 1987).

SEC, - - - - - , Shah et al. (1985)

D,  , DuBois (1985)

——Δ , t-matrix ionisation total for $0 \leq l \leq 3$ using $W(R) - U(R) = 2/R$.

is of the same size as the total ionisation cross section and both are much smaller than the combined Li(2p) and Li(3d) excitation cross sections. As in the case of the relatively small Li(3d) excitation cross section this suggests the cross sections for the states with small negative or positive energies are more difficult to determine accurately and that a small bias in the basis in favour of the negative energy states could result in an underestimation of the ionisation cross sections.

Due to the uncertainty associated with the DuBois data at low energies it is difficult to make a definitive comparison with the present result. However, the present curve L + K does agree remarkably well with the scaled data for ionisation of Li by e^- of Jalin et al. (1973) at high energies. The scaling procedure is to multiply the cross sections by 4, while multiplying the electron energies by the factor of 4 x 1836 to allow for the charge and mass ratios of e^- and He^{2+}. The simple scaling method only applies in the Born approximation and is invalid at the lower experimental energies.

Considering the uncertainties which have just been described it is rather remarkable that many features of the experimental curve SEG, shown in figure 4 in a wide range of E, can be explained in terms of the present quantal model. In the region $E < 1150$ keV lab. which includes the ionisation maximum at E = 100 keV lab., SEG shows a steep rise. In this region, coupling between all the channels is

strong and both DI and CTTC give sizeable contributions (separate DI and CTTC contributions to the total ionisation are shown in Figure 5.16). At higher energies there is a plateau region, 150 < E < 800 keV lab, where the coupling becomes weaker and where the CC cross sections converge to the Born result. This region is followed by a relatively short interval, 800 < E < 1500 keV. lab, where SEG is close to a linear function of log E (a nearly asymptotic region for the L-shell ionisation). For E > 1500 keV lab, where the K-shell gives an increasing contribution, a steeper rise of the curve SEG is recorded again.

Figure 5.16 also shows the CTMC results for ionisation. These were obtained using a form of the IEM to include the K-shell effects. The L-shell data was computed using an almost identical potential model to that used in the present quantal calculations in expression (5.5.1). The results agree in general with experiment except for E < 100 keV. lab but contain statistical uncertainties of some 10 per cent at low energies, rising to 30 per cent for the highest energies and they also have considerable scatter so that the agreement may be fortuitous.

We shall now describe the results obtained for excitation in the present calculations.

The close coupled calculations of ionisation using AO54 and AO65 also give cross sections for direct excitation of the low-lying final states nl included in either target centre set.

In Table 5.25 we list cross sections for direct excitation (5.6.2) of the $\overline{2p}$, $\overline{3p}$, $\overline{3d}$, $\overline{4d}$, and $\overline{4f}$ final states of Li, computed for energies from 22 keV. lab to 10 MeV lab.

The AO54 calculations show that the 2s - > 2p transition in Li has a large cross section (of the order 10^{-14} cm^2) which peaks at an energy about 100 keV. lab whereas transitions to higher np (n > 3) states have a very small probability.

Figure 5.17 presents a summary of theoretical results. A comparison is made with the experimental data (Kadota et al. 1982c) for the 2p - > 2s emission and 2s - > 2p excitation. There is an excellent agreement between the quantal and experimental cross sections. We note that the optical method used by Kadota et al. (1982c) directly determines the cross section for the 2p - > 2s emission. Experimental cross sections for the 2s - > 2p excitation are then obtained from the emission data by subtracting the cascade contribution. The cascade correction Δ_{cas} is mainly due to the primary excitation of the 3d level in the neutral lithium and is given (Kadota et al. 1982c) as

$$\Delta_{cas} = (1.0 \pm 0.8)\, \sigma_{em}^{(3d \rightarrow 2p)} \qquad (5.6.14)$$

assuming that Born cross sections for the e^- + Li collisions

Table 5.25 Computed close-coupled target excitation cross sections for some transitions $Li(2s) \rightarrow Li^{*}(nl)$ caused by He^{2+} ion impact. All cross sections are in units of 10^{-16} cm^{2}.

E(keV lab)	Basis	Final state $(\overline{nl})$				
		2p	3p	3d	4d	4f
22.0	a	54.2	5.59	22.3	14.2	6.42
	b,c	48.5	1.52	3.80	2.38	1.84
40.0	a	68.9	4.47	12.3	7.29	5.01
	b	78.5	--	8.85	2.46	1.27
65.0	a	77.1	3.18	6.82	3.39	3.53
	b,c	85.0	4.93	10.8	2.94	1.49
80.0	a	82.1	2.90	5.80	2.25	3.28
	b	86.8	--	11.1	2.60	1.65
100.0	a	86.0	2.69	5.49	1.51	3.03
	b,c	90.9	5.96	10.6	2.11	1.99
150.0	a	87.3	2.26	5.85	1.19	2.19
	b	86.7	--	8.18	1.39	1.38
200.0	a	78.8	1.79	5.85	1.17	1.20
	c		4.07			
300.0	a	65.7	1.38	4.67	1.13	0.78
600.0	a	41.2	0.80	2.48	0.63	0.23
	c		1.17			
1000.0	a	27.1	0.51	1.44	0.36	0.096
	b	29.2		1.66	0.38	0.092
2000.0	a	14.7	0.27	0.68	0.165	0.0354
3000.0	a	10.1	0.18	0.44	0.106	0.0208
6000.0	a	5.25	0.091	0.213	0.050	0.0096
10000.0	a	3.21	0.055	0.126	0.029	0.0056

a) CC calculation using the AO54 basis .

b) CC obtained using the AO65 basis(for all transitions except 2s->3p)

c) CC calculation using the 33-pseudostate basis AO33 (section 5.2.1) only for the 2s -> 3p transition.

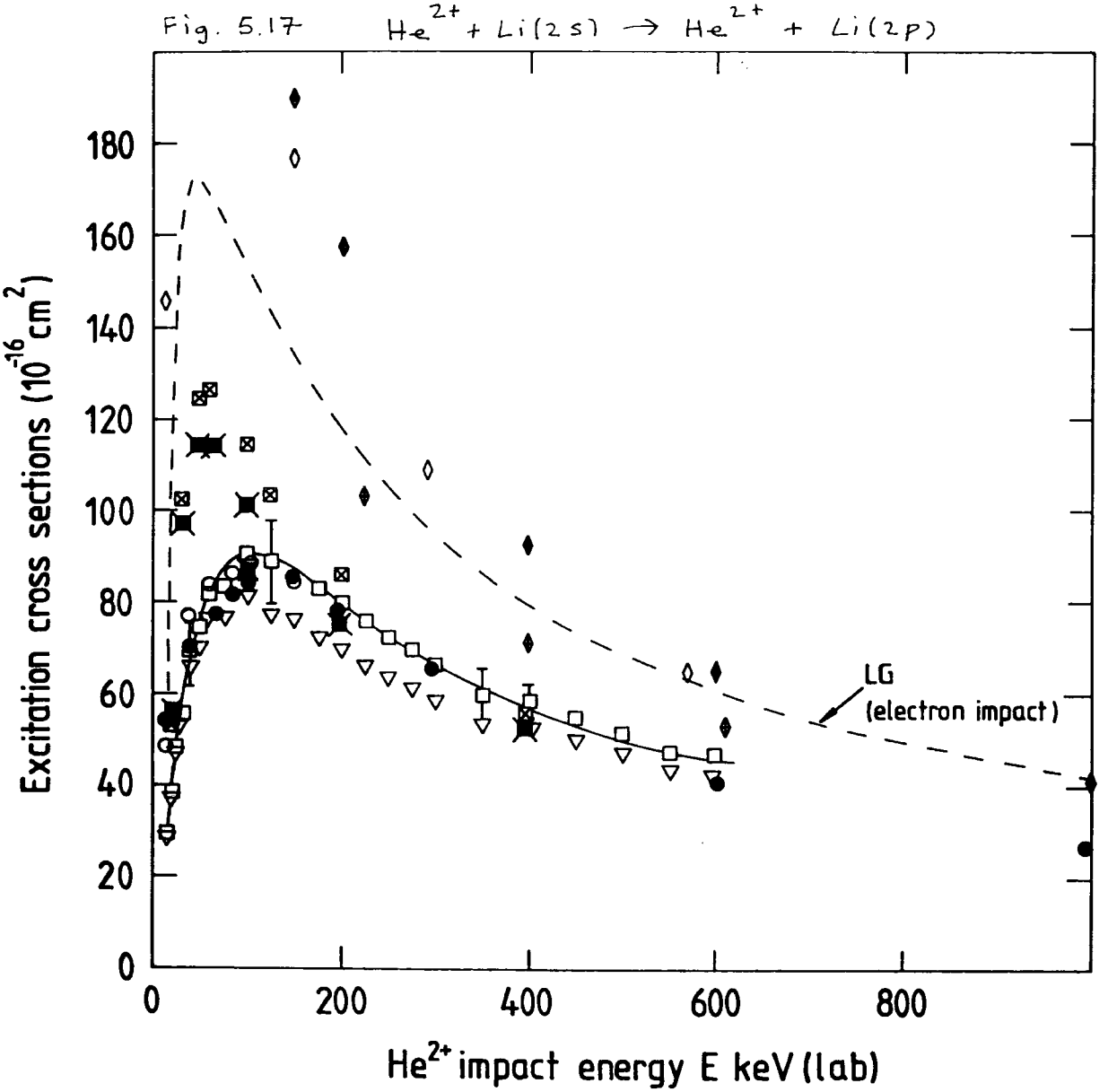
Fig. 5.17 $He^{2+} + Li(2s) \rightarrow He^{2+} + Li(2p)$
Excitation cross sections (10^{-16} cm^2)
180
160
140
120
100
80
60
40
20
0
0
200
400
600
800
He^{2+} impact energy E keV (lab)
LG
(electron impact)

Key to Figure 5.17

Direct excitation of Li(2s) by He^{2+} impact. Cross sections for Li(2s -› 2p) and Li(2p -› 2s) transitions.

Excitation of Li(2s -› 2p).

Theoretical results

⊠ , 20-state (AO20) results, present work.

✖ , 32-state (AO32) results, present work.

● , 54-state (AO54) results, present work.

○ , 65-state (AO65) results, present work.

◆ , FB results , present work.

Experimental data for Li(2s -› 2p) excitation.

▽ , Kadota et al. (1982c).

Experimental data for Li(2p -› 2s) emission.

□ , Kadota et al. (1982c).

Scaled e^- + Li data.

----- , experimental data of Leep and Gallagher (1974).

◇ , FB calculation by Vainshtein (1966) , (cited by Moiseiwitch and Smith (1968)).

⊕ , FB calculation by Mathur et al. (1971).

can be used for estimates in the present case. This correction appears to be generally adequate for high energies but may have to be re-examined for E < 200 keV. lab, using more realistic ion-atom theoretical results.

A comparison of the 2s - > 2p cross sections shows that even at E = 22 keV. lab where capture and direct excitation are comparable, the AO54 and AO65 bases give excitation cross sections which differ from each other no more than by some 12 per cent. This is a surprising result because the projectile sets are competely dissimilar in these two cases. A similar conclusion follows from a comparison of the results from the AO32 and AO20 basis sets described in section (5.2.1), which demonstrates the effect of introducing projectile continuum pseudostates. It appears that coupling between the main excitation channel and capture channels is relatively weak even at low E.

On the other hand, coupling between states centred on the target appears to be much stronger. The basis AO32 described in Section (5.2.1) could approximately be obtained from the AO65 basis by deleting a total of 14 negative energy states and 19 positive energy states from the target centre. Figure 5.17 shows that this truncation produces changes of about 25 - 30% in the 2p excitation especially around the maximum in the cross section. The FBA results for 2p excitation have also been computed and compare well with similar calculations as the energy increases.

Experimental data is also available for excitation of

the 3d state.

The experimental cross sections of Kadota et al. (1982c) are compared with the quantal results in Figure 5.18. For slow collisions with energy below 80 keV. lab, AO65 is better than AO54, particularly for energies as low as E = 22 and 40 keV. lab. Figure 5.18 shows that AO54 overestimates the 2s - > 3d cross section by a factor of six at E = 22 keV lab and by a factor of two at E = 40 keV. lab.

Figure 5.18 shows that the cross sections ocmputed using AO32 are consistent with the present results obtained with AO65 and that, at low energies, the enlarged basis AO65 brings the cross sections closer to the experimental values. For higher energies, near the 3d excitation maximum at 125 keV. lab, both the AO32 and AO65 bases overestimate experiment by some 40 per cent. This is larger by a factor of two than the experimental uncertainty. For energies higher than 80 keV. lab, there is excellent agreement between the quantal cross sections obtained with the AO54 basis and data of Kadota et al. (1982c).

The cross sections for excitation of higher states are small and are therefore difficult to calculate accurately. The 5d and 5f states of our basis overlap with higher-lying bound states so that they represent, effectively, all bound states lying above n = 4. An inspection of the results for n = 4, and 5 (1 = 2, and 3) presented in Table 5.26, shows that cross sections for the n > 4 excitation computed with AO54 are apparently too large if E < 100 keV. lab. It may

Fig. 5.18 $He^{2+} + Li(2s) \rightarrow He^{2+} + Li(3d)$

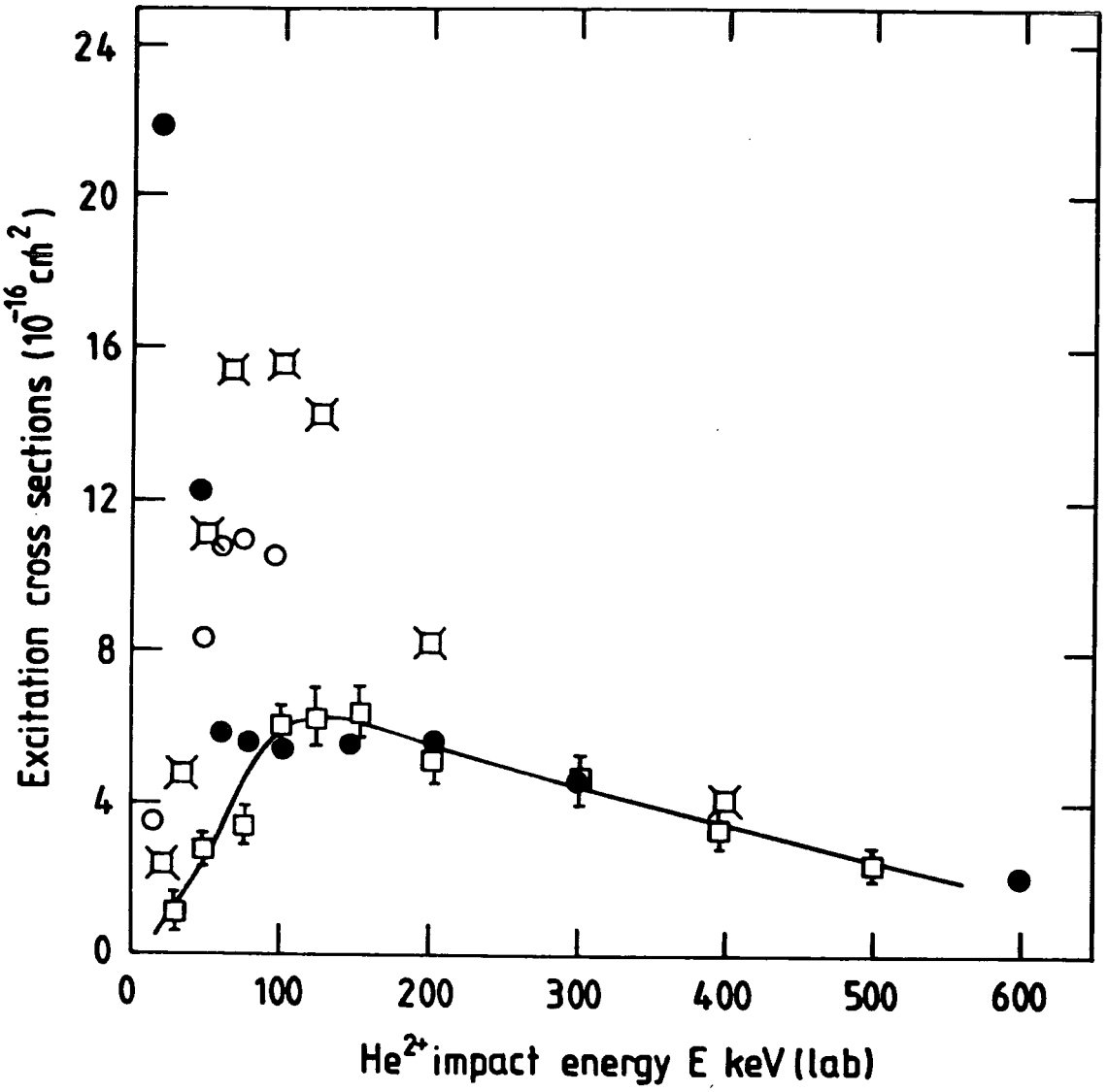

Key to Figure 5.18.

Direct excitation of Li(2s) by He^{2+} impact.

Cross sections for Li(2s -› 3d) excitation and Li(3d -› 2s) emission.

Experimental data

□ , Li(3d -› 2s) emission , Kadota et al. (1982c).

Theoretical results for Li(2s -› 3d) excitation.

⌑ , 32-state (A032) results, present work.

● , 54-state (A054) results, present work.

○ , 65-state (A065) results, present work.

Table 5.26

Computed cross sections for He^{2+} ion impact excitation of the n=4,5 (d,f) states in Li. All cross sections are in units of 10^{-16} cm^2.

E (keV lab)	40.0		100.0		300.0		1000.0	
Final state ($\overline{nT}$)	a	b	a	b	a	b	a	b
4d	7.3	2.5	1.51	2.11	1.13	1.32	0.37	0.38
5d	38.9	4.5	15.6	7.5	1.62	1.57	0.44	0.44
4f	5.0	1.27	3.0	2.0	0.80	0.60	0.085	0.092
5f	9.3	1.57	7.0	4.4	1.63	1.16	0.135	0.146

a Calculated using the AO54 basis .

b Calculated using the AO65 basis .

probably cast a doubt on the quality of the AO54 basis, particularly, near the ionisation threshold. In order to assess the properties of the basis we shall consider relevant oscillator strength sums listed in Table 5.19. For the sums of the 2p - > nd and 3d - > nf transitions, the negative energy states of AO54 give 0.89 and 1.36 to be compared with the exact values (Cowan 1981) of 0.94 and 1.30, respectively. This suggests that AO54 is adequate, within a few per cent error, for calculating excitation cross section for transitions to d and, even, to f states.

The reason for enlarged excitation cross section is the strong coupling between charge exchange and excitation channels at low energy. Table 5.26 shows that the omission of the corresponding n = 2, and 3 states from the projectile centre set is responsible for this effect: the cross sections are reduced considerably if these projectile centre states are included (as in the case of AO65). We have now completed the description of the coupled-channel results and shall consider next the t-matrix results for ionisation of the L-shell.

5.7 The t-matrix calculations and results for ionisation.

5.7.1 Numerical methods.

The t-matrix theory has been discussed in chapter 4. In this section we shall discuss the numerical details of the calculation of the ionisation of the L-shell of Li by He^{2+} impact. This will allow a comparison with the results presented in section 5.6. The first part of the calculation was to obtain an approximation for the function which is used in (4.1.35). This was obtained by solving the close-coupled equations as formulated in Chapter 3, using an expansion basis which consisted of the fifty-three target states defined in section (5.5.2) for AO54. This basis is given in table 5.18. The He^{+}(1s) state was omitted from the AO54 basis. This was because it had been found that the inclusion of this state did not make a significant difference (see Figure 5.13). This corresponds to the expansion shown in expression (4.3.1). The solution of the close-coupled equations was accompanied by the output of the corresponding transition amplitudes (defined by the $b_j(t)$) in expression (4.3.1) at a total of 127 intermediate values of z between z = -70.0 a.u. and z = +70.0 a.u., as described in section 4.3. The evaluation of the matrix elements $I_{klm}(t)$ in (4.1.37) could then begin using the methods described in section 4.2. . It was necessary initially to

choose a set of values of $k^2/2$ which represented the ionised electron energies in expression (4.1.34). The initial choice consisted of fifteen values between 0.05 and 2.0 a.u. as the primary AO54 calculations had shown that this was the most important range of energies for ionisation, using L^2 pseudostastes.

The two dimensional integration method that was used was tested using various numers of quadrature points in the Gauss-Legendre and Gauss-Laquerre integrals and initially 25 points were used in both integrations.

However this combination of parameters was found to produce some uncertainty in the final amplitudes. This was due to some uncertainty in the numerical integration over $k^2/2$ in (4.1.34) and also because of some uncertainty in the matrix elements in (4.1.37). It was found that it was necessary to reduce the upper limit of the $k^2/2$ integration to 1.0 a.u. to get a smoother integral (it often contained some structure) and to increase the number of points to be twenty-five in the Gauss-Legendre and forty in the Gauss-Laguerre quadratures. The b grid used for the numerical integrals over b in (4.1.40) was the same as in the original close-coupled calculation and contained either twelve or thirteen b values between 0.05 and 24.0 a.u. The above parameters were used for all the partial waves ($0 <= 1 <= 3$) of the final state electron. The corresponding cpu time needed to obtain a complete set of partial wave results for one impact energy from the t-matrix

codes was approximately 21 hours on the Newcastle Amdahl 5860 or about 60 hours on the Durham Amdahl 470/V8. To this must be added the cpu time for the initial coupled-state calculations, which decreased with increasing energy, but was of the order of 20 to 40 per cent of the t-matrix cpu time. The length of these calculations suggests that it would be worthwhile to investigate other methods of calculating the t-matrix matrix elements.

It is possible to make a check of the t-matrix codes by calculating the transition amplitudes defined by (4.1.35) for a final state which is identical to one of the states in the initial close-coupled expansion. The coupled-equations defined by expression (3.3.5) for the case where there are no projectile expansion states can be written as

$$i \underset{\sim}{I} \dot{\underset{\sim}{A}} = \underset{\sim}{H} \underset{\sim}{A} \qquad (5.7.1)$$

which has the solution

$$\underset{\sim}{A}(t_b) = -i \int_{-t_a}^{t_b} \underset{\sim}{H} \underset{\sim}{A} \, dt + \underset{\sim}{A}(t_a) \qquad (5.7.2)$$

where $\underset{\sim}{A}(t=t_a)$ defines the initial condition. The transition amplitudes from this expression are equivalent to those obtained from using expression (4.1.15) provided the wavefunction $\Psi_i^+(\vec{r}_B, t)$ is replaced by the close-coupled solution obtained from (5.7.1) and the final state is one of the same close-coupled states (except the initial state

because we have used (4.1.14) to get (4.1.15)). Tests were made to check that the computer codes could satisfactorily confirm this. For example consider the four 1 = 3 states in the close-coupled expansion. The values obtained from the initial close-coupled solution and the amplitudes obtained from expression (4.1.15) are given in table 5.27 and the agreement is very good in general. This is also a check that the initial solution of the coupled equations which produces the amplitudes is accurate.

During the evaluation of (4.1.40) the upper limit of the $k^2/2$ integration was varied to test how the integral converged. It was found that changing the limit from 1.0 a.u. to 0.65 a.u. produced less than 5 per cent difference in the results. The effect of changing the upper limit of the t integration in expression (4.1.35) was also studied but no significant effect was found and an upper limit corresponding to z = + 70.0 a.u. was sufficiently accurate. The codes used for the FBA calculations were developed from the t-matrix codes and were known to also provide results in excellent agreement with independent results of Peach (1986) for ionisation of the L-shell for $0 \leqslant 1 \leqslant 3$. We shall now describe the results obtained using the t-matrix method.

5.7.2 The t-matrix ionisation results.

The present results are shown in Table 5.28 and in Figure 5.16. Three different choices of the function (W(R) - U(R)) as defined in expression (4.1.35) were used as given below

Table 5.27

A comparison of the transition amplitudes obtained from the t-matrix method and the values obtained from the original close-coupled solution.

State $(\overline{nlm})$	t-matrix amplitude [a]	Close-coupled amplitude [b]
$\overline{4f0}$	$-0.04005 , -0.00783i$	$-0.03985 , -0.00758i$
$\overline{4f1}$	$0.09022 , -0.02799i$	$0.09029 , -0.02792i$
$\overline{4f2}$	$0.01060 , 0.06887i$	$0.01061 , 0.06881i$
$\overline{4f3}$	$-0.01582 , 0.01196i$	$-0.01583 , 0.01198i$
$\overline{6f0}$	$0.08348 , -0.12366i$	$0.08370 , -0.12363i$
$\overline{6f1}$	$0.14401 , 0.07602i$	$0.14377 , 0.07610i$
$\overline{6f2}$	$0.00034 , 0.08157i$	$0.00043 , 0.08164i$
$\overline{6f3}$	$-0.02485 , 0.02353i$	$-0.02485 , 0.02350i$

a) Computed using equation (5.7.2)

b) Obtained from solution of the close-coupled equations in (5.7.1).

Table 5.28 A comparison of the partial wave t-matrix results with the corresponding FBA and close-coupled results for ionisation.

l		E keV lab 40	65	100	150	200	600	1000	2000	6000
l=0	a	1.81	1.34	1.14	1.23	1.16	0.765	0.524	0.280	0.0975
	b	1.78	1.35	1.12	1.21	1.16	0.757	0.511	0.273	0.0951
	c	0.289	0.283	0.213	0.157	--	--	--	--	--
	d	1.74	0.983	0.664	0.653	0.672	0.687	0.437	0.220	0.0730
l=1	a	7.20	7.38	5.08	3.39	2.40	1.19	0.903	0.566	0.240
	b	7.20	7.29	5.09	3.39	2.39	1.19	0.903	0.566	0.240
	c	0.945	0.755	1.28	1.12	--	--	--	--	--
	d	1.25	1.55	1.55	1.51	1.42	1.35	0.983	0.624	0.282

a t-matrix results with (W(R) - U(R)) = 2 / R

b t-matrix results with (W(R) - U(R)) = 2 * (1 - e^{-R}) / R

c AO65 basis results for projected direct ionisation only.

d AO54 basis results for ionisation for E < 200 keV lab only.
FBA results from expression (4.1.40) using the exact continuum states for E > 200 keV lab.

Table 5.28 continued . A comparison of the partial wave t-matrix results with the corresponding FBA and close-coupled results for ionisation.

		E keV lab								
		40	65	100	150	200	600	1000	2000	6000
l=2	a	14.8	17.8	12.6	9.17	6.67	2.29	1.37	0.673	0.224
	b	14.2	17.9	12.6	9.22	6.69	2.30	1.37	0.673	0.224
	c	1.97	3.71	4.16	4.00	--	--	--	--	--
	d	5.24	7.91	7.83	6.28	4.81	2.17	1.31	0.661	0.221
l=3	a	22.6	29.6	26.1	19.1	13.6	2.47	1.15	0.447	0.131
	b	30.0	40.5	36.9	25.5	17.2	2.48	1.15	0.447	0.131
	c	1.78	5.09	7.83	7.80	7.58	--	--	--	--
	d	7.29	12.0	15.4	12.8	9.18	1.32	0.791	0.396	0.132

a t-matrix results with (W(R) - U(R)) = 2 / R

b t-matrix results with (W(R) - U(R)) = 2 * (1 - e^{-R}) / R

c AO65 basis results for projected direct ionisation only.

d AO54 basis results for ionisation for E < 200 keV lab only. FBA results from expression (4.1.40) using the exact continuum states for E > 200 keV lab.

$$W(R) - U(R) = \frac{2}{R} \qquad (5.7.3)$$

$$W(R) - U(R) = \frac{2}{R}(1 - e^{-R}) \qquad (5.7.4)$$

$$W(R) - U(R) = 0 \qquad (5.7.5)$$

Formula (5.7.4) has been used by Reading et al. in their investigation of charge transfer using a similar t matrix formulation as described in Section 2.4.10. Both (5.7.3) and (5.7.4) have the property that for R -> ∞ the potential in the matrix element (4.1.35) falls off faster than 1/R, assuming condition (4.1.6), that is

$$R\,(V_{eA}(r_A) + W(R) - U(R)) \underset{R \to \infty}{\longrightarrow} 0 \qquad (5.7.6)$$

Figure 5.16 shows that the results are rather dependent upon the choice of (W(R) - U(R)) and that they are in general well above the close-coupled results. The partial wave results in Table 5.27 show that the results for 1 = 0, 1, 2 and 3 are very similar when using either (5.7.4) or (5.7.5). The 1 = 3 total is the dominant contribution in the total cross section as in the close coupled results. The reason that the use of (5.7.5) gives different cross sections is because they do not obey (5.7.6), and the amplitudes (4.1.35) have not converged in the integration over t. The

results seem to be independent of the form of (W(R) - U(R)) for a reasonable choice.

There are several possible reasons for the above results. Of the assumptions made in calculating the amplitude (4.1.35) probably the least justified is in the approximation to the total wavefunction from equation (4.1.23). This was replaced by the solution of a large one centre expansion (OCE) with the neglect of the projectile centre. It was hoped initially that the large OCE could effectively reproduce the total wavefunction (including the charge exchange channels) for some interval around t = 0. Then if the major contribution to (4.1.35) came from the same interval the use of the OCE would be a reasonable approximation to the wavefunction in (4.1.23). However from table 5.27 it appears that even when the total capture is small compared to the direct excitation and ionisation cross sections, and presumably the OCE is a good approximation to $\Omega_i^+(\vec{r}_B, t)$ the t-matrix total still differs considerably from the AO54 and AO65 target ionisation totals. One reason could be that the final continuum states used in (4.1.35) with the corresponding integration over $K^2/2$ in (4.1.39) provide a better representation of the continuum than the pseudostates used in the initial close coupled expansion but the agreement between the exact and pseudostate representations of the continuum in the FBA, as shown in Figure 5.12, would suggest this is not the case, even for the 1 = 3 states.

As discussed in Section 5.6, we expect this difference in representation to lead to an increase of only some 10-15 per cent, in the computed cross sections, provided there are no other approximations made. The present t-matrix results are however a factor of more than two greater than any close coupled results near the ionisation maximum.

Another assumption in deriving (4.1.35) is using (4.1.16) to obtain the final continuum states. The close-coupled results from the AO54 basis and the AO65 basis had shown thay the dominant contribution to the positive energy cross sections is from states with energies less than 0.7 a.u. and the same is true of the t-matrix results, for impact energies below 600 keV. lab. An electron energy of 0.7 a.u. corresponds to an electron velocity of $v = 1.18$ a.u. The corresponding impact energy of an He^{2+} ion with this velocity is 139 keV. lab. This suggests that the use of (4.1.16) may only be justified for impact energies above 140 keV. lab or some slightly higher energy. At lower energies the incident projectile may screeen the ionised target and the ejected electron will see some Screened potential. This is one of the main problems in ionisation calculations. Unfortunately we have not been able to make calculations using final wavefunctions other than those obtained from (4.1.16).

In general the t-matrix results agree better with experiment than with the close-coupled results at impact energies below 600 keV lab., and converge towards the Born

results (for the same final continuum states) at higher energies. However if the experimental data is renormalized to agree with the supposedly more correct ionisation curve at high energies, discussed in Section 5.6, this would spoil the agreement of the t-matrix and experiment at lower energies. Hence there is some doubt as to the best theoretical data near the ionsation maximum, and this could be resolved by new experimental results we feel.

5.8 Remarks on the present methods.

In this section we shall make some comments upon the relationship between the present calculations and some of the methods described in Chapter 2. In Section 5.3 we have seen that there is agreement between the present results and the AO+ results of Fritsch and Lin (1983) for electron capture from the L-shell of lithium. In the AO+ method the basis sets used contained STO's with a range of exponential decay parameters from 0.352 to 3.80 on the Li centre, in order to optimise the United Atom (UA) energies. The increased nuclear charge of the UA is the reason for the large decay parameters. In the present method we have found it necessary to include STO's with exponential decay parameters between 0.5 and 1.7, on the He^{2+} centre. For the p and d states decay parameters which were larger than the

$\bar{z}$/n hydrogenic values were needed in order to obtain the correct oscillator sums. This reflects the fact that although both methods are trying to take the continuum into account by apparetly different methods they have in common the need to include larger decay parameters than is the case in a purely bound state calculation. This is also the case in the present calculations for ionisation from both the L- and K- shells.

The present AO54 basis for L-shell ionisation and the AO50 and AO43 basis sets used for K-shell ionisation were similar to the OHCE method of Reading et al. (1981, 1982a,b) as described in Section 2.4.10. The present results were obtained with unconstrained projectile time dependent amplitudes whereas the OHCE projectile amplitude was constrained to have the form of a Heaviside function O(t) with the discontinuity at T = 0, in the case of the p + H system. We can now compare the results from our AO54 basis with the OHCE method. Figure 5.19 shows that for a particular value of b and an impact energy of 100 keV. lab the actual unconstrained form of the He^{+}(1s) is not of the Heaviside form but rather of the form of a sharp peak centred upon T = 0. At B = 300 keV. lab the corresponding projectile amplitude is slightly more like a Heaviside funcion. This suggests that the OHCE method may not be very sensitive to the actual form assumed for the projectile amplitude b(t) as Reading et al. obtained good agreement with experiment. We cannot make any more general comments

Fig 5.19

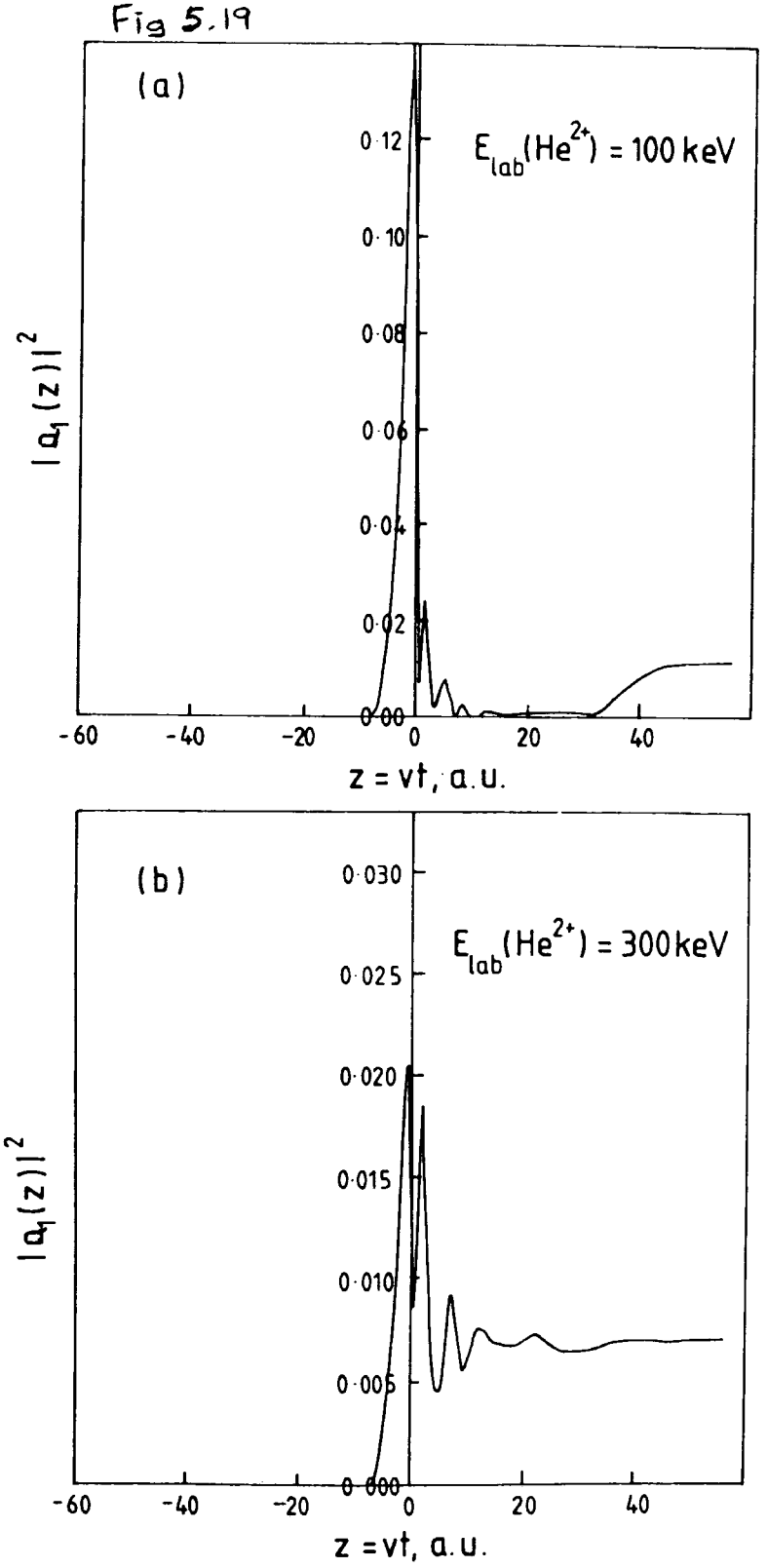

Key to Figure 5.19

The probability $|a_1(z)|^2$ for the valence 2s electron in Li to be captured into the 1s state of He^+ as a function of z = vt. Computed using the AO54 basis set for an impact parameter b = 1.5 a.u.

(a) E = 100 keV lab. (b) E = 300 keV lab. The point z = 0 corresponds to the point of closest approach.

however but we can say that for the special case where the projectile amplitude is constrained to be identically zero, this is equivalent to the AO53 basis (i.e. the OCE). The ionisation results from AO54 were not very different from the AO54 results for ionisation and therefore it may be that for the case of He^{2+} + Li interactions there is little advantage between the OCE, the OHCE and the AO54 type expansion. From previous experience it is evident that it is difficult to make more general conclusions than this, but possibly the OHCE is useful in systems which are more nearly symmetrical than those which are not.

In the present calculations we have used basis sets constructed in the spirit of the DACC approach (Section 2.4.9). The results we have obtained for varous single-electron processes show that this is a reasonably effective manner in which to include the continuum states in a basis set expansion. However, the success of this method should be judged when it is applied to other systems. Another method based upon the selection of oscillator strengths is suggested in the work of Hermann and Langhoff (1983). They have considered the Stieltjes-Chebyshev representation which provides a Gaussian quadrature scheme of the bound and continuum states, thus generating an optimal representation of these states. Such states have been generated in the present work but unfortunately some preliminary calculations were not successful due to computational problems. It remains to be seen if such

states can be successfully employed in coupled-channel calculations.

In the comparison between the quantal and classical calculations, discussed in this chapter, it has been found that in the intermediate energy range 12.5 keV amu^{-1} to 500 keV amu^{-1} the agreement is of the order of 30 per cent for total capture cross sections, and n-shell distributions, while the classical method is about a factor of twenty times as fast. This could be an important factor in subsequent calculations. A lengthier discussion of the two methods is given in Ermolaev, Hewitt and McDowell (1987).

We have described the main calculations that have been made to investigate the role of the continuum in single electron processes. However the present method is not limited but could be applied to two-electron processes which are currently being investigated (Shingal, Bransden and Flower, 1987). In some early calculations the method of Burke and Mitchell (1974) (in Section 2.4.3) was used to obtain a pseudostate basis to represent the continuum in p + H^- collisions using a two electron model (Shingal, 1983). However, it was found that the results were more sensitive to the form of the initial H^- wavefunction than to the inclusion of the continuum and therefore the pseudostates were not retained in the calculations.

In the final chapter we shall make some final comments upon the results presented in this chapter.

CHAPTER SIX

Conclusions

6.1 Discussion of results

The suggestion that is made in this thesis is that reasonably accurate results can be obtained for various single electron processes in ion-atom collisions by using a small number of states, chosen to represent certain physical criteria. In particular the continuum states can be represented by choosing pseudostates which satisfy certain oscillator sums. This is just one of the many possible approaches to this problem as shown in Chapter 2. We consider that this idea has been reasonably justified by the results in Chapter 5. Firstly we can consider the charge exchange results for capture from the L-shell in reaction (5.2.1). Table 5.9 has shown the direct effect of including states which represent both the continuum and high n states, to a bound state basis set. The largest effects are found in the energy region above 40 keV. lab. This coincides with the region where ionisation is significant, and coupling between the charge exchange and projectile continuum states is therefore relatively important. The continuum states were added to the projectile centre in these calculations.

However, both the direct and CTTC contributions have

maxima at similar positions and it is possible that the same results would be found by adding pseudostates to the target. For E > 200 keV. lab capture from the K-shell is the dominant process. The present results extend the previous close coupled calculations of Ermolaev and Hewitt (1985) to E = 2 MeV lab and reproduce the experimental behaviour of the cross section. For K-shell capture the continuum states (upon the target) have been seen to be less important than in the case of L-shell capture, and the K-shell capture cross sections appear to converge more readily than the L-shell results. The reason for this is presumably due to the large energy defect between the initial and final states.

The ionisation results we have presented are the first close coupled calculations for reaction (5.6.1) and there are several important conclusions to be made. Firstly we have confirmed the prediction of Ermolaev and Hewitt (1985) concerning the importance of both the d and f-state contribution to the target ionisation total for impact energies in the range 65 - 200 keV lab. As predicted by Ermolaev and Hewitt, the inclusion of charge exchange channels does not greatly alter their relative importance. However this has made the accurate calculation of the ionisation cross section much more difficult because of the number of states involved and the computational difficulties this produces. We have also shown that the CTTC contribution is always much less important than the direct

ionisation total, in contrast to the case for p + H(1s) for example. We believe that the best ionisation cross sections we have determined (using the close-coupled and FBA results) are accurate and do not anticipate that further calculations would show more than about 15 per cent difference around the maximum. Only accurate measurements could confirm this but they are difficult to perform.

The excitation cross sections for reaction (5.4.2) have been more difficult to determine than was originally thought. The results for Li(2s → 2p) excitation show that coupling between the target states is more important than the influence of the charge exchange channels and the AO65 and AO54 basis sets differ by less than 15 per cent over all impact energies. However the Li(2s → 3d) cross section is much more sensitive to the choice of basis set and good agreement with experiment is found only for E > 100 keV lab. Excitation of states with higher n values is also sensitive to the inclusion of the charge exchange channels.

The t-matrix results for ionisation reported in Section 5.6 are not very conclusive. They suggest that more complete calculations using two centre expansions are necessary in order to see if any improvement over the present L^2 expansion methods is obtained. This would be an interesting subject for further study. However, the results do not change the previous conclusions made in this section concerning the ionisation cross sections.

We shall conclude by making some comments upon the

motivation for the basis sets used in the calculations. Apart from investigating the role of the continuum in ion atom collisions, we were interested in trying to find the most efficient way to perform the calculations while obtaining results of a reasonable accuracy. That is why we tried to use a relatively small basis set for the capture calculations. We also tried to use a basis for the ionisation results which would be efficient computationally and also physically, which was the motivation for the AO54 type basis set. However, we found this was justifiable mainly for the K-shell calculations and less so for the L-shell.

The conclusion we make is that the methods that have been discussed in this thesis should be extended to other collision systems to see their effectiveness, and that for certain processes a high degree of accuracy can be expected. The least certain aspect of the present results is in the IEM model for the K-shell which shows the need for more investigation of the correlation effects present.

APPENDIX A1

Evaluation of the direct primitive matrix elements in the space fixed frame.

The primitive integrals to be found have the form given in expressions (3.4.4), (3.4.5) and (3.4.6). In order to demonstrate the numerical methods we shall consider the three following integrals

$$I^1_{jk} = -Z_1 \int d\vec{r}\, r^n e^{-\alpha r} \bar{Y}_{l_j m_j}(\theta,\phi)\, \bar{Y}_{l_k m_k}(\theta,\phi)\, \frac{1}{|\vec{R}-\vec{r}|} \qquad (A1.1)$$

$$I^2_{jk} = -Z_1 \int d\vec{r}\, r^n e^{-\alpha r} \bar{Y}_{l_j m_j}(\theta,\phi)\, \bar{Y}_{l_k m_k}(\theta,\phi)\, \frac{e^{-\gamma|\vec{R}-\vec{r}|}}{|\vec{R}-\vec{r}|} \qquad (A1.2)$$

$$I^3_{jk} = -Z_3 \int d\vec{r}\, r^n e^{-\alpha r} \bar{Y}_{l_j m_j}(\theta,\phi)\, \bar{Y}_{l_k m_k}(\theta,\phi)\, e^{-\gamma|\vec{R}-\vec{r}|} \qquad (A1.3)$$

The coordinate system which is used in the expressions (A1.1), (A1.2) and (A1.3) is shown in figure A1.1.

The polar angles (θ,ϕ) refer to the polar angles of $\vec{r}$ in the (x,y,z) coordinate system. Similarly the polar angles of $\vec{R}$ in the (x,y,z) system are defined by (θ_R,ϕ_R). The angular functions $\bar{Y}_{lm}(\theta,\phi)$ have been defined in the space fixed frame, as in section 3.2. In order to evaluate A1.1 we use the formula (Weissbluth 1978).

$$\frac{1}{|\vec{R}-\vec{r}|} = \sum_{l=0}^{\infty} \sum_{m=-l}^{l} \frac{4\pi}{2l+1} \frac{r_<^l}{r_>^{l+1}} Y^*_{lm}(\theta_R,\phi_R)\, Y_{lm}(\theta,\phi) \qquad (A1.4)$$

where as usual $r_<$ is the smaller of the two values , R , and

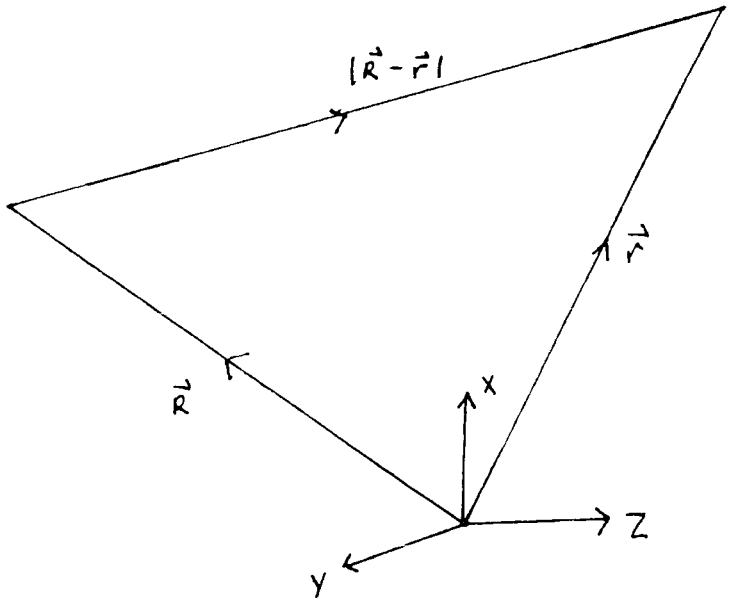

Fig. A1.1

The co-ordinate system used in evaluating the direct matrix elements.

$r_<$ and $r_>$ is the greater of the same two values. Then we can write I^1_{jk} as follows:

$$I^1_{jk} = -4\pi Z_1 \sum_{l=0}^{\infty} \frac{1}{2l+1} \int_0^{\infty} dr \left\{ r^{n+2} e^{-\alpha r} \frac{r_<^l}{r_>^{l+1}} \right\} \qquad (A1.5)$$

$$\times \sum_{m=-l}^{l} Y^*_{lm}(\theta_R, \phi_R) \int d\Omega_r \, \bar{Y}_{l_j m_j}(\theta,\phi) \bar{Y}_{l_k m_k}(\theta,\phi) Y_{lm}(\theta,\phi).$$

Thus we can separate out the term from expression A1.5 which contains the dependence upon $|\vec{R}|$ and this term is

$$\bar{f}^1_l(\alpha, n, R) = \int_0^{\infty} dr \, r^{n+2} e^{-\alpha r} \frac{r_<^l}{r_>^{l+1}} \qquad (A1.6)$$

$$= \frac{1}{R^{l+1}} \int_0^R dr \, r^{n+2} e^{-\alpha r} r^l + R^l \int_R^{\infty} dr \, r^{n+2} e^{-\alpha r} \frac{1}{r^{l+1}}$$

Expression A1.6 can readily be evaluated.

The summation over l in expression A1.5 is limited by the fact that the integral over $d\Omega_r$ vanishes unless the following condition is obeyed

$$|l_j - l_k| \leq l \leq l_j + l_k \qquad (A1.7)$$

The integral over $d\Omega_r$ can be written as

$$g(l_j, m_j, l_k, m_k, l, m) = \int d\Omega_r \, \bar{Y}_{l_j m_j}(\theta,\phi) \bar{Y}_{l_k m_k}(\theta,\phi) Y_{lm}(\theta,\phi) \qquad (A1.8)$$

and then combining A1.7, A1.8 and A1.5 we have an expression for I^1_{jK} as follows

$$I^1_{jK} = -4\pi z_1 \sum_{\ell} \frac{1}{2\ell+1} \tilde{f}^1_{\ell}(\alpha, n, R) \sum_{m=-\ell}^{\ell} Y^*_{\ell m}(\theta_R, \phi_R)\, g(\ell_j, m_j, \ell_K, m_K, \ell, m) \tag{A1.9}$$

We shall now consider the evaluation of I^2_{jK} as defined by expression A1.2. In order to reduce it to a suitable form the expansion series by Watson (1966) is used where

$$\frac{e^{-\gamma|\vec{R}-\vec{r}|}}{|\vec{R}-\vec{r}|} = \sum_{\ell=0}^{\infty} (2\ell+1) \frac{1}{\sqrt{r_>}} K_{\ell+\frac{1}{2}}(\gamma r_>) \frac{1}{\sqrt{r_<}} I_{\ell+\frac{1}{2}}(\gamma r_<) P_\ell(\cos\beta) \tag{A1.10}$$

and $\cos(\beta) = \dfrac{\vec{r}.\vec{R}}{rR}$

$K_{\ell+\frac{1}{2}}(\gamma w)$ and $I_{\ell+\frac{1}{2}}(\gamma w)$ are modified Bessel functions and w represents r or R. We use the following results

$$K_{\ell+\frac{1}{2}}(\gamma w) = \sqrt{\frac{\pi}{2\gamma w}}\, e^{-\gamma w} \sum_{s=0}^{\ell} \frac{(\ell+s)!}{s!(\ell-s)!(2\gamma R)^s} \tag{A1.11}$$

$$I_{\ell+\frac{1}{2}}(\gamma w) = \frac{1}{\sqrt{2\pi\gamma w}}\, e^{\gamma w} \sum_{s=0}^{\ell} \frac{(-1)^s(\ell+s)!}{(\ell-s)!\, s!\, (2\gamma r)^s} \tag{A1.12}$$
$$+ (-1)^{\ell+1} e^{-\gamma w} \textstyle\sum_{s=0}^{\ell} (\ell+s)!/[s!(\ell-s)!(2\gamma w)^s \sqrt{2\pi\gamma w}])$$

The expansion of $P_\ell(\cos\beta)$ is given in Weissbluth (1978)

$$P_\ell(\cos\beta) = \frac{4\pi}{2\ell+1} \sum_{m=-\ell}^{\ell} Y_{\ell m}(\theta, \phi)\, Y^*_{\ell m}(\theta_R, \phi_R) \tag{A1.13}$$

when A1.10 and A1.13 are substituted into A1.2 we finally obtain

(A1.14)

$$I^2_{jK} = -z_2 4\pi \sum_{\ell=0}^{\infty} \frac{1}{\sqrt{R}} K_{\ell+\frac{1}{2}}(\gamma R) \int_0^R dr\, r^{n+2} e^{-\alpha r} \frac{1}{\sqrt{r}} I_{\ell+\frac{1}{2}}(\gamma r)$$

$$\times \sum_{m=-\ell}^{\ell} Y^*_{\ell m}(\theta_R, \phi_R) \int d\Omega_r\, \bar{Y}_{j,m_j}(\theta, \phi)\, \bar{Y}_{\ell_K, m_K}(\theta, \phi)\, Y_{\ell, m}(\theta, \phi)$$

$$- z_2 4\pi \sum_{\ell=0}^{\infty} \frac{1}{\sqrt{R}} I_{\ell+\frac{1}{2}}(\gamma R) \int_R^{\infty} dr\, r^{n+2} e^{-\alpha r} \frac{1}{\sqrt{r}} K_{\ell+\frac{1}{2}}(\gamma r)$$

$$\times \sum_{m=-\ell}^{\ell} Y^*_{\ell m}(\theta_R, \phi_R) \int d\Omega_r\, \bar{Y}_{\ell, m}(\theta, \phi)\, \bar{Y}_{\ell_K, m_K}(\theta, \phi)\, Y_{\ell m}(\theta, \phi)$$

The form of I^2_{jK} as given in A.14 is similar to the form of I^1_{jK} as given in A1.9 and we have the final form of I^2_{jK} as follows

$$I^2_{jK} = -4\pi Z_2 \sum_{\ell} \bar{f}^2_{\ell}(\alpha, \gamma, n, R) \sum_{M=-\ell}^{\ell} Y^*_{\ell M}(\theta_R, \phi_R)\, g(\ell_j m_j \ell_K m_K \ell m) \qquad (A1.15)$$

where we define the function $\bar{f}^2_{\ell}(\alpha, \gamma, n, R)$ by

$$\bar{f}^2_{\ell}(\alpha, \gamma, n, R) = \frac{1}{\sqrt{R}} K_{\ell+\frac{1}{2}}(\gamma R) \int_0^R dr\, r^{n+2} e^{-\alpha r} \frac{1}{\sqrt{r}} I_{\ell+\frac{1}{2}}(\gamma R)$$

$$+ \frac{1}{\sqrt{R}} I_{\ell+\frac{1}{2}}(\gamma R) \int_R^{\infty} dr\, r^{n+2} e^{-\alpha r} \frac{1}{\sqrt{r}} K_{\ell+\frac{1}{2}}(\gamma R) \qquad (A1.16)$$

The integrals in expression A1.15 can readily be evaluated, by using expressions A1.11 and A1.12. In order to find I^3_{jK} as defined in expression A1.3 we use the result

$$I^3_{jK} = -(Z_3/Z_2) \frac{\partial}{\partial \gamma} I^2_{jK} \qquad (A1.17)$$

which follows from A1.2 and A1.3.

Thus combining A1.15 and A1.17 we obtain

$$I^3_{jK} = 4\pi Z_3 \sum_{\ell} \frac{\partial}{\partial \gamma} \bar{f}^2_{\ell}(\alpha, \gamma, n, R) \sum_{m=-\ell}^{\ell} Y^*_{\ell m}(\theta_R, \phi_R)$$

$$\times g(\ell_j m_j \ell_K m_K \ell m) \qquad (A1.18)$$

$$= 4\pi Z_3 \sum_{\ell} \bar{f}^3_{\ell}(\alpha, \gamma, n, R) \sum_{M=-\ell}^{\ell} Y^*_{\ell m}(\theta_R, \phi_R)$$

$$\times g(\ell_j, m_j, \ell_K, m_K, \ell, m)$$

APPENDIX A2

The Chebychev interpolation method

In this appendix we shall state the Chebychev interpolation formulae as used in the present work. The same method was used in solving the close-coupled equations (Section (3.5.2)) as in evaluating the t-matrix elements (Section (4.3)). The Chebychev polynomial of order N , for ($-1 \leq x \leq 1$) , is given by the formula

$$P_N(x) = \sum_{r=0}^{N}{}'' \, c_r \, T_r(x) \qquad \text{(A2.1)}$$

where $''$ means that the first and last terms are multiplied by 0.5. The coefficients c_r are determined by

$$c_r = \frac{2}{N} \sum_{k=0}^{N}{}'' \, f(x_k) \, T_r(x_k) \qquad \text{(A2.2)}$$

where f(x) is the function which to be inteprolated upon. The x_k are given by

$$x_k = \cos \frac{k\pi}{N} \qquad \text{(A2.3)}$$

and $T_r(x)$ is given by

$$T_r(x) = \cos r(\cos^{-1} x) \qquad \text{(A2.4)}$$

In order to transform to another interval given by ($a \leq y \leq b$) we use the formula

$$x = \frac{2y - (a+b)}{b-a} \qquad \text{(A2.5)}$$

APPENDIX A3

The numerical solution of the Schrodinger equation for the case of the continuum states.

In this appendix we shall indicate how the differential equation of the general form given in (4.1.32) was solved , that is to say

$$\left(-\frac{1}{2}\frac{d^2}{dr^2} - \frac{K^2}{2} + V(r) + \frac{\ell(\ell+1)}{2r^2}\right) u_{K\ell}(r) = 0 \qquad (A3.1)$$

where V(r) is given in general by expression (3.3.7).

Firstly we expand the general form of the potential as a polynomial in r , so that

$$V(r) = \sum_{j=0}^{\infty} v_j r^{j-1} \qquad (A3.2)$$

Then we write the solution $u_{K\ell}(r)$ as

$$u_{K\ell}(r) = r^{\ell+1} \sum_{i=1}^{\infty} a_i r^{i-1} = r^{\ell+1} F(r) \qquad (A3.3)$$

and substitute (A3.2) and (A3.3) into (A3.1) . By equating the coefficients of the powers of r as usual we obtain recurrence relations for the coefficients . This means we can obtain the solution $u_{K\ell}(r)$ out to a value of r = 0.5 , for example. Then the equation (A3.1) can be written as

$$y_2' + 2\frac{(\ell+1)}{r} y_2 + (2V + 2E) y_1 = 0 \quad , \quad y_1' = y_2 \qquad (A3.4)$$

where

$$y_1 = F(r), \quad y_2 = F'(r) \qquad (A3.5)$$

and this can be solved by using the subroutine DE as described in section (3.5.2).This solution must be normalised to have the asymptotic behaviour defined by expression (4.1.33).This can be done using the method described by Cooper (1962).The results of this method were checked by solving (A3.1) by the Numerov method . The solution was normalised by using the method described in Cowan (1981).

APPENDIX A4

Expressions used in the numerical integration of the body-fixed integrals in terms of the prolate spheroidal co-ordinates (ξ,η,ϕ).

In Chapter 4 the two dimensional integration method was described for evaluating the t-matrix matrix elements. In this Appendix we shall give the relationships between various quantities in the body-fixed frame and in the (ξ,η,ϕ) co-ordinate system. In Figure A4.1 the co-ordinate system for describing the one electron system is shown.

The prolate spheroidal co-ordinates are defined as follows

$$\xi = \frac{1}{R}(r_A + r_B) \quad , \quad 1 \leq \xi \leq \infty \qquad \text{(A4.1)}$$

$$\eta = \frac{1}{R}(r_A - r_B) \quad , \quad -1 \leq \eta \leq 1 \qquad \text{(A4.2)}$$

$$\phi \text{ (azimuthal angle)} \quad , \quad 0 \leq \phi \leq 2\pi \qquad \text{(A4.3)}$$

Then

$$r_A = \frac{R}{2}(\xi + \eta) \qquad \text{(A4.4)}$$

$$r_B = \frac{R}{2}(\xi - \eta) \qquad \text{(A4.5)}$$

It is straightforward to obtain the following relationship

$$\cos\theta_B = \frac{\xi\eta - 1}{\xi - \eta} \qquad \text{(A4.6)}$$

$$\sin\theta_B = \frac{[(\xi^2-1)(1-\eta^2)]^{1/2}}{\xi - \eta} \qquad \text{(A4.7)}$$

Therefore we can express a function of r_B and θ_B in terms of ξ and η.

Fig. A4.1

Co-ordinates in the body fixed frame.

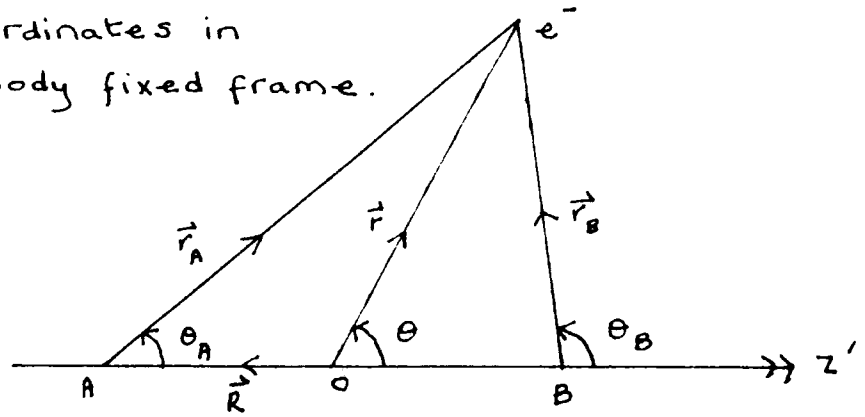

REFERENCES

Aberenkov I.V. and Heine V., 1965, Phil. Mag. 12, 529.

Anderson D.G.M., Antal M.J. and McElroy M.B., 1974, J. Phys. B: At. Mol. Phys. 7, L118.

Angel G.C., Dunn K.F., Sewell E.C. and Gilbody H.B., 1978, J. Phys. B: At. Mol. Phys. 11, L49.

Antal M.J., McElroy M.B. and Anderson D.G.M., 1975, J. Phys. B: At. Mol. Phys. 8, 1513.

Arbines R. and Percival I.C., 1966, Proc. Phys. Soc. 88, 861.

Arfken G., 1970, " Mathematical methods for physicists", (Academic Press: New York).

Banyard K.E. and Shirtcliffe G.W., 1979, J. Phys. B: At. Mol. Phys 12, 3247.

Barrett J.L. and Leventhal J.J., 1981, Phys. Rev. A23, 485.

Basu D., Mukherjee S.C. and Sural D.P., 1978, Phys. Reports 42C, 145.

Bates D.R. and Griffing G., 1953, Proc. Phys. Soc. A66, 961.

Bates D.R., 1958, Proc. Roy. Soc. A247, 294.

Bates D.R. and McCarroll R., 1958, Proc. Roy. Soc. A245, 175.

Bayfield J.E., 1969, Phys. Rev. 185, 105.

Becker R.L., Ford A.L. and Reading J.F., 1980, J.Phys. B: At. Mol. Phys. 13, 4059.

Bethe H.A. and Saltpeter E., 1977,"Quantum Mechanics of One- and Two-Electron Atoms", 1st edn. in pbk,(Plenum:New York).

Boellard A., 1984, FOM-Report 58.245.

Bransden B.H., 1983, "Atomic Collision Theory", 2nd ed., (Benjamin/Cummings : New York).

Bransden B.H., Newby C.W. and Noble C.J., 1980, J. Phys. B: At. Mol. Phys. 13, 4245.

Bransden B.H. and Ermolaev A.M., 1981, Phys. Lett. 84A, 316

Bransden B.H. and Noble C.J., 1981, J. Phys. B: At. Mol. Phys. 14, 1849

Bransden B.H. and Noble C.J., 1982, J. Phys. B: At. Mol. Phys. 15, 451.

Bransden B.H., Noble C.J. and Chandler J., 1983, J. Phys. B: At. Mol. Phys. 16, 4191.

Browne J.C., 1965, Proc. Phys. Soc. 86, 419.

Burke P.G., Gallaher D.F. and Geltman S., 1969, J. Phys. B: At. Mol. Phys. 2, 1142.

Burke. P.G. and Mitchell J.F.B., 1974, J. Phys. B: At. Mol. Phys. 6, 1974.

Callaway J., 1978, Phys. Repts. 45, 89.

Callaway J. and Wooten J.W., 1974, Phys. Rev. A9,1924.

Castillejo L., Percival I.C. and Seaton M.J., 1960, Proc. Roy. Soc. A254, 259.

Cheshire I.M., 1967, Proc. Phys. Soc. 92, 862.

Cheshire I.M., 1968, J. Phys. B: At. Mol. Phys. 1, 428.

Cheshire I.M., Gallaher D.F. and Taylor A.J., 1970, J. Phys. B: At. Mol. Phys. 3, 813.

Cooper J.W., 1962, Phys. Rev. 128, 681.

Cowan R.D., 1981,"The Theory of Atomic Structure and Spectra", 1st ed., (University of California Press: Berkeley).

Damburg R. J. and Karule E., 1967, Proc. Phys. Soc. 90, 637.

Damburg R. J. and Geltman S., 1968, Phys. Rev. Lett. 20, 485.

Danielle R., 1979, J. Chem. Phys. 70, 3462.

Dettmann K. and Leibfried G., 1969, Z. Phys. 218, 1.

DuBois R.D., 1985, Phys. Rev. A32, 3319.

DuBois R.D. and Toburen L.H., 1985, Phys. Rev. A31, 3603.

Eichler J. and Chan F.T., 1979, Phys.Rev. A20, 104.

Ermolaev A.M., 1984, J. Phys. B: At. Mol. Phys. 17, 1069.

Ermolaev A.M., 1987, unpublished.

Ermolaev A.M., Noble C.J. and Bransden B.H., 1982, J. Phys. B: At. Mol. Phys. 15, 457.

Ermolaev A.M. and Bransden B.H., 1984, J. Phys. B: At. Mol. Phys. 17, 1083.

Ermolaev A.M. and Hewitt R.N., 1985,Proc. Int. Conf. on the Physics of Highly Ionized Atoms, (Oxford), eds: J.D. Silver and N.J. Peacock, (Amsterdam: North Holland) , 487.

Ermolaev A.M., Hewitt R.N. and McDowell M.R.C., 1987, J. Phys. B: At. Mol. Phys. 20, 3125.

Ermolaev A.M., Hewitt R.N., Shingal R. and McDowell M.R.C., 1987, J. Phys. B: At. Mol. Phys. 20,

Fennema J.W.R., 1968, Physica 39, 13.

Fitchard E., Ford A.L. and Reading J.F., 1977, Phys. Rev. A16, 1325.

Fite W.L., Stebbings R.F., Hummer D.G. and Brackmann R.T., 1960, Phys. Rev. 119, 663.

Ford A.L., Fitchard E. and Reading J.F., 1977, Phys. Rev. A16, 133.

Ford A.L., Becker R.L., Swafford G.L. and Reading J.F., 1979a, J. Phys. B: At. Mol. Phys. 12, L491.

Ford A.L., Reading J.F. and Becker R.L., 1979b, J. Phys. B: At. Mol. Phys. 12, 2905.

Ford A.L., Reading J.F. and Becker R.L., 1981, Phys. Rev. A23, 510.

Ford A.L., Reading J.F. and Becker R.L., 1982, J. Phys. B: At. Mol. Phys. 15, 3527.

Fox L. AND Parker I.B., 1968," Chebyshev Polynomials in Numerical Analysis", 1st edn., (Oxford U.P.:Belfast).

Fritsch W. and Lin C.D., 1982, J. Phys. B: At. Mol. Phys. 15, 1255

Fritsch W. and Lin C.D., 1983a, J. Phys. B: At. Mol. Phys. 27, 3361.

Fritsch W. and Lin C.D., 1983b, J. Phys. B: At. Mol. Phys. 16, 1595.

Gallaher D.F. and Wilets L., 1968, Phys. Rev. 169, 139.

Geltman S., 1969, "Topics in Atomic Collission Theory", 1st edn., (Academic Press: London).

Geltman S. and Burke P.G., 1970, J. Phys. B: At. Mol. Phys. 3, 1062.

Ghosh M., Mandal C.R. and Mukherjee S.C., 1985, J. Phys. B: At. Mol. Phys. 18, 3797.

Gill P.E. and Miller G.F., 1972, Comp. Journal. 15, 80.

Green T.A., 1965, Proc. Phys. Soc. 86, 1017.

Greenland P.T., 1982, Phys. Reports. 81, 131.

Guffey J.A., Ellsworth L.D. and MacDonald J.R., 1977, Phys. Rev A15, 1863.

Hansteen J.M. and Mosebekk O.P., 1972, Phys. Rev. Lett. 29, 1361.

Hardie D.J.W. and Olson R.E., 1983, J. Phys. B: At. Mol. Phys. 16, 1983

Harris F.E. and Michels H.H., 1969, Phys. Rev. Lett. 22, 1036.

Hasse H.R., 1931, Proc. Camb. Phil. Soc. 26, 542.

Hatton G.J., Lane N.F. and Winter T.G., 1979, J. Phys. B: At. Mol. Phys. 12, L571.

Haugen H.K., Andersen L., Hvelplund P. and Knudsen H., 1982, Phys. Rev. A25, 1950.

Helbig H.F. and Everhart E., 1965, Phys. Rev. 140, A715.

Herman F. and Skillman S., 1963, "Atomic Structure Calculations", 1st edn., (Prentice-Hall: New Jersey).

Hermann M.R. and Langhoff P.W., 1983, Phys. Rev A.28, 1957.

Holt A.R. and Moiseiwitsch B.L., 1968, J. Phys. B: At. Mol. Phys. 1, 36.

Hvelplund P., Haugen H.K., Knusden H., 1980, Phys. Rev. A22, 1930.

Hylleraas E.A. and Undheim B., 1930, Z. Phys. 65, 759.

Inokuti M., 1971, Rev. of Mod. Phys. 43, 297.

Jalin R., Hagemann R., and Botter R., 1973, J. Chem. Phys. 59, 952.

Janev R.K. and Presnyakov L.P., 1980, J. Phys. B: At. Mol. Phys. 13, 4233.

Janev R.K. and Hvelplund P., 1981, Comm. Atom. Mol. Phys. 11, 75.

Janev R.K., Presnyakov L.P. and Shevelko V.P., 1985, "Physics of Highly Charged Ions", 1st ed., (Springer Verlag : Berlin).

Kadota K., Dijkkamp D., van der Woude R.L., Pan Guang Yan and de Heer F.J., 1982a, J. Phys. B: At. Mol. Phys. 15, 3275.

Kadota K., Dijkkamp D., van der Woude R.L., Pan Guang Yan and de Heer F.J., 1982b, Phys. Lett. 88A, 135.

Kadota K., Dijkkamp D., van der Woude R.L., Pan Guang Yan and de Heer F.J., 1982c, J. Phys. B: At. Mol. Phys. 15, 3297.

Kimura M. and Thorson W.R., 1981a, Phys. Rev. A24, 3019.

Kimura M. and Thorson W.R., 1981b, Phys. Rev. A24, 1780.

Kislyakov A.I. and Petrov M.P., 1971, Sov. Phys. - Tech. Phys. 15, 1252.

Klapisch M., 1967, C. R. Acad. Sci. (Paris) Ser. B 265, 914.

Kolker H.J. and Michels H.H., 1965, J. Chem. Phys. 43, 1027.

Lal M., Srivastava M.K. and Tripathi A.N., 1982, Phys. Rev. A26, 305.

Landau L.D. and Lifshitz E.M., 1977, "Quantum Mechanics : Non-Relativistic Theory", 3rd edn., (Pergamon Press: England).

Leep D. and Gallagher A., 1974, Phys. Rev. A10, 1082.

Lin C.D., 1978, J. Phys. B: At. Mol. Phys. 11, L185.

Lin C.D., Winter T.G. and Fritsch W., 1982, Phys. Rev. A25, 2395.

Lockwod G.L. and Everhardt E., 1962, Phys. Rev. 125, 567.

Louisell W.H., Scully M.O. and McKnight W.B., 1975, Phys. Rev A11, 989.

McCarthy I.E. and Stelbovics A.T., 1986, private communication.

McClure G.W., 1966, Phys. Rev. 148, 47.

McCorkle R.A., 1972, Phys. Rev. Lett. 29, 982.

McCullough R.W., Goffe T.V., Shah M.B., Lennon M. and Gilbody H.B., 1982, J. Phys. B: At. Mol. Phys. 15, 111.

McDowell M.R.C., 1985p, private communication.

McDowell M.R.C. and Coleman J.P., 1970, "Introduction to the Theory of Ion-Atom Collisions", (North Holland : Amsterdam).

McDowell M.R.C. and Ferendici A.M. (eds.), 1980, "Atomic and Molecular Processes in Controlled Thermonuclear Fusion", (Plenum : New York).

McDowell M.R.C., 1985, Seminar (University of California, Santa Cruz) 1985, invited paper.

McGuire E.J., 1968, Phys. Rev. 175, 20.

McGuire E.J., 1971, Phys. Rev. A3, 267.

McGuire J.H. and Weaver L., 1977, Phys. Rev. A16, 41.

Mapleton R.A., 1972,"Theory of Charge Exchange", 1st edn, (Wiley:New York).

Matese J.J. and Oberoi R.S., 1971, Phys. Rev. A4, 569.

Mathur K.C., Tripathi A.N. and Joshi S.K., 1971, Phys. Lett. 35A, 139.

Merzbacher E. and Lewis H.W., 1958, Encyclopedia of Physics, vol. 37, ed: S. Flugge, (Berlin : Springer Verlag), p. 166.

Moiseiwitch B.L. and Smith S.J., 1968, Rev. Mod. Phys. 40, 238.

Morse P.M. and Feshbach H., 1953, "Methods of Theoretical Physics", (McGraw-Hill: New York).

Murray G.A., Stone J., Mayo M and Morgan T.J., 1982, Phys. Rev. A25, 1805.

Nesbet R.K., 1969, Phys. Rev. 179, 60.

Neumann J. Von. and Wigner E., 1929, Physik Zeit. 30, 467.

Newby C.W., 1983, Ph.D Thesis, University of Durham.

Noble C.J., 1980, Comp. Phys. Commun. 19, 327.

Olson R.E., 1981, Phys. Rev. A24, 1726.

Olson R.E., 1982, J. Phys. B: At. Mol. Phys. 15, L163.

Olson R.E. and Salop A., 1976, Phys. Rev. A14, 579.

Olson R.E., Salop A., Phaneuf R.A. and Meyer F.W., 1977, Phys. Rev. A16,1867.

Oppenheimer J.R., 1928, Phys. Rev. 31, 349.

Peach G., 1965, Proc. Phys. Soc. 85, 709

Peach G., 1986, private communication

Peach G., Willis S.I. and McDowell M.R.C., 1985, J. Phys. B: At. Mol. Phys. 18, 3921.

Peart B., Grey R. and Dolder K.T., 1977, J. Phys. B: At. Mol. Phys. 10, 2675.

Peterkop R.K., 1977," Theory of Ionization of Atoms by Electron Impact", 1st edn, (Colorado Associated University Press, Colorado).

Post D., Mikkelsen D., Hulse R., Stewart L. and Weisheit J., 1981, Journal of Fusion Energy 1, 129.

Presnyakov L.P., 1964, Trudy (Proc.) of Lebedev Phys. Inst., Moscow 30, 256 (in Russian).

Prokofjew W., 1929, Z. Physik 58, 255.

Reading J.F., Ford A.L. and Fitchard E., 1976, Phys. Rev. Lett. 56, 573.

Reading J.F. and Ford A.L., 1979, J. Phys. B: At. Mol. Phys. 12, 1367.

Reading J.F., Ford A.L., Swafford G.L. and Fitchard A., 1979, Phys. Rev. A20, 130.

Reading J.F., Ford A.L. and Becker R.L., 1981, J. Phys. B: At. Mol. Phys. 14, 1995.

Reading J.F., Ford A.L. and Becker R.L., 1982a, J. Phys. B: At.Mol.Phys. 15, 625.

Reading J.F., Ford A.L. and Becker R.L., 1982b, J. Phys. B: At.Mol.Phys. 15, 3257.

Regemorter H. van., 1962, Astrophys. J. 132, 906.

Rose M.E., 1957, " Elementary Theory of Angular Momentum", (Wiley: New York).

Rotenberg M., 1970, Adv. Atom. Mol. Phys. 6, 233.

Rudge M.R.H. and Seaton M., 1964, Proc. Roy. Soc. A283, 262.

Sachdeva M.L. and Puri S.P., 1978, Phys. Rev. A14, 1603.

Salin A., 1969, J. Phys. B: At. Mol. Phys. 2, 631.

Sasao M., Matsumoto A., Nishizawa A., Sato K.N., Takagi S., Amamiya S., Masuda T., Tsurita Y., Kanamori Y., Hzuyama Y.

and Fukuzawa F., 1983, Proc. 13th Int. Conf. on the Physics of Electronic and Atomic Collsions (Berlin), ed J. Eichler et al., (Amsterdam: North Holland), abstracts p 569.

Sasao M., Sato K.N., Matsumoto A., Nishizawa A., Takagy S., Amamiya S., Masuda T., Tsurita Y., Fukuzawa F., Haruyama Y., and Kanamori Y., 1986a, J. Phys. Soc. (Japan) 55, 102.

Sasao M., Sato K.N., Nakamura Y. and Wakatani M., 1986b, Research Report IPPJ-57., Institute of Plasma Physics, Nagota University, Japan.

Sato H. and Kimura M., 1983, Phys. Lett. 96A, 286.

Seitz F., 1935, Phys. Rev.47, 300.

SethuRaman V., Thorson W.R. and Lebeda C.F., 1973, Phys. Rev. A8, 1316.

Sewell E.C., Angel G.C., Dunn K.F. and Gilbody H.B., 1980, J. Phys. B: At.Mol.Phys. 13, 2269.

Shah M.B. and Gilbody H.B., 1978, J. Phys. B: At. Mol. Phys. 11, 121.

Shah M.B. and Gilbody H.B., 1981a, J. Phys. B: At. Mol. Phys. 14, 2361.

Shah M.B. and Gilbody H.B., 1981b, J. Phys. B: At. Mol. Phys. 14, 2831.

Shah M.B. and Gilbody H.B., 1982, J. Phys. B: At. Mol. Phys. 15, 413.

Shah M.B., Elliott D.S. and Gilbody H.B., 1985, J. Phys. B: At. Mol. Phys. 18, 4245.

Shakeshaft R., 1975, J. Phys. B: At. Mol. Phys. 8, 1114.

Shakeshaft R., 1976, Phys. Rev. A14, 1626.

Shakeshaft R., 1978, Phys. Rev. A18, 1930.

Shakeshaft R. and Spruch L., 1973, Phys. Rev. 8, 206.

Shampine L.F. and Gordon M.K., 1975, "Computer Solution of Ordinary Differential Equations: The Initial Value Problem.", (Freeman, San Francisco).

Shingal R., 1983, unpublished.

Shingal R., 1987, unpublished.

Shingal R., Bransden B.H. and Flower D.R., 1987, to be published.

Shipsey E.J., Redmon L.T., Browne J.C. and Olson R.E., 1978, Phys. Rev. A18, 1961.

Silk J. and Steigman G., 1969, Phys. Rev Lett. 23, 597.

Sin Fai Lam L.T., 1967, Ph.d Thesis, University of Durham.

Smith F.J., 1964, Proc. Phys. Soc. 84, 889.

Tai H. and Gerjuoy E., 1973, J. Phys. B: At. Mol. Phys. 6, 1426.

Taylor J.R., 1983," Scattering Theory:The Quantum Theory of Nonrelativistic Collisions", 2nd edn., (R.E. Kreiger Publishing Company , Florida).

Temkin A., 1957, Phys. Rev. 107, 1004.

Temkin A., 1960, Phys. Rev. Lett. 4, 566.

Vainshtein L.A., Presnyakov L.P. and Sobelman I.I., 1962, Zh. Eksp. Teor. Fiz. 43, 518.

Vainshtein L.A., Sobelman I.I. and Yukov E.A., 1981, "Excitation of Atoms and Broadening of Spectral Lines", 1st edn, (Springer Verlag: Berlin).

Varghese S.L., Waggoner W. and Cocke C.L., 1984, Phys. Rev. A29, 2453.

Vinogradov A.V. and Sobelman I.I., 1973, Sov. Phys. JETP 36, 115.

Watson G.N., 1945,"Treatise on the theory of Bessel Functions", 2nd. edn., (MacMillan :New York).

Weinberg S., 1962, Phys. Rev. 126, 1899.

Weissbluth M., 1978, "Atoms and Molecules", 1st edn., (Academic Press: London).

Wilets L. and Gallaher D.F., 1966, Phys. Rev. 147, 13.

Willis S.L., Peach G., McDowell M.R.C. and Banerji J., 1985, J. Phys. B: At. Mol. Phys. 18, 3939.

Winter H., Bloeman E. and Reheer F.J., 1977, J. Phys. B: At. Mol. Phys. 10, L599.

Winter T.G., 1980, Bull. Am. Phys. Soc. 25,1135.

Winter T.G., 1982, Phys. Rev. A25, 697.

Winter T.G. and Hatton G.J., 1980, Phys. Rev. A21, 793.

Winter T.G., Hatton G.J. and Lane N.F., 1980, Phys. Rev. 22, 930.

Winter T.G. and Lin C.D., 1984, Phys. Rev. A29, 3071.

Zimmerman I.H., 1972, Ph.D Thesis, University of Washington, unpublished.